Multiscale Modelling *of* Tunnel Ventilation Flows *and* Fires

FRANCESCO COLELLA

Thesis submitted for the degree of Doctor of Philosophy

Politecnico di Torino, Dipartimento di Energetica.

May 2010

DECLARATION

This thesis and the research described and reported herein have been completed solely by Francesco Colella under the supervision of Professor Romano Borchiellini, Dr Vittorio Verda, Dr Guillermo Rein and Professor Jose L. Torero. Where other sources are quoted, full references are given.

Francesco Colella

TABLE OF CONTENTS

1 INTRODUCTION 1

1.1. Introduction 1

1.2. Fundamentals of tunnel fires 2

1.3. The role of the ventilation system 7

1.3.1. Natural ventilation systems 8

1.3.2. Mechanical ventilation systems 9

1.3.3. Hybrid ventilation systems 13

1.4. Interaction between fire and ventilation system 14

1.4.1. Ventilation velocity and back-layering 14

1.5. Analysis of tunnel ventilation systems and fires 22

1.5.1. Small and large scale experiments 23

1.5.2. Numerical modelling 23

1.6. Test cases 26

1.6.1. Case A: Frejus Tunnel, Bardonecchia (It) 26

1.6.2. Case B: Norfolk road Tunnels, Sydney (Au) 26

1.6.3. Case C: Wu-Bakar small scale tunnel 27

1.6.4. Case D: Dartford Tunnels, London (UK) 27

1.6.5. Case E: Test case tunnel 27

2 ONE-DIMENSIONAL MODELLING 29

2.1. Introduction 29

2.2. Literature overview 30

2.3. Typical mathematical formulation for 1D models 32

2.3.1. Topological representation 32

2.3.2. Fluid dynamics model 33

2.3.3. Thermal model 35

2.3.4. Steady state problem 36

2.3.5. Time dependent problem 40

2.3.6. Solving algorithm 42

2.3.7. Typical input parameters and boundary conditions 44

2.4. A case study: the Frejus Tunnel 47

2.5. Concluding remarks 51

3 CFD MODELLING 53

3.1. Introduction 53

3.2. Literature overview 55

3.3. Governing equations 67

3.4. Turbulence modelling 68

3.5. Boundary conditions 74

3.5.1. Pressure boundary conditions 74

3.5.2. Velocity boundary conditions 75

3.5.3. Wall boundary conditions 75

3.5.4. Boundary conditions for the transport equations of turbulent quantities 78

3.5.5. Fire representation 79

3.5.6. Jet Fan representation 82

3.6. Numerical features 83

3.7. Case Studies 85

3.7.1. Ventilation flows in the Norfolk road Tunnels 85

3.7.2. Assessment of the mesh requirements 87

3.7.3. Simulations of the ventilation scenarios and comparison to on-site measurements 89

3.7.4. Critical velocity calculation 93

3.7.5. Assessment of the mesh requirements 94

3.7.6. Critical velocity results 97

3.7.7. Effect of the fire Froude number on the critical velocity 102

3.8. Concluding Remarks 103

4 FUNDAMENTALS OF MULTISCALE COMPUTING 105

4.1. Introduction 105

4.2. Fundamental of domain decomposition methods 108

4.3. Formulation of the multiscale problem 112

4.4. Coupling technique 114
4.4.1. Direct coupling 114
4.4.2. Indirect coupling 119

4.5. Concluding remarks 120

5 MULTISCALE MODELLING OF TUNNEL VENTILATION FLOWS 121

5.1. Introduction 121

5.2. A case study: the Dartford tunnels 122

5.3. Overview on the experimental setups 125

5.4. Characterization of the jet fan discharge cone 126
5.4.1. Assessment of the mesh requirements 127
5.4.2. Effect of the 1D-CFD interface location 130
5.4.3. Comparison to experimental data 132

5.5. Characterization of the ventilation system 135
5.5.1. Calculation of the jet fan characteristic curves 135
5.5.2. Comparison to experimental data 138
5.5.3. Analysis of all the ventilation strategies 139
5.5.4. Assessment of the redundancy in the Dartford Tunnels 140

5.6. Concluding remarks 142

6 MULTISCALE MODELLING OF TUNNEL FIRES 145

6.1. Introduction 145

6.2. A case study: a modern tunnel 1.2 km in length 146

6.3. Characterization of the fire near field 147
6.3.1. Assessment of the mesh requirements 148
6.3.2. Effect of the 1D-CFD interface location 151
6.3.3. Comparison to full CFD solutions 155

6.4. Characterization of the ventilation system performance 161
6.4.1. Calculation of the fan and fire characteristic curves 161

6.4.2. Comparison to full CFD solutions 162
6.4.3. A note of the fire throttling effect 165

6.5. Concluding remarks 166

7 MULTISCALE MODELLING OF TIME-DEPENDENT TUNNEL VENTILATION FLOWS AND FIRES 169

7.1. Introduction 169

7.2. A case study: a modern tunnel 1.2 km in length 170

7.3. Multiscale model results 175

7.4. Concluding remarks 182

8 CONCLUSIONS AND FUTURE WORKS 185

LIST OF FIGURES

Figure 1: Typical traffic flow and induced ventilation in the 1.8 tunnel in Taipei City. Traffic density and induced ventilation as presented in [23] 8

Figure 2: A schematic of a Saccardo longitudinal ventilation system [26] 10

Figure 3: A schematic of a jet fan longitudinal ventilation system [26] 10

Figure 4: A schematic of a fully transverse ventilation system 12

Figure 5: A schematic of a supply semi-transverse ventilation system 13

Figure 6: A schematic of a exhaust semi-transverse ventilation system 13

Figure 7: Photograph of a small scale tunnel fire during the occurrence of back-layering. The fire size in 15 kW. The tunnel has an arched cross section (width 274mm, height 244 mm). Adapted from [3]. 15

Figure 8: Variation of dimensionless critical velocity against dimensionless heat release rate. (O) measurements of critical velocity; (continuous line) equations (8) and (9): (dashed line) Thomas correlation (4). (from [29]). 17

Figure 9: Two step approximation of fire growth rate phase for the Second Benelux tunnel fire Tests and Runehamar Fire Test Program (from [18]) 22

Figure 10: A schematic of a hybrid computational grid for multiscale calculation of tunnel ventilation flows and fires 25

Figure 11: Example of the network representation of a tunnel showing branches between nodes 33

Figure 12: Schematic of the control volumes adopted for the numerical solution 37

Figure 13: Meteorological pressure difference measured between the portals of Mont Blanc Tunnel [73] 45

Figure 14: Frejus tunnel: top) cross section; down) Schematic of the ventilation system layout 48

Figure 15: Schematic of the network used for the 1D calculation corresponding to the tunnel region between section T_2 and T_3 of Figure 14. 49

Figure 16: Velocity distribution computed with the developed 1D model and comparison to experimental data recorded in the Frejus tunnel. Longitudinal velocity as function of the tunnel length 50

Figure 17: Velocity distribution computed with the developed 1D model and comparison to experimental data recorded in the Frejus tunnel. Longitudinal velocity as function of the tunnel length at 4 different times 51

Figure 18: Schematic of the simplified fire representations used in this work. 80

Figure 19: Schematic of mesh used the fan representations used in this work. 83

Figure 20: Schematic of the CFD segregated solution algorithm. 84

Figure 21: Schematic of the Norfolk road tunnels cross section. 85

Figure 22: Schematic of the jet fan longitudinal position in the Westbound Norfolk road tunnel; jet fans are numbered from 13 to 24. 86

Figure 23: Examples of the different meshes used for half of the tunnel cross section and number of cells per unit length of tunnel. 88

Figure 24: Comparison of the longitudinal velocity contours for meshes #1 to #4 in the tunnel at the reference section 1. Velocity values are expressed in m/s. 88

Figure 25: Comparison of the longitudinal velocity contours for meshes #1 to #4 in the tunnel at the reference section 2. Velocity values are expressed in m/s. 89

Figure 26: Computed velocity profile in the tunnel for scenarios 1.1, 1.2, 1.3, 2.1, 2.2, 4.2, 5.1, 5.2, 6.1 from Table 8. The plotted velocity fields are relative to plane 1 of Figure 21. Velocity values are expressed in m/s. 91

Figure 27: Comparison between predicted velocity and experimental measurements provided by the Sickflow 200 Units located at the centre of each tunnel tube. 92

Figure 28: 3D visualisation of the computed velocity fields for ventilation scenario 3.4 involving all the 6 jet fan pairs. Velocity values are expressed in m/s. (not to scale). 93

Figure 29: Schematic of the experimental rig accordingly to Wu and Bakar [3]. Section B has been used in this study. 94

Figure 30: Examples of the different meshes used for half of the tunnel cross section and number of cells per unit length of tunnel. 95

Figure 31: Computed temperature and velocity fields for mesh #1 to #4 at reference sections 1 for a 30 kW fire at critical ventilation conditions. Temperature and velocity values are expressed in K and m/s respectively. 96

Figure 32: Computed temperature and velocity fields for mesh #1 to #4 at reference sections 2 for a 30 kW fire at critical ventilation conditions. Temperature and velocity values are expressed in K and m/s respectively. 97

Figure 33: Computed temperature and velocity fields in the vicinity of the fire source for a 30 kW fire at critical ventilation conditions. Temperature and velocity values are expressed in K and m/s respectively. 98

Figure 34: Computed temperature and velocity fields at reference sections 1 and 2 for a 30 kW fire at critical ventilation conditions. Temperature and velocity values are expressed in K and m/s respectively. 99

Figure 35: Computed temperature and velocity fields in the vicinity of the fire source for a 3 kW fire at critical ventilation conditions. Temperature and velocity values are expressed in K and m/s respectively. 100

Figure 36: Computed temperature and velocity fields at reference sections 1 and 2 for a 3 kW fire at critical ventilation conditions. Temperature and velocity values are expressed in K and m/s respectively. 101

Figure 37: Effect o fire Froude number on the predicted critical for a 3 kW and a 30 kW fire 102

Figure 38: up) Example computed velocity field for a pair of operating jet fans (jet fan discharge velocity ~34 m/s; down) Example computed temperature field for a 30MW fire subject to supercritical

ventilation conditions. The velocity and temperature values are expressed in m/s and K, respectively. 107

Figure 39: Example of domain decomposition with and without overlapping [65]. 108

Figure 40: Example of domain decomposition for solution of Navier-Stokes problem using a Dirichlet-Neumann iterative method. 110

Figure 41: Example of domain decomposition for solution of Navier-Stokes problem using a Schwartz (Dirichlet-Dirichlet) iterative method. 111

Figure 42: Example of a domain decomposition in 1D and 3D sub-domains. 113

Figure 43: Visualization of a three stage coupling procedure. 117

Figure 44: Visualization of the interaction procedure between 1D and 3D grids at the left CFD domain boundary (1D-CFD interfaces highlighted in green) 117

Figure 45: left) Evolution of total pressure and mass flow rate at a 1D-3D interface during a multiscale calculation. The maximum deviation allowed was 10^{-6}. right). Deviation of the mass flow rate and total pressure at a 1D-CFD interface during a multiscale calculation 118

Figure 46: Diagram of the East and West Dartford Tunnels showing the relative positions of jet fans and extract shafts. (Drawn approximately to scale but with vertical distances five times larger) 122

Figure 47: East Dartford Tunnel; Picture taken approximately 1100 m from the Kent portal facing south (refer to Figure 46). 123

Figure 48: West Dartford Tunnel; Picture taken approximately 500 m from the Kent portal facing south (refer to Figure 46). 123

Figure 49: Layout and general dimensions of the tunnel cross sections (west tunnel to the left; East tunnel to the right) including the points 1-9 where the air velocities where measured (dimensions are expressed in mm). 125

Figure 50: Schematic of multiscale coupling between mono-dimensional and CFD models for the multiscale calculation of the jet fan discharge cone (1D-CFD interfaces highlighted in green) 127

Figure 51: Examples of the different meshes used for half of the tunnel cross section and number of cells per unit length of tunnel. 128

Figure 52: Comparison of the longitudinal velocity contours for meshes #1 to #4 in the tunnel at the reference section 1. Velocity values are expressed in m/s. 129

Figure 53: Comparison of the longitudinal velocity contours for meshes #1 to #4 in the tunnel at the reference section 2. Velocity values are expressed in m/s. 130

Figure 54: Convergence of the predicted mass flow rate as a function of the location of the interface 131

Figure 55: Comparison of horizontal velocities between predictions (lines) and experimental measurements (symbols) in the West Tunnel. The two profiles and the numbers refer to locations in the tunnel section described in Figure 49. 132

Figure 56: Comparison of horizontal velocities between predictions (lines) and experimental measurements (symbols) in the East Tunnel. The two profiles and the numbers refer to locations in the tunnel section described in Figure 4.b. 134

Figure 57: Typical flow pattern produced by a series of seven jet fan pairs operating in the West Tunnel (not to scale). Velocity isocontours from 2 m/s to 20 m/s in steps of 2 m/s; Velocity expressed in m/s. 136

Figure 58: Computational mesh for the CFD module around the jet fans in the West (right) and East (left) tunnels. (Note: the West tunnel's jet fans are installed in niches on the ceiling, in the East tunnel they are not.) 137

Figure 59: CFD calculated jet fan thrust vs. tunnel average velocity for the Dartford tunnels. 137

Figure 60: Comparison between experimental data and model predictions. 139

Figure 61: Results for the West Tunnel, using the strategy for Zone C (Kent supply on, Essex extract on), varying the number of active jet fan pairs. (Note: Zone C extends from approximately 700 m into the tunnel to 1370 m). 141

Figure 62: Results for the East Tunnel, using the strategy for Zone C (Kent supply on, Essex extract on), varying the number of active jet fans. (Note: Zone C extends from approximately 700 m into the tunnel to about 1300 m) 142

Figure 63: Layout of the tunnel used as case study showing the relative positions of the fire, jet fans and portals (Not to scale). 146

Figure 64: Schematic of the multiscale model of a 1.2 km tunnel including portals, jet fans, and the CFD domain of the fire region. Contours of the temperature field show the fire plume. (Not to scale). The 1D-CFD interfaces have been highlighted in green 148

Figure 65: Examples of the different meshes used for half of the tunnel cross section and number of cells per unit length of tunnel. 149

Figure 66: Comparison of the longitudinal velocity (left) and temperature (right) contours for meshes #1 to #4 in the tunnel at Reference Section 1 for a 30 MW fire. The velocity and temperature values are expressed in m/s and K respectively. 150

Figure 67: Comparison of the longitudinal velocity (left) and temperature (right) contours for meshes #1 to #4 in the tunnel Reference Section 2 for a 30 MW fire. Velocity and temperature values are expressed in m/s and K respectively 150

Figure 68: Effect of the CFD domain length, L_{CFD}, on the average longitudinal velocity and temperature at the outlet boundary of the CFD module. Units are in m/s and K respectively. Note that the shortest module length is 20 m. 152

Figure 69: Effect of the CFD domain length L_{CFD} on the error for the average longitudinal velocity and average temperature. Results for top) Reference Section 1; bottom) Reference Section 2. Error calculated using Eq. (76). 153

Figure 70: Effect of the CFD domain length L_{CFD} on the horizontal velocity and temperature fields at Reference Section 1 for a 30MW fire. The velocity and temperature values are expressed in m/s and K respectively 154

Figure 71: Effect of the CFD domain length L_{CFD} on the horizontal velocity and temperature fields at Reference Section 2 for a 30MW fire. Velocity and temperature values are expressed in m/s and K respectively 154

Figure 72: Comparison of results near the fire for the multiscale and the full CFD simulations for a fire of 30 MW and ventilation scenario 1. Velocity and temperature values are expressed in m/s and K respectively. The longitudinal coordinates start at the upstream boundary of the corresponding CFD domain. 157

Figure 73: Comparison of results near the fire for the multiscale and the full CFD simulations for a fire of 30 MW and ventilation scenario 2. Velocity and temperature values are expressed in m/s and K respectively. The longitudinal coordinates start at the upstream boundary of the corresponding CFD domain. 158

Figure 74: Comparison of results near the fire for the multiscale and the full CFD simulations for a fire of 30 MW and ventilation scenario 3. Velocity and temperature values are expressed in m/s and K respectively. The longitudinal coordinates start at the upstream boundary of the corresponding CFD domain. 159

Figure 75: Comparison of results near the fire for the multiscale and the full CFD simulations for a fire of 30 MW and ventilation scenario 4. Velocity and temperature values are expressed in m/s and K respectively. The longitudinal coordinates start at the upstream boundary of the corresponding CFD domain. 160

Figure 76: Characteristic curves of a tunnel region 50 m long where an activated jet fan pair (and a single jet fan) is located: Pressure drop between inlet and outlet vs. Mass flow rate across the inlet. (CFD calculated). 161

Figure 77: Characteristic curves of the tunnel region 400 m long where the fire is located: Pressure drop between inlet and outlet vs. Mass flow rate across the inlet (CFD calculated) 162

Figure 78: Longitudinal velocity iso-contours, calculated using full CFD for 10 operating jet fans pairs. (Not to scale) 163

Figure 79: Predictions of average velocity for cold flow scenarios. Comparison and error between multiscale and full CFD results. 164

Figure 80: Layout of the tunnel used as case study showing the relative positions of the fire, jet fans and portals (Not to scale). 171

Figure 81: Fire growth curve, delay phase and detection times considered in the time dependent multiscale simulations. The fire growth curve is based on the work of Carvel (2008) [18]. 172

Figure 82: Schematic of the multiscale model of a 1.2 km tunnel including portals, jet fans, and the CFD domain of the fire region. Contours of the temperature field show the fire plume. (Not to scale). The 1D-CFD interfaces have been highlighted in green 173

Figure 83: Time dependent evolution of the mass flow rate through the tunnel for scenario 1, 2 and 3 (see Table 17). The time to detection is 2 min. Supercritical conditions (v_{air}> 3m/s) are reached after 244 s, 190 s and 160 s for scenario 2 and 3 respectively 175

Figure 84: Multiscale results in the vicinity of the fire computed 2 min after the fire outbreak for scenario 1, 2 and 3 (see Table 17). The ventilation system is about to be started. Velocity and temperature values are expressed in m/s and K respectively. The longitudinal coordinates start at the upstream boundary of the corresponding CFD domain. (not to scale) 176

Figure 85: Temperature profiles computed by the multiscale model 3 min after the fire outbreak for scenario 1, 2 and 3 (see Table 17). The ventilation system is operative since 1 min. Temperature values are expressed in K. (not to scale) 176

Figure 86: Longitudinal velocity profiles computed by the multiscale model 3 min after the fire outbreak for scenario 1, 2 and 3 (see Table 17). The ventilation system is operative since 1 min. Velocity values are expressed in m/s. (not to scale) **177**

Figure 87: Temperature and velocity profiles 5 min (left column) and 10 min (right column) after the fire outbreak for scenario 1, 2 and 3 (see Table 17). Temperature and velocity values are expressed in K. and m/s, respectively (not to scale) 178

Figure 88: Dependence between number of operating jet fan pairs, TD, and time required to remove back-layering computed from the moment of the ventilation system activation. **181**

Figure 89: Dependence between number of operating jet fan pairs, TD, and time required to remove back-layering computed from the fire outbreak **182**

LIST OF TABLES

Table 1: Extension of tunnels in Europe 1

Table 2: Approximate energy contents of typical tunnel fire loads [11,12] 4

Table 3: Approximate max HRR for typical tunnel fires 4

Table 4: Approximate smoke production from tunnel fires [12] 6

Table 5: Maximum peak temperature recorded on full scale experimental tunnel fires [1,2,14,19,20]. 6

Table 6: Summary of the observed correlation between ventilation rate, delay phase length and fire growth rate (from [18]). 22

Table 7: Summary of the published CFD studies related to tunnel fires discussed in the literature review. 66

Table 8: Summary of ventilation scenarios explored during the experimental campaign conducted in the Westbound Norfolk road tunnel. Scenarios having the measurement unit located in the vicinity of an operating jet fan have been highlighted in grey. 86

Table 9: Grid Independence Study for a scenario involving an operating jet fan pair in the Norfolk tunnels 87

Table 10: Grid Independence Study for a scenario involving a 30 kW fire scenario 96

Table 11: Grid Independence Study for a scenario involving an operating jet fan pair in the West tunnel 128

Table 12: Summary of ventilation flows in the tunnels resulting from various ventilation strategies. The operating ventilation devices in each scenario are indicated by “ON”. The predicted ventilation velocities in the incident zones are highlighted in bold 140

Table 13: Summary of ventilation and fire scenarios analysed with the multiscale technique 147

Table 14: Grid independence study of the full CFD domain for a 30 MW fire and 3 operating jet fan pairs. 149

Table 15: Comparison between Full CFD and Multiscale predictions for the 7 scenarios investigated. The multiscale results are obtained with direct coupling. The table presents only bulk flow data. 155

Table 16: Comparison between Full CFD, Multiscale, and 1D model predictions for the 7 scenarios investigated. The multiscale results are obtained with indirect coupling. The table presents only bulk flow data. 164

Table 17: Summary of the ventilation scenarios considered in the time dependent analysis 173

Table 18: Summary of the ventilation scenarios considered and numerical findings 180

ACKNOLEDGEMENTS

I would like to thank my supervisors Prof. Vittorio Verda and Prof. Romano Borchiellini for their constant support, their precious advices and feedbacks. They are the original masterminds behind this work. A special “Thank You” to Vittorio for the patience he had dealing with me during the last four years and above all and for being, besides an enthusiastic advisor, a good friend.

I would also like to thanks my supervisors Dr. Guillermo Rein and Prof. Jose Luis Torero for welcoming me at University of Edinburgh half the way through this project and for hosting me for more than 2 years. I thank them for tens of helpful discussions, for their invaluable feedback and for their contagious optimism. I have been very fortunate to learn about fire from them.

I owe my gratitude to Dr. Ricky Carvel for his expert comments and for providing insightful discussions. His help has been invaluable for the completion of this work.

I would like to thank Le Crossing Company Ltd., Jacob (UK) Ltd. and the Highways Agency for allowing access to the Dartford tunnels, assistance with the on-site measurements and permitting the completion of this work and the publication of several papers. Special thanks to Stuart Lowe of Jacobs (UK) Ltd. for all his help with the on-site measurements.

I am grateful to Transurban Ltd (AU) for supplying useful experimental measurements adding significant quality to this thesis. Special thanks to Cameron Torpy of Transurban Ltd (AU) for being a kind and expert interlocutor.

I would like to show my gratitude to all my colleagues in Torino, Adriano, Flavio, Chiara e Giorgia for many fruitful discussions but also for their friendship. The have been always around whenever I needed a break. A special thanks goes to Adriano for our innumerable conversations on CFD and music related topics and to Giorgia for being always so helpful while I was away.

I am also thankful to all the people I have meet in the last years at University of Edinburgh. Thanks to Nicolas and Cristián for all the interesting talks, the laughs and the culinary arguments we had since the beginning. They are among the best flatmates I have ever had. Thanks to Hubert and Wolfram for being always around for a talk, a joke or a serious discussion. I am thankful to Pedro for our endless conversations and for sharing his experiences. I cannot forget Thomas and his family for several enjoyable dinners and for introducing me to the pleasures of the “Deutsche Sprache”. Thanks to Albert for all the interesting research related conversations and for our long discussions on the Italo-Corsican culture. Thanks to all my office mates Paolo, Adam, Cecilia, Rory, Angus, Joanne, Kate and Susan for never denying a smile or a chat.

I am thankful to all my old friends and flatmates in Torino, Sergio, Michele, Antonio, Pierluigi and Michele for making, whenever I am there, my life pleasant and never boring. Thanks to them for all those late dinners, pool and poker games, sport activities and for always keeping the doors of their flats open for me to stay.

I also have to thank my father, my mother and my sister for encouraging and supporting me to follow my own choices and for insisting to invest in my education. I am grateful to them for all the sacrifices and efforts they did and they still do for me. To them I dedicate this thesis.

Finally, I would like to express my deepest thanks to Daniela. Thanks not only for coming into my life, but for the special person she is, for her enthusiastic support to my choices. Without her care and encouragements, this work would not have been successfully completed.

THANK YOU ALL

ABSTRACT

Tunnels represent a key part of world transportation system with a role both in people and freight transport. Past events show that fire poses a severe threat to safety in tunnels. Indeed in the past decades over four hundred people worldwide have died as a result of fires in road, rail and metro tunnels. In Europe alone, fires in tunnels have brought vital parts of the road network to a standstill and have cost the European economy billions of euros. Disasters like Mont Blanc tunnel (Italy, 1999) and the more recent three Channel Tunnel fires (2008, 2006 and 1996) show that tunnel fire emergencies must be managed by a global safety system and strategies capable of integrating detection, ventilation, evacuation and fire fighting response, keeping as low as possible damage to occupants, rescue teams and structures. Within this safety strategy, the ventilation system plays a crucial role because it takes charge of maintaining tenable conditions to allow safe evacuation and rescue procedures as well as fire fighting. The response of the ventilation system during a fire is a complex problem. The resulting air flow within a tunnel is dependent on the combination of the fire-induced flows and the active ventilation devices (jet fans, axial fans), tunnel layout, atmospheric conditions at the portals and the presence of vehicles.

The calculation of tunnel ventilation flows and fires is more economical and time efficient when done using numerical models but physical accuracy is an issue. Different modelling approaches can be used depending on the accuracy required and the resources available. If details of the flow field are needed, 2D or 3D computational fluid dynamics (CFD) tools can be used providing details of the flow behaviour around walls, flames, ventilation devices and obstructions. The computational cost of CFD is very high, even for medium size tunnels (few hundreds meters). If the analysis requires only bulk flow velocities, 1D models can be adopted. Their low computational cost favours large number of parametric studies involving broad range ventilation scenarios, portal conditions and fire sizes/locations.

Another class of methods, called multiscale methods, adopts different levels of complexity in the numerical representation of the system. Regions of interest are described using more detailed models (i.e. CFD models), while the rest of the system can be represented using a simpler approach (i.e. 1D models). Multiscale methods are characterized by low computational complexity compared to full CFD models but provide the same accuracy. The much lower computational cost is of great engineering value, especially for parametric and sensitivity studies required in the design or assessment of ventilation and fire safety systems. Multiscale techniques are used here for the first time to model tunnel ventilation flows and fires.

This thesis provides in Chapter 1 a general introduction on the fundamentals of tunnel ventilation flows and fires. Chapter 2 contains a description of 1D models, and a case study on the Frejus tunnel (IT) involving some comparisons to experimental data. Chapter 3 discusses CFD techniques with an extensive review of the literature in the last 30 years. The chapter provides also two model validations for cold ventilation flows in the Norfolk Tunnels (AU) and fire induced flows in a small scale tunnel. Chapter 4 introduces multiscale methods and addresses the typical 1D-CFD coupling strategies. Chapter 5 applies multiscale modelling for cold flow steady-state scenarios in the Dartford Tunnels (UK) where a further validation against experimental data has been introduced. Chapter 6 present the calculations from coupling fire and ventilation flows in realistic modern tunnel layout and investigates the accuracy of the multiscale predictions as compared to full CFD. Chapter 7 represents application of multiscale computing techniques to transient problems involving the dynamic response of the ventilation system.

The multiscale model has been demonstrated to be a valid technique for the simulation of complex tunnel ventilation systems both in steady-state and time-dependent problems. It is as accurate as full CFD models and it can be successfully adopted to conduct parametric and sensitivity studies in long tunnels, to design ventilation systems, to assess system redundancy and the performance under different hazards conditions. Time-dependent simulations allow determining the evolution of hazardous zones in the tunnel domain or to determine the correct timing for the activation of fixed fire fighting systems. Another significant advantage is that it allows for full coupling of the fire and

the whole tunnel domain including the ventilation devices. This allows for an accurate assessment of the fire throttling effect that is shown here to be significant and for a prediction of the minimum number of jet fans needed to cope with a certain fire size. Furthermore, it is firmly believed that the multiscale methodology represents the only feasible tool to conduct accurate simulations in tunnels longer than few kilometres, when the limitation of the computational cost becomes too restrictive.

1 Introduction

1.1. Introduction

Tunnels represent a key part of world transportation system playing a fundamental role both in people and freight transportation system, especially in developed countries. Around the world most major cities and metropolitan areas have metro systems accounting for hundreds of kilometres of underground tunnels and networked system. Similarly, in some mountainous regions, tunnels represent a vital part of the network transportation system. At present, the overall length for operational transportation tunnels throughout the whole of Europe is larger than 15000 km [1]. An overview on the extension of the underground transportation systems in Europe is given in Table 1 including road and rail tunnels.

	Italy	Austria	Switzerland	Germany	France	UK	Norway	Spain
Railways	1200	105	360	380	650	220	260	750
Roads	1160	210	140	70	180	30	370	100
Total	2360	315	500	450	830	250	630	850

Table 1: Extension of tunnels in Europe

The issue of tunnel fire safety has become more important in the last decades due to the social impact of disaster like King's Cross underground station in 1987 (31 deaths),

Baku Underground fire in 1995 (289 deaths), Gotthard Tunnel in 2001 (11 deaths), Tauern Tunnel in 1999 (12 deaths), Mont Blanc Tunnel in 1999 (39 deaths), Frejus Tunnel in 2005 (2 deaths) and Channel tunnel fires in 1996, 2006 and 2008.

According to French statistics [2] it appears that there are only one or two car fires (per km of tunnel length) every hundred million cars passing through the tunnel. Same order of magnitude can be expected for fire involving heavy good vehicles (HGVs). In this case, 8 fires per hundred millions of HGVs are expected, but only one will be enough serious to produce damage to the structure [3]. On the basis of such values, one can expect that the chance of an accidental tunnel fire can be negligible. However given the high number of tunnels in Europe, their high traffic density (several millions of vehicles per year) and their length (sometimes up to several tens kilometres), the probability of accidental fires become significant. For instance statistics indicates that, on average, one fire incident occurred practically every month within the Elb tunnel in Germany, from 1990 to 1999. And this is not an isolate case. Indeed in the past decade over four hundred people worldwide have died as a result of fires in road, rail and metro tunnels. In Europe alone, fires in tunnels have destroyed over a hundred vehicles, brought vital parts of the road network to a standstill - in some instances for years - and have cost the European economy billions of euros [4]. This serious problem has the potential to get worse it the future due to the drastic increase in the volume of dangerous goods transported and in the number of new operative tunnels.

1.2. Fundamentals of tunnel fires

This section is intended to provide a general overview of the fundamentals of tunnel fires. Fire behaviour in tunnel as well as in compartment is different from the behaviour in open space (free burning conditions). In particular, due to the confined enclosure, the heat feedback from the walls and hot gases enhances the fire burning rate. Furthermore, for very intense enclosure fires the oxygen supply can be reduced inducing a change in the combustion regime from fuel-controlled (also over-ventilated fires) to ventilation-controlled (under-ventilated fires). In the last case the combustion process generate a large amount of incomplete combustion products and toxic effluents.

Ingason identifies three main differences between compartment fires and tunnel fires [5]. The first is related to the maximum heat release rate (HRR) that can be attained. Typically, in small compartment fires the maximum HRR is controlled by the 'ventilation factor' that can be calculated as $A_o\sqrt{h_o}$ $[m^{5/2}]$ where A_o and h_0 are the area and the height of the opening, respectively. In the case of the tunnel fires, given the size of the tunnel cross section and the air flow eventually delivered by the ventilation system, the oxygen supply to the fire zone is at least one order of magnitude larger than typical compartment fires. Therefore, in tunnel fire scenarios, the limiting factor to the maximum HRR is not represented by the ventilation conditions but by the fuel available. Under-ventilated conditions can be only achieved in severe tunnel fires with multiple vehicles involved in the burning process.

The second difference is related to the likelihood of attaining flashover. Flashover is defined as a transition from a localized fire to the general conflagration within the compartment when all the fuel surfaces are burning [6], and limited by ventilation flows. External flames typically appear at the vents of the compartment. Indeed, flashover is unlikely to take place in a tunnel due to the large convective losses from the fire to the surroundings and lack of full containment of hot fire effluents. Nonetheless, it must be stressed that the ventilation system plays an important role in the development of a tunnel fire, especially during the under-ventilated regime [7].

The third difference is related to the smoke stratification. Early stage compartment fires are generally characterized by a buoyant layer of hot gases under the ceiling. The same smoke pattern can be observed in the early stages of tunnel fires but in absence of longitudinal ventilation. In this condition, the smoke front will spread away from the fire zone, cooling down and partially mixing with the air layer underneath. However, after a certain distance and time the smoke layer will descend and touch the road deck. The distance from the fire at which such phenomenon takes place is mainly dependent on the tunnel geometry and fire characteristics. The activation of the ventilation system generally produces important change in the structure of the smoke layer. Moderate ventilation velocities (< 3 m/s) generate a certain degree of back-layering in the fire upstream region while the stratification is lost in the fire downstream region. A more

detailed discussion on the interaction between ventilation system and smoke movements will be presented in the next sections.

Tunnel fires usually involve material from vehicles including seats, tyres, plastic material from the finishing, fuel from the tanks and eventually the loading. The latter can be very variable. Evaluations of the energy content for typical load involved in tunnel fires are presented in Table 2.

Type of vehicle	Approx. energy content [MJ]
Private car	3000-7000
Public bus	41000
TIR fire load	65000
HGV	88000 - 247000
Tanker with 50 m3 of petrol	1500000

Table 2: Approximate energy contents of typical tunnel fire loads [8,9]

Besides the global energy content other characteristics are required to assess the hazard of a given fire scenario. Typically the design of the ventilation system and structures requires an evaluation of the fire heat release rate (HRR), the smoke production and the temperature distribution and the maximum temperature at the tunnel walls.

Indeed the fire HRR represents the single most important variable to evaluate fire hazard [10] and its design value has a great influence on the tunnel construction and operating costs. Several guidelines have been formulated on the basis of large scale tests [8,11-13]. An overview is given in Table 3.

Type of vehicle	Maximum HRR [MW]
1 passenger car	2.5 - 5
2-3 passenger cars	8
1 van	15
1 bus	20
1 lorry with burning goods	20-30
1 HGV	70-200
Tanker	200-300

Table 3: Approximate max HRR for typical tunnel fires

The time evolution of the fire HRR (i.e. growth rate) is another important parameter to be evaluated when designing a ventilation system or an evacuation procedure. This task is much more complicated and only rough estimations can be provided with the current state-of-the-art. Fire growth is indeed linked to flame spread. Flame spread is directly

dependent on material properties with geometry layout and ventilation conditions playing a crucial role. Material properties controlling flame spread can be evaluated by using small-scale flammability testing within an acceptable degree of accuracy for material ranking purposes [14]. However, the extrapolation of small scale data to predict full scale behaviour is also a critical point still under active research, especially when attempting to span multiple orders of length scales. Typical tunnel fires involve a wide range of material, including thermo-plastics which show complex melting and dripping behaviour with burning surfaces highly convoluted. In typical full-scale fire scenarios every burning face sees a variety of radiant fluxes coming from the fire plumes and from other hot surface. The resulting heat release rate of a full-scale object is the sum of the heat release rate from a complex distribution of melting and burning surface, seeing a full spectrum of heat fluxes [15]. In general this distribution depends on the particular geometric configuration and it is not unique.

The geometry of the fire load also is critical issue when evaluating flame spread and the consequent fire growth curve. In opposed spread the flame develops against the air flow. In this case the heated region of the material produced by the radiant feedback from the flame is small and then the flame propagates slowly and steadily. In the case of concurrent flame spread, the air flow and the flame spread direction are the same. In this scenario the heated region of the material produced by the flame has the same dimensions of the flame itself. Concurrent flame spread rate is in between one and two orders of magnitude larger than opposite spread rates [14] and it is self-accelerating. Tunnel fires experience a wide range of geometry and consequently different spread regimes are present at different stages.

Further complexity is added when introducing the effect of the ventilation system controlling the oxygen supply into the fuel bed, the flame shape and amount of heat which is re-irradiated back to the burning surfaces [16].

Given the large uncertainty incurring on flame spread from all the previous considerations, a meaningful prediction the fire growth is a complex task and only rough estimation can be provided with the current state of the art. Most of them are based on experimental evidences. For example observations of the above cited tunnel

fire experiments have shown that the typical t^2 fire representation [6] does not explain the growth of any of the experimental data available, while a two-step linear approximation provided a better estimation [17]. During the first growth stage, the fire would grow slowly up to 1÷2 MW, while during the second stage, the growth rate would be significantly higher (up to 15 MW/min). A more detailed explanation will be given in the following sections.

Same rough estimations can be provided for smoke production. Average values given by PIARC and confirmed by the EUREKA fire test program [12] are resumed in Table 4.

	Smoke flow [m3/s]	
Type of vehicle	**PIARC**	**EUREKA TEST**
passenger car	20	-
passenger van	-	30
2 -3 passenger cars	-	-
1 van	-	-
lorry without dangerous goods	60	50 -60
HGV	-	-
Petrol tanker	100 - 200	-

Table 4: Approximate smoke production from tunnel fires [9]

Temperature distributions and peak temperature attained during a tunnel fire scenario represent important variable for design purposes. Also in this case the actual knowledge is based on experimental data. Table 5 gives an overview of the maximum temperatures recorded during full scale tunnel fires including MTFTVP, EUREKA, Second Benelux tunnel test and Runehamar tunnel fire tests [11-13,18,19]. As it can be seen, the temperature ranges are quite large mainly depending on the specific conditions including ventilation conditions, fire load and tunnel cross section geometry. A larger set of experimental measurements of tunnel fire peak temperature is available in [19].

Type of vehicle	**Peak Temperature [˚C]**
passenger car	200-400
bus	700
HGV	1000-1365
petrol tanker	1000 -1400

Table 5: Maximum peak temperature recorded on full scale experimental tunnel fires [11-13,18,19].

The test involving HGVs fires showed that the temperatures measured downstream of the fire were very high with flaming zone expanding up 70–100 m. Such high

temperature could affect the entire tunnel ceiling downstream of the fire causing considerable spalling of the unprotected tunnel ceiling and eventually flame spread to other vehicles. Same considerations can be given for the upstream region.

1.3. The role of the ventilation system

The ventilation system plays a fundamental role in tunnel safety both in normal operating conditions and in case of fire. In normal operating conditions, the ventilation has to dilute contaminants emitted from the travelling vehicles keeping the air quality within safety levels for the tunnel users. The dilution of smoke will have a direct improvement on the tunnel visibility. The first attempts of installing mechanical ventilation systems in tunnels have been made in the 1920s. This was mainly triggered by the concern on the increasing temperature which was taking place in the underground metro system in New York and London [20]. Previously, the ventilation of such environments was accomplished by utilizing the piston effect produced by moving trains and it was enhanced by the presence of vertical shafts permitting a continuous exchange of air with the exterior. Analogously, the introduction of the first mechanical ventilation devices in road tunnels was triggered by the concern on air quality and the impact of exhaust gases emitted by internal combustion engines.

Due to the growing concern on tunnel fire safety, the ventilation system has gained great importance also in the management of emergency fire scenarios in tunnels. In these cases it has the complex task of smoke management. Which ventilation system is to be selected depends mainly of the tunnel layout and the fire safety strategies chosen for the specific tunnel. However, ventilation systems fall in two broad categories: natural and mechanical. In the first case, the air movement is induced by temperature or pressure gradients across the tunnel portals (i.e. due to meteorological effects) which have importance for long tunnels, and by the piston effect induced by the traffic itself. Mechanical ventilation systems instead, use complex combinations of fans, ducts and dampers for the scope. Depending on the configuration, mechanical ventilation systems are classified in longitudinal, fully transverse ventilation systems and semi-transverse ventilation systems. However for specific reasons (i.e. enhance smoke control capabilities) hybrid configurations can be encountered.

1.3.1. Natural ventilation systems

Natural ventilation systems manly rely on meteorological conditions and piston effect from moving vehicles to guarantee acceptable environment conditions within a tunnel. Meteorological conditions, including temperature and static pressure difference across tunnel portals as well as the effect of the wind, can have a significant impact in long tunnels. Eventually, natural ventilation phenomena can be promoted by including vertical shafts due to an enhanced chimney effect. Unfortunately none of the previous variables can be relied upon when designing tunnel ventilation strategies.

Same considerations can be drawn when considering the ventilation flows due to piston effects. Indeed, it depends on a large number of factors, vehicle speed, vehicle spacing, traffic direction, vehicle drag coefficient, and tunnel geometry, and as expected, many of them cannot be controlled. Small-scale experiments have demonstrated that the ratio between air bulk airflow velocity and vehicle velocity is mainly dependent on the traffic conditions and ranges between 15% and 26% [21]. Full scale measurements under various realistic traffic situations performed in a 1.8 km long tunnel in Taipei City provided lower values: the ratio between vehicles and bulk flow speed ranged between 2% and 7% when the traffic density varied between 2 and 20 vehicles per km of tunnel length and the average traffic velocity is 90 km/h [22]. Figure 1 depicts the typical correlation between traffic density and induced ventilation flows in a tunnel in the Taipei City tunnel.

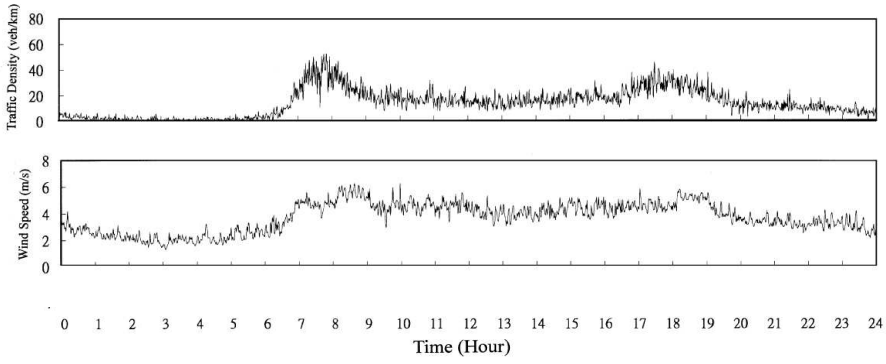

Figure 1: Typical traffic flow and induced ventilation in the 1.8 tunnel in Taipei City. Traffic density and induced ventilation as presented in [22]

Similar values have been encountered for railway tunnels during the passage of a train [23]. However, the same authors confirmed that, in two-way traffic conditions, the

effectiveness of the piston effect is compromised and the ratio between bulk flow velocity and vehicle velocity is radically reduced.

For this reason, natural ventilation systems are applied to short tunnels. Depending on the specific national guidelines, the boundary between short and long tunnels ranges between 350 m÷ 700 m in Germany or 400 m in UK [24].

In case of fire, smoke cannot be controlled due to the absence of mechanical ventilation devices, and naturally stratifies and spreads longitudinally along the tunnel. Due to stratification, the lower portion of the tunnel cross section is free of smoke promoting a safe evacuation of the tunnel users. The depth of the smoke layer underneath the ceiling varies with fire size and fire growth rate, tunnel layout (i.e. dimensions, slope, and cross section), distance from the fire source and eventually with the natural ventilation phenomena (i.e. environment conditions and piston effects). Due to the heat losses through walls, mixing at the interface with the fresh air which is recirculated beneath the smoke layer, the natural smoke stratification breaks down after a certain distance and the vitiated gases occupy the entire tunnel cross section. The smoke recirculation towards the fire source induces also a serious deterioration of the environmental conditions in the vicinity of the fire. Experimental observations demonstrate that stable stratification can be maintained initially for a distance ranging between 400 m and 600 m from the fire [24]. Eventually, the presence of intermediate chimneys can improve the smoke removal from the tunnel but usually this is not a reliable approach. For this reason, it is easy to understand that natural ventilation becomes significantly risky for long tunnels and it represents a viable approach only for tunnels shorter than few hundred meters.

1.3.2. Mechanical ventilation systems

1.3.2.1. Longitudinal ventilation systems

Longitudinal ventilation systems are designed in order to generate a longitudinal ventilation flow within the tunnel with air introduced or extracted from a limited number of points. The longitudinal movement can be induced by the presence of air injection points into the tunnel or by using fans installed on the ceiling providing

longitudinal thrust. The first design option uses Saccardo nozzles located in the vicinity of the tunnel portals which inject air with high velocity and induce longitudinal ventilation flow. A schematic of a Saccardo longitudinal ventilation system is depicted in Figure 2.

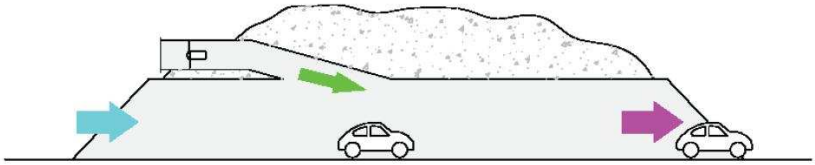

Figure 2: A schematic of a Saccardo longitudinal ventilation system [25]

Longitudinal ventilation systems based on jet fans use series of axial fans (known as jet fans or boosters) installed on the tunnel ceiling characterized by high thrust (hundreds of N) and high discharge ventilation velocities (around 30 m/s). The jet fans can be installed individually, in pairs or even more. A schematic of a jet fan longitudinal ventilation system is depicted in Figure 3.

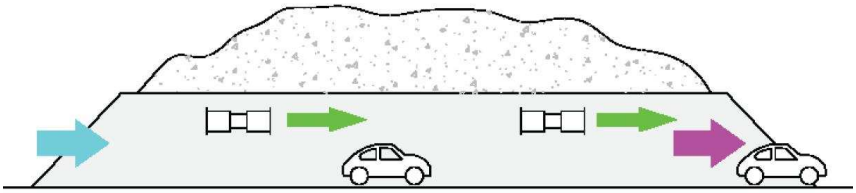

Figure 3: A schematic of a jet fan longitudinal ventilation system [25]

Both the previous ventilation systems are characterized by an almost uniform ventilation velocity through the whole tunnel domain with pollutant concentrations and air temperature increasing in direction of the ventilation flows. In comparison to other more complex ventilation systems (i.e. transverse and semi-transverse ventilation system), longitudinal ventilation systems require less space for ventilation building and ductworks, and a lower capital investment. On the contrary, the tunnel cross section has to be large enough to accommodate their installation. The maintenance and operating cost break-even point associated with a large number of jet fans must be considered. If the system is characterized by a number of jet fans larger than 20, it may be economically convenient to move to other centralized ventilation layouts [26].

The typical ventilation strategies adopted in longitudinally ventilated tunnel require the ventilation system to push the smoke downstream of the incident region in the same direction as the road traffic flow, avoiding the smoke spreading against the ventilation flow (back-layering effect). The vehicles downstream of the fire zone are assumed to leave the tunnel safely. All the studies on back layering show that the maximum critical velocity is in the range from 2.5 m/s to 3 m/s [27-30]. Thus, an adequate ventilation system must guarantee air velocities higher than this range in the region of the fire incident. A more detailed overview on the critical velocity will be given in the following sections. Longitudinal ventilation systems are very effective for tunnel with uni-directional traffic flows, providing enhanced smoke control for a wide range of fire sizes. The ventilation strategies to be adopted are also straightforward. Nowadays, their applicability is limited mainly by the tunnel length.

1.3.2.2. Transverse ventilation systems

Transverse ventilation systems are characterized by uniform air supply and extraction along the tunnel length realized by means of full-length ducts. Supply ducts are usually located either beneath the road deck or above a false ceiling and are connected to the tunnel environment through grills or dampers that can be automatically opened in specific location to promote smoke extraction. The ducts lead to ventilation stations equipped with axial fans. A schematic of a transverse ventilation system is presented in Figure 4. In long tunnels the supply ducts are usually divided in sections in order to limit the size of each ventilation station and the air velocities. Given the dimensions of the duct work and the size of the ventilation stations, the initial investment cost is high.

In normal operating conditions the concentration of pollutants is uniform along the tunnel length (if there is no longitudinal air flow) making this systems well suited for long tunnels also for bi-directional traffic operation.

In case of fire, the ventilation system is operated in order to maintain a smoke clear zone for evacuation purposes by creating a stable stratification of the smoke. The latter is extracted through dampers which are opened in the vicinity of the fire. Eventually fresh air can be supplied. More complex ventilation strategies can be used depending on the specific tunnel layout or boundary conditions.

Globally, transverse ventilation systems are operated in order to avoid the smoke spreading in the tunnel by promoting smoke confinement, stratification and extraction. An optimum strategy would provide limited air velocity (~ 1 m/s) in the fire vicinity. A velocity profile converging towards the fire zone is also desired in order to promote faster smoke confinement. Transverse ventilation systems are proved to be effective for smoke control in case of relatively small fires (< 20 MW). In these scenarios, the extraction efficiency appears to depend mainly on the air flow velocity while the shape of the dampers, for equal opening area, does not have any significant effect [31]. The same authors show that the efficiency of transverse ventilation systems mainly depends on the air flow velocity for small fire size. However, ineffective smoke and temperature managements have been observed for larger fire sizes [11].

It is worth to note that a viable longitudinal flow control is difficult to achieve, even if the system has a large capacity because there are not compensating forces acting in the longitudinal direction. Fire detection and localization are also critical issues for transverse ventilation system.

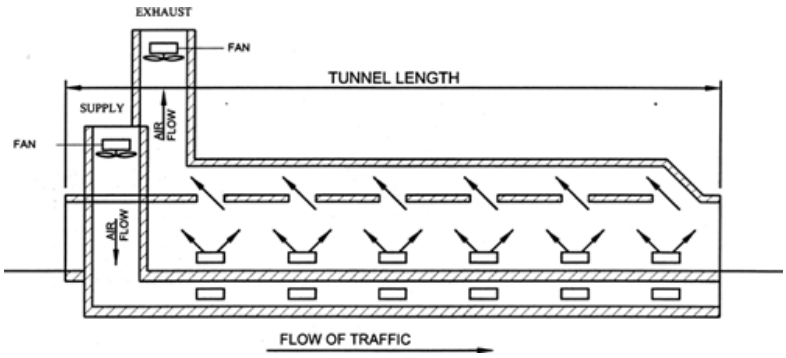

Figure 4: A schematic of a fully transverse ventilation system

1.3.2.3. Semi-transverse ventilation systems

Transverse ventilation systems are characterized by uniform air supply or extraction along the tunnel length realized by means of one full-length duct. Depending on the way the ventilation system is operated, semi-transverse ventilation systems can be classified as supply semi-transverse ventilation systems (see Figure 5) or exhaust semi-transverse ventilation systems (see Figure 6). The former are characterized by a uniform air supply while the latter have a uniform collection of air along the tunnel length. In normal operating conditions supply semi-transverse systems are activated in order to provide

dilution to the traffic pollution. In emergency conditions the air supply could be used to dilute fire effluents; however, reversible fans should be preferably adopted and used to extract smoke during fire scenarios. In fire scenarios, exhaust semi-transverse systems are operated to extract smoke promoting smoke stratification and extraction.

The same limitations presented for fully transverse ventilation systems apply to semi-transverse systems. They have limited capability in controlling longitudinal ventilation flows and they are likely to be unable in managing smoke and temperature in large fire scenarios.

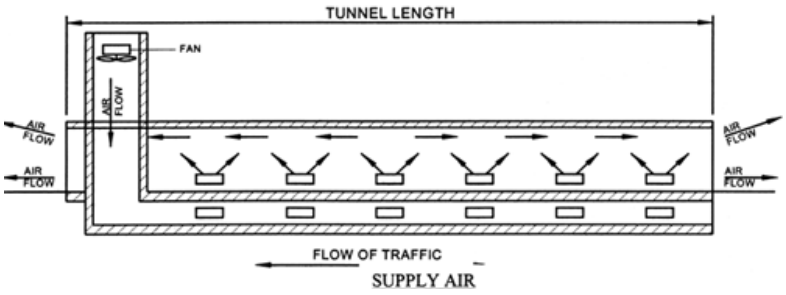

Figure 5: A schematic of a supply semi-transverse ventilation system

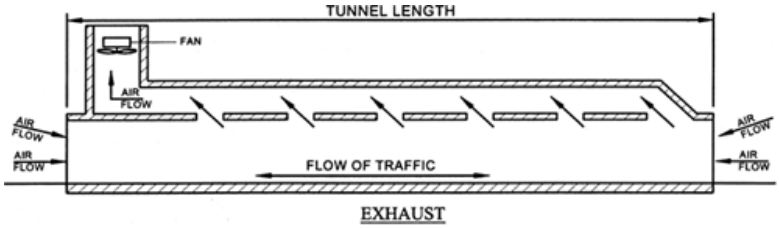

Figure 6: A schematic of a exhaust semi-transverse ventilation system

1.3.3. Hybrid ventilation systems

Beside the previous classification, ventilation systems with intermediate characteristics are often encountered worldwide. In most of the cases they are hybrid combinations of longitudinal and transversal layouts resulting from refurbishments or updating of old un-effective ventilations systems. This is the case of the Mont Blanc tunnel (11.6 km), which has been converted, after the catastrophic fire in 1999, from fully transverse ventilation system to hybrid transverse-longitudinal. Another example is represented by the Dartford Tunnels (UK) converted from semi-transverse ventilation system to hybrid semi-transverse-longitudinal. In both the previous cases the existing ventilation systems

have been updated with the introduction of jet fans for enhancing longitudinal smoke control.

In general hybrid ventilation systems are designed in order to provide high smoke control capabilities both in bi-directional and uni-directional traffic operation. In some cases they are operated in order to generate smoke-clear zones on both sides of fire site. The ventilation strategies used in hybrid ventilation systems are generally very complex requiring a careful analysis of all the variables involved including fire location, tunnel layout, boundary conditions at the portals and ventilation system settings.

1.4. Interaction between fire and ventilation system

The management of indoor ambient quality in underground structures both in ordinary operating and emergency conditions involves the use of the ventilation system.

Here it is stressed that a tunnel and the corresponding ventilation plant constitutes a single system. Its thermo-fluid-dynamic behaviour is affected by several internal and external factors, such as barometric pressure at the portals, tunnel slope, set-points of the ventilation system and traffic conditions [32]. Besides these, in emergency scenarios, fire dynamics, smoke movements, stratification and dilution, heat transfer with the tunnel linings are deeply coupled with the ventilation flows.

Mainly two aspects must be taken into account when considering the interaction between ventilation flows and fires: firstly, it controls the movements of smoke, stratification and dilution and secondly it supplies the fire with the oxidizer. A good understanding of the interaction between ventilation and a fire is therefore vital when developing a fire safety strategy.

1.4.1. Ventilation velocity and back-layering

The critical velocity is by definition the minimum longitudinal air flow required to prevent the occurrence of back-layering in tunnel fire scenarios. The back-layering phenomenon is the reverse smoke flow that can spread against the tunnel longitudinal ventilation if it is too low. An example of back-layering occurrence is depicted in Figure 7.

Figure 7: Photograph of a small scale tunnel fire during the occurrence of back-layering. The fire size in 15 kW. The tunnel has an arched cross section (width 274mm, height 244 mm). Adapted from [33].

The exact value of the critical velocity depends mainly on the buoyant plume characteristics including smoke temperature, smoke flow rate, fire source size as well as tunnel height and width. The simplest techniques to predict the critical velocity are based on semi-empirical equations obtained by Froude Number preservation combined with some experimental data.

The Froude Number is defined as

$$Fr = \frac{Inertia\ forces}{gravity\ forces} = \frac{U^2}{gD} \tag{1}$$

where g is the gravity, D and U are the characteristics length and velocity scales respectively. Equation (1) can be rearranged by using the density ratio of the smoke in order to include the effects of stratification. When rearranged in this for it is usually called Richardson number or modified Froude number:

$$Ri = \frac{gD}{v^2} \cdot \frac{\Delta\rho}{\rho} = \frac{1}{Fr} \cdot \frac{\Delta\rho}{\rho} \tag{2}$$

where ρ represents the density.

The first empirical relation based on Froude theory is due to Thomas (1958) [27] who argued that the characteristics of the flow are dependent on the ratio of buoyancy to inertial forces on the tunnel cross section. Thomas concluded that, when the ventilation

velocity is close to the critical value, the modified Froude number is close to 1 and therefore the back-layering does not occurs. Under this assumption, it can be written that

$$U_c \approx \frac{\Delta\rho}{\rho_0} gH \tag{3}$$

where, U_C is the critical velocity value, H represents the tunnel height and ρ_0 is the ambient temperature. After substituting an expression correlating the convective part of the fire heat release rate (HRR) and fire induced smoke characteristics (temperature, density and flow rate), a final correlation can be obtained

$$U_c = k\left(\frac{gQ(1-\lambda)H}{\rho_o T_o c_p A}\right)^{\frac{1}{3}} \tag{4}$$

where k is a proportionality constant, Q is the total HRR, T_o is the ambient temperature, c_p is the air specific heat, A is the tunnel cross section and λ is the radiative fraction of the HRR. On the basis of experiment conducted in short corridors, the proportionality constant was found to be equal to 0.8 [34].

A similar correlation has been developed by Kennedy and co-workers:

$$U_c = k_g K\left(\frac{gQ(1-\lambda)H}{\rho_o T c_p A}\right)^{\frac{1}{3}} \tag{5}$$

$$T_f = T_o + \frac{Q(1-\lambda)}{\rho_o U_c c_p A} \tag{6}$$

$$k_g = 1 + 0.037(\alpha)^{0.8} \tag{7}$$

where K is an dimensionless empirical constant equal to 0.61, α is the tunnel gradient and T_f is an average temperature of the fire effluents [35]. This correlation has been

built on the basis of small scale experiments conducted by Lee and co-workers in 1979 [36].

Thomas correlation is valid within a limited range of heat release rates where the 1/3 law well fits the experimental data. For higher heat release rates, the correlation fails because it is not able to represent the asymptotic behaviour of the critical velocity. Indeed, on the basis of small scale experiments, Oka and Atkinson pointed out that for high HRR the critical velocity reaches an asymptotic value which is independent from the HRR [28]. This behaviour is clearly presented in Figure 8 showing the correlation between dimensionless critical velocity and dimensionless heat release rate. Oka and Atkinson proposed a modified correlation whish is presented hereafter (equations from (8) to (11)):

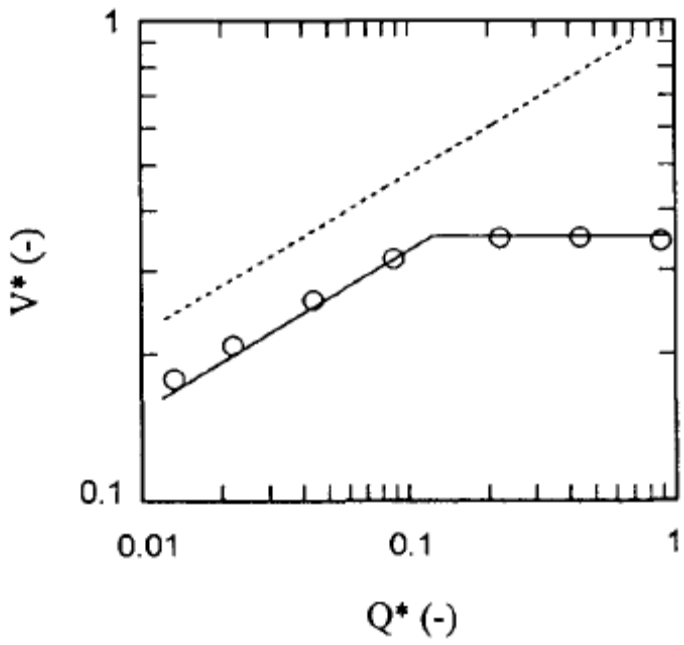

Figure 8: Variation of dimensionless critical velocity against dimensionless heat release rate. (O) measurements of critical velocity; (continuous line) equations (8) and (9): (dashed line) Thomas correlation (4). (from [28]).

$$U_c^* = K_v \left(\frac{Q^*}{0.12} \right)^{\frac{1}{3}} \quad for \quad Q^* < \quad 0.12 \tag{8}$$

$$U_c^* = K_v \qquad for \quad Q^* > \quad 0.12 \tag{9}$$

where Q^* and U_c^* are the dimensionless heat release rate and dimensionless critical velocity that can be obtained by using equation (10) and equation (11). The proportionality constant K_v ranges between 0.22 and 0.38 depending on the burner geometry.

$$Q^* = \frac{Q}{\rho_o T_o c_p g^{1/2} H^{5/2}} \tag{10}$$

$$U_c^* = \frac{U_c}{\sqrt{gH}} \tag{11}$$

Such asymptotic behaviour has been also observed in full scale experimental campaigns such as Memorial tunnel fire ventilation test program (MTFVTP) [11] or EUREKA [12]. A theoretical explanation has been given by Wu and Bakar [33] attributing such behaviour to the positioning of the intermittent flames in the tunnel cross section. Indeed, free fire plumes are characterized by three different regimes [6]

1. persistent flame region, located close to the fire source and characterized by an accelerating flow of combustion gases
2. Intermittent flame region, characterized by intermittent flaming and a near-constant flow velocity
3. The buoyant plume characterized by a decreasing velocity and temperature with the height.

For relative small fires having flame length smaller that the tunnel height, only the buoyant smoke impinges the ceiling and in under-ventilated conditions, it will generate back-layering. Obviously the characteristics of the buoyant plume will be depending on the fire HRR. However, for large enough fires, the intermittent flames will impinge the ceiling occupying the upper portion of the tunnel cross section and in under-ventilated conditions they will be present in the back-layering. Intermittent flame are characterized by constant speed regardless the fire source and therefore, they build up a buoyancy force with is not sensitive to the fire HRR. Consequently the critical velocity will tend

to its asymptotic values. A similar explanation has been given also by Hwang and Edwards [37].

However, it must be stressed that simplified analysis based on Froude scaling theory cannot take into account the effect of the tunnel geometry (i.e. tunnel width) and tunnel slope on the critical velocity. Based on the classical Thomas theory it is easy to obtain a linear correlation between the critical velocity and the quantity $(1/W)^{1/3}$ where W represents the tunnel width. Indeed, small scale experiments have confirmed that for aspect ratios greater than 1 (width W to height H) the critical velocity decreases with the tunnel width but following a trend different from the $(1/W)^{1/3}$ law proposed by Thomas. Furthermore, it appears that for aspect ratios smaller than 1 the critical velocity increases with the tunnel width [30]. Analogous deviations from the classical theory have been encountered when introducing blockages upstream the fire source or when varying the fire source geometry; in particular the critical velocity appears reducing when wider fire sources are adopted [28].

The effect of the tunnel slope on the critical velocity has been investigated by Atkinson and Wu [38] and by Ko and co-workers [39] on the basis of small scale experiments involving a propane gas burner for the former and methanol, acetone and n-heptane pool fires for the latter. In both the cases the results showed that the critical velocity increases with the tunnel slope due to the enhanced stack effect following equation (12)

$$U_{C,\vartheta} = U_{C,0}\left(1 + K_\theta \cdot \vartheta\right) \tag{12}$$

where $U_{C,\theta}$ and $U_{C,0}$ are the critical velocities in a inclined and horizontal tunnel, ϑ the tunnel slope, K_θ an empirical constant ranging between 0.014 and 0.033 in accordance with [38] and [39], respectively.

On the basis of the previous theoretical considerations supported by experimental measurements, it can be claimed that the maximum critical velocity value to be expected in any tunnel fire scenario is between 2.5 m/s and 3 m/s. If the ventilation velocity is in this range (or eventually larger) the back-layering is usually avoided and

the smoke are pushed downstream of the fire region. Smoke stratification is usually compromised.

For ventilation velocities between 1 m/s and 2.5÷3 m/s, depending on the fire source size, back-layering can occur. The back-layering distance usually varies between zero and 17 times the tunnel hydraulic diameter [5]. For even lower ventilation velocities (between 0 m/s and 1 m/s) the back-layering distance can be very large (several hundred meters) and it is almost uniform in both directions.

Ingason proposed an approximated correlation to predict back-layering distance based on small scale experiments [5] and Froude scaling theory.

$$\frac{L_b}{H} \propto \left(\frac{gQ}{\rho_o c_p T_o U^3 H} \right)^{1/3} \tag{13}$$

Equation (13) correlates the back-layering distance L_b to the tunnel geometry, the ventilation velocity U and the fire HRR Q. The proportionality constant, deduced from small scale experiments, ranges between 0.6 and 2.2. Given the lack of large scale tests, great care must be adopted when predicting the back-layering distance on the basis of equation (13). Indeed, in a recent work, it appears that equation (13) seriously under-predicts the back-layering distance (up to 1 order of magnitude) [40]. This conclusion has been drawn on the basis of a recent large scale set of experiments in a 1 km long tunnel (W ~ 10 m, H ~ 7 m, slope ~ 2%) involving fires between 1.8 MW and 3.2 MW.

1.4.1.1. Ventilation velocity and fire HRR

Ventilation flows have a direct impact on the tunnel fire dynamics. By using a probabilistic approach, Carvel and co-workers demonstrated that the HRR of a HGV could increase in size by a factor 4 when the ventilation velocity is around 3 m/s and by a factor 10 when the ventilation is up to 10 m/s [41]. The authors found that a similar behaviour could be expected for the fire growth rate asserting that it can increase by a factor of 5 at 3 m/s and by a factor of 10 at 10 m/s.

Such behaviour is mainly dependent on the enhanced heat transfer from tilted flames and on the improved transport of oxygen into the fuel bed. However, it can be expected that for ventilation flows higher that a certain limit, the cooling effect due to the ventilation flows counteracts against the improved radiative heat transfer from the flames; in this conditions peak HRR and fire growth rate can be reduced.

The enhancing effects of the ventilation flows on the fire peak HRR and growth rate have been observed experimentally both on large and small scale tests. In particular this behaviour has been recorded during the Second Benelux Tunnel fire tests for canvas covered trucks loaded with wooden cribs and tyres. The fire growth rate with ventilation velocity ranging between 4 m/s ÷ 6 m/s was almost 2 times higher when compared to the fire development in no-ventilation scenarios. The peak HRR was about 1.5 times higher [13]. A similar behaviour has been observed on small scale experiments and described by Lonnemark and co-workers [16]. The increase in the peak HRR ranged between 1.3÷1.7 and 1.8÷2 times for high and low porosity wood cribs respectively. They also found that the fire growth rate increased by a factor 5 to 10 depending on the tunnel cross section. Beyond a certain velocity limit the HRR and the fire growth rate did not seem to vary significantly.

A more recent literature review presented by Carvel addressed other significant aspect of the fire dynamics in tunnel [17]. The work reviewed a large number of tunnel fire experiments including the Second Benelux Tunnel fire tests [13], the Runehamar fire tests [8], and the EUREKA fire test program [12] and performed regular observations on the effect of the ventilation velocity on the fire growth phase.

The author observed that the typical t^2 fire representation [6] was not fitting any of the experimental data and proposed a two-step linear approximation. During the first step the fire would grow slowly up to 1÷2 MW, while during the second step, the growth rate would be significantly higher (up to 15 MW/min). Figure 9 shows a two steps approximation of the fire growth phase as observed in [8] and [13].

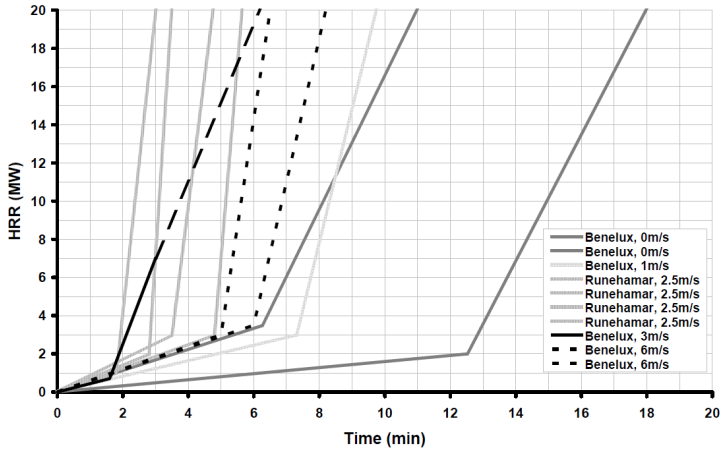

Figure 9: Two step approximation of fire growth rate phase for the Second Benelux tunnel fire Tests and Runehamar Fire Test Program (from [17])

The changing in the fire regimes usually takes place after a *delay phase* usually as long as few minutes (from 2 to 6). The author observed also that the delay phase length and the fire growth rate are somehow correlated to the ventilation flows experienced by the fire during its development. A table resuming the observed trends is introduced hereafter.

Ventilation rate	Delay phase	Growth rate
Low (less than 1ms^{-1})	6 minutes or longer	About 5 MW/min
Medium (about 3ms^{-1})	5 minutes or less	15 MW/min or more
High (about 6ms^{-1})	5 or 6 minutes	About 10 MW/min

Table 6: Summary of the observed correlation between ventilation rate, delay phase length and fire growth rate (from [17]).

1.5. Analysis of tunnel ventilation systems and fires

On the basis of the previous discussions it is easy to understand that fire behaviour, smoke dynamics and ventilation flows are deeply coupled and they cannot be studied separately. In other words, the resulting air flow within a tunnel is dependent on the combination of fire-induced flows, active ventilation devices (jet fans, axial fans), tunnel layout, atmospheric conditions at the portals and the presence of vehicles. Although an overall analysis of tunnel ventilation flows and fires can be very complex, the resulting information is crucial for tunnel fire safety purposes. Studies of tunnel ventilation flows and fires are indeed fundamental to assess the capabilities of a

ventilation system to manage smoke, to design ventilation and evacuation strategies, to predict loss of tenability in the environment and to minimize damages to the structure.

Depending on the accuracy required and the resources available, a solution to the problem can be reached using different ways.

1.5.1. Small and large scale experiments

Full scale tests, generally conducted within unused tunnels, require very large financial investments but provide large amounts of collected data. Some examples have already been cited. The Memorial Tunnel fire ventilation test program [11], the EUREKA fire test program [12] and the Second Benelux Tunnel fire test program [13] are only few examples. A wide review of the experimental tunnel fires conducted in the last 4 decades is available in [42]. Because of the huge costs associated, only a limited number of tests can be carried out. Furthermore they are highly specific and their outcome is strictly related to the specific tunnel layout, fire load material and geometry. Design procedures sometimes use small scale tunnel models in order to represent ventilation and fire scenarios. Interpretation of their results is dependent on the relevant scaling laws and model scale results may not have a general validity in relation to the full scale case. Nevertheless, experimental data are widely used to extrapolate proportionality constant used in semi-empirical correlation to predict back-layering occurrence and distance, smoke production and smoke front velocity and temperature.

1.5.2. Numerical modelling

The analysis of tunnel ventilation systems can be also conducted using numerical models based on a mathematical representation of the physical phenomena involved. Numerical models are usually highly flexible, significantly more economic than experimental test, and allow for large parametrical studies and sensitivity analysis. The accuracy of numerical models must be always addressed on the basis of a direct comparison of the results to experimental findings in order to assess range of applicability and limitations.

Several numerical approaches have been adopted by the international community to address tunnel fire safety issues.

The overall behaviour of the ventilation system can be approximated using 1D fluid dynamics models under the assumptions that all the fluid-dynamic quantities are uniform in each tunnel cross section and gradients are only present in the longitudinal direction. 1D models have low computational requirements and are specially attractive for parametric studies where a large number of simulations have to be conducted. In the last two decades several contributions on the application of 1D models to tunnel ventilation flows and fires flows have been published; a literature review as well as a wide description of their accuracy and range of applicability will be presented in chapter 2.

Zone models are based on the experimental evidence that, under certain conditions, fire effluents tend to stratify generating a cold air layer underneath and a hot smoke layer containing the fire effluents [43]. Zone models have been widely used to simulate compartment fires but their applicability in tunnel fire scenarios is limited. Indeed, they are not able to simulate tunnel smoke dynamics due to the lack of a dedicated horizontal momentum equation needed to represent the longitudinal smoke transport in a tunnel environment. Furthermore, they are not able to take into account mixing between hot and cold layers or to simulate fire scenarios where smoke stratification is lost (i.e. critical or supercritical ventilation scenarios).

Modified version of zone models have been developed trying to extend their use to tunnel fire scenarios. Charters and co-workers developed a modified version of zone models having a three layer domain: a hot smoke layer, a mixing layer and a cold air layer underneath [44]. As for any zone model, the accuracy of the new one mainly relies on calibration constants needed to predict the mixing between layers, hot layer velocity and plume entrainment. A similar approach has been followed by Kunst who developed a zone model and used it to predict back-layering [29]. Kunst model is in qualitative agreement with former, widely used models and it has been validated by comparison with mostly large-scale experiments in instrumented galleries. A more recent application has been presented by Suzuki and co-workers [45]. The model uses several horizontal layers and provides reasonably accurate temperature distributions when compared to small scale fire scenarios. However also in this case, the accuracy of the

model relies on calibration constants needed to predict plume entrainment and further validations test must be conducted.

CFD techniques are usually adopted in fire safety science when flow field data are needed. Such techniques are able to provide detailed temperature and velocity fields, smoke movement and stratification, toxic species evolution, heat fluxes mapping, time to untenability conditions and other important variables. The computational cost of this class of methods is high even for medium size tunnels and they are typically used for design verification. A literature review as well as a wide description of their accuracy and range of applicability will be presented in chapter 3.

Another class of methods, called multiscale methods, adopt different levels of complexity in the numerical representation of the system. The multi-scale concept is an extension of the conventional 1D and CFD modelling techniques where the two models are coupled together with the latter providing the boundary condition to the former and vice-versa. The multi-scale model is solved on a hybrid computational grid, where 1-dimensional elements are linked to 3-dimensional ones generating a continuous domain in the streamwise direction (see Figure 10). The 3D elements are modelled by means of a CFD tool while 1D elements by using a conventional 1D model. During the solution procedure 1D and CFD models dynamically exchange information at the 1D-3D interfaces and thus run in parallel. A literature review as well as a wide description multiscale modelling technique for tunnel ventilation flows and fires will be presented in chapters from 4 to 7.

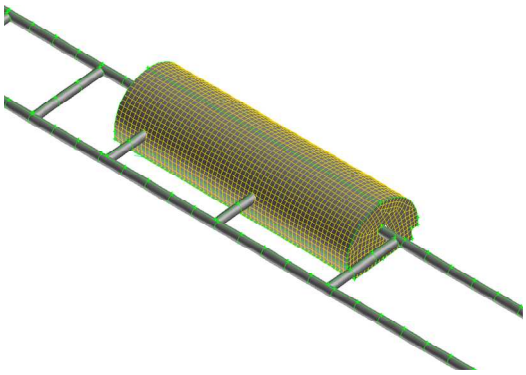

Figure 10: A schematic of a hybrid computational grid for multiscale calculation of tunnel ventilation flows and fires

1.6. Test cases

This thesis contains in different chapters several applications of 1D models, CFD models and multiscale models. In most of the cases the developed models have been applied to predict the behaviour of real operative road tunnels. In some cases, experimental campaigns have been undertaken to characterize the behaviour of tunnel and ventilation system. The collected data have been used to validate the developed models and to assess their accuracy.

1.6.1. Case A: Frejus Tunnel, Bardonecchia (It)

In Chapter 2, the Frejus tunnel behaviour is simulated with a 1D model. This tunnel is a two-way link between Italy and France with a total length of 12870 m and an approximated hydraulic diameter of 6 m. The ventilation system is fully transverse and it is operated by means of full length supply and exhaust duct located over the tunnel ceiling. Ordinary ventilation is operated by introducing fresh air along the tunnel through 3 U-shaped fresh air ducts which have 2 fans at each end. Fresh air openings are installed each 5 m. Emergency ventilation is operated using the fresh air ducts and 3 U-shaped extraction ducts. The extraction dumpers are installed each about 130 m. A more detailed description of the Frejus tunnel including typical emergency ventilation strategies will be given in chapter 2. Experimental data will be used to validate the developed 1D model when simulating the tunnel ventilation system behaviour.

1.6.2. Case B: Norfolk road Tunnels, Sydney (Au)

In Chapter 3 the Norfolk road tunnels ventilation systems are simulated by using a CFD tool. These are two two-lanes unidirectional road tunnels located in Sydney (AU). The tunnels are 460 m long with a virtually flat gradient. Each tunnel, longitudinally ventilated, is equipped with 6 pairs of jet fans. A large set of air velocity measurements in the tunnel central section were made available by the tunnel operator and they have been used to validate the capability of CFD tools to model tunnel ventilation flows at ambient conditions.

1.6.3. Case C: Wu-Bakar small scale tunnel

In Chapter 3 a CFD tool has been also used to simulate small-scale fire scenarios. Experimental data have been provided by Wu and Bakar [33] that carried out a series of small scale experiments on five horizontal tunnels with different cross-sections. They assessed, on the basis of accurate measurements in a controlled environment, the effect on the critical velocity of tunnel cross section and fire heat release rate. Among the different cross sections, the data relative to the square cross-sectional tunnel (0.25×0.25 m^2 cross section) will be considered in this document. The small scale tunnel is around 15 m long and it is equipped with a circular porous bed propane burner (diameter equal to 0.106 m) located at a distance of 6.21 m from the tunnel inlet. The tunnel outlet is located at a distance of 8.7 m from the burner centre. The burner heat release rate, controlled by the propane flow rate, was varied during the tests ranging between 1.5 kW and 30 kW. The measured values of critical velocities in two different fire scenarios (3 kW and 30 kW) will be used in the next sections to validate the fire CFD model.

1.6.4. Case D: Dartford Tunnels, London (UK)

In chapter 5 the multiscale model has been used to simulate the ventilation flows in the Dartford tunnels. They are two twin-lane, uni-directional road tunnels under the River Thames, crossing from Dartford at the south (Kent) side of the river to Thurrock at the north (Essex) side, about 15 miles east of London in the UK. Both tunnels have complex ventilation system consisting of a semi-transverse system together with additional jet fans to control the longitudinal flow. Both the Dartford tunnels have two shafts with axial extraction fans located at relatively short distance from each of the tunnel portals. They length is around 1.5 km while the approximate internal diameter is 8.6 m and 9.5 for the West and the East tunnels, respectively. A more detailed description of the Dartford tunnel including typical emergency ventilation strategies will be given in chapter 5. A large set of experimental data measured in the both the tunnels will be used to corroborate the developed multiscale model.

1.6.5. Case E: Test case tunnel

A different test case has been used in chapters 6 and 7 to discuss the multiscale model formulation when dealing with tunnel fire scenarios both in steady state and time-

dependent conditions. The tunnel is 1.2 km long with a standard horseshoe cross section. The ventilation is longitudinal and uses 10 pairs of 50 m spaced jet fans. The jet fans are arranged in two groups, each group installed near each portal. A more detailed description of the geometry and typical emergency ventilation strategies will be given in chapters 6 and 7.

2
One-dimensional modelling

2.1. Introduction

The main advantage of using 1D models for the analysis of complex network systems, (i.e. the tunnel main gallery and ventilation ducts), is that it allows for a complete and compact description of the system. This characteristic has two major consequences: 1) it is possible to define with adequate precision the boundary conditions, such as the ambient conditions at the portals, and 2) it is suitable for applications requiring the computation of a large number of scenarios, such as during the assessment of safety strategies for complex tunnels.

Its intrinsic limit is instead due to the fact that the flow in each cross section is assumed homogeneous; it is then identified by a unique value of the variables pressure, velocity, temperature, smoke concentration, etc. This peculiar assumption makes 1D models unsuitable to simulate the fluid behaviour in regions characterized by high temperature or velocity gradients. Regions characterized by high temperature gradients are typically

encountered close to the fire where well-defined smoke stratification is found. In the case of small fires, smoke stratification is important along large section of the tunnel and determines a peculiar propagation of the smoke front. In fact it proceeds with larger velocity than if it were to occupy the entire cross section. Thus, if 1D models are applied to fire events (particularly in the case of small fires where the smoke is stratified), it is necessary to properly introduce corrections to account for non-homogeneity caused by the stratification, otherwise the calculated propagation velocity of the smoke front would be significantly underpredicted [46]. Once the smoke away from the fire has occupied the entire, or nearly entire, tunnel cross section, the conditions are close to homogenous and the prediction of the propagation velocity is accurate.

Regions with high velocity gradients are also typically encountered close to ventilation devices (i.e. jet fans) where the fan thrust produces highly 3D (tri-dimensional) flows and the flow homogeneity assumption of 1D model fails. Usually, 1D models describe the behaviour of such regions on the basis of empirical correlations that must be calibrated on the specific tunnel layout. Indeed, the jet fan thrust curve provided by the manufacturer only applies to the isolated jet fans and it does not describe its behaviour once installed in a particular tunnel gallery.

2.2. Literature overview

The first reported codes for digital calculation of a fluid networks were produced in the late 50s. They were mainly developed to design mine ventilation systems and, in the late 60s, they became a fundamental part of any ventilation planning [47]. In spite of the fact that an increasing number of attempts were made during the early years to adapt such network calculation codes for the simulation of fire scenarios, none of them progressed enough. A first significant attempt of including the effect of fire in network system calculation has been made in the late 70s when Greuer and co-workers produced a tool able to perform steady state calculation of networked system providing temperature velocity and pollutant distributions [47]. The resulting code was able to perform steady state simulations of complex networked system computing the solution by using a hardy-cross-like method [48]. The numerical method adopted was based on the solution of longitudinal momentum equations on closed airway loops whose

definition was not straightforward as erroneous loop definition could lead to slow convergence.

In the last two decades, several national Institutions proposed contributions to the subject. Models such as MFIRE [49], ROADTUN [50,51], RABIT and SPRINT [52] and [53], Express'AIR and SES [54] and [55] are now commonly used to perform complete studies of tunnel ventilation systems and fires.

MFIRE, developed by the US Bureau of Mines is able to perform steady state fluid-dynamic simulations of underground network system. The model has been tested by Cheng et al. [56] on experimental data from a small scale underground transportation network constituted of 27 branches about 0.1 m diameter and 1-2 m length, and then applied to simulate a hypothetical fire outbreak in the Taipei Mass Rapid Transit System. The simulations were designed to investigate the direction and rate of air flows, temperature distribution and emergency ventilation responses. The same theoretical approach has been used by Ferro et al. [57-58] and Jacques [59]. The former presented a 1D computer model for tunnel ventilation. The model was designed to deal with complex tunnel network including phenomena like the piston effect from moving vehicles and the distribution of pollutant concentration in the tunnel domain. The model was able to perform steady state calculations. Similar approach has been used in [59] where numerical simulations of urban tunnel 2.5 km in length have been presented.

The Subway Environmental Simulation code (SES), developed by Parson Brinckerhoff Inc.[61], is a 1D simulation tool able to predict steady state ventilations scenarios in tunnel networks. The tool includes a simplified model to predict the occurrence of back-layering as function of the fire size and ventilation conditions (see equations 5 to 7). The model, based on Froude scaling analysis, has been calibrated on small scale experiments. The experiments were conducted in a 10 m long tunnel with a 0.09 m^2 cross section with the fire source represented by the tunnel wood lining [36]. No information on the fire HRR was made available.

A more recent application is represented by the code SPRINT [53]. It is able to perform time dependent analysis of fire scenarios in tunnel ad to handle gravity-driven smoke propagation due to thermal stratification. The latter effect is accounted by superposition

of the mean flow velocity, and the front velocity is estimated on the basis of semi-empirical correlation. The model validated against experimental data recorded during Memorial Tunnel Fire Ventilation Test Program [11] and in the Mont Blanc Tunnel, has been applied to simulate real tunnel fire scenarios.

In a recent application, a 1D model has been used in an optimization procedure used to determine the aerodynamic coefficient in a highway tunnels 1.8 km in length [62]. The optimization, performed on the basis of detailed experimental measurements, is able to provide the pressure rise coefficients of the jet fans, the wall friction coefficient and the averaged drag coefficients of small-sized and large-size vehicles.

2.3. Typical mathematical formulation for 1D models

The vast majority of the 1D models for tunnel applications found in the literature are based on a generalized Bernoulli formulation [63]. Most of them are designed to account for buoyancy effects, transient fluid-dynamic and thermal phenomena, piston effect and transport of pollutant species. They are usually developed to handle complex layouts typical of modern tunnel ventilation system (especially true for transverse ventilated tunnel) on the basis of a topological representation of the tunnel network.

2.3.1. Topological representation

The topological structure of complex flow distribution systems, as pipelines, tunnels, mines, etc, is easily described using matrix representation and graph theory (see as example [64]). This representation lays on two concepts: node and branch. A node is a section where state properties as temperatures, pressures, mass or molar fractions, etc. are defined. A unique value of these properties is defined in a node. A branch is an element bounded by two nodes and characterized by geometrical properties as length and cross section, together with flow and thermal properties, as roughness, wall temperature, etc. Branches are associated to mass flow rates and velocities. A conventional flow direction is also selected for each branch, so that inlet and outlet nodes are defined. Resulting negative flows refer to flows directed from the outlet towards the inlet.

The flow network is described through the interconnections between nodes and branches (multiple branches can join in the same node), with the former playing the role of flow splitter and/or junction. In graph theory, *incidence matrix A* is used to express the interconnections. This matrix is characterized by a number of rows equal to the total number of nodes and a number of columns equal to the number of branches (in some analyses, the incidence matrix is defined as the transpose of that presented here). The general element A_{ij} is 1 if the *i-th* node is the inlet node of *j-th* branch, it is -1 if the *i-th* node is the outlet node of the *j-th* branch and it is 0 in the other cases. A typical layout of a tunnel network system is presented in Figure 11.

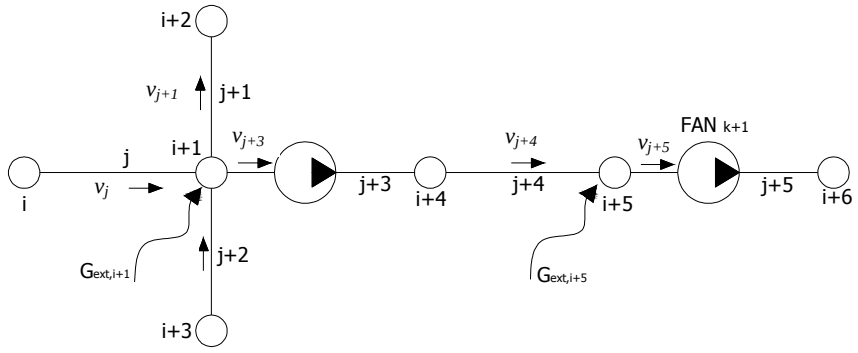

Figure 11: Example of the network representation of a tunnel showing branches between nodes

The corresponding *incidence matrix A* is presented below:

$$A = \begin{array}{c|cccccc} & j & j+1 & j+2 & j+3 & j+4 & j+5 \\ \hline i & +1 & 0 & 0 & 0 & 0 & 0 \\ i+1 & -1 & +1 & -1 & +1 & 0 & 0 \\ i+2 & 0 & -1 & 0 & 0 & 0 & 0 \\ i+3 & 0 & 0 & +1 & 0 & 0 & 0 \\ i+4 & 0 & 0 & 0 & -1 & +1 & 0 \\ i+5 & 0 & 0 & 0 & 0 & -1 & +1 \\ i+6 & 0 & 0 & 0 & 0 & 0 & -1 \end{array} \qquad (14)$$

2.3.2. Fluid dynamics model

Modelling flow system requires that continuity and momentum equations are written with spatial dependence on one single coordinate, which, in the case of tunnels, is the longitudinal coordinate, *x*. The starting points are the Navier-Stokes equations, as

described in their classical form for a time dependent three dimensional fluid flow [66] and [65],

$$\begin{aligned} &a) \quad \frac{\partial \rho}{\partial t} + \nabla \cdot \rho\, \mathbf{u} = 0 \\ &b) \quad \frac{\partial \rho \mathbf{u}}{\partial t} + \nabla \cdot (\rho \mathbf{u}\mathbf{u}) = -\nabla p + \nabla \cdot \boldsymbol{\tau} + \sum \mathbf{S} \end{aligned} \tag{15}$$

where **u** is the velocity vector, *t* the temporal coordinate, *p* the static pressure, ρ the fluid density, $\boldsymbol{\tau}$ is the stress tensor, **S** a vector containing momentum source terms per unit volume (including the gravity term). Equation (15).a, known as continuity equation, states that the rate of flow into a volume must be equal to the rate of change of mass within the volume. Equation (15).b, known as momentum equation, states that the rate of change in the fluid momentum is equal to the sum of forces acting on it.

After eliminating the *y* and *z* spatial dependences, and neglecting the viscous stress term which loses its significance in a 1D formulation, the equations become

$$\begin{aligned} &a) \quad \frac{\partial \rho}{\partial t} + \frac{\partial \rho u}{\partial x} = 0 \\ &b) \quad \rho \frac{\partial u}{\partial t} + \rho u \frac{\partial u}{\partial x} = -\frac{\partial p}{\partial x} + \sum S_{Mx} \end{aligned} \tag{16}$$

where *u* is the longitudinal velocity and S_{Mx} is the longitudinal momentum source term. The momentum source term contains all the terms related to the chimney effect, wall friction, losses due to flow separation at the portals or after obstacles. Eventually, pressure rise due to fan operation and piston effect are also accounted for. Equation 16.b, after integration along a branch *j* (which is also a streamline) from node *i-1* to node *i*, leads to the generalized Bernoulli formulation for transient flows (see equation (17)). The buoyancy term has been also included.

$$\int_{i-1}^{i}\frac{\partial(u)}{\partial t}dx+\left(\frac{u_i^{\,2}-u_{i-1}^{\,2}}{2}\right)+\int_{i-1}^{i}\frac{dp}{\rho}+g(z_i-z_{i-1})=\int_{i-1}^{i}\frac{1}{\rho}\sum S_{Mx}dx \qquad (17)$$

where z represents the vertical elevation and g the gravity acceleration. After defining the total pressure P as sum of the kinetic, pressure and gravity terms, and after making explicit all the sources of momentum, equation (17) can be expressed as

$$\rho_j\frac{d(u_j)}{dt}L_j+(P_i-P_{i-1})+\Delta P_{FAN,j}+\Delta P_{PIST,j}-\Delta P_{FRICT,j}=0 \qquad (18)$$

where ρ_j represents the average density in the branch j between nodes i and i-1, u_j the average velocity in the branch j, and $\Delta P_{FAN,j}$ $\Delta P_{PIST,j}$ and $\Delta P_{FRICT,j}$ the source of momentum due to the fan action, the piston effect and the friction.

Equations (18) can be solved only after discretizing the computational domain in branches interconnected by nodes. Such discretization generates control volumes allowing the integration of the momentum and continuity equations. In this model a staggered arrangement is used where pressure and densities are defined in nodes while the velocities are defined in the branches. An overview on the numerical solution of the problem will be given in the next sections.

2.3.3. Thermal model

In this section the features of the thermal problem are described. In the case of thermal analysis, the problem is complicated by the temperature definition in the nodes. Whereas pressures in nodes are univocally defined, temperatures are not. In the case of a flow junction, two flows at different temperature can converge in the same node and the total mass flow rate exits at the average temperature.

The thermal analysis requires the solution of the energy equation. The general formulation, valid for constant pressure, constant heat capacity and low Mach number flows, is presented hereafter

$$\rho c \frac{\partial T}{\partial t} + \rho c \mathbf{u} \nabla T = \nabla \cdot (k \nabla T) + \sum S_E \tag{19}$$

where T represents the fluid temperature, c the fluid heat capacity, k the fluid conductivity, **u** the fluid velocity components, and S_E the energy source terms/sink per unit volume. Equation (19) must be simplified eliminating the spatial dependencies with the exception of the x-coordinate. Furthermore, the summation of the source/sink terms is split in two terms: the first one accounting for the heat generation due to fire (q_v) and the second one accounting for the heat losses through walls (q_l).

$$\rho \cdot c \cdot \frac{\partial T}{\partial t} + \rho \cdot c \cdot u \cdot \frac{\partial T}{\partial x} = k \cdot \frac{\partial^2 T}{\partial x^2} - q_l + q_v \tag{20}$$

The definition of q_v, which is particularly important in the case of fire, will be discussed in the next sections. In general the term, representing the heat conduction along the longitudinal coordinate can be neglected if compared to the other terms of equation (20).

In order to resolve the energy equation, a finite volume formulation has been used. More details on discretization techniques and numerical schemes will be given in the next section.

2.3.4. Steady state problem

The solution of the steady state problem requires the integration of the differential equations (18) and (20) over specific control volumes. Obviously, in this case the time derivatives must be neglected. The tunnel domain is first discretized in branches and nodes indicated as *i* and *j* in Figure 12. The variables are allocated in a staggered arrangement. In particular, pressures, temperatures are calculated in each node while velocities in each branch. Therefore, continuity, momentum and energy equations are applied on different control volumes. In particular, a control volume included between two nodes (red dashed volume in Figure 12) is used for the momentum equations. A node centered control volume (blue dashed volume in Figure 12) is used for the integration of continuity and energy equations.

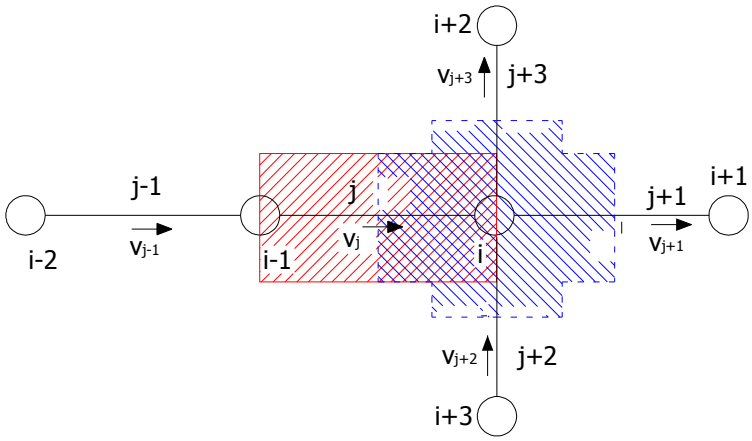

Figure 12: Schematic of the control volumes adopted for the numerical solution

Once defined the control volumes, the integration of continuity equations leads to equation 21.a. The momentum equation, which has been integrated along a streamline, is already in its final form.

$$\begin{aligned} &a) \quad \int_{CV} \frac{d\rho u}{dx} dV = 0 \\ &b) \quad (P_i - P_{i-1}) + \Delta P_{FAN,j} + \Delta P_{PIST,j} - \Delta P_{FRICT,j} = 0 \end{aligned} \tag{21}$$

The control volume integrals are rewritten as integrals over the entire bounding surface by using Gauss's divergence theorem leading to equations (22).

$$\begin{aligned} &a) \quad \int_{A} \mathbf{n} \cdot (\rho u) dA = 0 \\ &b) \quad (P_i - P_{i-1}) + \Delta P_{FAN,j} + \Delta P_{PIST,j} - \Delta P_{FRICT,j} = 0 \end{aligned} \tag{22}$$

The above equations integrated over the control volume surface lead to the following general algebraic continuity and momentum equations for a generic node *i* and a branch *j* respectively.

$$\begin{aligned} &a) \quad \sum_j \rho_j u_j A_j = 0 \\ &b) \quad \left(P_i - P_{i-1}\right) + \Delta P_{FAN,j} + \Delta P_{PIST,j} - \Delta P_{FRICT,j} = 0 \end{aligned} \tag{23}$$

Equation (23).a states that sum of the mass flow rates entering a generic node of the network must be equal to the sum of the mass flow rate exiting the node. In particular A_j is the cross section of the generic interconnected branch *j*. Equation (23).b states the total pressure difference across a generic branch *j* (delimited by the nodes *i* and *i-1*) is due to the sum of all the contributions due wall friction, losses due to flow separation at the portals and after obstacles, pressure rise due to fan operation and piston effect. Making explicit all the terms, equation (23).b becomes

$$P_i - P_{i-1} - \frac{1}{2}\left(f_j \frac{L_j}{D_{h,j}} + \sum \beta_j \right) \rho_j u_j^2 + \Delta P_{FAN,j} + \Delta P_{PIST,j} = 0 \tag{24}$$

where *f* the branch friction coefficient, β the minor loss coefficient, *L* the branch length, D_h the branch hydraulic diameter, while ΔP_{FAN} and ΔP_{PIST} represent the pressure gain inside the branch due to fans and piston effect respectively.

The pressure rise due to fans is commonly represented as generic polynomial of the second order known as fan characteristic curve (see equations (25)). The characteristics curve coefficients are *a*, *b*, and *c*. They are usually obtained from empirical correlations and they are specific for each tunnel layout.

$$\begin{aligned} &a) \quad \Delta P_{FAN,j} = a + b u_j + c u_j^2 \\ &b) \quad \Delta P_{FAN,j} = n_j \rho_j \frac{A_F}{A_j} K_j u_f \left(u_f - u_j\right) \\ &c) \quad \Delta P_{FAN,j} = \eta_j \frac{P_e}{A_j u_j} \end{aligned} \tag{25}$$

Alternatively, in some works, the pressure rise due to fans can be represented as described in equations (25).b and (25).c. In the last two cases, n, A_F, u_f and K respectively represent the number of operating fans, the fan discharging area, the fan discharging velocity and the pressure rise coefficient while, η, P_e are the fan efficiency and the fan electric power.

Commonly the piston effect term can be evaluated following the expression proposed by PIARC which includes the characteristics of the vehicles and the air velocity in the tunnel [67].

$$\Delta P_{PIST,j} = \varepsilon \frac{A_v}{A_j} \frac{\rho_j}{2} \left[N_1 \left(u_1 - u_j \right)^2 - N_2 \left(u_2 + u_j \right)^2 \right] \tag{26}$$

where ε is the aerodynamic factor of the vehicles (multiple terms should be considered for each kind of vehicles), A_v is the vehicle cross section, N_1 and N_2 the number of vehicles moving in the same direction and in the opposite direction of the branch j. The vehicle velocities are respectively u_1 and u_2.

The integration over the control volumes of the energy equation (20) leads to the expression (27) that can be rearranged to generate a generic algebraic equation for a node i (see equation (28)) .

$$\int_A \rho \cdot c \cdot u \cdot T \, dA = \int_A k \frac{dT}{dx} dA - \int_{CV} q_l dV + \int_{CV} q_v dV \tag{27}$$

$$\sum_j \rho_j \cdot c_j \cdot u_j \cdot A_j \cdot T_j = \sum_j k_j \left. \frac{dT}{dx} \right|_j A_j - Q_{L,i} + Q_i \tag{28}$$

The diffusive term at the RHS of equation (28) is usually neglected for these systems as the advective term is by far dominating the heat transfer in tunnels. The terms Q_L and Q represent the total heat losses and the heat generated (i.e. due to the fire) in a generic node i.

The term Q_L in this work is represented as

$$Q_{L,i} = \sum_j \frac{L_j}{2} \cdot \Omega_j U_j \left(T_i - T_{\infty,j}\right) \tag{29}$$

where Ω is the branch perimeter, L its length, U the global heat transfer coefficient and T_∞ is a fixed know temperature (i.e. the rock temperature in a tunnel bore). The global heat transfer coefficient can be computed by using well know heat transfer correlations [68]:

$$U_j = \left(\frac{1}{h_j} + R_j \right) \tag{30}$$

$$h_j = \frac{1}{8} f_j \rho_j c_j u_j \tag{31}$$

where h is the convective heat transfer coefficient and R is the global thermal resistance of rock and tunnel lining. Equation (31) is based on the applicability of the Reynolds analogy (valid for Prandlt number equal to 1) to air (Prandtl number around 0.7).

More care is required when estimating the summation on the LHS of equation (28) since temperature values are not defined in branches but in nodes. Therefore, the estimation of the temperature at the boundary of the control volume has been performed by using a first order upwind scheme [66].

2.3.5. Time dependent problem

In time dependent problems, the time derivative of equations (18) and (20) must be retained. Furthermore the finite volume integration over the control volume must be augmented with a further integration over a finite time step Δt. This procedure leads to

$$a) \quad \int_t^{t+\Delta t} \left[\int_{CV} \frac{\partial \rho}{\partial t} dV \right] dt = \int_t^{t+\Delta t} \left[\int_A \rho u \, dA \right] dt \tag{32}$$

$$b)\quad \int_t^{t+\Delta t} \rho_j \frac{d\left(u_j\right)}{dt} L_j dt + \int_t^{t+\Delta t} \left(P_i - P_{i-1}\right) dt = \int_t^{t+\Delta t} \left[\Delta P_{FAN,j} + \Delta P_{PIST,j} - \Delta P_{FRICT,j}\right] dt$$

$$c)\quad \int_t^{t+\Delta t} \left[\int_{CV} \rho \cdot c \cdot \frac{\partial T}{\partial t} dV\right] dt + \int_t^{t+\Delta t} \left[\int_A \rho \cdot c \cdot u \cdot T\, dA\right] dt = \\ = \int_t^{t+\Delta t} \left[\int_A k \cdot \frac{\partial T}{\partial x} dA\right] dt - \int_t^{t+\Delta t} \left[\int_{CV} q_l dV\right] dt + \int_t^{t+\Delta t} \left[\int_{CV} q_v dV\right] dt$$

The terms at the LHS of equation (32), under the hypothesis that the variable under the time derivative (i.e. density, velocity and temperature) prevails over the whole control volumes, lead to

$$a)\quad \int_t^{t+\Delta t} \left[\int_{CV} \frac{\partial \rho}{\partial t} dV\right] dt = \left(\rho_i^t - \rho_i^{t-\Delta t}\right) \Delta V_i$$

$$b)\quad \int_t^{t+\Delta t} \left[\int_{CV} \rho \frac{\partial u}{\partial t} dV\right] dt = \rho_j \left(u_j^t - u_j^{t-\Delta t}\right) L_j \qquad (33)$$

$$c)\quad \int_t^{t+\Delta t} \left[\int_{CV} \rho \cdot c \cdot \frac{\partial T}{\partial t} dV\right] dt = \rho_i c_i \left(T_i^t - T_i^{t-\Delta t}\right) \Delta V_i$$

where ΔV_i and ΔV_j are the volumes of integration and L_j is the length of the branch. The evaluation of the rest of the terms contained in (32) requires an assumption on the time evolution of the quantities contained in the time integrals. In this work an implicit formulation has been adopted; this means that such quantities are the ones of the next time level. This approach is first order accurate but unconditionally stable for any time step size [70]. After performing the double integration and after some rearrangements, equations (33) can be rewritten in the final fashion

$$a)\quad \left(\sum_j \frac{A_j L_j}{2\Delta t}\right)\left(\rho_i^t - \rho_i^{t-\Delta t}\right) + \sum_j A_j \rho^t{}_j u^t{}_j = 0 \qquad (34)$$

$$b) \quad \rho_j L_j \frac{u_j^t - u_j^{t-\Delta t}}{\Delta t} + P_i^t - P_{i-1}^t - \frac{1}{2}\left(\left(f_j \frac{L_j}{D_{h,j}} + \beta_j\right)\rho_j u_j^2\right)^t + \Delta P_{FAN,j}^t + \Delta P_{PIST,j}^t = 0$$

$$c) \quad \rho_i c_i \frac{\left(T_i^t - T_i^{t-\Delta t}\right)}{\Delta t} + \sum_j \rho_j^t \cdot c_j^t \cdot u_j^t \cdot A_j \cdot T_j^t = -Q_{L,i}^t + Q_i^t$$

Also for the time dependent formulation, a first order upwind scheme has been adopted to treat the convective fluxes in equations (34)

2.3.6. Solving algorithm

In both steady state and transient approaches, the continuity and momentum equations can be solved by using an iterative solution strategy known as the SIMPLE algorithm [71]. The method, based on a 'guess and correct' procedure has been rearranged in order to improve its applicability for complex mono-dimensional networks. The procedure is presented hereafter for the unsteady formulation of the problem but can be directly applied for steady state problems. For sake of simplicity the number of nodes and branches in the network will be indicated as n_n and n_b respectively.

The whole set of continuity equations can be rearranged by using the incidence matrix A ($n_n \times n_b$) as follow

$$[A] \cdot [M]\{u\} = \{b\} \tag{35}$$

where M is a ($n_b \times n_b$) matrix containing the product $A_j \rho_j$ on the principal diagonal and b is vector containing the term at the LHS of equation (34).a which are treated explicitly during the iteration procedure.

Analogously, the complete set of momentum equations (34).b can be expressed as

$$[A]^t \{P\} = [Y]\{u\} + \{t\} \tag{36}$$

where Y is a ($n_b \times n_b$) matrix containing the term $\rho_j L_j \frac{u_j^t}{\Delta t} + \frac{1}{2}\left(\left(f_j \frac{L_j}{D_{h,j}} + \beta_j\right)\rho_j u_j\right)$ on the principal diagonal and t is a vector containing the rest of the terms contained in equation (34).b. In particular the pressure gains due to the piston effect or fan action are treated explicitly by the model.

The iterative procedure starts by guessing a pressure field P^* which allows for the calculation of a guessed flow field u^* by a rearranged version of equation (36)

$$\{u^*\} = [Y]^{-1}[A]^t\{P^*\} - [Y]^{-1}\{t\} \tag{37}$$

After defining pressure and velocity correction vectors u' and P' (see equation (38))

$$\begin{aligned} &a) \quad \{u'\} = \{u\} - \{u^*\} \\ &b) \quad \{P'\} = \{P\} - \{P^*\} \end{aligned} \tag{38}$$

and after some rearrangements a correlation between velocity vector and pressure correction can be obtained. As for the original SIMPLE algorithm formulation, the term $-[Y]^{-1}\{t\}$ is dropped to keep the iteration procedure simpler [66], leading to equation (39)

$$\{u\} = \{u^*\} + [Y]^{-1}[A]^t\{P'\} \tag{39}$$

By substituting equation (39) into equation (35) a final set of equations for the pressure correction is obtained.

$$[A]\cdot[M][Y]^{-1}[A]^t\{P'\} = -[A]\cdot[M]\{u^*\} + \{b\} \tag{40}$$

At each iteration step, equation (40) is used to calculate the pressure correction to update pressure and flow fields. Obviously, in the nodes where the values of pressure or

velocities are known (i.e. domain boudaries), the pressure or velocity corrections are set to zero.

The developed numerical algorithm requires an under-relaxation step in order to reach convergence. In particular the new update values for pressure and velocities are calculated by means of relaxation factors that can provide more stable computations. The status of the convergence is checked by monitoring the scaled values of the residuals.

The main steps of the solution procedure of the 1D model are resumed as follows:

1. Guess a pressure field P^*
2. Solve the momentum equations to obtain u^* (equations (37))
3. Solve the pressure correction equations to calculate P' (equation (40))
4. Update pressures and velocities
5. Solve energy equations (34).c and update temperatures and densities
6. Iterate from step 2 to step 5 until convergence is reached.

2.3.7. Typical input parameters and boundary conditions

Given the substantial simplifications introduced in the 1D models (i.e. one-dimensionality of the fluid pattern), their accuracy mainly rely on the calibration constants and semi-empirical parameters contained in previous equations. Furthermore, the boundary conditions to be input into the model are known only with low accuracy given all the uncertainties related to the estimation or static pressure at the portals or at the chimneys, wind conditions and variability, fire load and HRR.

The pressure difference at the portals usually plays a negligible role for short tunnels (few hundred meters) while is a dominant parameter for long tunnels under relevant meteorological barriers (such as mountains). The evaluation of this effect to input reliable boundary conditions is subject to long term measurements. A first rough

approximation (based on measurements carried out on the tunnels Frejus, Mont Blanc and Lioran) is given in [72] and is presented hereafter

$$\Delta p \approx 0.4 \cdot \Delta z \tag{41}$$

where *Δp* is the barometric pressure difference at the portals in *Pa,* and *Δz* it the difference in the portal altitude. Nevertheless, this value represents only a statistic average and significantly higher pressure difference can be achieved.

As example, the pressure differences measured over a long term experimental campaign for the Mont Blanc tunnel are reported in Figure 13. It shows that while average statistic pressure is larger at the French portal, the largest pressure differences (up to 1000 Pa) are in the opposite direction. Therefore the whole ventilation system has to be set up to cope with such critical environment conditions. In the case of the Mont Blanc Tunnel after the refurbishment, the ventilation system is designed to counteract against pressure differences of ±750 Pa with 76 jet fans.

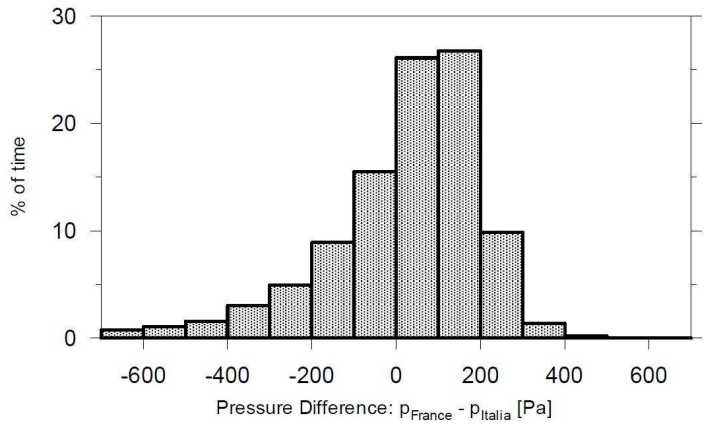

Figure 13: Meteorological pressure difference measured between the portals of Mont Blanc Tunnel [73]

Similar arguments can be given when including the wind pressure as boundary condition. The portal load due to the effect of the wind is proportional to the stagnation pressure as presented in equation (42)

$$\Delta p \approx \zeta \frac{\rho}{2} u_{w,por}^2 \tag{42}$$

where ζ is a pressure loss coefficient at the portals (~0.6) and $u_{w,por}$ is the wind velocity at the average portal height. If the wind velocity at the average portal height is not known, it can be scaled by using standard power laws to take into account the atmospheric boundary layer.

Another key parameter is represented by the effective tunnel friction coefficient *f*. Indeed, it takes into account not only the wall roughness but it must include the "apparent roughness" induced by all the appliances and auxiliary facilities installed on the tunnel lining. Typical values can differ significantly from the standard values measured for pipes. The tunnel friction coefficients can range between 0.1 and 0.3. An average value of 0.026, calculated on the basis of a statistical analysis of experimental measurements for a longitudinally ventilated tunnel with horse-shoe cross section, is provided in [62].

The modelling of jet fans and ventilation devices require the adoption of a fan characteristic curve. In most of the cases the fan characteristics curves are completely unknown or not well defined because their behaviour is strongly dependent on their surroundings and their installation; distance from the ceiling, eccentricity, presence of niches etc. The values provided by the manufacturer are in fact measured in laboratory whose environment is different from a real tunnel. Usually, in situ measurements or further CFD analysis are required to adequately define their behaviour. Typical values of jet fan thrust range between 500 N and 1400 N while the nominal jet fans pressure rise coefficients ranges between 0.8 and 0.9. However, the latter values can be highly variable, especially if the fans are installed in niches. Indeed Jang and co-workers [62], on the basis of experimental measurements conducted in a real operating tunnel, proposed a value of 0.56 significantly lower that the nominal values.

The evaluation of the piston effect is a complex task since it depends on a large set of ill-defined parameters including, vehicle drag coefficients and speed and traffic conditions. Experimental studies [62] assert that the average drag coefficients of the small-sized vehicles and the large-sized vehicles fall in the ranges 0.32–0.35 and 0.36–0.4, respectively, when the averaged traffic density in the tunnel is below 8 vehicles/lane/km and the vehicular tailgating effect is weak. However, as the averaged

traffic density in the tunnel increases to 8–23 vehicles/lane/km during the morning rush hours, the averaged drag coefficients of the small-sized vehicles and the large-sized vehicles would be reduced to 0.20 and 0.24.

Besides, a large set of semi-empirical correlations to model the hydraulic resistance in complex intersections between galleries, shafts or large obstructions can be found in [75]

The estimation of the heat generation due to fire is a complex process and 1D models cannot provide any accurate result. Therefore, data on the fire growth curve are required. They can be derived from available experimental data or from design prescriptions. Alternatively the same approach as presented by Carvel in [4] or by Ingason and co-workers can be adopted [74]. The former has been vastly described in the first chapter of this work. The latter consist of a parabolic growth followed by a constant heat flux over a period of time and an exponential decrease:

$$\begin{aligned} &Q = \alpha \cdot t^2 \qquad for \qquad t \le t_1;\ t_1 = \sqrt{Q_{\max}/\alpha} \\ &Q = Q_{\max} \qquad for \qquad t_1 < t < t_2 \\ &Q = Q_{\max} \cdot e^{-\beta(t-t_2)} \qquad for \qquad t \ge t_2 \end{aligned} \tag{43}$$

This expression depends on parameters α and β, which values are suggested for fast fires (buses: α=0.1 kW/s^2; β=0.0007 s^{-1}) and medium fires (cars: α=0.01 kW/s^2; β=0.001 s^{-1}). Time t^2 is calculated on the basis of the total energy released.

2.4. A case study: the Frejus Tunnel

The developed 1D model has been used to simulate the behaviour of the Frejus tunnel and the installed ventilation system. The analysis aims at defining ventilation strategies to be used in case of fire and illustrates the approach.

The Frejus tunnel is a two-way link between Italy and France with a total length of 12870 m. A schematic of the typical Frejus tunnel cross section and ventilation system is presented in Figure 14. The hydraulic diameter of the semicircular sections is 6 m. Ventilation is fully transversal. Figure 14 depicts 6 groups of fresh air fans (AF) and the

six groups of extraction fans (AV). The French portal is located on the left side (x=0 m) while the Italian on the right side (x=12870 m). Ordinary ventilation is operated by introducing fresh air along the tunnel through 3 U-shaped fresh air ducts which have 2 fans at each end. Fresh air openings are installed each 5 m. Emergency ventilation is operated using the fresh air ducts and the 3 U-shaped extraction ducts connected to extraction dumpers installed each about 130 m.

The Frejus tunnel ventilation system is operated in order to create a stagnation point as close as possible to the fire position with positive velocity upstream the fire and negative velocity downstream the fire. In this scenario the smoke does not tend to propagate along the tunnel but is extracted close to the section where it is generated.

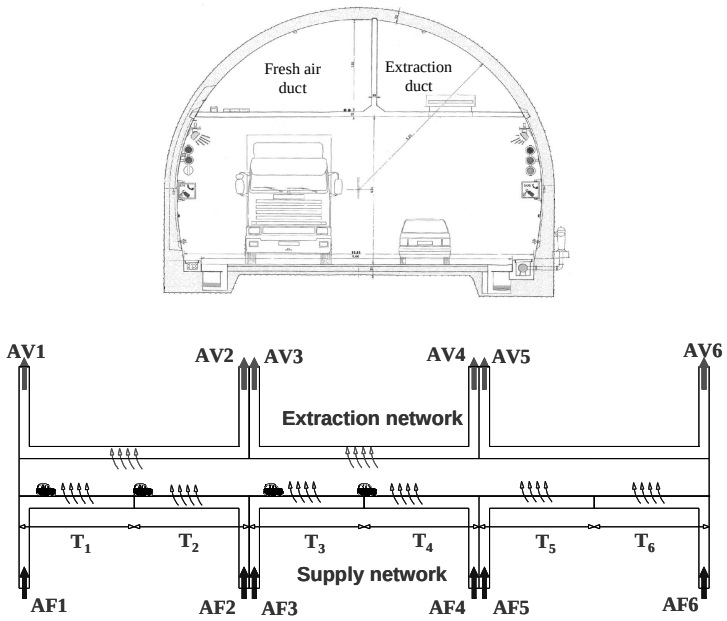

Figure 14: Frejus tunnel: top) cross section; down) Schematic of the ventilation system layout

The most effective strategy to be applied in case of fire depends on the fire location along the tunnel and the pressure difference between the two portals.

The pressure difference, assumed to be positive when inducing the air flowing from the French towards the Italian portal, can reach values of several hundreds Pascals, as typical for long tunnels across the Alps. Furthermore, given a certain positive pressure difference across the portals, the ventilation scenario to be adopted depends on the location of the fire.

If the fire takes place in the first tunnel portion (between the French portal and the tunnel central section), 10 extraction dumpers over the fire (5 upstream and 5 downstream) are opened. In addition, if the pressure difference is large, fresh air is supplied downstream of the fire to enhance smoke confinement *(opposite supply strategy)*. Some fresh air is also supplied all along the tunnel mainly in order to prevent from smoke propagation in the fresh air ducts, which may be used as escape route.

If the fire takes place in the last portion (between the tunnel central section and the Italian portal), a proper air extraction in the first portion of the tunnel is used to oppose the effect of pressure difference between the portals *(opposite extraction strategy).* Similar strategies are also defined for negative pressure difference.

In order to implement these conceptual strategies it is necessary to provide the operators with proper guidelines in the form of tables or algorithms relating pressure difference and fire position to the extraction dumpers to be opened and to the settings of each group of fans. This information is obtained through multiple numerical simulations, performed using the 1D approach. However, the model must be calibrated and validated against experimental data before being used as reliable simulation tool.

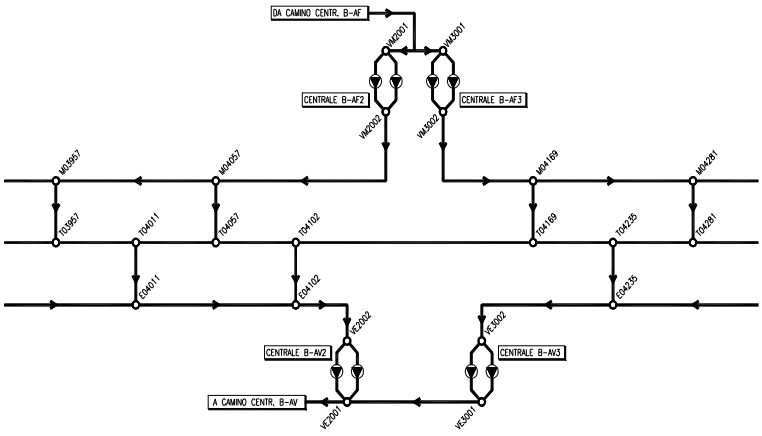

Figure 15: Schematic of the network used for the 1D calculation corresponding to the tunnel region between section T_2 and T_3 of Figure 14.

Two examples of validation for the developed code on specific ventilation scenarios are presented hereafter. The global network, built for the purpose, is composed by 650 branches and 450 nodes. A schematic is presented in Figure 15.

The volumetric flow rates of the axial fans at full charge range between 222÷257 m^3/s and 117÷124 m^3/s for supply and extraction units, respectively. The tunnel friction coefficient has been established on the basis of experimental measurements to be around 0.017.

A first comparison between numerical predictions and experimental data is relative to a steady state scenario with only the supply fans operating at 30% of full charge. The pressure difference across the Frejus tunnel during the test was negligible. This is confirmed by the computed and experimental velocity profiles which are almost specular with respect to the tunnel central section (see Figure 16). An accurate match between numerical and experimental prediction has been achieved.

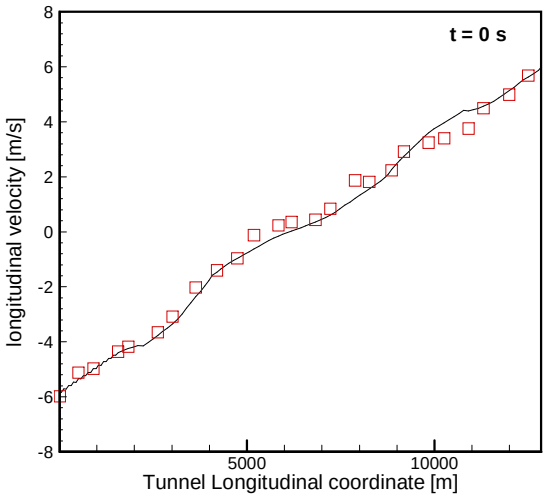

Figure 16: Velocity distribution computed with the developed 1D model and comparison to experimental data recorded in the Frejus tunnel. Longitudinal velocity as function of the tunnel length

A second validation has been performed for an emergency ventilation scenario including a small 8MW fire source located in the tunnel portion indicated as T_3 (see Figure 14). Given the high pressure difference across the portals (1000 Pa) and the location of the fire, an opposite supply ventilation strategy has been adopted. It consists of a localized extraction over the fire zone as well as an enhanced fresh air supply in the fire downstream region. The fans are supposed to be started at *t=0*.

Computed horizontal velocity profiles established along the tunnel and measured data are compared in Figure 17. An overall good agreement is obtained. The 1D model predicts well the overall flow behaviour of tunnel ventilation system.

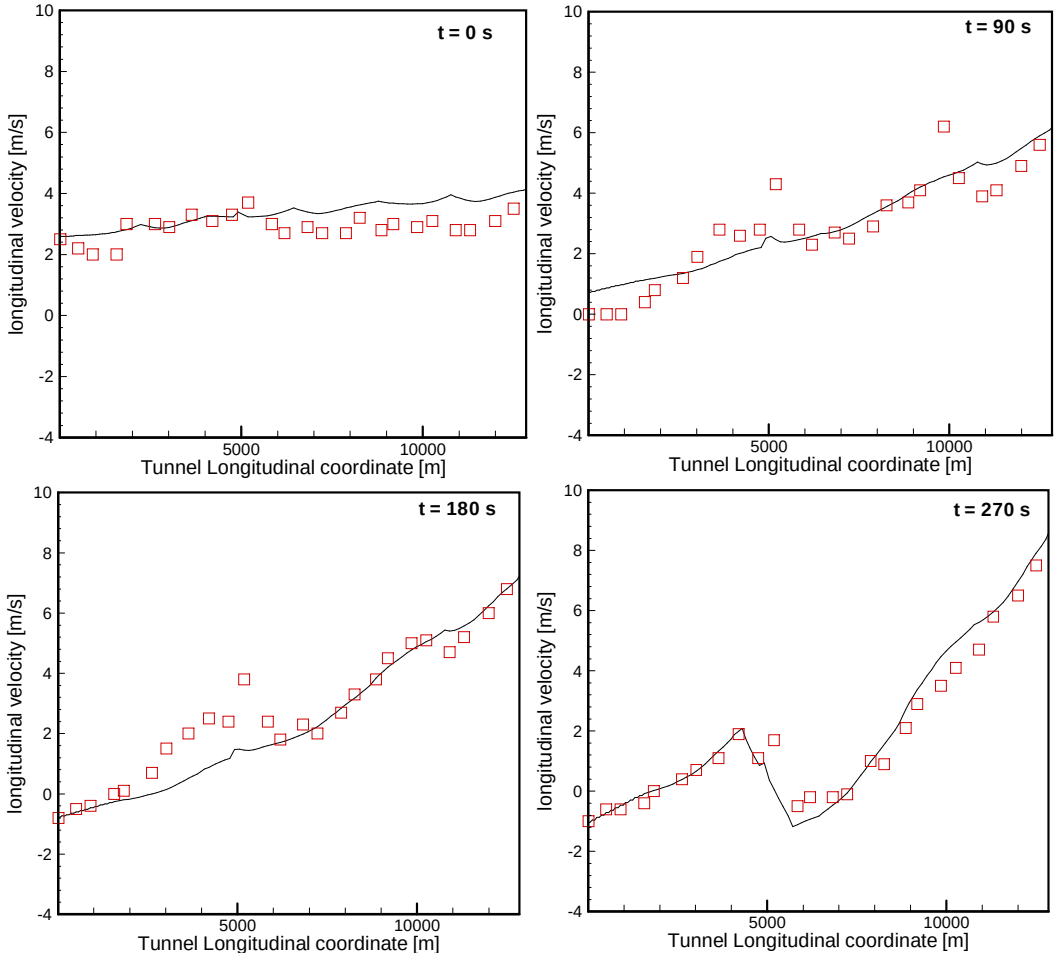

Figure 17: Velocity distribution computed with the developed 1D model and comparison to experimental data recorded in the Frejus tunnel. Longitudinal velocity as function of the tunnel length at 4 different times

2.5. Concluding remarks

The results obtained by 1D models can be used to assess whether the overall ventilation conditions are acceptable for the fire safety strategies. In the case of transversally ventilated tunnels, this can be made by determining the presence of a cross section where flow is stagnant, as close as possible to the fire. In the case of longitudinally ventilated tunnel 1D models can be used to assess whether or not the tunnel ventilation system is able to guarantee super-critical ventilation velocity in the fire zone and therefore avoid back-layering.

However, they are unsuitable to simulate the fluid behaviour in regions characterized by high temperature or velocity gradients typically encountered in the vicinity of the fire plume, ventilation devices of complex interconnections of galleries. In order to deal

with such complex flow conditions they mainly rely on empirical correlation or calibration constants to be defined on the basis of experimental measurements or detailed calculations.

Parts of this work have been published in *Building and Environment [102]* and *Fire Technology [105]*. A chapter titled *One Dimensional and Multi-scale Modelling of Tunnel Ventilation and Fires* is based on the work presented here and will be published in next edition of *The Handbook of Tunnel Fire Safety [104]*.

3
CFD modelling

3.1. Introduction

In the last two decades the application of CFD as fire safety engineering tool has become widespread. This tendency has reached also tunnel applications where CFD calculations are now part of many designs, assessments and investigations.

CFD simulations require the solution of the complete set partial differential equations asserting the conservation of mass, momentum and energy. Such set of equations is solved numerically leading to detailed predictions of velocity and temperature fields, species concentration, heat fluxes mapping and so forth. The calculations are performed by enforcing the conservation laws on a high number of control volumes generated by a numerical discretization of the computational domain.

Severe limitations to the full numerical solution of the governing equations are induced by the impossibility of resolving the whole range of spatial and time scales involved in the turbulent flows associated with any ventilation or fire scenarios in tunnels. This problem has been tackled by modifying the governing equations in order to model the

unresolvable turbulent transport phenomena. Typically, two main approaches have been used: the first one is based on a time-averaging of the Navier-Stokes equations (RANS) while the second one uses spatial averaging by means of specific filter functions. Such technique for turbulence modelling is known as Large Eddy Simulation (LES).

Besides to the uncertainty related to the modelling of turbulence, considerable difficulties are also introduced by the description of turbulent combustion chemistry, buoyancy, radiation heat transfer and burning of condensed-phase fuels. Great uncertainty, especially when dealing with tunnel fire and ventilation scenarios, is also expected at the definition of the boundary conditions due to the unknown meteorological conditions at the portals, actual fire load, effective lining roughness, presence of vehicles and obstructions, etc.

Further complexity is introduced by the numerical solution of the final set of partial differential equations where the choice of the numerical schemes and the accuracy of the grid influence strongly the quality of the CFD solution.

Nowadays, computational fluid dynamics (CFD) can be considered as a mature tool to predict the overall flow behaviour due to ventilation devices, large obstructions or fire as well as to predict smoke spread in enclosure. However, more complex issues related to flame spread, soot formation, oxygen vitiation and combustion modelling are far by being solved, and they will not be satisfactorily addressed in the next decades.

Given all these complexities, any CFD analysis requires two additional steps, *verification* and *validation,* in order to judge the appropriateness of its use and the level of confidence of its predictions [76]. *Verification* is a process to check the correctness of the solution of the governing equations. *Validation* is a process to check the appropriateness of the governing equations as model of the physical phenomena under investigation. Usually validation is made by comparing the model against experimental data. In this case, the differences that cannot be explained in terms of numerical issues, are attributed to uncorrected hypothesis and simplification introduced when building the governing equations.

There are a number of institutions dedicating a great effort in developing CFD tools for specific fire modelling purposes. A recent survey identified at least a dozen of CFD model for fire modelling including JASMINE from the Fire Research Station (UK), Fire Dynamic Simulator (FDS) from NIST (US), SMARTFIRE from University of Greenwich (UK) and SOFIE from a European Consortium [77]. Among the general purpose CFD codes used for simulation fire scenarios, the authors enumerate CFX, Flow3D, STAR-CD and Fluent. This work uses Fluent as CFD tool for simulating tunnel ventilation flows and fires.

3.2. Literature overview

The issue of CFD modelling of fire phenomena is too wide to be treated is a single literature overview. Several books and literature review papers on the subject have been published in the last decades, and the interested reader is referred to them [78-80]. In this section only the archival papers direct referring to the CFD modelling of tunnel ventilation flows and fires will be reviewed.

The first significant contribution on the subject is dated 1994 and was presented by Fletcher and co-workers [81]. The paper presents a comparison between numerical and experimental data recorded in a 120 m long tunnel (cross section ~ 13 m^2). The authors used a k-ε turbulence model and a mixture fraction model for combustion. Radiation heat transfer has been implemented by using a discrete transfer radiation model. A pool fire, whose size was estimated ranging between 2 MW and 2.4 MW was located in the middle of the tunnel. Three different ventilation velocity scenarios have been analysed (0.5 m/s, 0.85 m/s and 2 m/s). A qualitative good match between predicted and recorded temperature has been found with error ranging between 40÷100% in the vicinity of the flame and around 40% in the far field. The authors recorded that the addition of the turbulence production due to buoyancy was crucial to predict smoke stratification while soot production had a very little impact.

A comprehensive study has been presented by Woodburn and Britter in 1996 [82] and [83]. The study was performed by using a commercial CFD package Flow-3D and aims at predicting temperature and flow fields in a 360 m long tunnel under a 2.7 MW fire scenario. A k-ε turbulence model was implemented together with an eddy break-up

model for combustion. Radiation heat transfer was not included. The authors assessed the sensitivity of the results to several unknown parameters including wall friction coefficient, turbulence model, tunnel slope and so forth. They highlighted that maximum temperature, velocity profile and global heat transfer were significantly dependent on the input parameters; maximum temperatures showed variation within a 60% range of base case scenario, velocity profile up to 30% and convective heat transfer up to 45%. Temperatures were generally over-predicted showing deviation from measured values ranging between 260% in the vicinity of fire source and 200÷400% in the downstream area.

Only a qualitative assessment of temperature and velocity fields has been developed by Chow by using the commercial CFD package Phoenix [84]. The CFD model has been applied to a 20 m long tunnel (25 m^2 cross section) under a 5 MW and a 40 MW fire source. Fire has been modelled as source of heat and smoke without a dedicated combustion model.

A detailed analysis of CFD capabilities has been presented by Wu and Bakar (2000) [33]. The contribution presents a numerical analysis of two fire scenarios (1.4 kW and 28 kW) in 10.4 m long small scale tunnel. The corresponding full scale fires, using the canonical scaling laws presented in chapter 1, would range between 2.5 and 50 MW. The numerical model has been developed by using the commercial CFD package FLUENT adopting a standard k-ε model with buoyancy modifications for turbulence and a mixture fraction model for combustion. Radiation heat transfer has not been accounted for. The comparison to experimental data shows that the CFD model underpredicts the critical velocity by 20% as maximum. The comparison to detailed velocity field data shows a qualitative agreement to the experimental data but typically, higher deviations are recorded: velocity profiles in the back-layering region close to ceiling are slightly underpredicted (~12%), while deviations up to 100% are recorded in the velocity profiles located underneath the back-layering nose. Temperatures are significantly over-predicted and do not show any qualitative agreement to the experimental findings with deviation up to 500% recorded 30 cm downstream the fire source. The authors asserted that temperature overprediction is mainly due to the

hypothesis of fast chemistry embedded in the mixture fraction model adopted for combustion which overestimates the reaction rate.

Similar level of accuracy has been reached in the contribution by Karki and Patankar (2000) [85]. The numerical model has been developed by using the commercial CFD package COMPACT-3D adopting a standard k-ε model including buoyancy modifications for turbulence. The fire has been modelled as source of heat and smoke without any dedicated combustion model. Radiation heat transfer has not been modelled. This contribution has the merit of including the ventilation devices in the computational domain performing the simulation of the whole system. In particular the jet fans have been modelled as combination of sources and sink with the volume within the fan region treated as a solid. The numerical findings have been validated against experimental data recorded during the MTFVTP [11] test 606A (10MW pool fire) and 615B (100MW pool fire). After calibrating the CFD model on the basis of cold flow scenarios, good bulk flow predictions could be achieved at ambient conditions (deviation within 7%). Predicted bulk flow data resulted in good agreement also for the simulated fire scenarios bur show larger deviations (within 30%). Predicted flow field data show an overall agreement with the experimental findings; an average 20% deviation for temperature and velocity profiles could be achieved when simulating scenario 606. The CFD simulation of test 615B showed higher deviations, up to 50% and 30% for temperature and velocity profiles, respectively.

Jojo and co-workers adopted the CFD open source package FDS to simulate a 100 m long tunnel (35 m^2 cross section) under two different fire hazards (0.5 MW and 50 MW) [26]. The CFD tool adopts a LES model for turbulence and mixture fraction model for combustion. Several configurations of the ventilation system (i.e. longitudinal, transversal, semi-transversal and hybrid) have been considered. Since experimental data were not available, the CFD predictions have been compared to classical correlations for predicting critical velocity and average temperature which are generally overpredicted (deviations ranging between 30% and 100%).

Both the k-ε and LES turbulence models have been adopted in the contribution by Gao and co-workers (2004) [86]. The work uses the same experimental set-up and data

adopted by Fletcher and co-workers one decade before [81]. In general the authors find a good agreement when analysing the plume inclination angle with errors ranging between 10% and 30%. Overall flow behaviour could be accurately predicted (i.e. occurrence of back-layering) but local temperature fields were over-predicted by up to 250%.

A qualitative contribution has been presented by Bari and Naser (2005) [87]. The work addresses the spread of fire effluents within a longitudinally ventilated tunnel 1.6 km in length. The fire represented by a burning bus, was supposed to grow up to a HRR of around 44 MW in 10 s and to extinguish in 4 min. The fire was modelled as source of heat a smoke without dedicated combustion model. Besides the unrealistic design fire, the results were not corroborated by experimental measurements as well as no information about the smoke production modelling was provided.

More detailed descriptions of the CFD modelling procedure has been provided by Hwang and Edwards (2005) [37]. The authors adopted the open source CFD package FDS to simulate flow and temperature fields within two different tunnels. The first was a 4.9 m long (0.12 m^2 cross section) small scale tunnel including a 3.3 kW fire. The full scale experimental data were taken from the MTFVTP [11] and were relative to a 50MW fire under longitudinal ventilation conditions. The authors reported a general good agreement between predicted and experimental critical velocity for both the tunnels. Detailed flow field data show a satisfactory qualitative and quantitative agreement between experimental and numerical data for the small scale tunnel in the downstream region. In the upstream region velocities are overpredicted by up to 100%. The full scale simulations show a qualitative agreement to the experiments but higher deviations (up to 200%) are recorded.

Lee and Ryou (2006) used FDS to predict temperature and flow fields in a small scale tunnel having difference aspect ratio and fire sources ranging between 2 kW and 12 kW [88]. The experimental data were provided in [33]. An overall qualitative and quantitative agreement was reached when computing the critical velocity and back-layering distance. Temperature distribution under the ceiling was calculated within a 10% deviation from the experimental findings.

Same CFD tool was adopted by McGrattan and Hamins (2006) to perform a simulation of the Howard Street tunnel fire (2.65 km long) involving a 60 cars freight train powered by three locomotives [89]. The CFD tool was used to simulate natural ventilation scenarios involving fires ranging between 20MW and 50MW. The work provides only qualitative considerations on the peak temperatures and oxygen concentration in the tunnel without any corroboration from experimental data or canonical correlations.

The commercial CFD tool FLUENT was used by Ballesteros-Tajadura et al. to simulate velocity and temperature fields within a real 1.5 km long tunnel under a 30MW fire scenario [90]. Time dependent simulations have been conducted in order to predict smoke spread in the domain but the final results were not validated against experimental data. Furthermore, the adopted mesh density (~162 cells/m) was largely under the minimum required to achieve accurate field predictions. The effect of the ventilation system was taken into account by introducing a pressure difference across the tunnel domain which was previously computed on the basis of cold flow simulations.

The CFD package FLUENT was also used by Vauquelin and Wu (2006) to predict the effect of the tunnel width on the critical velocity [30]. The CFD data were corroborated against small scale experimental data provided in [33]. Turbulence was addressed by using a k-ε turbulence model with buoyancy modification while combustion was implemented by using a mixture fraction model. The authors confirmed that the model was able to predict critical velocity with an uncertainty ranging between 5% and 14%. No conclusions on the accuracy of the predicted flow fields have been given.

Lin and Chuah performed a qualitative analysis on the effectiveness of different extraction strategies in a semi-transverse ventilated tunnel by using FDS. The tunnel considered for the case study was 4 km long (~50 m^2 cross section) while the fire is supposed to have a 100 MW peak HRR [91]. No comparisons to experimental data are provided.

The same numerical tool has been used by Jae Seong Roh et al. to simulate temperature and flow fields within a 10 m long small scale tunnel (~0.14 m^2 cross section) [92]. The average fire size ranged between 2 kW and approximately 13 kW. The numerical model

has been validated against temperature measurements recorded along the tunnel ceiling. The predicted temperature values deviated from the experimental findings as maximum as 20% for a 5 kW fire and 90% for a 13 kW fire.

A hypothetic fire outbreak in the Louis-Hippolyte-Lafontaine tunnel under a river in the Montreal area represented the test case for the work by Abanto and co-workers (2006) [93]. The simulations have been conducted by using the commercial CFD package FLUENT and an in-house CFD code. The fire has been modelled as a volumetric heat source while a un-specified combustion model has been used for the second run. In both the cases a k- ε turbulence model has been adopted. The authors provide only qualitative results and most of them are questionable (e.g. temperature higher than 3000 K in certain domain regions). No comparison to experimental data has been provided.

A more comprehensive validation of FDS has been performed by Kim and co-workers (2007) [94]. The authors performed a detailed sensitivity study to several modelling parameters (i.e. Smagorisky constant, turbulent Prandlt number, Schmidt number, grid size) and included a systematic comparison to experimental findings from a 100MW fire test performed during the MTFVTP [11]. More detailed analyses were performed to refine the smoke layer predictions but without much success. The authors showed that FDS produces predictions that are in qualitative agreement with the actual fire phenomena in the near-fire and downstream region: simulated temperatures and flow velocities showing an error distribution of approximately +56% to +37%, and ±91% to ±30%, respectively. For the upstream region of the tunnel, FDS shows serious limitations in predicting the smoke layer near the ceiling. Some inconsistencies were also reported when trying to reproduce transient ventilation scenarios with FDS.

The MTFVTP was the source of experimental data also for Galdo-Vega and co-workers (2007) [95]. In particular 3 different ventilation scenarios involving 10MW and 50MW fires have been modelled. The whole computational domain was meshed including the ventilation devices (jet fans) modelled as source and sinks of mass. The mesh density adopted for the calculation (117 cells/m) is by far under the minimum requirements for accurate predictions. The fire has been modelled as source of heat and smoke while turbulence has been addressed by using a k-ε turbulence model with buoyancy

modifications. Nonetheless, the authors showed an overall agreement between numerical predictions and experimental data confirming that simplified fire modelling approaches lead to accurate predictions of the global ventilation system behaviour. However, higher deviations are expected in the vicinity of the fire.

A small scale experimental and numerical study has been presented by Rusch and co-workers (2008) [96]. The small scale experiments were performed in a 10 m long tunnel (0.64 m^2 cross section) including a buoyant hot jet released in cross flow. Velocity and temperature were recorded by using thermocouples and laser doppler anemometry. The numerical predictions were performed by using the CFD commercial package CFX. Turbulence was addressed by using several models including k-ε turbulence model with buoyancy modifications, k-ω, k-ω SST, and RSM. Steady simulations showed that all the previous models tend to overpredict temperature under the ceiling since unable to predict the entrainment of cold air from the cross-flow into the hot jet. The reason for the failure was found to be the inability of the models to solve un-isotropic vortical structures in steady simulations. Unsteady simulations showed a tiny improvement in the temperature predictions; better accuracy could be achieved when adopting a DES (Detached Eddy Simulations) turbulence model. The authors asserted that an accurate wall treatment and well resolved large scale vortical structures are required to improve CFD predictions.

A comparison between LES and k-ε turbulence models for critical velocity prediction has been presented by Van Maele and Merci (2008) [97]. The k-ε turbulence model has been implemented in the commercial CFD package FLUENT. Radiation heat transfer was not considered while combustion was addressed by using a mixture fraction model. The LES calculations are performed by using the CFD tool FDS. Experimental data are provided by Wu and Bakar (2000) [33] for a 15 long tunnel (0.0625 m^2 cross section) under a 3 kW and a 30 kW fire scenario. The authors showed that both the modelling approaches are able to provide good predictions of the critical velocity with deviations ranging between 20% to 38% and 31% to 8% for k- ε and LES turbulence model, respectively. Flow and temperature fields are no validated against experimental data.

Some data on the back-layering occurrence in a 1.8 km long operative tunnel are presented by Kashef and Benichou (2008) [98]. The tunnel is equipped with a semi-transverse ventilation system which is supposed to cope with a 20 MW fire scenario. The model, developed with FDS, is validated against data recorded during some tests involving a 2 MW fire. Generally, the authors find a good agreement between experimental and numerical findings but the extrapolation of the model up to fire sizes 10 times larger is questionable.

A qualitative analysis on the capabilities of CFD and zone models is presented by Jain and co-workers [99]. The CFD and zone model calculations are performed by using CFX and CFAST respectively. A 150 m long tunnel (80 m^2 cross section) represents the test case. The numerical predictions are not compared to experimental data.

In a recent work FDS has been used to predict the fire growth, temperature and velocity fields established during the Runehamar fire test 1 characterized by a peak release rate around 200MW [8,100]. The authors performed several attempts to reproduce the measured fire growth by tuning the model parameters including fire load geometry, grid size and domain size. Following this approach, which is fundamentally questionable, the authors were able to reproduce the actual fire growth within an acceptable degree of accuracy. However, their conclusion are case dependent and cannot be generalized to any other tunnel, fire load, geometry of the fire source and ventilation velocities.

Nmira and co-workers (2009) performed a CFD analysis of a thermoplastic tunnel fire under a water mist mitigation agent (i.e. water mist) [101]. The CFD model uses a k- ε turbulence model, an Eddy-break-up-Arrhenius model for turbulent combustion and a multiphase radiative transfer equation including the contribution of soot, combustion products and water droplets. A dedicated pyrolysis model for PMMA was also introduced in order to calculate the time evolution of combustible gases released into the tunnel environment. The model was applied to simulate the behaviour of a PMMA fire in a 25 m long tunnel (3×5 m^2 cross section). A large set of CFD data have been presented but none of them has been corroborated by experimental measurements.

Table 7 summarizes the main characteristics of the tunnel fire related CFD studies discussed in the literature review.

CFD models of tunnel fires have been shown to predict critical ventilation velocity, and back layering distance within an acceptable level of accuracy (deviation smaller than 30%). The overall flow data (i.e. bulk velocity and temperature) are also accurately predicted with deviations from experimental values typically within 20%. The literature study, including the main reference paper of the last 25 years, shows that prediction of local flow field data (i.e. velocity and temperature fields), especially if calculated in the vicinity of the fire source, can be affected by error higher than 100% when compared to experimental measurements.

It has been shown that CFD analysis of fire phenomena within tunnels suffers from the limitations set by the size of the computational domains. The high aspect ratio between longitudinal and transversal length scales leads to very large meshes. The number of grid points escalates with the tunnel length and often becomes impractical for engineering purposes, even for short tunnels less than 500 m long. An assessment of the mesh requirements for tunnel flows is made by Colella et al. [102,105] for active ventilation devices and for fire-induced flows. Grid independent solutions could be achieved only for mesh density larger that 4000 cells/m and 2500 cells/m for ventilation and fire induced flows, respectively.

The high computational cost leads to the practical problem that arises when the CFD model has to consider the boundary conditions or flow characteristics in locations far away from the region of interest. This is the case of tunnel portals, ventilation stations or jet fan series located long distances away from the fire. In these cases, even if only a limited region of the tunnel has to be investigated (i.e. to simulate the fire) an accurate solution of the flow movement requires that the numerical model includes all the active ventilation devices and the whole tunnel layout. For typical tunnels, this could mean that the computational domain is several kilometres long.

This limitation is the reason why only a limited number of CFD studies directly focus on the performance of tunnel ventilation systems. In most of the works reviewed the computational domain is limited to a small region close to the fire and the ventilation velocity at the domain boundaries is considered to be known (i.e. estimated with crude correlations or determined by cold flow ventilation tests). Obviously, if the

performances of a ventilation system have to be assessed, this kind of approach is completely useless because it produces a de-coupling between ventilation system and fire.

Reference	Domain size [m]	fire size	Small scale	ventilation devices	Code	Turbulence	Combustion	Validation	note
Fletcher et al. (1994)	90	2 and 2.4 MW	-	-	Furnace	k-ε	Mixture fraction	√	Octane pool fires were used in the experiments
Woodburn et al. (1996)	366	2.3 MW	-	-	FLOW 3D	k-ε	Eddy break-Up	√	The combustion model is used when modelling the fire area (40 m).
Chow (1998)	20	5 and 40 MW	-	-	PHOENIX	N.A.	N.A.	-	Only qualitative observations are given
Wu et al. (2000)	8.1	3 to 45 kW	√	-	Fluent	k-ε	Mixture fraction	√	Different tunnel cross section investigated
Karki et al. (2000)	850	10 MW and 100 MW	-	√	COMPACT - 3D	k-ε	Volumetric heat source	√	Also cold flow scenarios are simulated
Jojo el al. (2003)	100 m	0.5 to 50 MW	-	-	FDS	LES	Mixture fraction	-	Different ventilation systems are analysed
Gao et al. (2004)	90	2 and 2.4 MW	√	-	N.A.	LES	Volumetric heat source	√	A comparison to k-ε turbulence model results is provided
Bari et al. (2005)	1600	44 MW	-	-	Fluent	N.A.	Volumetric heat source	-	The fire behaviour is questionble and the smoke production parameters are unclear
Hwang et al. (2005)	4.9	1 to 100 kW	√	-	FDS	LES	Mixture fraction	√	Also large scale simulations are performed and validated against Memorial tunnel data. Large scale fire HRR up to 50 MW. Large scale tunnel length 853 m.
McGrattan et al. (2006)	2650	50 MW	-	-	FDS	LES	Mixture fraction	-	Only observation on the maximum temperature are given
Ballestreros-Tajadura et al. (2006)	1500	30 MW	-	-	Fluent	k-ε	Volumetric heat source	-	The effect of the ventilation system is modelled as total pressure difference across the portals
Vauquelin et al. (2006)	8.1	15 kW	√	-	Fluent	k-ε	Mixture fraction	√	Different tunnel cross section investigated
Lee et al. (2006)	10.4	2.47 to 12.30kW	√	-	FDS	LES	Mixture fraction	√	Different tunnel cross section investigated
Abanto et al. (2006)	1800	N.A.	-	-	Fluent	k-ε	Volumetric heat source	-	Fire model, fire sizes and are not clear. Qualitative description of the results are not given.

Reference	Domain size [m]	fire size	Small scale	ventilation devices	Code	Turbulence	Combustion	Validation	note
Lin et al. (2007)	550	100MW	-	-	FDS	LES	Mixture fraction	-	Only 550 m of tunnel have been simulated.The real tunnel length is 4000
Roh et al. (2007)	7	2 to 13 kW	√	-	FDS	LES	Mixture fraction	√	N-heptane pool fires are used in the experiments
Galdo Vega et al. (2007)	850	10 and 50 MW	-	√	Fluent	k-ε	Volumetric heat source	√	Memorial tunnel fire tests are used as case studies
Kim et al. (2007)	350	100 MW	-	-	FDS	LES	Mixture fraction	√	Only 350 m of tunnel have been simulated.The real tunnel length is 850. Memorial tunnel data are used for the validation
Jain et al. (2008)	150	9 MW	-	-	CFX/Cfast	k-ε	Volumetric heat source	-	Only qualitative observations are given
Van Maele (2008)	8	3 kW and 30 kW	√	-	FDS/Fluent	LES and k-ε	Mixture fraction	√	GGDH hypothesis used for k-ε modelling
Kashef et al. (2008)	1400	2 and 20 MW	-	-	FDS	LES	Mixture fraction	√	The validation was conducted only for the 2 MW fire scenario
Rusch et al. (2008)	10	N.A.	√	-	CFX	:-ε/k-ω/RSM/DES	N.A.	√	CFD simulations of a hot jet in cross flow conditions are presented
Cheong et al. (2009)	36 to 102	up to 200 MW	-	-	FDS	LES	Mixture fraction	√	The FDS model was calibrated agaist the Runehamar fire test experiments
Nmira et al. (2009)	25	N.A.	-	-	N.A.	k-ε	Eddy break-Up	-	A pyrolysis model for PMMA was used to estimate the amount of combustible products generated. The interaction with a water mist agent is also considered.

Table 7: Summary of the published CFD studies related to tunnel fires discussed in the literature review.

3.3. Governing equations

The physics of fluid flows can be described by a set of partial differential equations known as governing equations describing the conservation of mass, momentum and energy. Each of these can be derived for an elemental fluid particle having volume *dx·dy·dz*. An interested reader can refer to [66,70]. The CFD commercial package FLUENT [106], used in this work, solves the mass conservation equation in the following form

$$\frac{\partial \rho}{\partial t} + \nabla \cdot \rho \, \mathbf{u} = 0 \tag{44}$$

where ρ is the fluid density and $\mathbf{u}$ the velocity vector. The momentum conservation equation states

$$\frac{\partial \rho \mathbf{u}}{\partial t} + \nabla \cdot (\rho \mathbf{u}\mathbf{u}) = -\nabla p + \nabla \cdot \boldsymbol{\tau} + \sum \mathbf{S} \tag{45}$$

where p the static pressure, $\boldsymbol{\tau}$ is the stress tensor, g the gravity vector, and $\mathbf{S}$ a vector containing the momentum source terms per unit volume. The stress tensor $\boldsymbol{\tau}$ is given by

$$\boldsymbol{\tau} = \mu \cdot \left[\left(\nabla \mathbf{u} + \nabla \mathbf{u}^T \right) - \frac{2}{3} \nabla \cdot \mathbf{u} \mathbf{I} \right] \tag{46}$$

where μ is the molecular viscosity, $\mathbf{I}$ the unit tensor while the second term on the RHS contains the effect of volume dilation which is typically negligible for low mach number flows.

FLUENT solves the energy equation in the following form

$$a) \quad \frac{\partial}{\partial t}[\rho E] + \nabla \cdot (\mathbf{u}(\rho E + p)) = \nabla \cdot \left(k_{eff} \nabla T + \boldsymbol{\tau}_{\mathbf{eff}} \cdot \mathbf{u} \right) + \sum S_E \tag{47}$$

$$b) \quad E = h - \frac{p}{\rho} + \frac{u^2}{2}$$

where h is the sensible enthalpy, S_E the energy source term, k_{eff} the effective conductivity and $\boldsymbol{\tau}_{\mathbf{eff}}$ is the global stress tensor including the Reynolds turbulent stresses. The effective conductivity k_{eff} can be obtained by summing molecular and turbulent conductivity.

The equation of state for a fluid is used to relate the material properties to each other. By assuming thermodynamic equilibrium, pressure and internal energy are functions of density and temperature:

$$\begin{aligned} &a) \quad p = p(\rho, T) \\ &b) \quad i = i(\rho, T) \end{aligned} \tag{48}$$

For a perfect gas, for instance, the above equations are $p=\rho RT$ and $i=c_vT+i_0$ where R is the specific gas constant, c_v is the specific heat capacity at constant volume and i_0 is the reference internal energy.

In the solid region the energy transport equation solved by model has the following form

$$\frac{\partial}{\partial t}(\rho h) + \nabla \cdot (\mathbf{v}\rho h) = \nabla \cdot (k \nabla T) + S_E \tag{49}$$

where h is the sensible enthalpy, k is the solid heat conductivity and S_E is the volumetric heat source, and $\boldsymbol{v}$ is the velocity field eventually specified for the solid zone.

3.4. Turbulence modelling

Typical tunnel ventilation flows and fire induced flows are characterized by a turbulent regime in which the fluid velocities as well as other properties vary in a random and chaotic way. The turbulent nature of the flow precludes any economical description of the motion of all the fluid parcels.

Typically, the description of turbulent flows can be addressed by decomposing the instantaneous fluid velocity *u(t)* into a steady mean value *U* and a fluctuating component *u'(t)*. This approach, known as Reynolds decomposition, allows a turbulent flow to be characterized in term of mean value properties *(U, V, W, P, T)* and some statistical properties of their fluctuations *(u', v', w', p', T')*[66]. Visualization of turbulent flows shows that, even if the mean velocity components or pressure vary in 1 or 2 dimensions, the turbulent fluctuations have always a three-dimensional character. In practice, turbulent flows are characterised by trains of vortices, also called eddies. Turbulent eddies take place over a continuous and wide spectrum of length scale; fluid parcel with are initially separated by a long distance can be brought closed by turbulent eddies motions.

Due to the convective transport of eddies, faster moving fluid parcels are brought in regions characterized by slower fluid motions and viceversa. This causes faster moving layer to be decelerated and slower moving layer to be accelerated inducing additional shear stresses in the fluid flow known as Reynolds stresses. Same conclusions could be drawn when analyzing the turbulent transport of heat or species. Due to turbulent transport, heat, mass and momentum transfers are extremely enhanced in turbulent flows. Effective mass, heat and momentum diffusion coefficients are therefore higher in turbulent flows than the correspondent laminar values.

Given the impact of turbulent transport phenomena in fluid dynamics and the fact that most of the industrial flows are turbulent, it is easy to understand the great effort done by the international community to address such issues. Indeed, a large number of different turbulence models have been developed but there is no universal turbulence modelling approach which is suitable for all the CFD applications.

However, for most of the engineering purposes it is unnecessary to resolve the details of the turbulent fluctuations since the information provided by the time averaged fluid properties are adequate. Turbulence models for Reynolds-averaged Navier-Stokes equations (RANS) have been developed in this context.

The averaging of Navier-Stokes equations is performed under the assumption that the time averaged value of the fluctuating components of any fluid variable is zero. After

substituting the decomposed variables into equations from (44) to (46), it can be easily shown that additional terms appear in the RANS equations due to the interactions between various turbulent fluctuations (see equations (50)).

a) $$\frac{\partial \rho}{\partial t} = \frac{\partial}{\partial x_i}\left(\rho U_i\right)$$

b) $$\frac{\partial}{\partial t}\left(\rho U_i\right) + \frac{\partial}{\partial x_i}\left(\rho U_i U_j\right) = \\ = -\frac{\partial p}{\partial x_i} + \frac{\partial}{\partial x_j}\left[\mu\left(\frac{\partial U_i}{\partial x_j} + \frac{\partial U_j}{\partial x_i} - \frac{2}{3}\delta_{ij}\frac{\partial U_l}{\partial x_l}\right)\right] + \frac{\partial}{\partial x_j}\left(-\rho\overline{u_i' u_j'}\right) \tag{50}$$

The additional terms, containing the products of velocity oscillating components, are commonly called Reynolds stresses and they have to be modelled to close the equations. Similar transport terms will arise when derivating a transport equation for any other scalar quantity; therefore a closure equation will be needed also for them.

A common closure method employs the Boussinesq hypothesis to model the Reynolds stresses which are related to the mean velocity gradients as shown in equation (51)

$$-\rho\overline{u_i' u_j'} = \mu_t\left(\frac{\partial U_i}{\partial x_j} + \frac{\partial U_j}{\partial x_i}\right) - \frac{2}{3}\left(\rho k + \mu_t \frac{\partial U_k}{\partial x_k}\right)\cdot \delta_{ij} \tag{51}$$

where $k = \frac{1}{2}\left(\overline{u'^2} + \overline{v'^2} + \overline{w'^2}\right)$ is defined as turbulent kinetic energy per unit mass and μ_t is the turbulent viscosity . The Boussinesq hypothesis is used in several turbulence model including, k-ε, k-ω and Spalart-Allmaras models. The disadvantage of the Boussinesq hypothesis is that it assumes μ_t to be an isotropic scalar quantity, which is not strictly true. Indeed, turbulence models based on such assumptions typically fail in situations where the anisotropy of turbulence has a dominant effect on the mean flow.

In this work turbulence modelling has been addressed by using the standard *k-ε* turbulence model whose first version was developed by Lauder and Spalding (1974) [107]. The standard *k-ε* model is a semi-empirical model based on the transport

equations for the turbulence kinetic energy *(k)* and its dissipation rate *(ε).* The transport equation for *k* is derived from the exact equation, while the transport equation for ε is obtained using physical reasoning since its exact transport equation contains many unknowns and unmeasurable terms. Both of them are presented hereafter

$$\text{a)}\quad \frac{\partial \rho k}{\partial t}+\frac{\partial}{\partial x_i}\left(\rho k U_i\right)=\frac{\partial}{\partial x_j}\left[\left(\mu+\frac{\mu_t}{\sigma_k}\right)\frac{\partial k}{\partial x_j}\right]+G_k+G_B-\rho\varepsilon+S_k$$

$$\text{b)}\quad \frac{\partial \rho \varepsilon}{\partial t}+\frac{\partial}{\partial x_i}\left(\rho \varepsilon U_i\right)=\frac{\partial}{\partial x_j}\left[\left(\mu+\frac{\mu_t}{\sigma_\varepsilon}\right)\frac{\partial \varepsilon}{\partial x_j}\right]+C_{1,\varepsilon}\frac{\varepsilon}{k}\left(G_k+C_{3,\varepsilon}G_B\right)+ -C_{2,\varepsilon}\rho\frac{\varepsilon^2}{k}+S_\varepsilon \qquad (52)$$

In the above equations, G_k represents the generation of turbulence kinetic energy due to the mean velocity gradients, G_B is the generation of turbulence kinetic energy due to buoyancy. $C_{1\varepsilon}$, $C_{2\varepsilon}$, and $C_{3\varepsilon}$ are constants; σ_k and σ_ε are the turbulent Prandtl numbers for *k* and ε, respectively. S_k and S_ε are source terms for turbulent kinetic energy and dissipation rate.

The turbulent viscosity μ_t is computed by combining *k* and ε as follows

$$\mu_t=\rho C_\mu\frac{k^2}{\varepsilon} \qquad (53)$$

where C_μ is a constant of the model.

The constants $C_{1\varepsilon}$, $C_{2\varepsilon}$, C_μ, σ_k and σ_ε have the following default values determined from experiments with air and water for common flow conditions including shears flows and decaying isotropic grid turbulence:

$C_{1\varepsilon}=1.44$, $C_{2\varepsilon}=1.92$, $C_\mu=0.09$, $\sigma_k=1$ and $\sigma_\varepsilon=1.3$.

The constant $C_{3\varepsilon}$ which determines how ε is affected by the buoyancy should be close to one for vertical buoyant shear layers and close to the zero for horizontal buoyant shear

layers [108]. In order to make possible the use of a single expression for $C_{3\varepsilon}$ Fluent uses the following relation

$$C_{3,\varepsilon} = \tanh\left(\frac{v}{u}\right) \tag{54}$$

where v is the component of the flow velocity parallel to the gravity vector and u is the perpendicular component [106].

The generation of turbulent kinetic energy due to the mean velocity gradients G_k can be computed as

$$G_k = \mu_t S^2 \tag{55}$$

where S is the modulus of the mean rate-of-strain tensor, defined as

$$S = \sqrt{2S_{ij}S_{ij}} \tag{56}$$

The generation of turbulence due to buoyancy is computed by

$$G_B = \beta g_i \frac{\mu_t}{\mathrm{Pr}_t}\frac{\partial T}{\partial x_i} \tag{57}$$

where β Is the coefficient of thermal expansion. g_i is the component of the gravity vector in the i^{th} direction, Pr_t is the turbulent Prandtl number by default assumed to be equal to 0.85. This approach is known as single gradient diffusion hypothesis (SGDH).

Once computed, turbulent kinetic energy *(k)* and turbulent dissipation rate *(ε)* can be used to define velocity scale θ and length scale l which are representative of the large scale turbulence [66]

$$\theta = k^{\frac{1}{2}} \qquad l = \frac{k^{\frac{3}{2}}}{\varepsilon} \tag{58}$$

The Reynolds stresses can be computed by using the Boussinesq approximation (see equation (51).

As already pointed out in the previous literature review, the standard k- ε model has been used and largely validated by the scientific community to simulate fire induced flows in tunnels. Several contributions assert that, if the model accounts for turbulence production and destruction due to the buoyancy effects, it is able to predict with reasonable accuracy the overall behaviour of tunnel fire induced flows [30,33,81-83,85,96,97]. Back-layering occurrence and back-layering distance are reasonably well predicted.

Some limitations of the k- ε turbulence model are evident when modelling highly anisotropic flow regions (i.e. the fire plume). Several works on the assessment of the k-ε model performance in this specific region are available in literature.

Nam and Bill (1993) noticed that the use of the standard k-ε model for simulating free plumes generates overpredictions in velocities and temperature at the central axis of the plume underpredicting the vertical spreading rate [109]. The same authors tried to correct the results by tuning the turbulent viscosity coefficient C_μ and the effective Prandtl number reporting an agreement to experimental data within 2%.

Most of the uncertainties are related to the source term due to buoyancy in the transport equation for ε which is poorly understood. Several variants for determining the coefficient $C_{3\varepsilon}$ have been resumed in [108]. Some authors reported that the modification of such coefficient has only a marginal effect in the final solution when simulating free plumes. The latter could in fact achieve a 10% accuracy when comparing numerical and experimental predictions [110]. However it must be noted that the grid resolution adopted was significantly poor. Controversial aspects on the value to be adopted for $C_{3\varepsilon}$ are also pointed out by [111].

Nevertheless, it is well known that, for any value of $C_{3\varepsilon}$, the k-ε model tends to underestimate vertical plume spread and to overestimate the spreading rate of horizontal ceiling layers [112]. Some improvements could be achieved by treating the buoyancy with a generalized gradient diffusion hypothesis (GGDH) which introduced the transversal density gradients into the buoyancy production term [108].

Several authors have tried this approach and, after tuning the model constants, they could improve the model predictions. However, the results are still limited given the lack of general applicability of the tuned models. For instance, Merci and co-workers adopted a GGDH approach to predict the critical velocity in a small scale tunnel; the accuracy of the numerical predictions, when compared to experimental findings, ranged between 8% and 38% depending on the fire scenario which is comparable with standard k- ε turbulence modelling.

3.5. Boundary conditions

3.5.1. Pressure boundary conditions

Constant pressure boundary conditions are used in situations where the exact details of the flow field are unknown but the boundary value of the pressure is known. When performing CFD simulations of tunnel ventilation flows and fires, pressure boundary conditions are usually enforced at the tunnel portals or at the top open surface of vertical shafts or chimneys.

There are several variations on how to apply pressure boundary conditions; the numerical tool adopted for the simulations (Fluent), in case of inflow conditions, requires the definition of a total stagnation pressure just outside the domain which is used by the solver to compute the static pressure just inside the domain. In case of outflow conditions, static pressure can be directly fixed.

From a mathematical point of view, more natural boundary condition would require the prescription of force per unit area as a normal component of the stress tensor [65] as described hereafter

$$\boldsymbol{\tau} \cdot \mathbf{n} - p\mathbf{n} = \psi_{\mathrm{N}} \tag{59}$$

where n is the unit vector normal to the specific boundary, $\boldsymbol{\tau}$ is the stress tensor, p is the pressure and ψ_{N} is the boundary value to be fixed. Clearly, being first derivatives of the velocity involved, equation (59) represents a *Neumann type boundary condition*. Under the assumption of negligible velocity gradients ($\boldsymbol{\tau} \cdot \mathbf{n} \sim 0$), the force per unit area indeed corresponds to the value of the pressure. However, the positioning of pressure boundary condition boundaries is a critical step as it must be always verified that the flow has reached a fully developed state having negligible gradients in the flow direction [66].

3.5.2. Velocity boundary conditions

Velocity inlet boundary conditions require all the flow variables to be specified at inlet boundaries. Typically, this approach is used to enforce a velocity profile or to model a solid wall moving with a prescribed velocity under no slip conditions. From a mathematical point of view this corresponds to a *Dirichlet type boundary condition* [65]. When performing CFD simulations of tunnel ventilation flows and fires, velocity boundary conditions are usually enforced when the ventilation conditions are known. This requires previous experimental test to be carried out in order to assess the ventilation conditions within a certain degree of accuracy. However, such approach is questionable as induces a decoupling between fire and ventilation flows.

3.5.3. Wall boundary conditions

No-slip conditions have been applied to all the velocity components at solid walls. Typically, a zero velocity component in the direction normal to the wall is the appropriate condition for the discretized continuity equation and discretized momentum equation in the direction normal to the wall. The estimation of the tangential and normal stresses at the wall (contained in the discretized momentum equations) requires extreme care given the typical turbulent nature of the flow. Indeed, a thin viscous sub-layer is located immediately adjacent to the wall followed by a buffer layer and a turbulent core. An extensive overview on the subject is given in [119] and is outside the scope of this document. However, the number of mesh points required to solve a turbulent boundary layer would be extremely large and commonly *wall functions* are used.

Wall functions are a collection of semi-empirical formulas and functions that interpolate the solution variables at the near-wall cells and the corresponding quantities at the wall. They usually comprise *laws-of-the-wall* for mean velocity and temperature (or other scalars) and correlations to prescribe near-wall turbulent quantities (k and ε specifically). In this work standard wall functions, based on the work of Lauder and Spalding [107], have been used. They are collected hereafter

$$u^+ = \frac{1}{\kappa}\ln\left(Ey^+\right)$$

where

$$u^+ = \frac{U}{u_\tau} \qquad (60)$$

$$y^+ = \frac{y\rho u_\tau}{\mu}$$

$$u_\tau = \sqrt{\frac{\tau_w}{\rho}}$$

and κ is the Von Karman constant (=0.4187), E wall roughness parameter (=9.8 for smooth walls), U is the mean fluid velocity, y the distance of the first grid point from the wall, u_τ a velocity scale, μ the fluid molecular viscosity and ρ the fluid density.

The log-law (equation (60)) is valid as long as the first grid point is located in the fluid region characterized by $30 < y^+ < 300$. Fluent by default uses the wall functions as described in (60) if $y^+ > 11.63$; if otherwise the code uses the laminar stress relationship known as linear law of the wall.

$$u^+ = y^+ \qquad (61)$$

However, intrusion of the first grid point in the viscous sub-layer should be avoided as the wall functions are based on the assumption that the rate of production of turbulent

kinetic energy equals the rate of dissipation which is true in the log-layer but not strictly true in the viscous sub-layer. This hypothesis is on the basis of two relationships between *k*, ε and the wall shear stress τ_w.

$$k = \frac{\tau_w / \rho}{\sqrt{C_\mu}}$$

$$\varepsilon = \frac{\left(\tau_w / \rho\right)^{\frac{3}{2}}}{\kappa\, y} \tag{62}$$

For heat transfer, a wall function approach based on the universal near wall temperature distribution has been used [107]. For uncompressible flow calculation Fluent uses the following relationships

$$T^+ = \frac{\left(T_w - T_P\right)\rho\, c_p u_\tau}{q_w} = \mathrm{Pr}_t\left(u^+ + P\right) \tag{63}$$

where T_w is the wall temperature, ρ the fluid density, c_p the fluid specific heat at constant pressure, q_w the wall heat flux, Pr_t the turbulent Prandtl number (=0.85 at the wall), and P is a correction function Pee-function, dependent on the ratio between laminar and turbulent Prandtl numbers [107]. Equation (63) is applied as long as y is larger than the non-dimensional sub-layer thickness defined as the intersection distance between the linear and the log-law of the wall. For smaller values of y a linear relationship between T^+ and y^+ is used

$$T^+ = \mathrm{Pr}\, y^+ \tag{64}$$

where *Pr* is the molecular Prandtl number of the fluid.

The previous relationships are valid for smooth walls where the changeover from laminar to turbulent flows is assumed to take place at $y^+=11.63$. For no smooth walls

the constant E contained in (60) and indirectly in (63) is adjusted accordingly. Further details are given in [106,119].

By combining equations (60) and (64) it is easy for example to determine the wall shear stress to be input as boundary condition for a near wall cell in turbulent flow conditions

$$\tau_w = \rho \frac{C_\mu^{1/4} k^{1/2} u}{u^+} \tag{65}$$

where u^+ must be determined depending on the correspondent wall law. Equation (65) is a combination of the wall tangent velocity (u) and its derivative contained in τ_w resulting in a *non-linear Robin type boundary condition* [120].

Similarly a heat flux boundary conditions can be introduced as

$$q_w = -\rho c_p \frac{C_\mu^{1/4} k^{1/2} \left(T - T_w\right)}{T^+} \tag{66}$$

Equation (66) is also a *Robin type boundary condition*. In case of adiabatic walls a zero normal derivative is enforced. If not specified, all the following simulations are conducted under the assumption of adiabatic walls. Other heat transfer boundary conditions to the walls could be used, but the adiabatic condition represents the worst case in terms of buoyancy strength, threat to people and damage to the structure [121].

3.5.4. Boundary conditions for the transport equations of turbulent quantities

The solution of two additional transport equations for turbulent kinetic energy and dissipation rate requires boundary conditions to be specified also for them.

Typically a profile for k and ε must be specified at inlets (i.e. tunnel portals or chimneys). Since in most of the cases no information is available in the literature, a rough estimation for inlets distributions for k and ε is obtained from the turbulent intensity and characteristic length (assumed for this case to be proportional to the tunnel hydraulic diameter D_h) can be conducted by means of the following simple forms [66].

$$k = \frac{2}{3}\left(U_{ref} i_t\right)^2$$

$$\varepsilon = \frac{2}{3} C_\mu^{3/4} \frac{k^{3/2}}{\ell} \tag{67}$$

$$\ell = 0.07 D_h$$

where i is the turbulent intensity, U_{ref} the reference inlet velocity, k the turbulent kinetic energy, C_μ the k-ε turbulence model constant, ℓ a characteristic length scale and D_h the tunnel hydraulic diameter.

At outlets, commonly, a zero normal derivative is enforced for k and ε.

At walls, a zero normal derivative is fixed for the turbulent kinetic energy as prescribed in [107]. A Dirichlet boundary condition is instead enforced for ε which is assumed to be equal to

$$\varepsilon = \frac{C_\mu^{3/4} k^{3/2}}{\kappa y} \tag{68}$$

where, C_μ is the *k-ε* turbulence model constant, k is the turbulent kinetic energy, κ is the Von Karman constant and y is the distance from the wall of the first grid point.

3.5.5. Fire representation

The fire has been modelled as a volumetric source of energy without using a dedicated combustion model. It has been shown that this simplified approach, previously used to model tunnel fires [85,95], is the most practical given its low computational cost and its ability to reproduce the overall behaviour of tunnel fire induced flows. It avoids the burden and the complexity of combustion and radiation models and the large uncertainty associated to the burning of condensed-phase fuels. Furthermore, it has been demonstrated that the same order of accuracy could be achieved when modelling a fire as volumetric source of heat or by adopting sophisticated combustion models [111]. In

the previous reference, the accuracy of the model predictions has been estimated by comparing numerical data against experimental data from a number of enclosure fires including large atria and small scale tunnel. Detailed combustion models and the volumetric source of heat approach produce reasonable results in most cases, but none of them are consistently accurate overall cases considered.

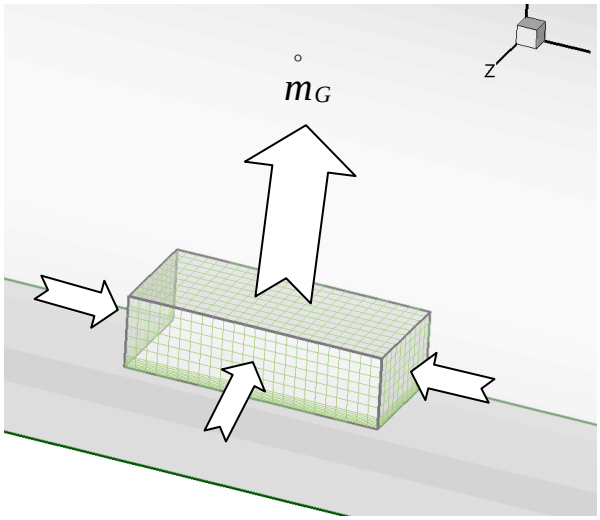

Figure 18: Schematic of the simplified fire representations used in this work.

In this work, the fire heat release rate (HRR), *Q*, has been introduced in the computational domain as a rectangular slab releasing hot gases from the top surface simulating a burning vehicle (see Figure 18). Mass conservation is applied by the extraction of air at the obstruction four lateral surfaces simulating air entrainment. For sake of generality the mass extraction from the lateral faces is uniform and independent from the ventilation conditions. This may not be completely true for high ventilation velocity but previous sensitivity studies have confirmed a minor impact of this modelling detail. The amount of gases injected into the domain ($\dot{m}_g$) is calculated using Equation (69) which correlates the convective part of the HRR, *Q(1-λ)*, to the temperature difference between air and hot gases:

$$\dot{m}_g = \frac{Q(1-\lambda)}{c_p(T_g - T_\infty)} \qquad (69)$$

where λ is the flame radiative fraction, $(T_g - T_\infty)$ is the temperature difference between ambient air and hot combustion products, Q the fire HRR and c_p the air specific heat.

The flame radiative fraction λ can be up to 50 % [113] but most measured values are around 35% (value used in this work). The main limitation of this approach is that the maximum flame temperatures are not accurate very close to the fire source. However, as demonstrated by Vega et al. [95] and by Karki and Patankar [85], this methodology produces a good overall agreement with experimental temperature measurements of away from the flames.

There is little information in the literature on the gas phase temperature in a tunnel close to the fire and its dependence on the ventilation conditions and fire size. Some experimental data are reported in the Runehamar tests in Norway, where the measured gas temperature above the centre of fire ranged between 1100 K and 1500 K [114]. The same temperature range has been considered in this paper and the corresponding sensitivity of the solution investigated.

This modelling approach requires the definition of the top slab surface dimensions and its dependence on the fire size. A surface too small would bring unrealistic air behaviour given the corresponding excessively high inlet velocity for the hot gases and the wrong balance between the momentum and buoyancy of the fire source. Thus, the fire Froude number Q* is used here to link HRR and size of the fire source [115], defined as

$$Q^* = \frac{Q}{\rho_\infty c_p T_\infty D_f^{\,2} \sqrt{g D_f}} \tag{70}$$

where D_f is the characteristic dimension of the fire source (hydraulic diameter of the slab top surface). Values of Q* above 2.5 are not realistic for diffusion flames [113]. Hence, the dimension of the fire source is calculated setting Equation (70) equal to 1, indicating a regime where the momentum and buoyancy strengths are of the same order of magnitude. This choice is supported by the fact that typical tunnel fires can be

represented as a crib fires [116,117] that, following [118], have Froude number in the range of 1.

3.5.6. Jet Fan representation

CFD modelling of tunnel ventilation flows requires also a representation of the jet fans. Previous CFD analyses of tunnel ventilation [85,95] simulated the jet fans as a combination of discharge source and intake sinks of momentum and mass. This kind of approach has not been used in this paper avoiding the discrepancies in energy, momentum and species conservations that are generated by uncoupling discharge sources and intake sinks. The methodology used here simulates the real construction of the jet fans as a cylindrical fluid region delimitated by walls and containing an internal cross surface where a constant positive pressure jump is enforced. Since no data on the specific jet fan characteristic curve were available, the pressure rise across the jet fan internal cross section has been supposed to be independent of the average normal air velocity. A schematic of the jet fan modelling approach is depicted in Figure 19; the internal jet fan surfaces used to fix the positive pressure difference have been highlighted in red.

However, in order to accurately predict the thrust with this approach or any other, it is highly recommended to use experimental data for calibration or validation of the results. This approach has been implemented successfully to model jet fan installed in a real tunnel where the comparison with experimental flow measurements is excellent (Colella et al. 2009 [102] and Colella et al. 2010 [103]).

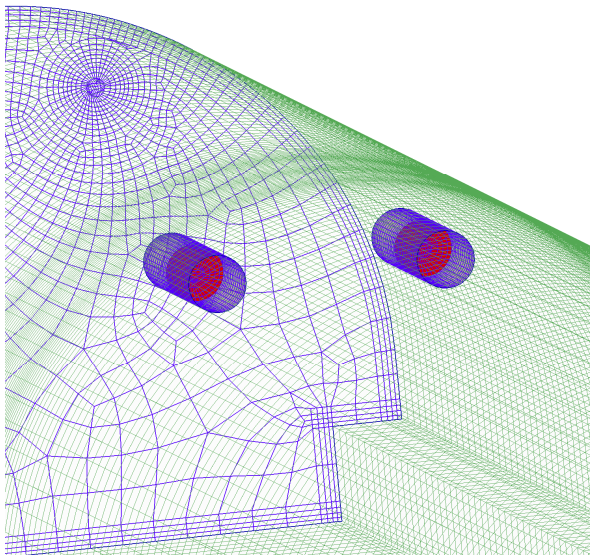

Figure 19: Schematic of mesh used the fan representations used in this work.

3.6. Numerical features

The complete set of partial differential equations including, mass, momentum, and energy conservation equations as well as the transport equations for turbulent kinetic energy and dissipation rate, cannot be solved directly. Numerical methods allow the conversion of the governing equations into a set of algebraic equations whose derivation can be performed using different strategies.

The first step involve a discretization of the domain, also knows as meshing, which allows the description of a continuous field variable θ into a set of discrete values θ_i defined at each mesh node.

The commercial CFD package Fluent adopts a finite volume approach to derive the set of algebraic equations. Such technique uses a formal volume integration of the governing equations over each of the control volumes generated by the meshing procedure. A simplified 1D control volume integration of the governing equations has been also presented in chapter 2. A detailed description of all the numerical aspects involved in the discretization of the governing equation is beyond the scope of this document but the interested reader can refer to [66]. However, some important aspects related to the settings of the CFD model are worth to be discussed.

The integration of the governing equation over the control volumes requires the estimation of the variable at the boundary interface. In this work the convective fluxes and have been approximated by using a second-order upwind scheme [69].

Temporal discretization has been treated by using a first order implicit time integration as already described in chapter 2. The advantage of the fully implicit scheme is that it is unconditionally stable for any time step size [70].

The pressure-velocity linkage has been resolved by adopting the SIMPLE algorithm due to Patankar and Spading (1972) [71]. An adapted version of the algorithm has been developed for fluid network systems and presented in chapter 2. A segregated solution algorithm has been adopted for the calculation. The sequence of operations performed by the CFD solver is resumed in Figure 20.

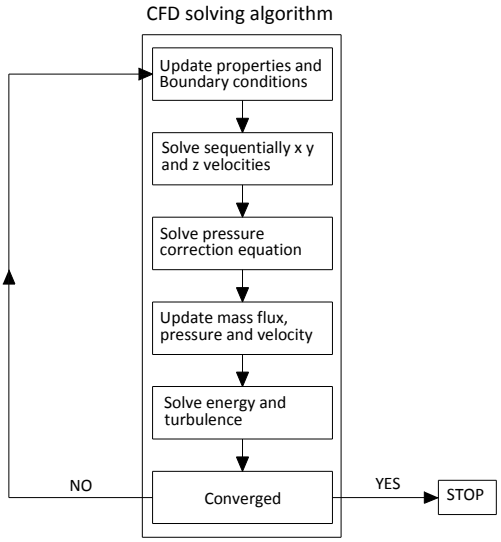

Figure 20: Schematic of the CFD segregated solution algorithm.

The degree of convergence of the solution has been estimated by using scaled residual and by monitoring integral values of relevant quantities (typically mass flow rate through tunnel portals) during the solution procedure. The simulations have been considered to be converged when the scaled residuals were lower than 10^{-5} with the exception of the energy equation where the maximum allowed value was 10^{-7}.

Given the complex geometries typically encountered in tunnel environments (i.e. horseshoe cross sections, intersections with shafts, jet fan geometry) a quasi-structured

meshing approach has been used. Once produced a base mesh case, the grid has been systematically refined in order to assess whether or not a grid-independent solution was reached. The refining has been iterated until no substantial variations both in the local field data and integral values were observed. A detailed grid independence analysis has been performed for any CFD or multiscale calculation presented hereafter.

3.7. Case Studies

3.7.1. Ventilation flows in the Norfolk road Tunnels

A CFD model been used to simulate the ventilation flows in the Norfolk tunnels, Sydney (AU). The tunnels are 460 m long with a virtually flat gradient. Each tunnel, longitudinally ventilated, is equipped with 6 pairs of jet fans, rated by the manufacturer at the volumetric flow rate of 34.2 m^3/s with a discharge velocity of 34.7 m/s. A schematic of the tunnel cross section including the jet fan installation arrangement is presented in Figure 21.

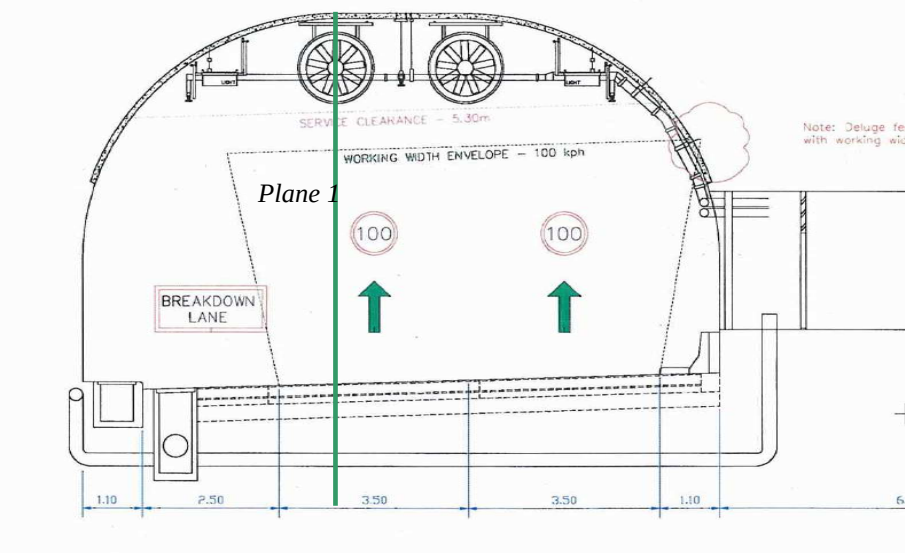

Figure 21: Schematic of the Norfolk road tunnels cross section.

On the basis of the data provided by the tunnel operator, we were not able of accurately defining the longitudinal position of the jet fans within each tube; therefore, they have been considered approximately 80 m spaced as depicted in Figure 22.

Ventilation flow measurements were made available for the Westbound tunnel; they were taken by SickFlow 200 units located at the centre of each tunnel tube (~ 230 m from the inlet portal). Being the units located in the vicinity of jet fans, for some ventilation scenarios the wind speed sensor readings are affected by adjacent jet fan. In these scenarios the accuracy of readings is compromised since they did not represent the real average velocity in the cross section.

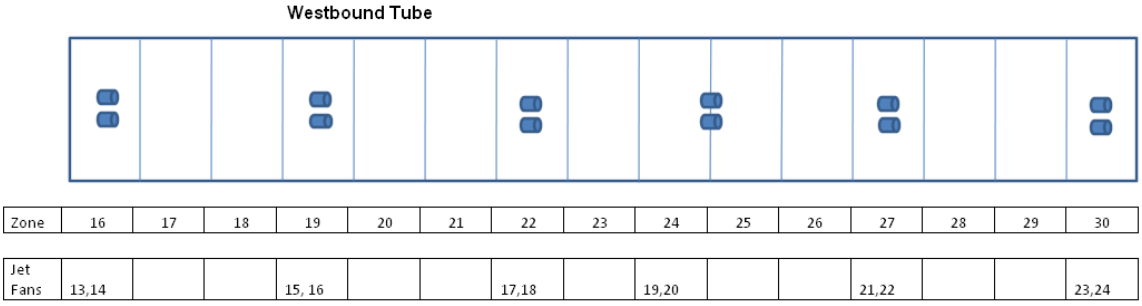

Figure 22: Schematic of the jet fan longitudinal position in the Westbound Norfolk road tunnel; jet fans are numbered from 13 to 24.

16 different ventilation scenarios have been considered during the experimental measurements. The main characteristics of each scenario are resumed in Table 8. Scenarios having the measurement unit located in the vicinity of an operating jet fan are highlighted in grey and they have been discarded. In these cases, the measured air velocity is strongly dependent on the distance between fan and measurement unit and too little information of the effective fan and sensor locations was available.

scenario	sub scenarios	Jet fan pairs						experimental velocity [m/s]	predicted velocity [m/s]	mass flow rate [kg/s]
		13-14	15,16	17,18	19,20	21,22	23,24			
1	1.1	OFF	OFF	OFF	OFF	OFF	ON	1.94	1.14	101.3
	1.2	OFF	OFF	OFF	OFF	ON	ON	4.16	4.28	379.3
	1.3	OFF	OFF	OFF	ON	ON	ON	5	5.77	510.8
2	2.1	ON	OFF	OFF	OFF	OFF	OFF	2.7	3.9	339.2
	2.2	ON	ON	OFF	OFF	OFF	OFF	5.27	5.66	470.7
	2.3	ON	ON	ON	OFF	OFF	OFF	15.3	-	
3	3.1	ON	ON	ON	OFF	OFF	OFF	15.3	-	
	3.2	ON	ON	ON	ON	OFF	OFF	15.8	-	
	3.3	ON	ON	ON	ON	ON	OFF	16.4	-	
	3.4	ON	ON	ON	ON	ON	ON	16.9	-	
4	4.1	OFF	OFF	ON	OFF	OFF	OFF	14.4	-	
	4.2	OFF	OFF	OFF	ON	OFF	OFF	3.33	3.83	339.4
	4.3	OFF	OFF	ON	ON	OFF	OFF	15.3	-	
5	5.1	OFF	ON	OFF	OFF	OFF	OFF	3.33	4.06	338.4
	5.2	OFF	ON	OFF	OFF	ON	OFF	5.83	5.2	470.5
6	6.1	OFF	ON	OFF	ON	OFF	ON	6.1	6.25	512.8

Table 8: Summary of ventilation scenarios explored during the experimental campaign conducted in the Westbound Norfolk road tunnel. Scenarios having the measurement unit located in the vicinity of an operating jet fan have been highlighted in grey.

3.7.2. Assessment of the mesh requirements

The computational domain has been discretized by using a quasi structured mesh arrangement. Various CFD runs have been also conducted to asses the mesh requirements. Four different meshes have been generated and the resulting solutions compared. The mesh density per meter of tunnel length ranged from 260 cells/m up to 6200 cells/m. The symmetry of the domain across the longitudinal plane was considered since the explored ventilation scenarios involved activated jet fan pairs arranged symmetrically in respect to the tunnel longitudinal section. Four examples of the mesh cross sections are presented in Figure 23. The test case used for the grid sensitivity analysis corresponds to scenario 2.1 and involves only 2 operating jet fans (#13 and #14 in Figure 22).

The solution is shown to converge as the mesh is made finer. A coarse mesh of 260 cells/m leads to a 16% underestimation of the average ventilation velocity. But a finer mesh of 2500 cells/m leads to results within 0.36% of the prediction made with the finest mesh.

	mesh density [cells/m]	predicted velocity [m/s]	deviation from mesh 4
mesh 1	260	3.125	16.41%
mesh 2	700	3.360	10.13%
mesh 3	2800	3.752	0.36%
mesh 4	6200	3.739	-

Table 9: Grid Independence Study for a scenario involving an operating jet fan pair in the Norfolk tunnels

Besides the comparison of the average quantities, detailed field solutions have been compared at Reference Sections 1 and 2, located 10 m and 100 m downstream of the jet fan discharge surface, respectively. The comparison of the longitudinal velocity is plotted in Figure 24 for the Reference Section 1 and in Figure 25 for the Reference Section 2

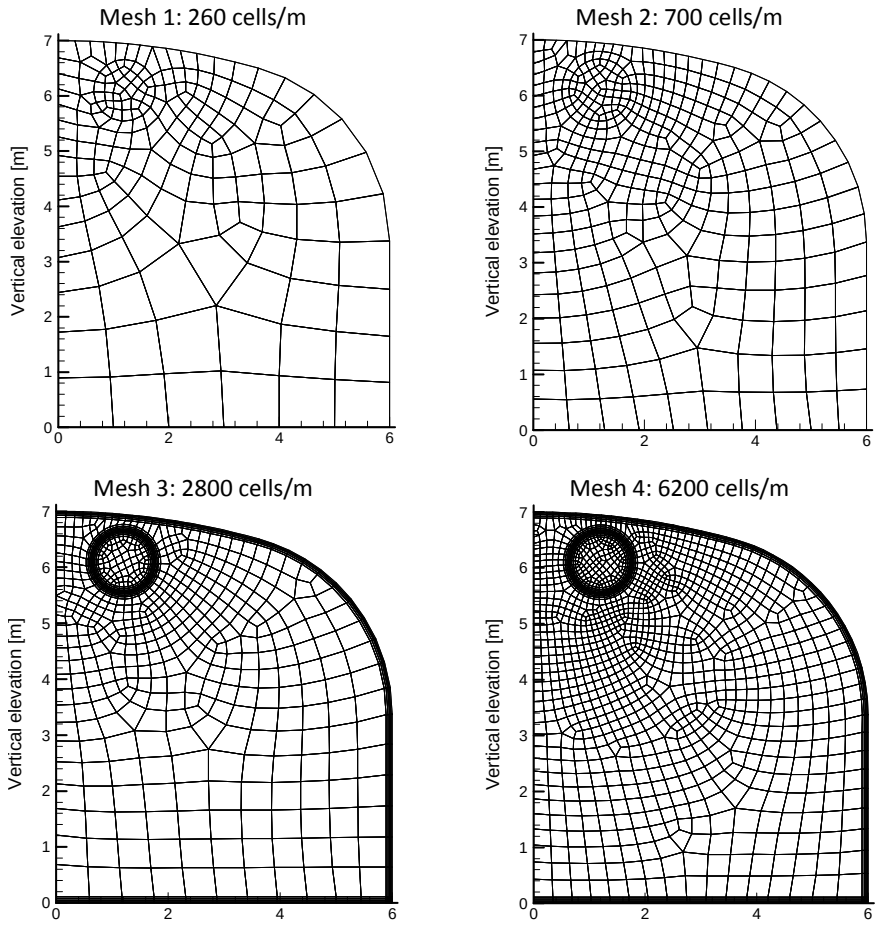

Figure 23: Examples of the different meshes used for half of the tunnel cross section and number of cells per unit length of tunnel.

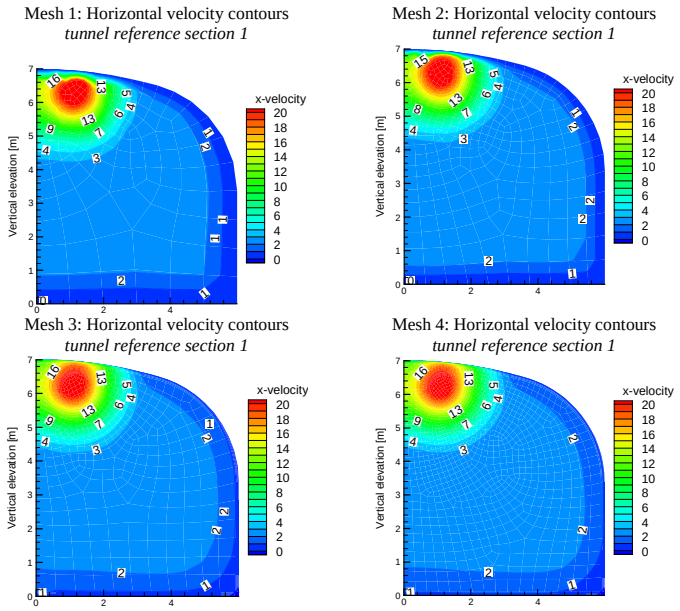

Figure 24: Comparison of the longitudinal velocity contours for meshes #1 to #4 in the tunnel at the reference section 1. Velocity values are expressed in m/s.

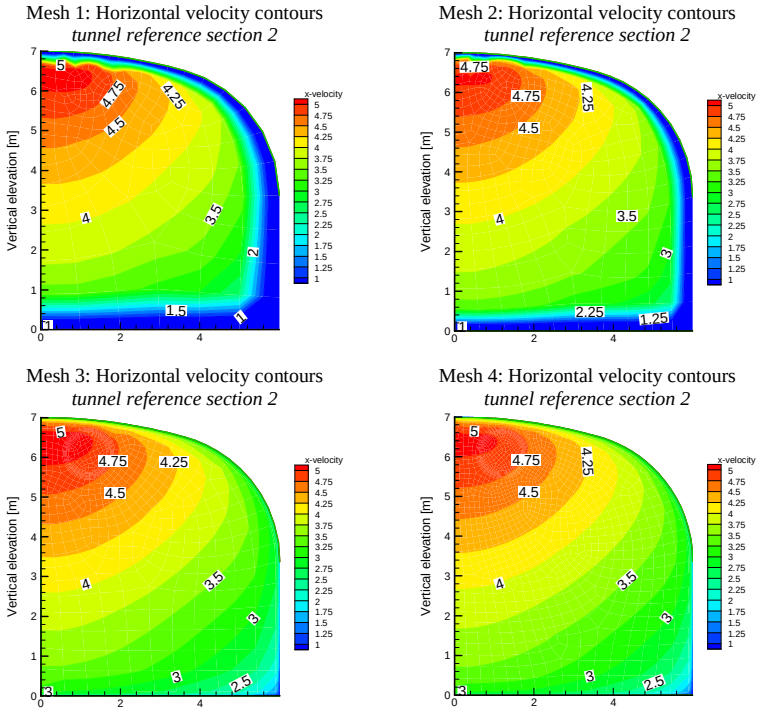

Figure 25: Comparison of the longitudinal velocity contours for meshes #1 to #4 in the tunnel at the reference section 2. Velocity values are expressed in m/s.

As expected from the previous results, the computed solutions show larger deviations for the coarse meshes 1 and 2 while convergence is obtained for finer meshes 3 and 4. Based on the results, grid independence is considered reached in mesh 3 and therefore, the following simulations have been conducted using this grid. The total number of nodes for the 460 m long tunnel is around 1.3 million and the resulting computing time for a steady state scenario ranged between 3 and 5 hours in a modern quad-core workstation.

3.7.3. Simulations of the ventilation scenarios and comparison to on-site measurements

The developed model has been used to simulate 9 ventilation scenarios from Table 8. The computed velocity profiles in the jet-fan longitudinal plane (plane 1 in Figure 21) are presented in Figure 26.

The available experimental data have been used to corroborate the model predictions. The comparison is presented in Figure 40. Generally, accurate velocity predictions could be achieved having an average relative deviation from experimental findings

around 17%. The maximum deviation (~40%) has been found for the ventilation scenario 2.1. Given the lack of detailed information on the jet fan installation arrangement, geometry and longitudinal position, the accuracy achieved is considered satisfactory and no other attempts to improve the numerical predictions have been performed. However it is believed that, if more detailed geometric details are provided, significantly better predictions can be achieved.

The model results confirm the very low efficiency of ventilation scenario 1.1 which was also observed experimentally. This is due to the unfavourable location of the jet fans 23 and 24 (see Figure 39). Indeed, they are too close to the tunnel outlet portal to allow their discharge velocity cones to develop and generate enough thrust.

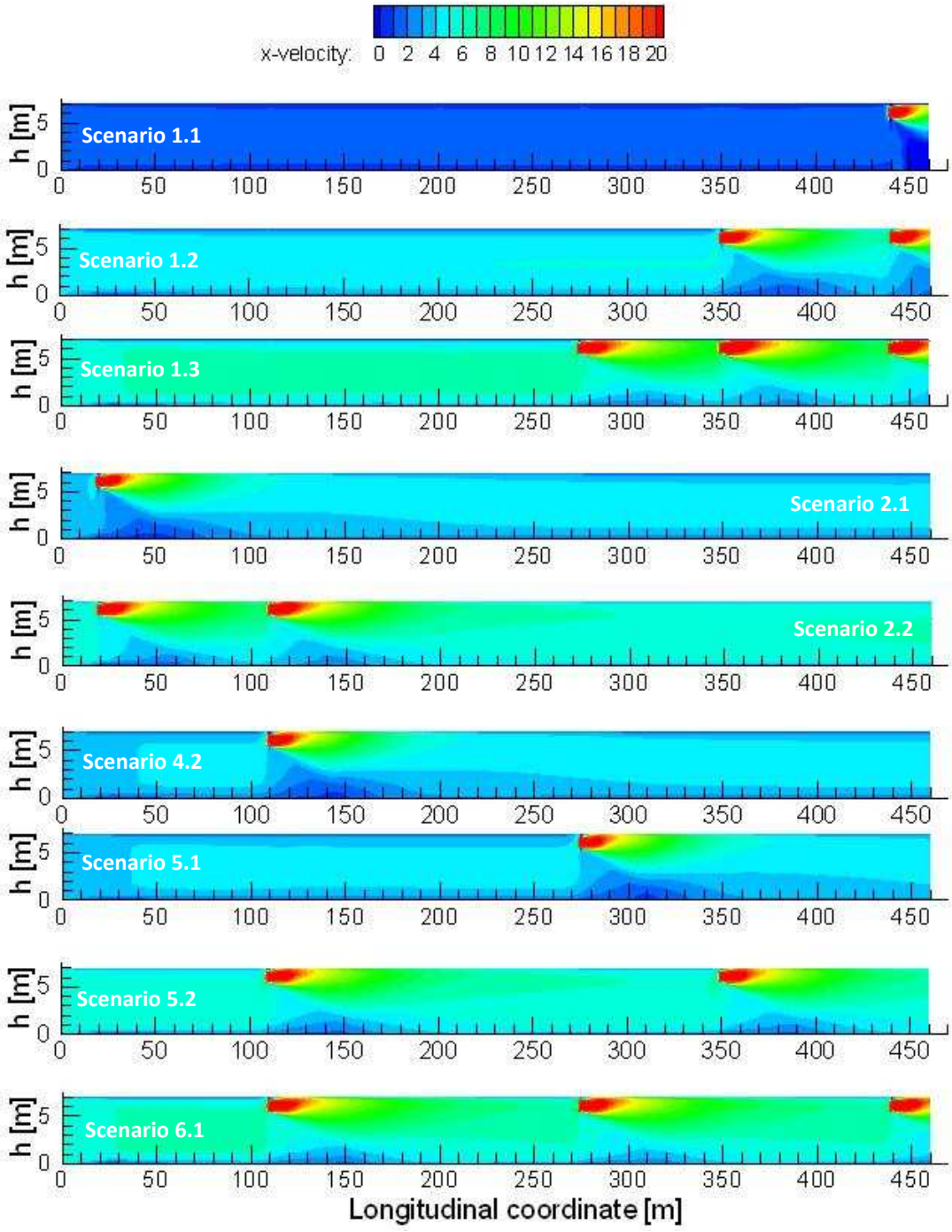

Figure 26: Computed velocity profile in the tunnel for scenarios 1.1, 1.2, 1.3, 2.1, 2.2, 4.2, 5.1, 5.2, 6.1 from Table 8. The plotted velocity fields are relative to plane 1 of Figure 21. Velocity values are expressed in m/s.

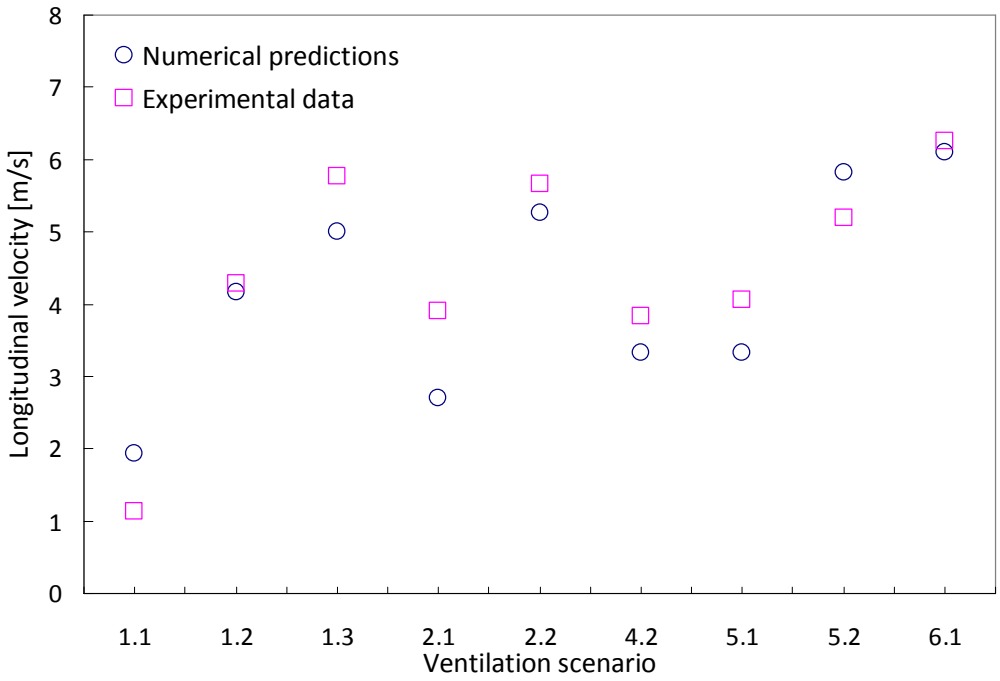

Figure 27: Comparison between predicted velocity and experimental measurements provided by the Sickflow 200 Units located at the centre of each tunnel tube.

Table 8 contains also the predictions of the mass flow rates through the tunnel for each ventilation scenario. It can be seen that, scenarios 2.1, 4.2 and 5.1, involving only one operating jet fan pair, are equivalent since the same mass flow rate through the tunnel is generated (~338 kg/s). Same conclusion can be deduced when analysing scenarios 2.2 and 5.2 which involve 2 operating jet fan pairs. In the last two cases the ventilation induced flow through the tunnel is around ~470 kg/s. In the ventilation scenarios involving 3 jet fan pairs (1.3 and 6.1) an average ventilation induced flow of 510 kg/s could be attained.

A final CFD run has been performed to assess the ventilation system performance when all the 6 jet fan pairs are operating (ventilation scenario 3.4 in Table 8). In this ventilation scenario the predicted mass flow rate through the tunnel is around 764 kg/s corresponding to an average longitudinal velocity of around 8.5 m/s. A schematic of the CFD predictions is presented in Figure 28.

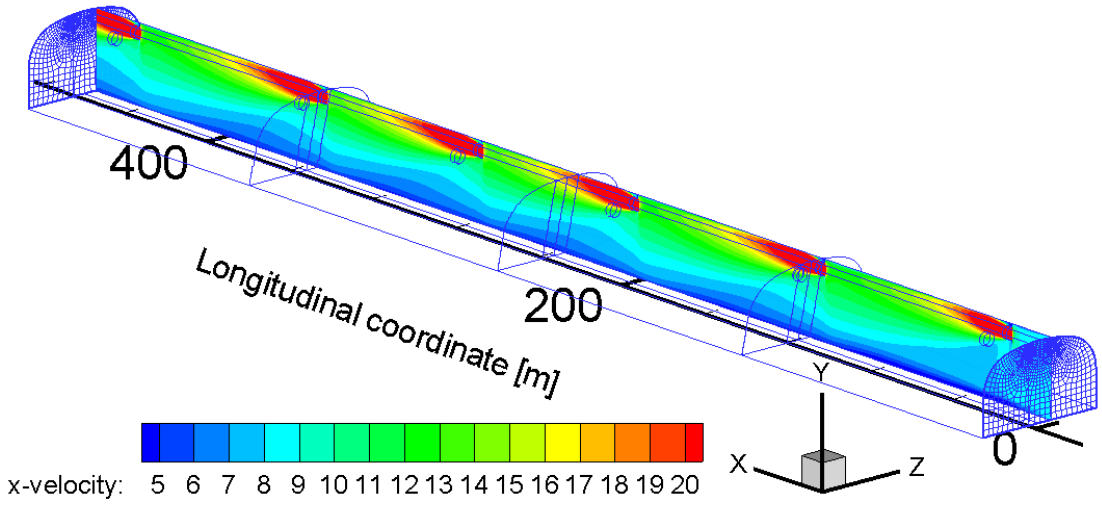

Figure 28: 3D visualisation of the computed velocity fields for ventilation scenario 3.4 involving all the 6 jet fan pairs. Velocity values are expressed in m/s. (not to scale).

3.7.4. Critical velocity calculation

Wu and Bakar [33] carried out a series of small scale experiments on five horizontal tunnels with different cross-sections. They assessed, on the basis of accurate measurements in a controlled environment, the effect on the critical velocity of tunnel cross section and fire heat release rate. Among the different cross sections, the data relative to the square cross-sectional tunnel (0.25×0.25 m^2 cross section) will be considered in this document. The small scale tunnel is around 15 m long and it is equipped with a circular porous bed propane burner (diameter equal to 0.106 m) located at a distance of 6.21 m from the tunnel inlet. The tunnel outlet is located at a distance of 8.7 m from the burner centre. The tunnel upstream section was constructed of PMMA, while, the fire and the fire downstream regions were constructed of steel. A water spray device was constructed to cool the tunnel walls near the fire source and was used only when the tunnel wall temperature was excessive. The ventilation flow during the experiments was driven by an air compressor. A schematic of the experimental rig is depicted in Figure 29.

The burner heat release rate, controlled by the propane flow rate, was varied during the tests ranging between 1.5 kW and 30 kW. These fire sizes correspond to fires of

approximately 2.5÷50MW in a tunnel of diameter around 5 m and 300 m long when a scaling procedure is applied (see equations (10) and (11)).

The measured values of critical velocities in two different fire scenarios (3 kW and 30 kW) will be used in this section to validate the fire CFD model. The same scenarios have been used by Van Maele and Merci [97] to validate two different turbulence modelling approaches (RANS and LES). They also adopted a mixture fraction model to simulate the combustion process. Their results will be taken into account when evaluating the performance of the simplified fire model previously presented in this chapter.

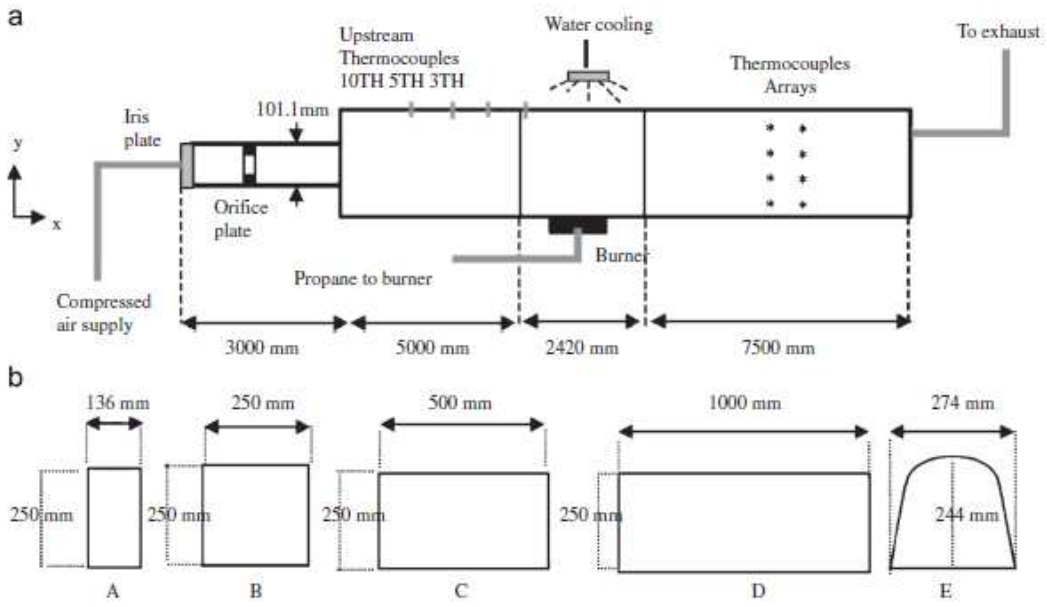

Figure 29: Schematic of the experimental rig accordingly to Wu and Bakar [33]. Section B has been used in this study.

3.7.5. Assessment of the mesh requirements

The computational domain has been discretized by using a structured mesh arrangement. The upstream edge of the fire source has been located 5 m downstream of the inlet section of the CFD domain. The length of the simulated CFD domain is 10 m. Various CFD runs have been also conducted to asses the mesh requirements. Four different meshes have been generated and the resulting solutions compared. The mesh size ranged from 37000 up to 1300000 nodes. The symmetry of the domain across the longitudinal plane was considered. Four examples of the mesh cross sections are presented in Figure 30.

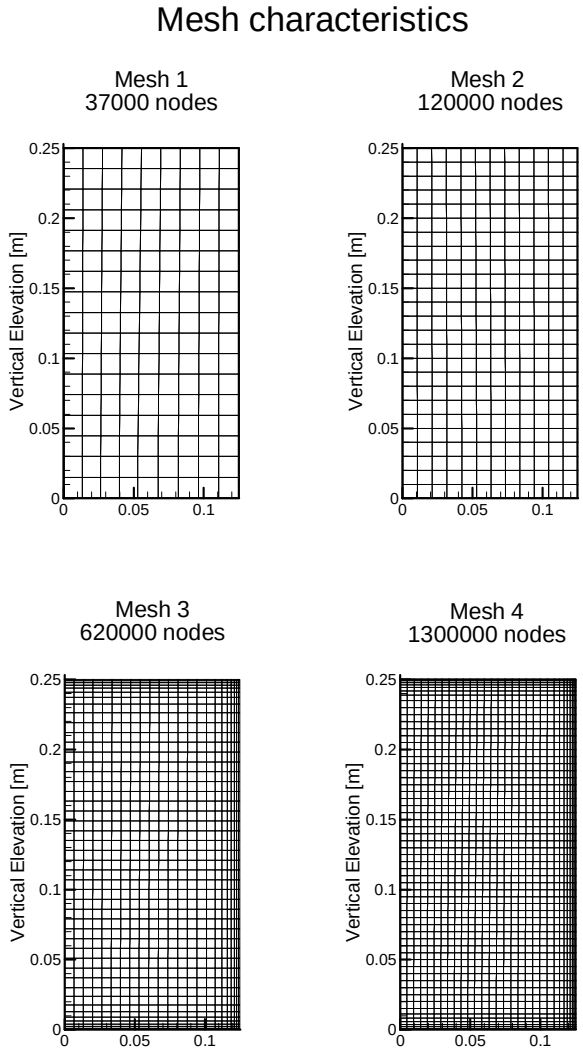

Figure 30: Examples of the different meshes used for half of the tunnel cross section and number of cells per unit length of tunnel.

The simulations, conducted for a 30kW fire scenario at critical ventilation conditions, have been compared first in terms of the predicted critical velocity (see Table 10).

The solution is shown to converge as the mesh is made finer. The adoption of mesh #1 leads to an 11% underestimation of the critical ventilation velocity when compared to the finest mesh (#4) results. No appreciable variation in the critical velocity predictions could be observed when the computations have been performed using mesh #3.

	mesh size [cells]	predicted critical velocity [m/s]	deviation from mesh 4
mesh 1	37000	0.49	8.89%
mesh 2	120000	0.46	2.22%
mesh 3	620000	0.45	0.00%
mesh 4	1300000	0.45	-

Table 10: Grid Independence Study for a scenario involving a 30 kW fire scenario

Besides, detailed field solutions have been compared at Reference Sections 1 and 2, located 1 m and 3 m downstream of the fire source, respectively. The predicted longitudinal velocities and temperature fields are plotted in Figure 31 for Reference Section 1 and in Figure 32 for Reference Section 2.

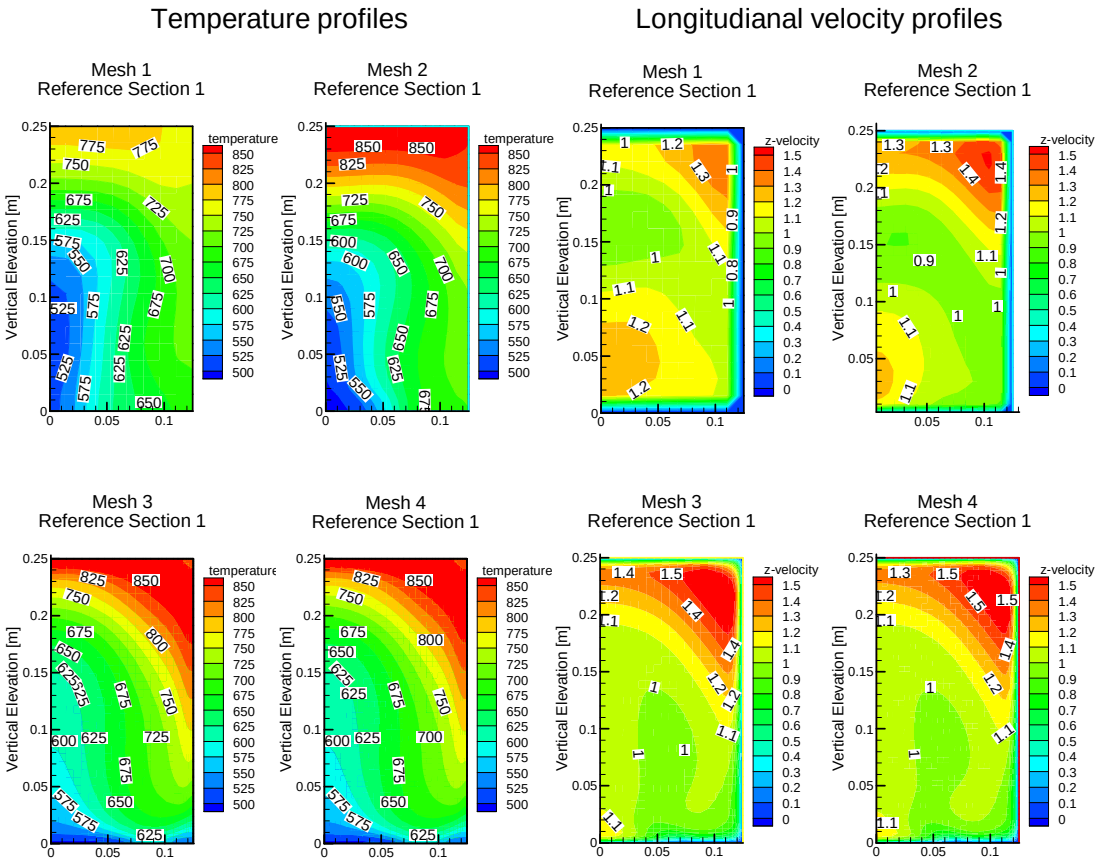

Figure 31: Computed temperature and velocity fields for mesh #1 to #4 at reference sections 1 for a 30 kW fire at critical ventilation conditions. Temperature and velocity values are expressed in K and m/s respectively.

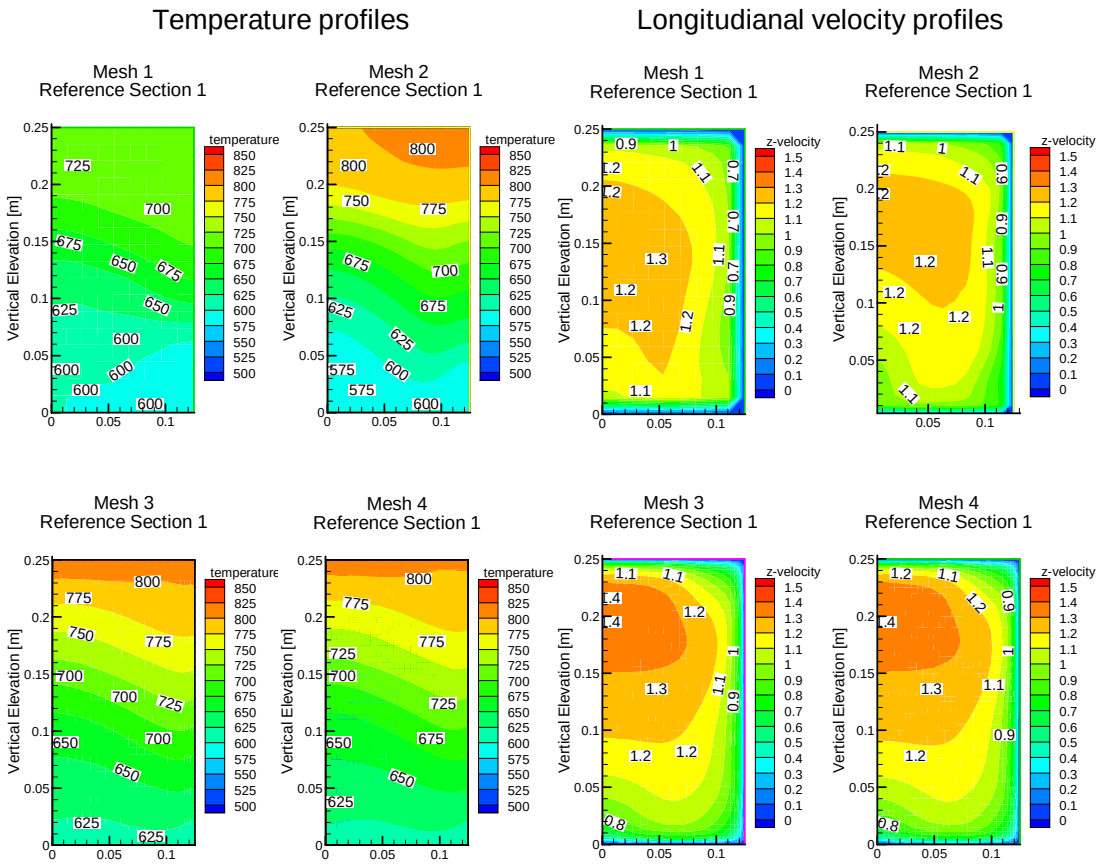

Figure 32: Computed temperature and velocity fields for mesh #1 to #4 at reference sections 2 for a 30 kW fire at critical ventilation conditions. Temperature and velocity values are expressed in K and m/s respectively.

As expected from the previous results, the computed solutions show larger deviations for the coarse meshes 1 and 2 while convergence is obtained for finer meshes 3 and 4. Based on the results, grid independence is considered reached in mesh 3 and therefore, all the following simulations have been conducted using this grid. The total number of nodes for the 10 m long small scale tunnel is around 1.3 million and the resulting computing time for a steady state scenario ranged between 2 and 4 hours in a modern quad-core workstation.

3.7.6. Critical velocity results

Two scenarios have been simulated first involving a 30 kW and a 3 kW fire. The size of the fire source has been calculated using the scaling relations as presented in equations (69) and (70) under the assumption of fire source Froude number equal to 1. The

corresponding sizes of the fire source are 0.042 m^2 and 0.007 m^2 for the 30 kW and 3 kW fire, respectively.

Following the same approach presented in [97], the simulated fire is considered to be at critical ventilation condition when the velocity component parallel to the tunnel axis becomes around zero in the computational cell adjacent to the tunnel ceiling and above the leading edge of the burner. The computed critical ventilation velocities are respectively 0.36 m/s and 0.45 m/s for 3 kW and the 30 kW fire scenarios, underestimating the experimental findings by around 25 % in both the cases. Indeed, the measured critical velocity values are 0.48 m/s and 0.6 m/s for the 3 kW and 30 kW fire, respectively.

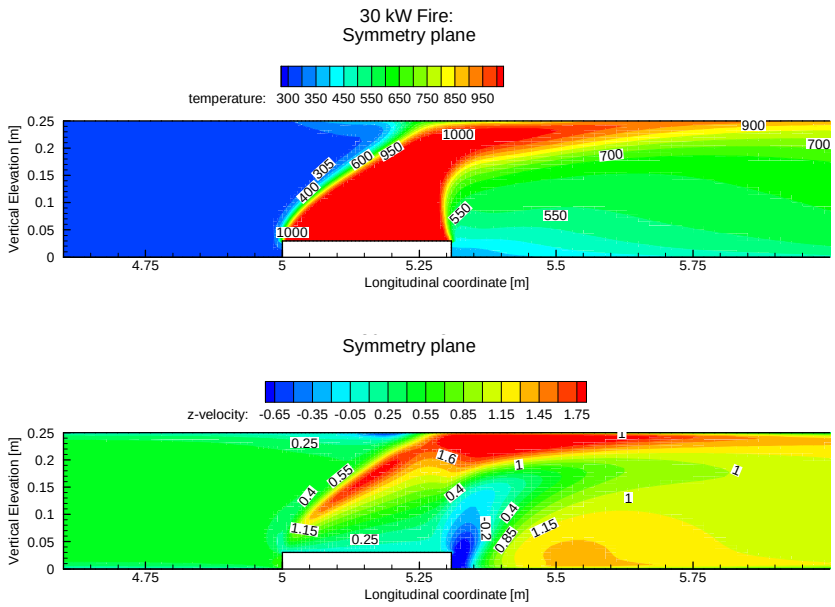

Figure 33: Computed temperature and velocity fields in the vicinity of the fire source for a 30 kW fire at critical ventilation conditions. Temperature and velocity values are expressed in K and m/s respectively.

A schematic of the computed temperature and longitudinal velocity field in the vicinity of a 30 kW fire source at critical ventilation conditions is presented in Figure 33. An initial stage of back-layering occurrence is confirmed by the presence of a region characterized by sustained backward motions in the region located immediately above the fire source. Same conclusion can be obtained by observing the high temperature gases stratified in same regions. Temperature and longitudinal velocity fields have been

also plotted for reference section 1 and reference section 2 located 1 and 3 m downstream of the fire source, respectively (see Figure 34).

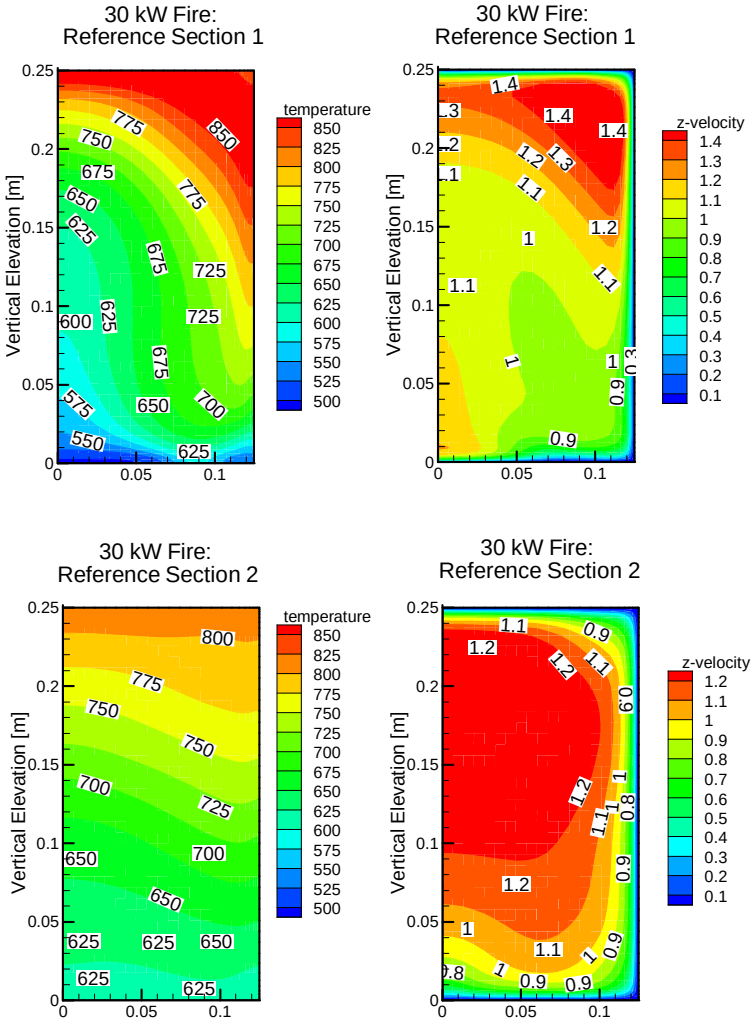

Figure 34: Computed temperature and velocity fields at reference sections 1 and 2 for a 30 kW fire at critical ventilation conditions. Temperature and velocity values are expressed in K and m/s respectively.

The velocity and temperature isocontours show a complex flow pattern at reference section 1. Instead, the temperature contours show that the flow has a stratified structure with almost horizontal layers at reference section 2. It has been verified that in this region the maximum transversal velocity components are almost two orders of magnitude smaller than the maximum longitudinal velocity. This confirms that, at reference section 2, the flow has evolved to fully developed channel flow which is essentially 1D with small recirculation patterns. As a consequence, the details of the

flow beyond this point do not influence the flow pattern near the burner surface and hence the prediction of the critical velocity.

Same considerations can be obtained for the 3 kW fire. The computed temperature and longitudinal velocity fields in the fire near field are presented in Figure 35 while temperature and longitudinal velocity fields at reference sections 1 and 2 are presented in Figure 36.

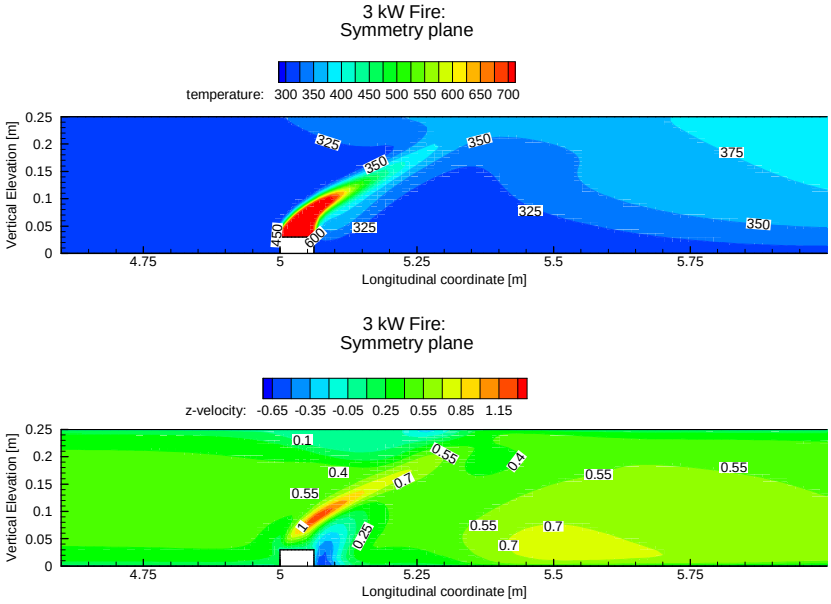

Figure 35: Computed temperature and velocity fields in the vicinity of the fire source for a 3 kW fire at critical ventilation conditions. Temperature and velocity values are expressed in K and m/s respectively.

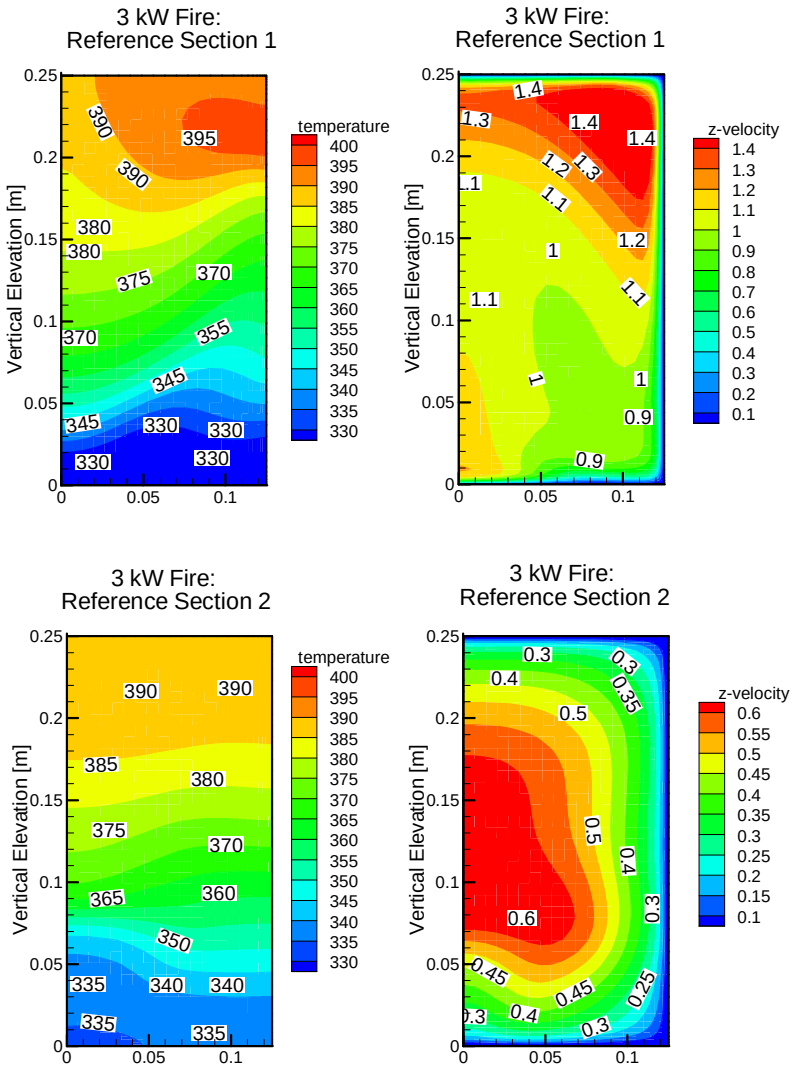

Figure 36: Computed temperature and velocity fields at reference sections 1 and 2 for a 3 kW fire at critical ventilation conditions. Temperature and velocity values are expressed in K and m/s respectively.

These two fire scenarios have been analysed by Van Maele and Merci [97] by using two different CFD tools: Fluent and FDS.

The first simulations have been conducted with Fluent by using a modified version of the k-ε turbulence model in which the turbulence production due to buoyancy has been treated by using the generalized gradient diffusion hypothesis briefly described in this chapter. Combustion has been addressed by adopting a mixture fraction approach. The critical velocity predictions underestimate the experimental values by around 8.5% and 31% for the 30 kW and 3 kW fire respectively.

Poorer predictions have been achieved when adopting the second CFD package (FDS) which is based on LES turbulence modelling. The LES model systematically over-predicted the experimental critical velocity data by 21% and 40% for the 3 kW and 30 kW fire scenarios, respectively. The simplified fire representation developed in this work, leads to a critical velocity under-estimation (25% in both the cases) which is comparable with the accuracy that could be achieved adopting higher sophisticated modelling approaches for turbulence and combustion. On the other hand, the resulting computing time is smaller since species transport equations and combustion phenomena are not solved. This is a point in favour of the simplified representation of the fire that will be used in the remaining part of this work.

3.7.7. Effect of the fire Froude number on the critical velocity

The previous simulations have been conducted under the assumption that the fire Froude number is equal to 1 and the temperature of the hot combustion gases released by the horizontal slab is equal to around 1100 K. An initial study conducted by varying the temperature of the combustion products between 1100 K and 1500 K has shown that it has a very minor impact on the predicted critical velocity. Therefore it has been omitted. A much larger impact on the critical velocity predictions was observed when varying the fire source Froude number and therefore a sensitivity study has been undertaken. A wide range of Froude numbers (between 0.5 a 5) has been investigated in order to include the largest portion of possible fire scenarios involving different fuels [6]. Also in this case two different fire sizes (3 kW and 30 kW) have been considered for the sensitivity study and the results are resumed in Figure 37.

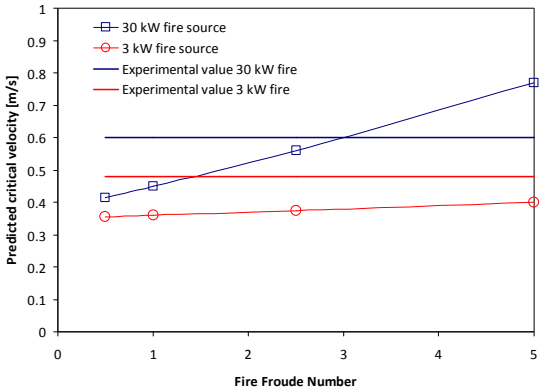

Figure 37: Effect o fire Froude number on the predicted critical for a 3 kW and a 30 kW fire

The numerical analysis shows that there is a linear correlation between the predicted critical velocity and the fire source Froude number at least within the range of Froude number investigated. As expected, the slope seems to be correlated to the fire HRR being higher for larger fire sizes. A 100 % increase in the predicted critical velocity has been found for the 30 kW fire scenario when the Froude number was increased from 0.5 to 5. Around 10 % increase has been found for the 3 kW fire source. An analysis of this behaviour on the basis of Froude scaling theory has been undertaken but no conclusive results have been obtained and therefore the subject is currently under investigation.

3.8. Concluding Remarks

The chapter describes the application of CFD techniques to tunnel ventilation flows and fires. An overview of the literature studies since the first application in the late 90s has been given. The review process showed that CFD models are able to predict critical ventilation velocity, and back layering distance within an acceptable level of accuracy (deviation usually smaller than 30%). The overall flow data (i.e. bulk velocity and temperature) are also accurately predicted with deviations from experimental values typically within 20%. On the other hand the literature study, showed that prediction on local flow field data (i.e. velocity and temperatures), especially if calculated in the vicinity of the fire source, can be affected by error significantly higher than 100% in comparison to experimental measurements.

An overview of CFD model characteristics including turbulence model, typical boundary conditions for tunnel ventilation flows and fires and numerical features has also been provided. A simplified approach to deal with the fire source has also been developed. The fire has been modelled as a rectangular slab releasing hot combustion products without using a dedicated combustion model. This approach does not provide accurate results in the flame region but allows for reasonable accuracy when dealing with the overall tunnel flow behaviour (i.e. far field temperature and velocity, critical velocity and back layering distance). A comparison to the experimental findings from two small scale tunnel fire scenarios (3 kW and 30 kW) studied by Wu and Bakar [33] confirmed the ability of the simplified fire model to predict the critical velocity with a reasonable level of accuracy (~ 25%). A similar level of accuracy for the same fire

scenarios was also achieved by Van Maele and Merci [97] that adopted a dedicated combustion model and more sophisticated turbulence models.

Furthermore, the ability of the developed CFD tool to deal with cold flow ventilation scenarios has been assessed. The developed model has been validated against experimental velocity data measured in 9 different ventilation scenarios in the Norfolk Tunnels in Sydney (AU). Also in this case a significant level of accuracy (average relative deviation around 17%) has been achieved.

The CFD analyses have shown that significant computational resources (several hours of computing time in a modern 4-core workstation) were required to simulate a single steady state ventilation or fire scenario in relatively short tunnels. Indeed the small-scale tunnel was 15 m long (300 m on large scale if the diameter is scaled up to 5 m) while the Norfolk tunnels are 460 m in length. The computational time would become a severe limitation when the full CFD approach is adopted to deal with fire or ventilation behaviour in tunnels several kilometres in length. For these scenarios, a way to avoid such high computational complexity is the adoption of multiscale methods based on hybrid 1D-3D computational techniques. The application of multiscale methods in the framework of tunnel ventilation flows and fires is the subject of the following chapters.

Parts of this work have been published in *Building and Environment [102]*, *Tunnelling and Underground Space Technology [103]* and *Fire Technology [105]*.

4

Fundamentals of multiscale computing

4.1. Introduction

CFD models of tunnel fires have been shown to predict the overall behaviour of the ventilation system (i.e. critical ventilation velocity and back-layering distance) within an acceptable range of accuracy (namely, within 10÷30% deviation). Several studies on the subject have been reviewed and discussed in the previous chapter. However, almost 90% of the reviewed papers focused only on the back-layering occurrence without directly referring to the capabilities of the installed ventilation system (i.e. how many fans to be activated in order to prevent back-layering). Indeed, the ventilation velocity to be input as boundary condition into the model is supposed to be known on the basis of rough estimations or cold flow experimental tests conducted in the tunnel. This kind of approach does not allow a critical evaluation of the ventilation system performance under different fire hazards as ventilation velocities and fire behaviour are not coupled together.

The reason for this trend highlighted in the literature review process, is due to the very large computational demand typical for comprehensive CFD studies of ventilation system performance during fires. The high computational cost leads to the practical problem that arises when the CFD model has to consider boundary conditions or flow characteristics in locations far away from the region of interest. This is the case of tunnel portals, ventilation stations or jet fan series located long distances away from the fire. In these cases, even if only a limited region of the tunnel has to be investigated (e.g. for the fire), an accurate solution of the flow movement requires that the numerical model includes all the active ventilation devices and the whole tunnel layout. For typical tunnels, this could mean that the computational domain is several kilometres long.

The study of ventilation and fire-induced flows in tunnels [30,33,85,95,97,102] provides the evidence that in the vicinity of operating jet fans or close to the fire source the flow field has a complex 3D behaviour with large transversal and longitudinal temperature and velocity gradients. The flow in these regions needs to be calculated using CFD tools since any other simpler approach would only lead to inaccurate results. These regions are hereafter named as the *near field*. However, it has been demonstrated for cold flow scenarios and for fire scenarios that some distance downstream of these regions, the temperature and velocity gradients in the transversal direction tend to disappear and the flow becomes essentially 1D. In this portion of the domain the transversal components of the velocity can be up to two orders of magnitude smaller than the longitudinal components. These regions are hereafter named as the *far field*. The use of CFD models to simulate the fluid behaviour in the far field leads to large increases in the computational requirements but very small improvements in the accuracy of the results. A visual example of typical velocity and temperature fields established in the vicinity of an operating jet fan or fire is presented in Figure 38.

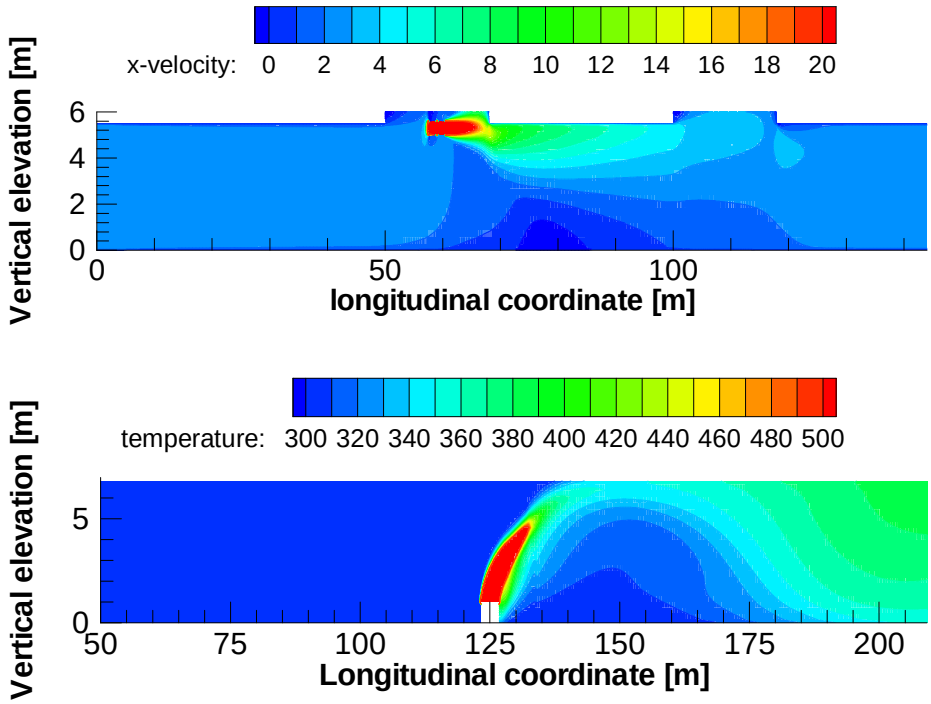

Figure 38: up) Example computed velocity field for a pair of operating jet fans (jet fan discharge velocity ~34 m/s; down) Example computed temperature field for a 30MW fire subject to supercritical ventilation conditions. The velocity and temperature values are expressed in m/s and K, respectively.

On the basis of these observations and for the sake of an efficient allocation of resources, CFD should be applied only to model the near field regions while the far field regions should be simulated using a 1D model. These types of hybrid model are commonly called *multiscale models.* Multiscale models allow a significant reduction in the computational time as the more time consuming tool is applied only to a limited portion of the domain.

In a multiscale approach, the CFD and the 1D models exchange flow information at the 1D-CFD interfaces. There are two general coupling options. The simplest one is the *1-way coupling* (or superposition). For example, in the case of inclined tunnels, it is possible to evaluate the global chimney effect using a 1D model of the entire tunnel [122]. Then, a CFD analysis of specific tunnel portions can be run using as boundary conditions the 1D results. This approach does not represent true multiscale modelling since there is no coupling of the CFD results to the 1D flow. This would be equivalent to assume that the flow behaviour in the high gradient regions does not affect the bulk tunnel flow.

A *2-way coupling* of 1D and CFD models, proper multiscale modelling, consists of a physical decomposition of the problem in two parts: a portion of the tunnel is simulated using a CFD model and the remaining portions through 1D model. The advantage of multiscale modelling resides on including in the flow calculations the effect of the fire on the entire ventilation system and vice versa. If the solver is able to receive the two sets of equations, the problem can be solved at once. In most of the cases there is a different solver for each model, and therefore iterative calculations are necessary with the two solvers continuously exchanging information at boundary interfaces.

Few examples of multiscale modelling fluid flow systems have been found in the literature. Examples include the simulation of blood flow in the circulatory system [123], the computation of gas flows in exhaust ducts of internal combustion engines [124], the characterization of the flow pattern over high speed trains moving through tunnels [125]. Recent applications of multiscale techniques address also the problem of naturally fractured oil reservoirs [127]. Multiscale methods have been only cited as possible techniques for simulating tunnel ventilation flows and fires by Rey and co-workers (2009) [126] without any significant results.

4.2. Fundamental of domain decomposition methods

Multiscale techniques are based on domain decomposition methods which have been developed for all the discretization techniques (i.e. finite difference, finite volume and finite elements) mainly in the framework of parallel computing. They allow the original single problem to be reformulated on several computational sub-domains. Eventually, this technique can be applied to solve heterogeneous problems which are described by different governing equation as in the present case.

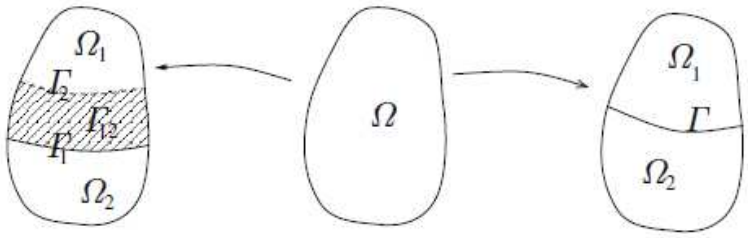

Figure 39: Example of domain decomposition with and without overlapping [65].

The basic idea is to decompose the global domain in several sub-domains and to solve the resulting problems characterized by smaller domain size eventually by means of parallel computing. Domain decomposition can be performed adopting two different techniques which generate overlapping and non-overlapping sub-domains. A visual example of sub-domain decomposition with and without overlapping is depicted in Figure 39.

Three iterative methods based on domain decomposition are available in the literature and they are mainly differentiated by the boundary conditions applied at the interfaces and by the presence of overlapping regions [128]:

- *Dirichlet-Dirichlet* or *Schwarz methods*
- *Dirichlet- Neumann methods*
- *Neumann - Neumann methods*

Schwarz methods are applied for overlapping domain decomposition and use Dirichlet type boundary conditions applied on Γ_1 and Γ_2 for the sub-domains Ω_1 and Ω_2, respectively (see Figure 39).

Dirichlet-Neumann methods are applied for non-overlapping domain decomposition and use one Dirichlet-type boundary condition and one Neumann-type boundary condition.

Neumann-Neumann methods are applied for non-overlapping domain decomposition and use only Neumann-type boundary conditions applied on Γ for the sub-domains Ω_1 and Ω_2, respectively (see Figure 39).

A description of the mathematical theory behind domain decomposition methods is beyond the scope of this document. The interested reader should refer to [128].

The exact structure of the boundary conditions to be applied at the interfaces depends on the differential operator defining the original set partial differential equations. In the case of Navier-Stokes equations only Dirichlet-Neumann and Schwartz methods are used. Being S the Navier-Stokes operator, a Dirichlet-Neumann iterative method must perform the following sequence of operating until convergence is achieved [65]

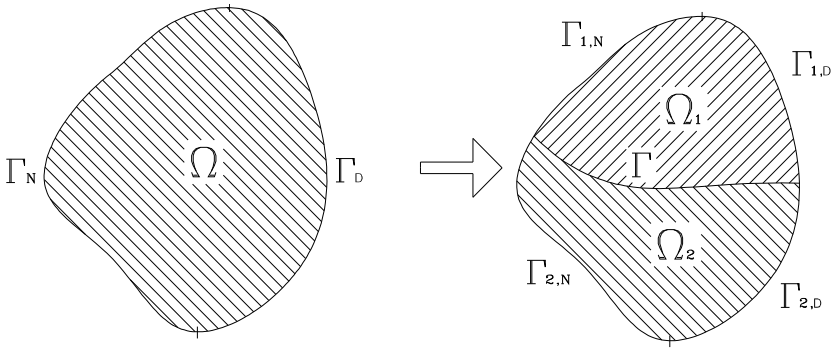

Figure 40: Example of domain decomposition for solution of Navier-Stokes problem using a Dirichlet-Neumann iterative method.

a.
$$\begin{cases} \mathbf{S}\left(\mathbf{u}_2^{k+1}, p_2^{k+1}\right) = \mathbf{f} \quad in\ \Omega_2 \\ \mu \dfrac{\partial \mathbf{u}_2^{k+1}}{\partial n} - p_2^{k+1} = \mu \dfrac{\partial \mathbf{u}_1^{k}}{\partial n} - p_1^{k} \quad on\ \Gamma \\ \mathbf{u}_2^{k+1} = \varphi_2 \quad on\ \Gamma_{2,D} \\ \mu \dfrac{\partial \mathbf{u}_2^{k+1}}{\partial n} - p_2^{k+1} = \psi_2 \quad on\ \Gamma_{2,N} \end{cases} \tag{71}$$

b.
$$\begin{cases} \mathbf{S}\left(\mathbf{u}_1^{k+1}, p_1^{k+1}\right) = \mathbf{f} \quad in\ \Omega_1 \\ \mathbf{u}_1^{k+1} = \alpha\, \mathbf{u}_2^{k+1} + (1-\alpha)\mathbf{u}_2^{k} \quad on\ \Gamma \\ \mathbf{u}_1^{k+1} = \varphi_1 \quad on\ \Gamma_{1,D} \\ \mu \dfrac{\partial \mathbf{u}_1^{k+1}}{\partial n} - p_1^{k+1} = \psi_1 \quad on\ \Gamma_{1,N} \end{cases}$$

where

- φ_2 a φ_1 are vectorial functions describing the Dirichlet boundary conditions (e.g. prescribed velocities) at the boundary $\Gamma_{2,D}$ and $\Gamma_{1,D}$ of the sub-domains Ω_1 and Ω_2 (refer to Figure 40)
- ψ_2 a ψ_1 are vectorial functions describing the Neumann boundary conditions (e.g. prescribed normal stresses) at the boundary $\Gamma_{2,N}$ and $\Gamma_{1,N}$ of the sub-domains Ω_1 and Ω_2 (refer to Figure 40)
- k is the multiscale iteration counter, α is a velocity under-relaxation parameter required to improve convergence and n the normal coordinate.

It is here stressed that when a Dirichlet-Neumann method is adopted, the sub-domains Ω_1 and Ω_2 must not overlap.

Schwartz methods require overlapping sub-domains and Dirichlet boundary conditions prescribed on both the resulting interfaces Γ_2 and Γ_1.

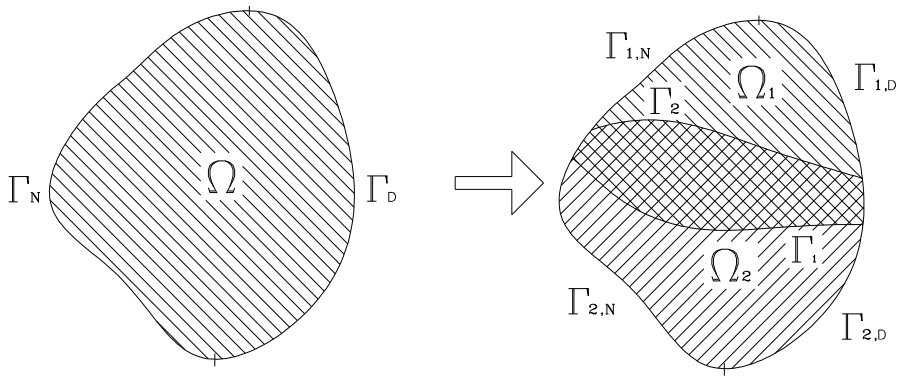

Figure 41: Example of domain decomposition for solution of Navier-Stokes problem using a Schwartz (Dirichlet-Dirichlet) iterative method.

Being *S* the Navier-Stokes operator a Schwartz iterative method must perform the following sequence of operating until convergence is achieved [65]

$$\text{a.}\quad \begin{cases} \mathbf{S}\left(\mathbf{u}_1^{k+1}, p_1^{k+1}\right) = \mathbf{f} \quad in\ \Omega_1 \\ \mathbf{u}_1^{k+1} = \mathbf{u}_2^{k} \quad on\ \Gamma_1 \\ \mathbf{u}_1^{k+1} = \varphi_1 \quad on\ \Gamma_{1,D} \\ \mu \dfrac{\partial \mathbf{u}_1^{k+1}}{\partial n} - p_1^{k+1} = \psi_1 \quad on\ \Gamma_{1,N} \end{cases} \qquad (72)$$

$$\text{b.}\quad \begin{cases} \mathbf{S}\left(\mathbf{u}_2^{k+1}, p_2^{k+1}\right) = \mathbf{f} \quad in\ \Omega_2 \\ \mathbf{u}_2^{k+1} = \mathbf{u}_1^{k+1} \quad on\ \Gamma_2 \\ \mathbf{u}_2^{k+1} = \varphi_2 \quad on\ \Gamma_{2,D} \\ \mu \dfrac{\partial \mathbf{u}_2^{k+1}}{\partial n} - p_2^{k+1} = \psi_2 \quad on\ \Gamma_{2,N} \end{cases}$$

where

- φ_2 a φ_1 are vectorial functions describing the Dirichlet boundary conditions (e.g. prescribed velocities) at the boundary $\Gamma_{2,D}$ and $\Gamma_{1,D}$ of the sub-domains Ω_1 and Ω_2 (refer to Figure 40)

- ψ_2 a ψ_1 are vectorial functions describing the Neumann boundary conditions (e.g. prescribed normal stresses) at the boundary $\Gamma_{2,N}$ and $\Gamma_{1,N}$ of the sub-domains Ω_1 and Ω_2 (refer to Figure 40)

- k is the multiscale iteration counter and n the normal coordinate.

The main advantage of Schwarz method is the easy way of dividing the sub-domains from a possibly complicated geometry. The main drawback is that the convergence of the iteration depends on the overlap [129].

4.3. Formulation of the multiscale problem

The multiscale model developed in this work is based on domain decomposition techniques which have been proved to be adequate to solve also heterogeneous problems described by different governing equations [128]. In this specific case the tunnel fluid-dynamic behaviour has been addressed by adopting two different numerical descriptions of the problem based on 1D and 3D-CFD tools.

For sake of simplicity and only in this section, it is supposed that the tunnel domain (Ω) is decomposed in two sub-domains Ω_{1D} and Ω_{3D} where the 1D model (see section 2) and the CFD model (see section 3) are respectively applied. Ω_{1D} and Ω_{3D} are built in order to be continuous in the streamwise direction. Figure 42 depicts a schematic of a 1D-3D domain decomposition. The 1D-3D interface Γ_a is located in $x=a$ in such way that there is no overlapping between the two sub-domains.

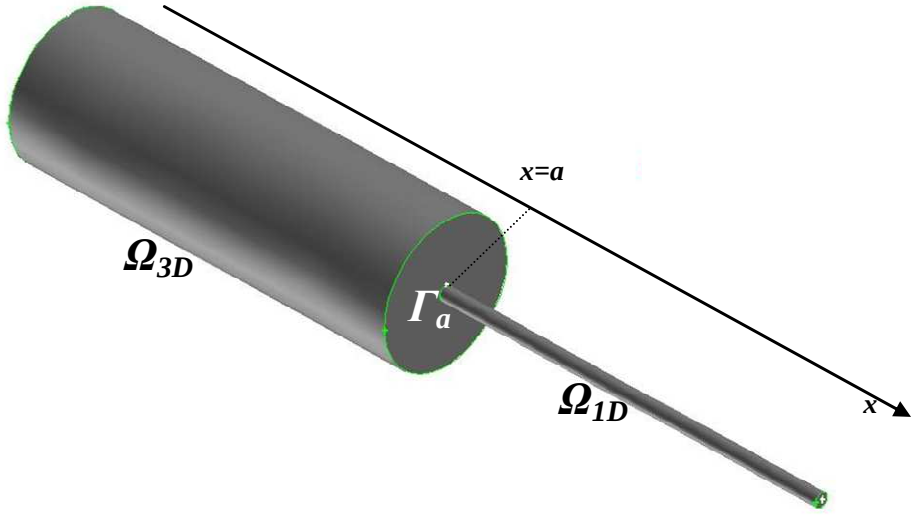

Figure 42: Example of a domain decomposition in 1D and 3D sub-domains.

On the right hand side of Γ_a the 1D domain provides average values for pressure, temperature, velocity and mass flow rate; they are indicated as $\overline{p}(a^+)$, $\overline{T}(a^+)$, $\overline{u}(a^+)$ and consequently $\dot{m}(a^+)$, respectively. Analogously, the same quantities can be defined for the left side of Γ_a but, since the left hand side of Γ_a belongs to the 3D domain, integral averaged values must be computed (see equation (73)).

$$
\begin{aligned}
&a)\quad \overline{u}(a^-) = \frac{1}{|\Gamma_a|}\int_{\Gamma_a} \mathbf{u}\cdot\mathbf{n}\, d\sigma \\
&b)\quad \overline{p}(a^-) = \frac{1}{|\Gamma_a|}\int_{\Gamma_a} p\, d\sigma \\
&c)\quad \overline{T}(a^-) = \frac{\int_{\Gamma_a} \rho T |\mathbf{u}\cdot\mathbf{n}|\, d\sigma}{\int_{\Gamma_a} \rho |\mathbf{u}\cdot\mathbf{n}|\, d\sigma} \\
&d)\quad \dot{m}(a^-) = \int_{\Gamma_a} \rho\mathbf{u}\cdot\mathbf{n}\, d\sigma
\end{aligned}
\qquad (73)
$$

where u represents the velocity vector, p the pressure, ρ the density, T the temperature, **n** the unitary vector normal to the interface $\Gamma_{a.}$

Following the same approach presented in [123], it is reasonable to look for the continuity of the following quantities at the interface:

a. Area $A(a^-) = A(a^+)$

b. Mean pressure $\overline{p}(a^-) = \overline{p}(a^+)$

c. Mean velocity $\overline{v}(a^-) = \overline{v}(a^+)$ (74)

d. Mean temperature $\overline{T}(a^-) = \overline{T}(a^+)$

The same authors underline that instead of the constraint (74).b, the continuity of the averaged normal stresses could also be prescribed; however, being the normal stresses partially neglected in the 1D model, and the 1D-3D interfaces located in regions where the flow is fully developed ($\frac{\partial u}{\partial x} \approx 0$), the previous constraint on the pressure is adequate. However, the accuracy of such assumption will be checked in each multiscale computation by assessing how its location affects the global results. The solution of the coupled multiscale problem cannot be reached by means of standard computing algorithm but it is based on iterative computing procedures developed in the framework of domain decomposition methods. Obviously, being the sub-domains without overlapping regions, a Dirichlet-Neumann coupling strategy will be adopted.

4.4. Coupling technique

4.4.1. Direct coupling

The solution to the multiscale problem requires the coupling of the 1D and CFD models which has been obtained by means of a Dirichlet-Neumann strategy. In particular Dirichlet boundary conditions (i.e. velocity boundary conditions) are prescribed at the interfaces for the 1D model. Neumann boundary conditions (i.e. pressure boundary conditions) are instead prescribed at the interfaces for the CFD model.

The iterative solving algorithm will be presented for a general case in which a CFD model of the near field domain (Ω_{3D}) is coupled with two 1D models of far field domains ($\Omega_{1,1D}$ and $\Omega_{2,1D}$) located upstream and downstream, respectively. Two interfaces Γ_i and Γ_j are therefore generated (see Figure 43).

The algorithm requires a dynamic exchange of information between the models during the computation. A three stage coupling has been adopted for the scope (see Figure 43).

A full 1D model of the whole system is solved during the first stage.

A CFD model of the near field domain Ω_{3D} is solved during the second stage. Its boundary conditions at Γ_i and Γ_j are provided by the full 1D model run at the first stage.

The global multiscale convergence is reached during the third stage when the 1D model of the far fields ($\Omega_{1,1D}$ and $\Omega_{2,1D}$) and the CFD model of the near field (Ω_{3D}) are run sequentially *k-times* exchanging periodically the boundary conditions at the interfaces Γ_i and Γ_j (see Figure 43).

In comparison to more traditional coupling approaches, a three stage coupling allows a significant reduction of the multiscale iterations needed to reach a global convergence.

The complete sequence of operations to be conducted during the solving procedure is described hereafter:

STAGE 1

a. Run the full 1D model of the whole system until convergence is reached

b. Total pressure and temperature values at the nodes corresponding to the interfaces Γ_i and Γ_j are recorded (to be used as boundary conditions of the Ω_{3D} CFD model in the next stage)

STAGE 2

a. Run the CFD model of the near field Ω_{3D} until a certain degree of convergence is reached

b. Calculate average velocity values at the interfaces Γ_i and Γ_j (to be used as boundary conditions for the 1D model of the far fields in the next stage)

c. Calculate average temperature values at the interfaces Γ_i and Γ_j (to be used as boundary conditions for the 1D model of the far field in the next stage)

STAGE 3

a. Run the 1D model of the far fields $\Omega_{1,1D}$ and $\Omega_{2,1D}$ until convergence is reached

b. Pressure and temperature values at the Γ_i and Γ_j are recorded as used as boundary conditions in step c.

c. Run the CFD model of the near field until a certain degree of convergence is reached

d. Calculate average velocity values at the interfaces Γ_i and Γ_j (to be used as boundary conditions for the 1D model in the next multiscale iteration)

e. Calculate average temperature values at the interfaces Γ_i and Γ_j (to be used as boundary conditions for the 1D model in the next multiscale iteration)

f. Check global convergence

   I. If global convergence is not reached go back to *point a* (eventually a relaxation step can be added as prescribed in equation (72))

   II. If global convergence is reached quit the calculation or proceed to the next time step for time dependent calculation

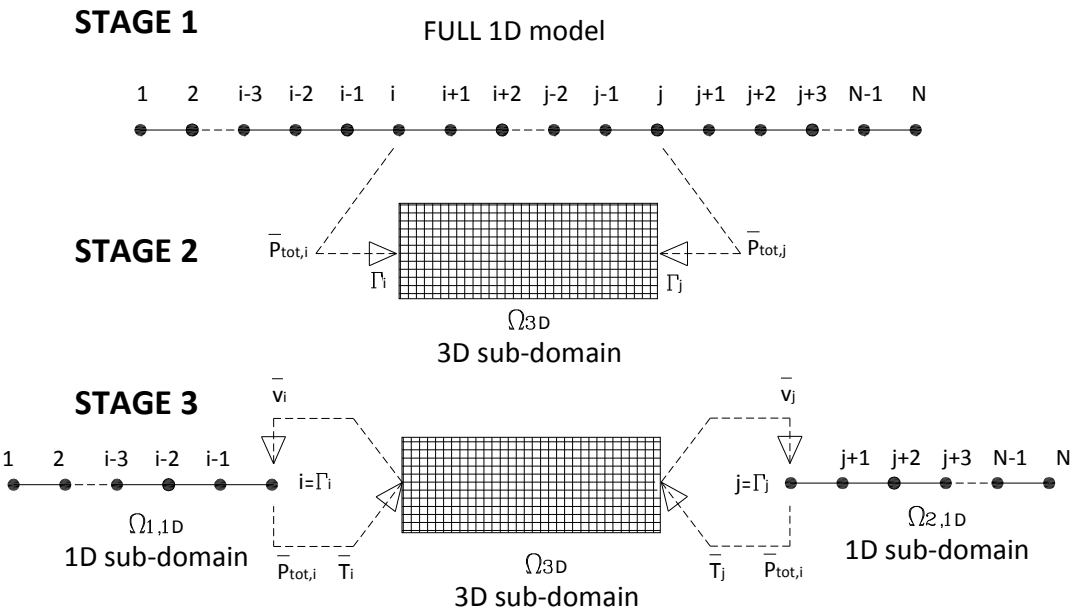

Figure 43: Visualization of a three stage coupling procedure.

It must be noted that, the coupling between grids is physically realized between the pressure nodes of the 1D grid (*i,j* in Figure 43) and the mesh faces lying on the interfaces Γ_i and Γ_j. Therefore, the prescription of a velocity boundary condition for the 1D sub-domain is performed by using a ghost velocity node (indicated as *t'* in Figure 44 for the left interface) located beyond the last 1D pressure node (indicated as *i* in Figure 44). The implementation of this boundary condition causes the *i* pressure cell to act as a source/sink of mass. Instead, temperature and pressure values can be directly transferred from the 3D to the 1D grid (and vice-versa) since naturally defined in the *i* node.

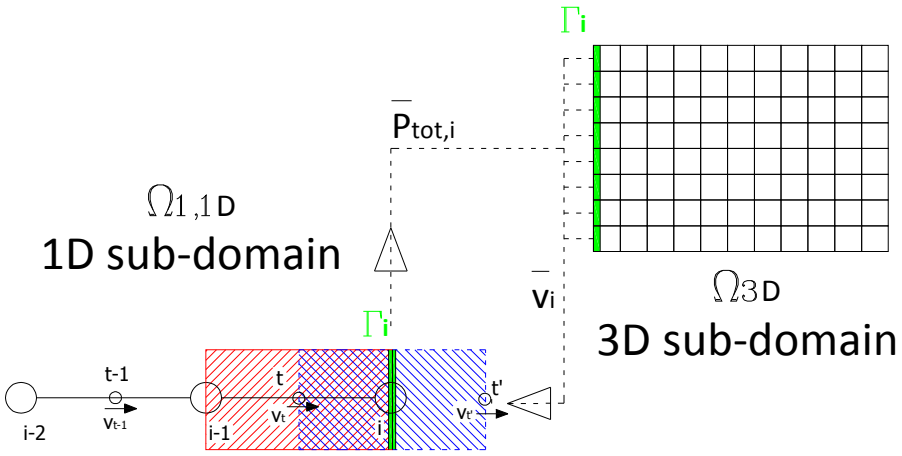

Figure 44: Visualization of the interaction procedure between 1D and 3D grids at the left CFD domain boundary (1D-CFD interfaces highlighted in green)

Further considerations are required when dealing with the turbulent kinetic energy and the dissipation rate at the interfaces. Since these quantities are not calculated by the 1D model, they are introduced as a function of turbulence intensity, turbulent length scale and Reynolds number using well known relations for fully developed flow within pipes. They have been resumed in equations (67).

This coupling approach is called *direct coupling*. It allows for a significant reduction in the computational time in comparison to the full CFD calculation of the same scenario. However, the timescale of the direct coupling calculations is limited by the computational speed of the CFD portion of the model. This can take from some minutes to up to many hours depending on the complexity of the scenario.

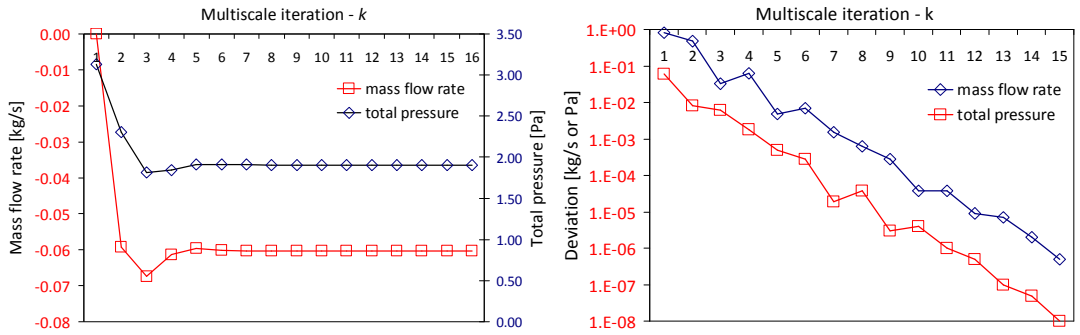

Figure 45: left) Evolution of total pressure and mass flow rate at a 1D-3D interface during a multiscale calculation. The maximum deviation allowed was 10^{-6}. right). Deviation of the mass flow rate and total pressure at a 1D-CFD interface during a multiscale calculation

The global convergence check is performed by monitoring the evolution of any average fluid-dynamic quantity at the *1D-CFD* interfaces during the *k-iterations* performed during step 3. In particular, the model checks whether or not the deviation of a certain fluid-dynamic quantity during two sequential multiscale iterations is lower than a fixed tolerance. Figure 45 shows the evolution of total pressure and mass flow rate computed at a *1D-CFD* interface during a multiscale calculation. The maximum deviation allowed was 10^{-6} which was reached after around 20 multiscale iterations. It is worth to note that, given the high uncertainty characterizing tunnel ventilation flow calculations, lower accuracy (i.e. 10^{-3}) can be used shortening significantly the computing time (~10 multiscale iterations).

The actual exchange of information between 1D and CFD tools has been performed by using *User-defined-Functions* (UDF) that can be dynamically loaded by FLUENT to enhance the standard features of the code [130]. UDF scripts are written in C++ programming language and are used to define user-defined source terms, boundary conditions and material properties. In the specific case *compiled UDF* have been used for mainly 3 purposes:

- Averaging fluid-dynamic quantities at the 1D-3D interfaces
- Launch the 1D model executable file
- Update and store the results before proceeding to the next time step calculation (for time-dependent simulations)

In particular the general-purpose "*DEFINE_ON_DEMAND" UDF* have been chosen as they can be are called automatically by the solver during the solution procedure. A large effort has been profused in order to produce "*parallelized"* version of the scripts in order to be used both during serial and parallel computations. A detailed description of the UDF programming technique is beyond the scope of this document; the interested reader can refer to [130].

4.4.2. Indirect coupling

Most of the ventilation studies require bulk flow velocities and average temperature values in steady state or quasi steady state conditions. In this case an *indirect coupling* method can be adopted allowing 1D and CFD simulations to be run separately. After identifying the near field, a series of CFD runs are conducted for a range of uniform boundary conditions at the interfaces. In this manner, the CFD results are arranged in terms of bulk flow velocities as a function of the total pressure differences across the near field allowing the definition of characteristic curves. These curves represent the coupling of the active element of interest (shaft, jet fan, or fire) with the surrounding tunnel gallery. The 1D model is designed in order to take into account these curves, accurately calculated by the CFD model and, hence, it couples them to the rest of the tunnel. In the next sections, indirect coupling techniques will be used to describe the behaviour of jet-fan and fire near field in terms of fan and fire characteristic curves. The

CFD computed curves will be then input in the 1D model improving its prediction capabilities.

Indirect coupling leads to higher set-up times, mainly dedicated to the calculation of the characteristic curves, but then provides almost instantaneous results for steady state calculation of tunnel flows and temperatures. The implementation of indirect coupling techniques for transient calculation is possible but complicated since the curves must be eventually updated each time step to follow the fire growth or the fan activation ramp.

4.5. Concluding remarks

In this section the fundamentals of multiscale computing have been presented. The developed model is based on the decomposition of the tunnel layout in sub-domains:

- The near field regions, characterized by high velocity or temperature gradients, modelled by means of CFD techniques;
- The far field regions, characterized by milder gradients modelled by using a 1D model.

Some practical issues related to the coupling methods between the 1D and 3D solvers have been also addressed in the framework of domain decomposition techniques. The application of multiscale modelling techniques to simulate tunnel ventilation flows and fire will be the subject of the next sections.

Parts of this work have been published in *Building and Environment [102]*, *Tunnelling and Underground Space Technology [103]* and *Fire Technology [105]*.

5

Multiscale modelling of tunnel ventilation flows

5.1. Introduction

In this section a multiscale model will be used to describe the behaviour of tunnel ventilation flows in normal operating conditions (i.e. cold flow). Computational analysis of tunnel ventilation flows are mainly interested in the characterization of the discharge cone from operating jet fans and in assessing the global performance of a given ventilation system. The first analysis is required for optimization purposes or to understand how the fan thrust depends on particular installation details (i.e. presence of niches, distance from the ceiling, eccentricity). Comprehensive analysis of ventilation systems are instead required to describe the ventilation flows in the overall tunnel domain depending on the specific settings of the ventilation devices (i.e. set points of the fans, activation of specific extraction or supply stations). Such analyses are mainly required for ventilation strategy design.

The characterization of the jet fan discharge cones and a comprehensive analysis of the installed ventilation systems have been performed for the Dartford tunnels located in

London (UK). The multiscale model results have been corroborated by an extensive experimental campaign we have conducted in the tunnels between 2007 and 2008.

5.2. A case study: the Dartford tunnels

The Dartford tunnels are two twin-lane, uni-directional road tunnels under the River Thames, crossing from Dartford at the south (Kent) side of the river to Thurrock at the north (Essex) side, about 15 miles east of London in the UK. Both tunnels have complex ventilation systems consisting of a semi-transverse system together with additional jet fans to control longitudinal flow.

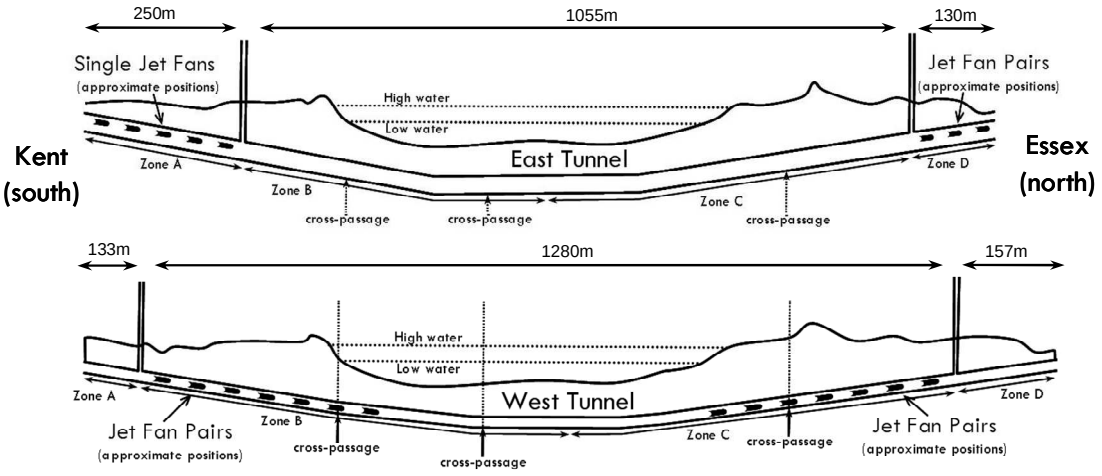

Figure 46: Diagram of the East and West Dartford Tunnels showing the relative positions of jet fans and extract shafts. (Drawn approximately to scale but with vertical distances five times larger)

The tunnels are approximately 1.5 km long and each tunnel carries unidirectional traffic in two lanes. Generally, both tunnels carry northbound traffic only, while southbound traffic uses the four lane Queen Elizabeth II bridge, which lies slightly to the east of the tunnels. In instances of extreme weather, the bridge may be closed and the traffic direction in the East Tunnel may be switched to southbound.

Figure 46 shows the general layout of the tunnels. The West Tunnel (approx. 8.6m internal diameter) was opened to traffic in 1963 and the East Tunnel (approx. 9.5m internal diameter) in 1980. The West Tunnel is constructed of a cast iron segmental lining, which has been infilled with concrete. The East Tunnel is constructed of three

different types of primary lining material: the central 600m of the tunnel are constructed of pre-cast concrete segments with steel face plates, on either side of the central section there is a portion of the tunnel (170m long at the north end and 100m long at the south) constructed of cast iron segments, the remainder of the tunnel (200m at the north and 355m at the south) was constructed of cast in-situ concrete using a cut and cover technique. The real tunnel environment is represented in Figure 47 and Figure 48.

Figure 47: East Dartford Tunnel; Picture taken approximately 1100 m from the Kent portal facing south (refer to Figure 46).

Figure 48: West Dartford Tunnel; Picture taken approximately 500 m from the Kent portal facing south (refer to Figure 46).

In both tunnels the semi-transverse ventilation system has two shafts with axial extraction fans located at relatively short distance from each of the tunnel portals. In

both tunnels the semi-transverse system supplies fresh air into the tunnel through grills along the side of the roadway between the extract shafts. The fresh air is pumped into the invert under the roadway by means of two axial fans, one at the Kent end and one at Essex. There are no transverse supply grills between the portals and the shafts. In the West tunnel, there are 14 pairs of unidirectional jet fans, located between the extract shafts. In the East tunnel there are five individual reversible jet fans between the southern portal and the southern extract shaft and three pairs of reversible jet fans between the northern shaft and the northern portal. The jet fan spacing is around 50 m in both the tunnels. The layout of the tunnels and the position of the jet fans is shown in Figure 46.

In the event of a fire, the emergency strategy currently implemented in the Dartford tunnels assumes that all vehicles ahead of the incident will be able to safely exit the outgoing portal, while a queue of traffic builds up behind the incident. Thus, the ventilation is configured in such a way as to blow any smoke away from the queuing traffic. To allow for a flexible emergency response, four different ventilation strategies are used, depending on the location within the tunnel where the fire occurs:

- If the incident occurs between the Kent portal and the southern extract shaft (hereafter referred to as ‘Zone A’), the ventilation strategy utilises the activation of all jet fans (blowing south to north) and both extract fans, but sets both supply fans off.

- If the incident occurs between the southern extract shaft and the mid point of the tunnel (‘Zone B’), the ventilation strategy utilises the activation of all jet fans (blowing south to north) and the northern extract fan, but sets both supply fans and the southern extract fan off.

- If the incident occurs between the mid point of the tunnel and the northern extract shaft (‘Zone C’), the ventilation strategy utilises the activation of all jet fans (blowing south to north), the southern supply fan and the northern extract fan, but sets the northern supply fan and the southern extract fan off.

- If the incident occurs between the northern extract shaft and the Essex portal ('Zone D'), the ventilation strategy utilises the activation of all jet fans (blowing south to north), both southern supply fans, but sets both extract fans off.

5.3. Overview on the experimental setups

In order to estimate the flow in the tunnels, the cross-section was divided into 9 equal areas, and the measurements of velocity were taken at the geometric centres of gravity of each section. However, in order to simplify the measurement process, the actual coordinates of the measurement points were slightly offset from the calculated values and are shown in Figure 49:

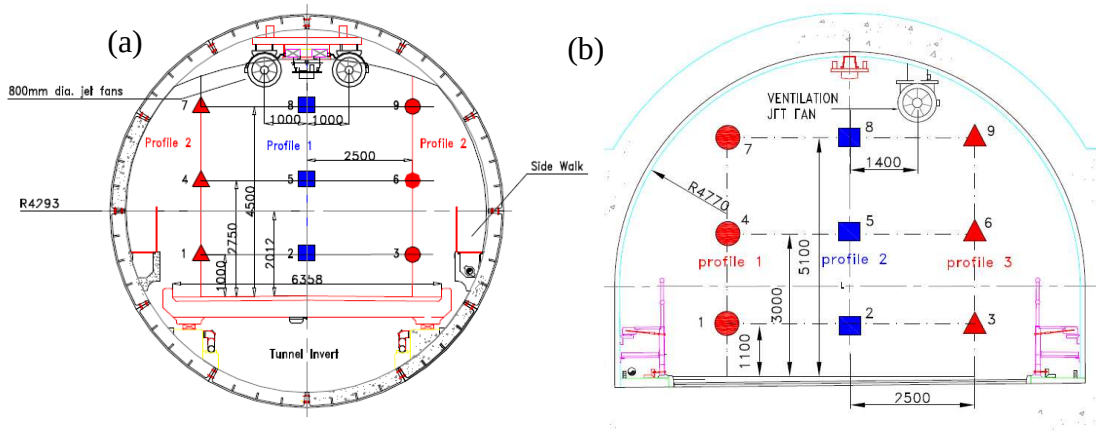

Figure 49: Layout and general dimensions of the tunnel cross sections (west tunnel to the left; East tunnel to the right) including the points 1-9 where the air velocities where measured (dimensions are expressed in mm).

The measurements of the jet fan discharge cones have been performed at 6 different locations, at 20 m intervals, starting 20 m downstream from the jet fan discharge surface. Furthermore, bulk flow velocities in the central section of the tunnels have been recorded for a wide range of fan combinations.

The measurements were carried out using 3 different types of instruments:

- hot wire anemometers
- rotating vane anemometers
- a Pitot tube

All these instruments were connected to Kimo portable data loggers. The instruments provide measurements in the range 0.3 to 35 m/s with an accuracy of 2%±0.1 m/s. They are also very robust in terms of their correct alignment with the flow: they present little error for angles of misalignment of up to 24° (in practice, anemometers positioned in the flow by hand, as in these tests, are unlikely to be misaligned by as much as 10°, so the results are well within the operating range of the equipment).

Error estimations were done for the rotating vane anemometer, the instrument used for most of the measurements. The greatest standard error was of ±14.5. This value was measured 20 m downstream from a pair of jet fans, with all the other fans turned off. This is caused by the unstable nature of the flow close to the jet fans, where the jet generated is probably not stable in space, especially when there are no other fans operating.

In order to avoid redundancy, the experimental measurements will be presented later together with the numerical predictions.

5.4. Characterization of the jet fan discharge cone

The characterization of the jet fan discharge cone for the East and West tunnel has been performed by adopting a multiscale model with direct-coupling. This approach allows for the computation of detailed flow field data in the 3D-CFD sub-domain (Ω_{3D} in Figure 50) while the rest of tunnel layout is represented by adopting a 1D modelling approach. Indeed, detailed simulations of the fluid flow behaviour in the jet-fan surroundings may be not fully accomplished without taking into account the interaction with the rest of the tunnel layout and ventilation devices.

A schematic of the coupling between 1D model of the far field and CFD model of the near field has been depicted in Figure 50.

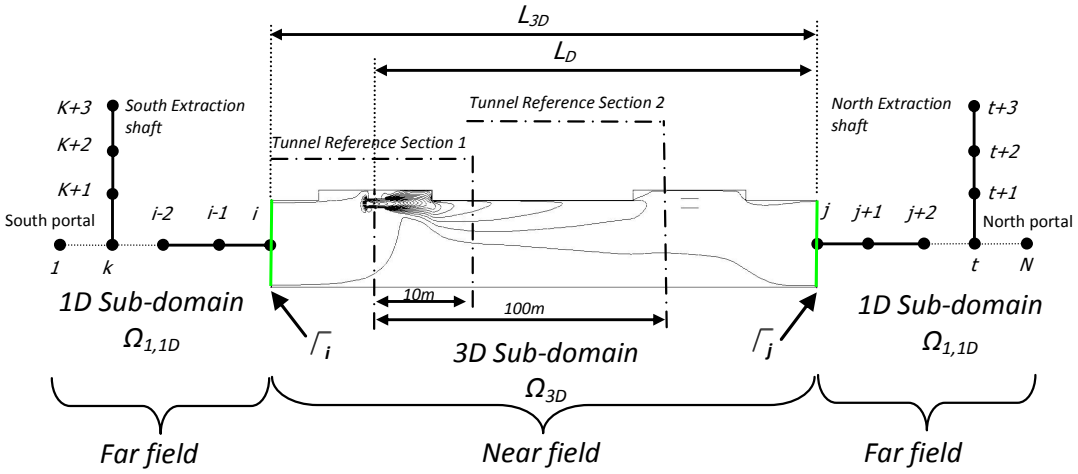

Figure 50: Schematic of multiscale coupling between mono-dimensional and CFD models for the multiscale calculation of the jet fan discharge cone (1D-CFD interfaces highlighted in green)

As already asserted in the previous sections, a critical point of the multiscale representation is the positioning on the 1D-3D interfaces Γ_i and Γ_j in Figure 50. Indeed, they must be located in a domain region where the flow is fully developed and is characterized by mild velocity gradients. Thus, the size of the 3D sub-domain (L_{3D}) plays a crucial role in the accuracy of the global solution. This issue will be addressed in the next sections.

5.4.1. Assessment of the mesh requirements

Various CFD runs have been conducted to asses the mesh requirements. Four different meshes have been generated and the resulting solutions compared. The mesh density per meter of tunnel length ranged from 272 cells/m up to 7000 cells/m. The symmetry of the domain across the longitudinal plane was considered only for the West tunnel calculations since the explored ventilation scenario involved a jet fan pair arranged symmetrically in respect to the tunnel longitudinal section. Four examples of the mesh cross section are presented in Figure 51.

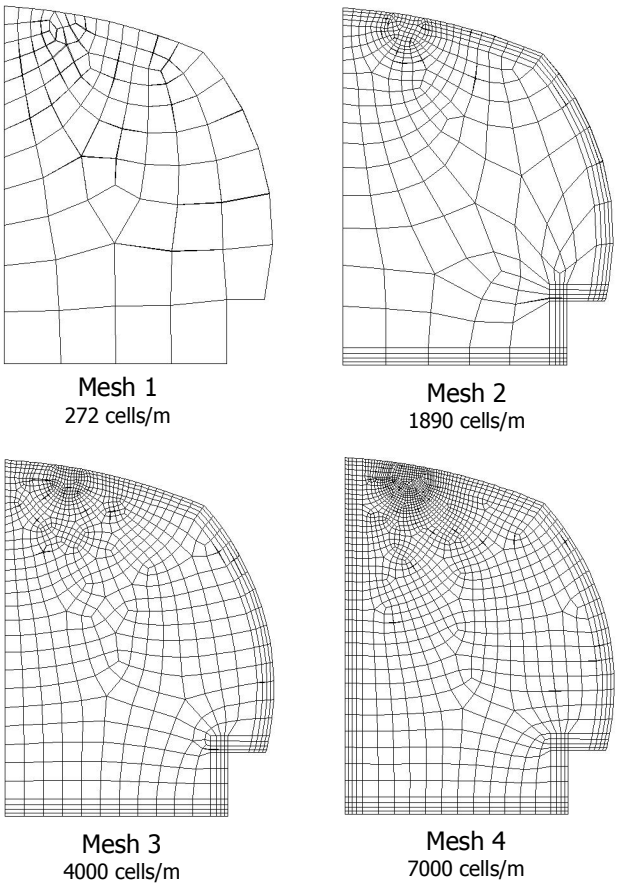

Figure 51: Examples of the different meshes used for half of the tunnel cross section and number of cells per unit length of tunnel.

The solutions have been compared in terms of bulk flow velocity and in terms of the flow field computed in two reference tunnel cross sections located 10 m and 100 m downstream of the jet fan discharge surface (see Figure 50).

	Mesh density [cell/m]	Predicted air velocity [m/s]	Deviation from mesh 4
Mesh 1	272	1.926	0.29%
Mesh 2	1890	1.927	0.34%
Mesh 3	4000	1.921	0.02%
Mesh 4	7000	1.920	-

Table 11: Grid Independence Study for a scenario involving an operating jet fan pair in the West tunnel

The dependence of the computed average velocity as function of the mesh density is resumed in Table 11. It shows that the solution converges as the mesh is made finer. For instance, the computation performed with mesh 3 deviates by 0.02% from the prediction performed with the finest mesh.

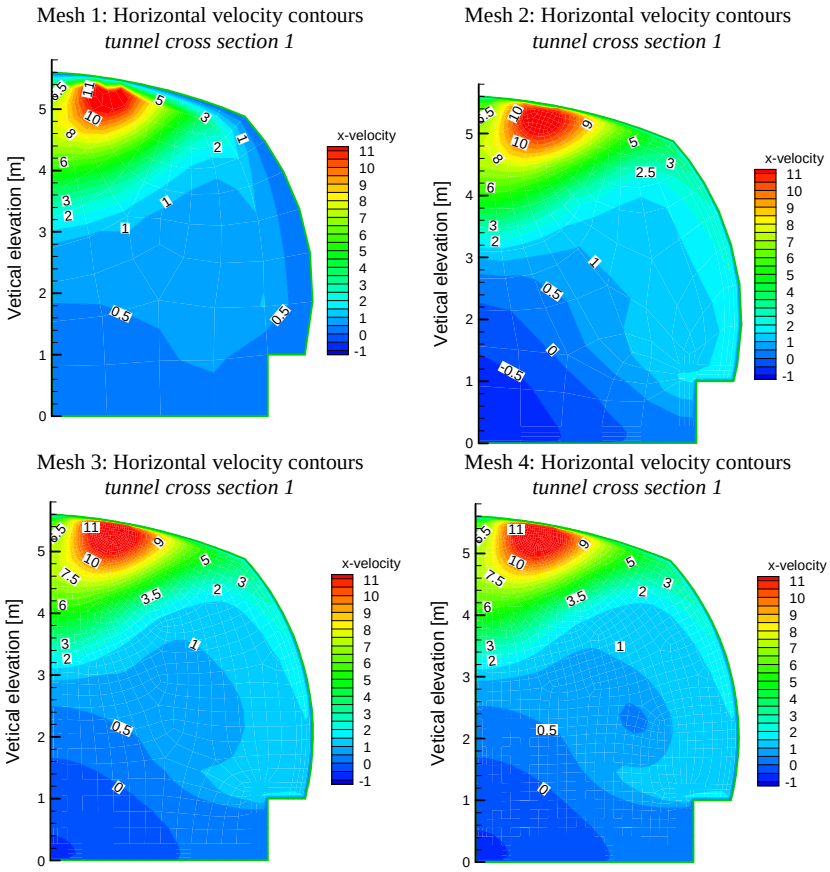

Figure 52: Comparison of the longitudinal velocity contours for meshes #1 to #4 in the tunnel at the reference section 1. Velocity values are expressed in m/s.

The comparison of the predicted velocity fields at the Reference Section 1 and Reference Section 2 is presented in Figure 52 and Figure 53. As expected from the previous results, the computed solutions show larger deviations for the coarse meshes 1 and 2 while convergence is obtained for finer meshes 3 and 4. Based on the results, grid independence is considered reached in mesh 3 and therefore, all the following simulations have been conducted using this grid.

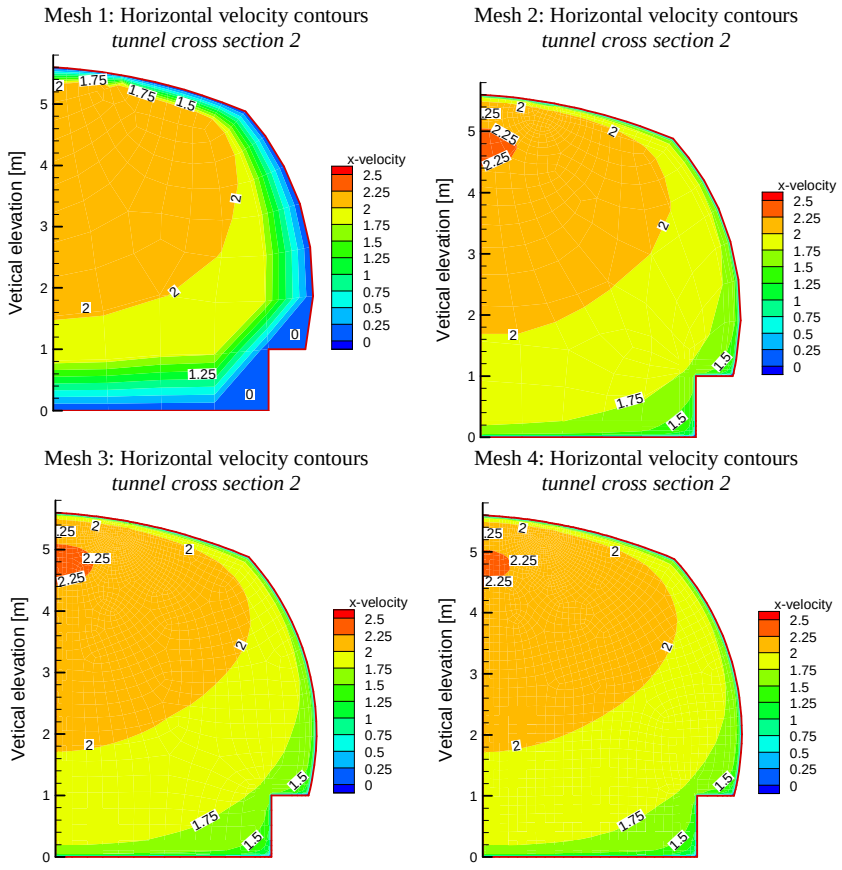

Figure 53: Comparison of the longitudinal velocity contours for meshes #1 to #4 in the tunnel at the reference section 2. Velocity values are expressed in m/s.

5.4.2. Effect of the 1D-CFD interface location

A sensitivity analysis has been conducted in order to asses how the position of the interfaces between mono-dimensional and CFD domain affects the calculated solution. An operating jet fan produces a region where the fluid field has high velocity gradients and a proper modelling approach would require a CFD tool. The high gradient region does not extend for a long distance and after the flow behaves as fully developed and it could be successfully represented using a mono-dimensional model. The interface between mono-dimensional and CFD domain must to be located in this region. In order to identify this distance, 14 different runs were performed. In each run the interfaces were placed progressively further away from the operating fans, increasing the longitudinal extension of the CFD domain (L_{3D} Figure 50) and consequently reducing the extension of the mono-dimensional domain. For each run the predict bulk flow (Figure 51) has been recorded. The reference value is the bulk flow calculated using a full scale CFD simulation of the whole tunnel.

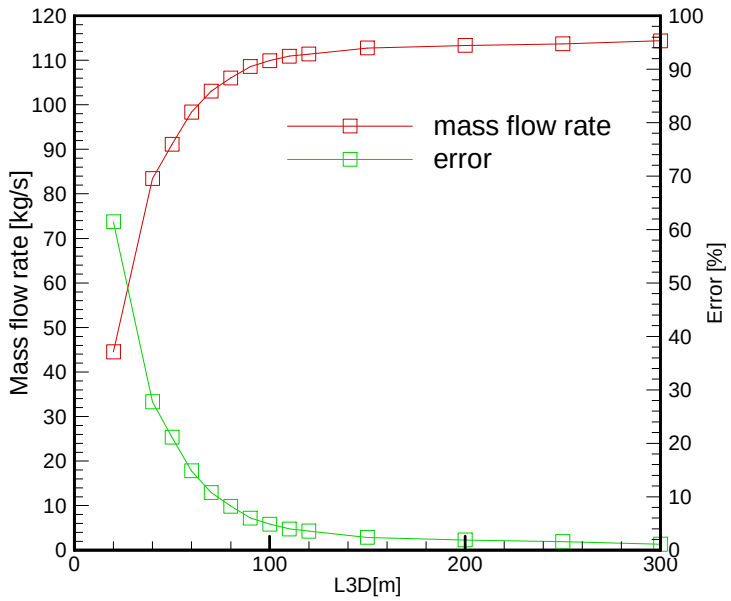

Figure 54: Convergence of the predicted mass flow rate as a function of the location of the interface

Being L_{3D} the length of the near field (see Figure 50), the error induced by an inappropriate location of the interfaces can be calculated as

$$\varepsilon_{MS} = 100 \cdot \frac{\left| \dot{m}_{CFD} - \dot{m}_{MS} \right|}{\dot{m}_{CFD}} \tag{75}$$

where $\dot{m}_{CFD}$ is the mass flow rate calculated using the full CFD model, and $\dot{m}_{MS}$ is the mass flow rate computed by the multiscale model for a given value of L_{3D}. Figure 54 shows the error calculated in each run and its dependence on the 3D domain length. It is clear that the multiscale approach can lead to accurate results when the dimensions of the CFD domain are only a fraction of the whole tunnel length (1.5km) with a significant reduction of the computational time. Results with less than 10% error can be obtained using a 3D domain longer than 80 m (5% of the tunnel length). The accuracy of the multiscale model is improved up to around 1% by using 300 m as length of the near field (20% of the tunnel length). The following calculations are then conducted with the length of the 3D model set to 300 m. The downstream 1D-CFD interface is then located at a distance from the jet fan discharge surface (L_D in Figure 50) larger than ~20 times the tunnel hydraulic diameter.

5.4.3. Comparison to experimental data

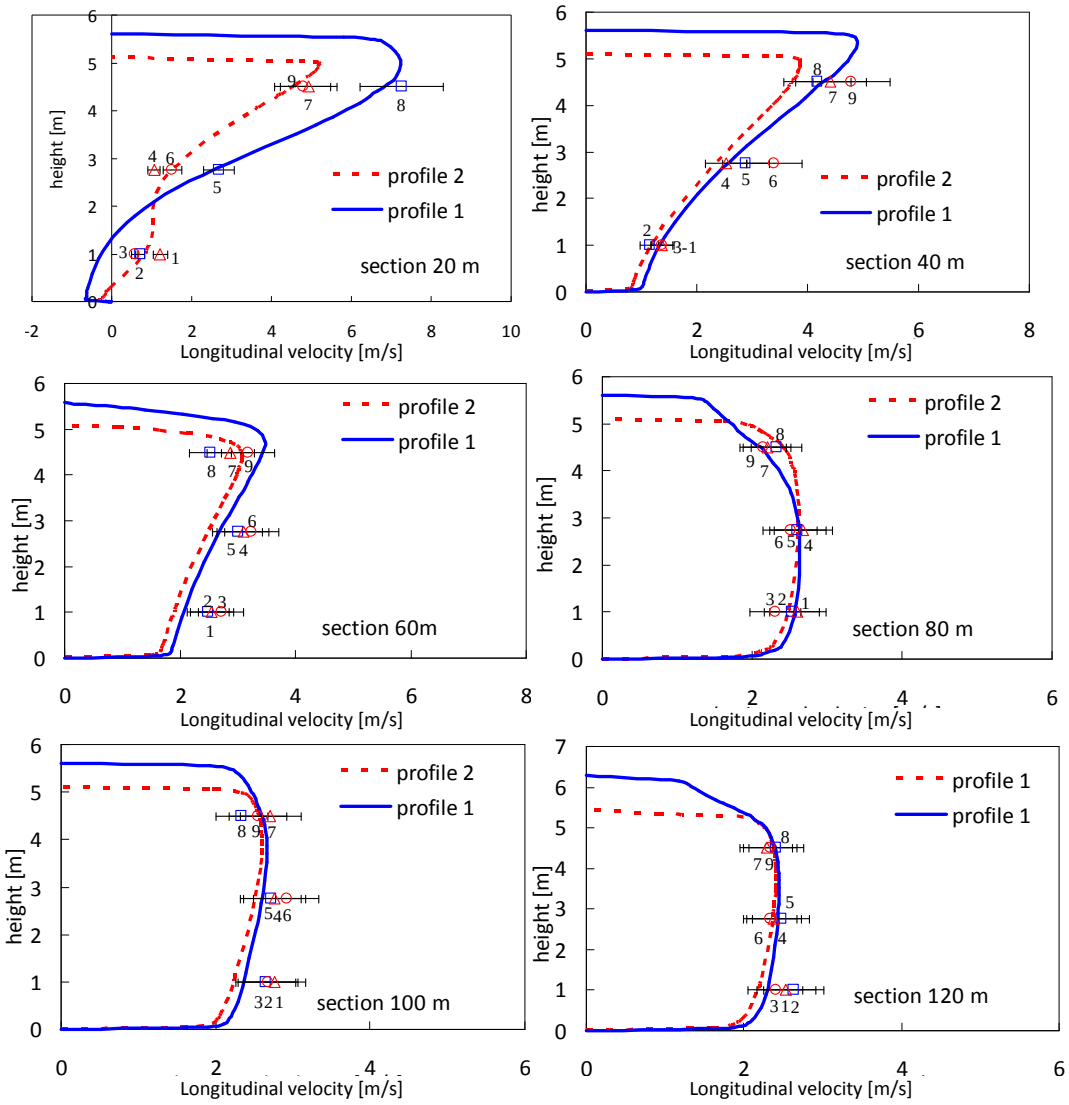

Figure 55: Comparison of horizontal velocities between predictions (lines) and experimental measurements (symbols) in the West Tunnel. The two profiles and the numbers refer to locations in the tunnel section described in Figure 49.

The comparison between predicted and experimental velocities measured in the West tunnel is presented in Figure 55. The blue continuous line represents the velocity profiles calculated in the middle of the tunnel cross sections (*profile 1* in Figure 49.a) while the red dashed ones represent the velocity profiles calculated along the vertical lines corresponding to the *profiles 2* in Figure 49.a.

The measured velocity values represented in Figure 55 are numbered from 1 to 9 following the same pattern as presented in Figure 49.a. The measurements have been

obtained with only the 5th jet fan pair operating in the West tunnel. The comparison is quite encouraging as in almost all the measurement sections there is a good agreement between experimental and numerical data.

All the CFD tests done during the development of the model have demonstrated that the niches where the jet fans are located, have a significant effect on the longitudinal development of the flow and their capability of producing thrust. The worst agreement between the model and the experimental data was found in the section 60m downstream of the fan; this peculiarity is most likely due to the presence of obstacles located on the tunnel ceiling (other fans and lighting devices) which are not included in the computational domain but influence the discharge cone characteristics.

A similar degree of accuracy is obtained when comparing predicted and measured velocity profiles in the East Tunnel (see Figure 56). In this case, only the 3rd single jet fan was operating and therefore the velocity profile is not symmetrical across the tunnel longitudinal plane, unlike in the West Tunnel.

The blue continuous line represents the velocity profiles calculated in the middle of the tunnel cross sections (*profile 2* in Figure 49.b). The red velocity profile with finer dashing represents the velocity calculated on the vertical line indicated as *profile 1* in Figure 49.b. The green velocity profile with coarser dashing represents the velocity calculated on the vertical line indicated as *profile 3* in Figure 49.b. The measured velocity values represented in Figure 56 are numbered from 1 to 9 following the same pattern as presented in Figure 49.b.

Also in this case the comparison is quite encouraging as in almost all the measurement sections there is a good agreement between experimental and numerical data. A poor agreement between experimental and numerical data has been encountered in the section 80 m downstream from the fan. This is most likely due to obstacles present in the specific region of the tunnel (luminaries or other jet fans) or to a sudden change in the meteorological conditions given the strong external winds recorded during the measurement campaign.

The analysis of the jet fan discharge cone confirmed that the flow is approximately one dimensional in nature beyond 80m downstream of the fan outlet in the case of the West tunnel. In the East tunnel the discharge cone is slightly longer at 100m. This is because the jet fans installed within the East tunnel are more powerful than in the West, and not installed in niches on the ceiling, as they are in the West Tunnel. When more than one jet fan pair is operating, the near field must include all operating devices within the module length.

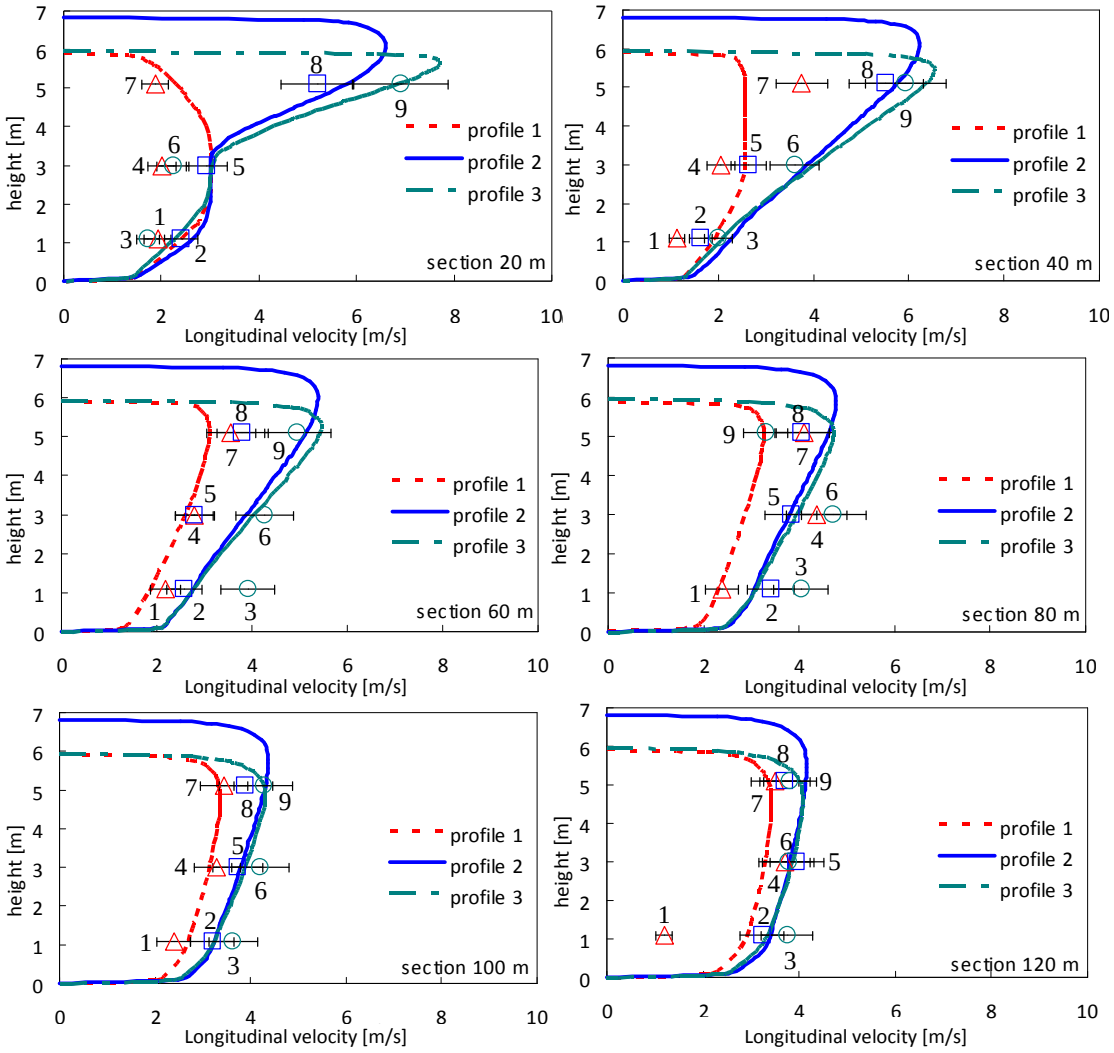

Figure 56: Comparison of horizontal velocities between predictions (lines) and experimental measurements (symbols) in the East Tunnel. The two profiles and the numbers refer to locations in the tunnel section described in Figure 4.b.

5.5. Characterization of the ventilation system

The assessment of the ventilation system performance required a comprehensive study of the ventilation strategies within the tunnels. In particular, the study aims to understand the consequences on the tunnel flow of making changes to the fan configurations. This kind of analysis does not require detailed flow field data but only bulk flow velocities within the tunnel domain.

The first modelling choice to address this problem was a purely 1D model. For this particular application, the main difficulty encountered when using the 1D approach was related to the assessment of the jet fan thrust and their losses induced by their peculiar installation locations (i.e. in niches in the West tunnel). In fact, it is well known that the pressure rise produced by the jet fans is strictly dependent on the specific surrounding environment [62]. Therefore, the prediction capability of a 1D model mainly relies on calibration constant to be defined arbitrarily or on the basis of literature data. Furthermore, some empirical correlations to estimate the thrust from jet fan pairs were adopted (see equations (25)) but, in several cases, they over-predicted the actual capabilities of the ventilation system.

In order to overcome this problem, a multi-scale modelling approach with indirect coupling was used.

5.5.1. Calculation of the jet fan characteristic curves

When using a multiscale model with indirect coupling, the behaviour of high gradient regions is represented in terms of characteristics curves. Such curves, computed by performing several CFD runs of the near-field sub-domain, are built in order to be directly implemented in a 1D model.

The region of high velocity gradients, in this case, is represented by the fluid domain close to the operating jet fan pair. In case of the activation of many jet fan pairs, the flow within the tunnel domain is characterized by many high gradients regions requiring to be modelled using a CFD approach. Obviously, depending on the number and location of the operating jet fans, different meshes for the near field must be built. To avoid this complexity, some preliminary CFD runs have been performed in order to

understand how a series of operational jet fan pairs operates. All the results have shown that a series of equidistant jet fans produces a flow field characterized by an almost periodic pattern. Figure 58 is a clear example. It shows the velocity isocontours calculated for a series of 7 jet fan pairs operating in the West tunnel where the periodicity of the flow field is evident.

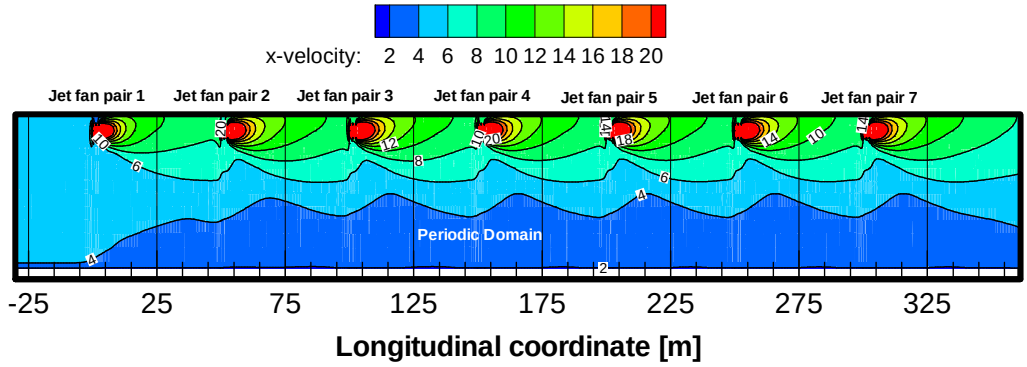

Figure 57: Typical flow pattern produced by a series of seven jet fan pairs operating in the West Tunnel (not to scale). Velocity isocontours from 2 m/s to 20 m/s in steps of 2 m/s; Velocity expressed in m/s.

As the flow periodicity has been accessed, the computational domain of the near field has been limited to the periodic portion of the tunnel geometry where the inlet and outlet boundaries have been defined as periodic surfaces. Thus, a jet fan series can be modelled by including a single representative module which operates in a periodic behaviour. The assumption of periodic flows implies that the velocity components repeat themselves in space while the pressure drop across the modules is periodic. This modelling approach is usually applied for periodic flows where a periodic pressure drop occurs across translationally repeated boundaries [69].

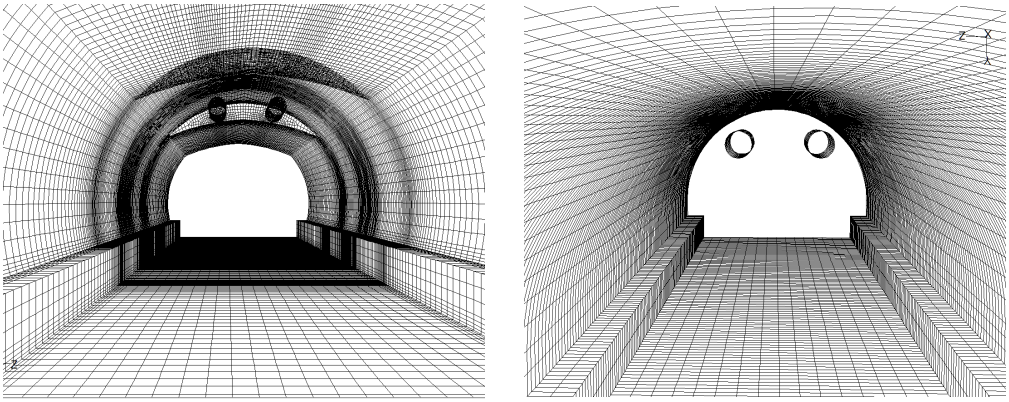

Figure 58: Computational mesh for the CFD module around the jet fans in the West (right) and East (left) tunnels. (Note: the West tunnel's jet fans are installed in niches on the ceiling, in the East tunnel they are not.)

Thus, once the near fields have been identified, the CFD mesh has been built following the available tunnel geometric data, in order to represent the jet fans installations and obtain a better estimation of the jet fans thrust. An example of the CFD meshes built for the East and West tunnels is presented in Figure 58.

Several runs of the near field CFD model have been performed, varying the pressure difference across the domain boundaries. The results can be presented in terms of bulk flow velocity and pressure difference across the domain (Figure 59). The curve obtained describes the capability of each pair of jet fans to produce thrust and its dependence on the bulk flow velocity.

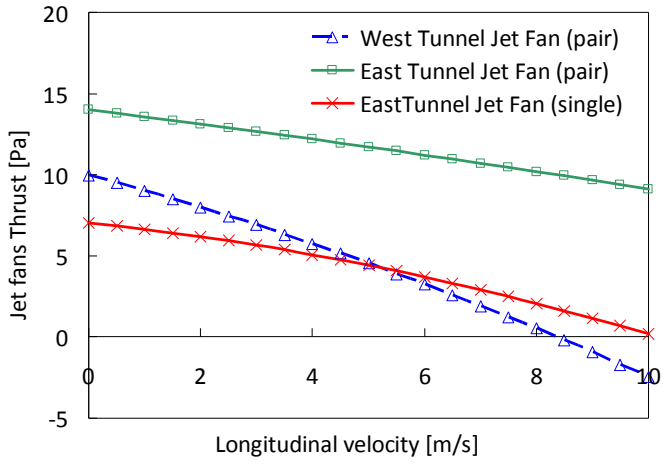

Figure 59: CFD calculated jet fan thrust vs. tunnel average velocity for the Dartford tunnels.

The results of this CFD study for the near fields are then coupled to the 1D model for the rest of the tunnel. Specifically, the computed curves are used as the characteristics of

any branch of the 1D model containing jet fans avoiding the uncertainties related to calibration constants.

It is worth to highlight that the assumed flow periodicity lasts as long as the supply fans within the tunnel are off. The introduction of fresh air will slightly modify the velocity patterns within the tunnel and the mass flow rate will not be constant along the longitudinal direction. However, these effects are small since the amount of fresh air introduced is negligible compared to the large mass flow rate through the main gallery. Thus, in also this case, the computed characteristic curves still provide a good approximation.

The same approach for the description of operating jet fan series has been used by Colella and co-workers (2010) [105] and the results have been compared to full CFD representation of the same scenarios. The authors showed that the simplified representation based on the periodic flow assumption leads to bulk flow velocities deviating as much as 1.5% from full CFD solutions.

5.5.2. Comparison to experimental data

The multiscale model with indirect coupling has been validated using bulk flow data recorded in the central section of the tunnels under a wide range of fan combinations. The comparison between predictions and recorded bulk velocities is presented in Figure 60 as a function of the number of operating jet fans. The agreement between the experimental data and the predictions is excellent, demonstrating accurate prediction capabilities. Some discrepancies can be observed for the East tunnel under some ventilation scenarios. The differences are due to changes in the weather (i.e. strong wind at the portals) during the on-site measurements.

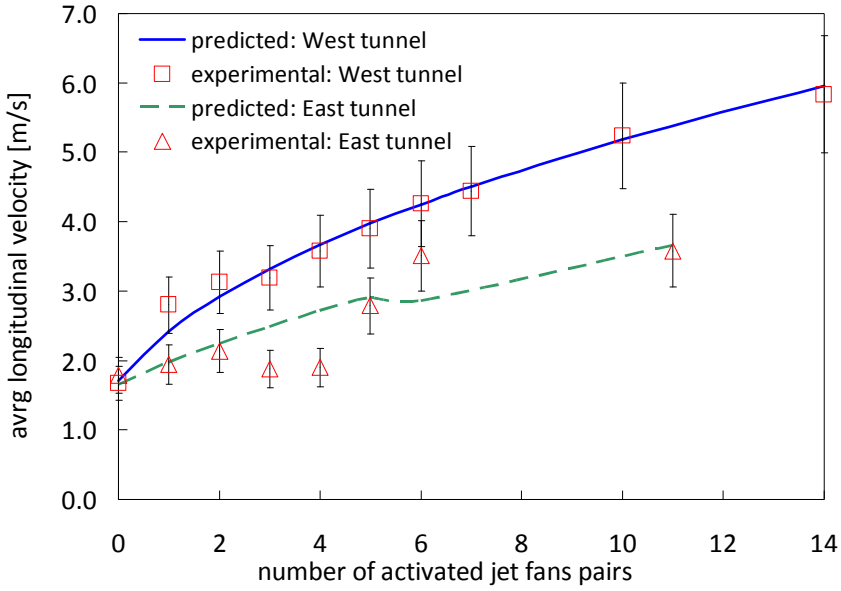

Figure 60: Comparison between experimental data and model predictions.

The simplicity of the model and its robustness allows the simulation of many different ventilation scenarios, as well as the effect of different fan combinations and their interaction with the extract and supply fans. The effect of wind or other external boundary conditions (e.g. difference between static pressures at the adits) can also be easily taken into account, as can the influence of the vertical shafts, stack effect, dampers or any obstacles within the tunnel. The model can also be used to calculate the distribution of pollutants or the influence of traffic flow on the average air velocity, as well as to make real time predictions of ventilation flows for control purposes. In the next section some results of the assessment of the ventilation system performance are presented.

5.5.3. Analysis of all the ventilation strategies

The model was used to analyse the flows resulting from each of the existing ventilation configurations, related to the strategies for each of the four zones. The results are summarised in Table 12.

Ventilation strategy		All Jet Fans	Kent Axial Extract Fan	Essex Axial Extract Fan	Kent Axial Supply Fan	Essex Axial Supply Fan	Between Kent portal and shaft (Zone A)	Midpoint of tunnel (Between Zones B & C)	Between Essex shaft and portal (Zone D)
							Ventilation velocities (m/s)		
West Tunnel	Zone A	ON	ON	ON	OFF	OFF	**9**	5.1	1.2
	Zone B	ON	OFF	ON	OFF	OFF	4.5	**5.9**	2
	Zone C	ON	OFF	ON	ON	OFF	3.5	**5.9**	3.3
	Zone D	ON	OFF	OFF	ON	ON	2.2	5.4	**5.1**
	JF only	ON	OFF	OFF	OFF	OFF	4.2	5.6	3.6
East Tunnel	Zone A	ON	ON	ON	OFF	OFF	**5**	2.2	5.2
	Zone B	ON	OFF	ON	OFF	OFF	5	**4.1**	1.4
	Zone C	ON	OFF	ON	ON	OFF	3.7	**4.1**	3
	Zone D	ON	OFF	OFF	ON	ON	1.5	2.9	**5.7**
	JF only	ON	OFF	OFF	OFF	OFF	4.7	3.2	4.7

Table 12: Summary of ventilation flows in the tunnels resulting from various ventilation strategies. The operating ventilation devices in each scenario are indicated by "ON". The predicted ventilation velocities in the incident zones are highlighted in bold

Studies of the ventilation required to control smoke from fires in tunnels [28,29,33] suggest that the critical velocity is generally of the order of 2.5 to 3 m/s. Thus, for the Dartford, all four ventilation strategies for both tunnels should provide more than adequate smoke control in an emergency.

Further analysis of the simulations for the East Tunnel showed that some of the airflow generated by the jet fans between the Kent portal and the extract shaft is diverted up the extract shaft as this short shaft poses a smaller resistance to the airflow than the main portion of the tunnel does. For example, in the 'jet fans only' case, the flow in Zone A is 4.7 m/s, while the flow in Zone B is only 3.2 m/s, some of the air is lost. Similar behaviour has been found in the East tunnel when activating the Essex jet fan pairs. Using the model it is possible to demonstrate, for example, that if dampers were fitted on the extract shafts, effectively blocking the losses, the resulting flow using all jet fans would be 3.7 m/s throughout the tunnel.

5.5.4. Assessment of the redundancy in the Dartford Tunnels

One of the advantages of using the multiscale model with indirect coupling is that it is comparatively easy and quick to assess the consequences of making small changes to the fan configuration, thus it is possible to assess the consequences of removing individual jet fans (or pairs) from a given scenario.

For example, Figure 61 shows the effects of varying the number of active jet fans in the Zone C ventilation strategy for the West Tunnel. If it is assumed that an airflow of at least 3 m/s is required throughout Zone C in this incident scenario, then it can be clearly seen that more than two pairs of jet fans are required to provide this magnitude of flow.

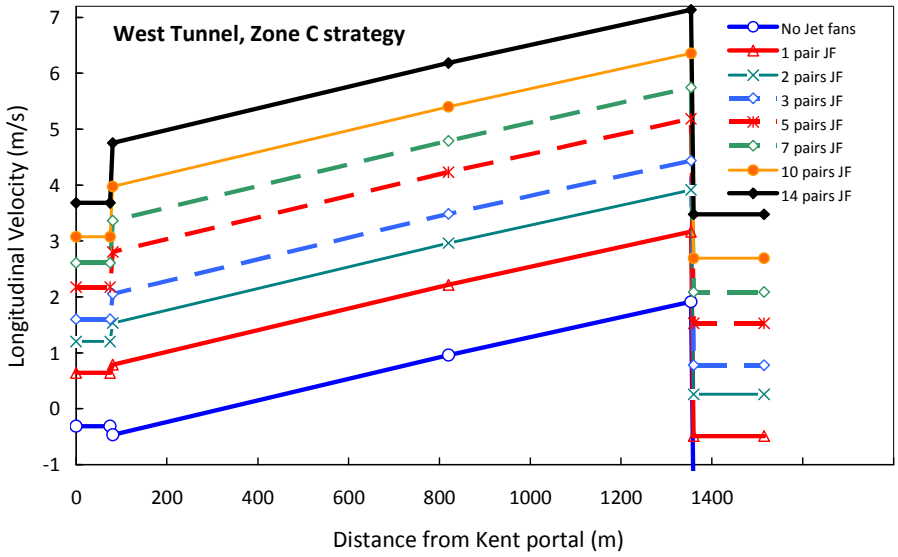

Figure 61: Results for the West Tunnel, using the strategy for Zone C (Kent supply on, Essex extract on), varying the number of active jet fan pairs. (Note: Zone C extends from approximately 700 m into the tunnel to 1370 m).

Similar calculations for the other zones reveal that, to generate a flow of at least 3 m/s in each of the incident zones, a minimum of three jet fan pairs are required in the Zone B scenario, only two pairs are required in the Zone D scenario and no jet fans are required in the Zone A scenario; in this instance sufficient flow can be generated by the axial extract fans on their own. Thus, it is clear that several pairs of jet fans in the West Tunnel may be safely taken out of use for maintenance or refurbishment, whilst still maintaining sufficient flow control capabilities for any of the considered incident scenarios.

In the East Tunnel the situation is more complex due to the positioning of the fans between the portals and the shafts. An example of the results for the Zone C strategy is shown in Figure 62. Here, it is generally found that the majority of jet fans are required to produce the required level of flow in the central section of the tunnel.

- For Zone A ventilation strategy, only one pair of jet fans on the Essex incline is required to produce a longitudinal flow of 3 m/s.

- For Zone B ventilation strategy, all three pairs of jet fans on the Essex incline (or four Kent fans and one pair at Essex) are required to produce a longitudinal flow of 3 m/s.

- For Zone C ventilation strategy, at least four Kent jet fans plus one pair of Essex jet fans are required to produce a longitudinal flow of 3 m/s.

- For Zone D ventilation strategy, at least three jet fans on the Kent incline are required to produce a longitudinal flow of 3 m/s.

Thus, while there is some redundancy in the East Tunnel ventilation system, there is considerably less redundancy than in the West Tunnel. However, it appears that one or two fans may be safely taken out of service in the East Tunnel at any given time for maintenance purposes.

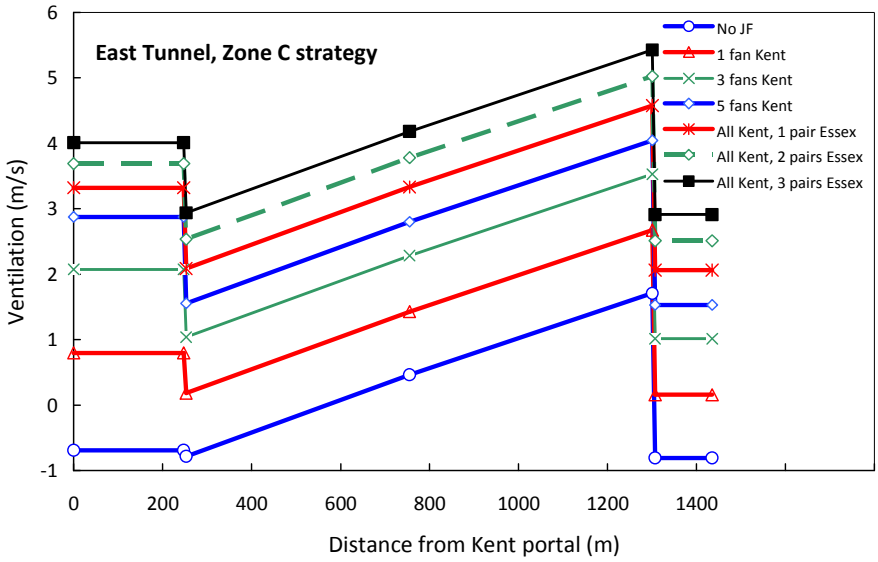

Figure 62: Results for the East Tunnel, using the strategy for Zone C (Kent supply on, Essex extract on), varying the number of active jet fans. (Note: Zone C extends from approximately 700 m into the tunnel to about 1300 m)

5.6. Concluding remarks

The chapter describes the application of multiscale computing techniques to model ventilation flows within road tunnels. The direct coupling approach has been adopted to

simulate the velocity field generated by operating jet fans in the Dartford tunnels (UK). The analysis on the positioning of the 1D-CFD interfaces shows that high accurate results (deviation from Full CFD calculation within 1%) can be achieved with CFD sub-domains whose longitudinal extension is around 300 m representing the 20% of the whole tunnel length. The corresponding multiscale model run-time is around 2 orders of magnitude shorter when compared to the requirements of full CFD calculations. The results obtained have been also compared to on-site velocity measurements.

The multiscale model with indirect coupling has been used to characterize the Dartford tunnel ventilation systems and its redundancy. Also in this case the results have been corroborated by on-site measurements. The analysis of the jet fan near field has confirmed that the niches in the West tunnel play a considerable role in the development of the discharge cone affecting the fan capability in producing thrust.

The multiscale model has been demonstrated to be a valid tool for the simulation of the complex behaviour of the tunnel ventilation systems in cold flow scenarios. It can be successfully adopted to design ventilation systems and to assess their redundancy and their performance under different operative conditions. An example of performance assessment has been performed in the case of the Dartford tunnels. The analysis demonstrates the capability of the actual ventilation systems to provide adequate levels protection for all the incident ventilation strategies. The model has also demonstrated that, for a given ventilation scenario, even if there are some jet fan failures, the tunnel ventilations system will still be able to provide adequate air flow levels.

Parts of this work have been published in *Building and Environment [102]* and *Tunnelling and Underground Space Technology [103]*.

6

Multiscale modelling of tunnel fires

6.1. Introduction

In the previous chapter, a multiscale modelling technique has been applied to address the behaviour of tunnel ventilation systems in cold flow scenarios (i.e. ambient conditions). The aim of the present section is to widen the range of applicability by addressing tunnel fire scenarios.

In this case further complexity is added by the presence of high temperature and velocity gradients in the plume region. However, as already asserted in the previous chapters, such high gradient regions do not extend too far downstream of the fire source since they evolve to fully developed flow regions.

The multiscale application discussed in this section is designed in order to include the fire near field region in the 3D-CFD sub-domain while the rest of the tunnel domain is modelled by means of a simple 1D modelling approach. It is in fact clear that detailed

simulations of the fire near field cannot be fully accomplished without accounting for the interaction with the remaining part of the tunnel domain. As result, detailed flow field data in the fire near field are made available by the CFD solver including, back-layering occurrence, back-layering distance, smoke stratification, smoke temperature, heat flux mapping, pollutant concentrations and so forth. At the same time, the overall interaction between fire near field and ventilation system, tunnel layout and eventually boundary conditions at the portals is maintained

6.2. A case study: a modern tunnel 1.2 km in length

The multiscale technique has been used to simulate a 1200 m long tunnel longitudinally ventilated. This layout is realistic and typical of a modern generic uni-directional road tunnel. A schematic of the tunnel layout is presented in Figure 63. The tunnel is 6.5 m high with standard horseshoe cross section of around 53 m^2 and hydraulic diameter around 7.3 m. The same geometry of the East Dartford tunnel cross section has been used for the scope (see Figure 49). The tunnel is equipped with two groups of 5 jet fans pairs 50 m spaced, each group installed near a tunnel portal. The jet fans are rated by the manufacturer at the volumetric flow rate of 8.9 m^3/s with a discharge flow velocity of 34 m/s.

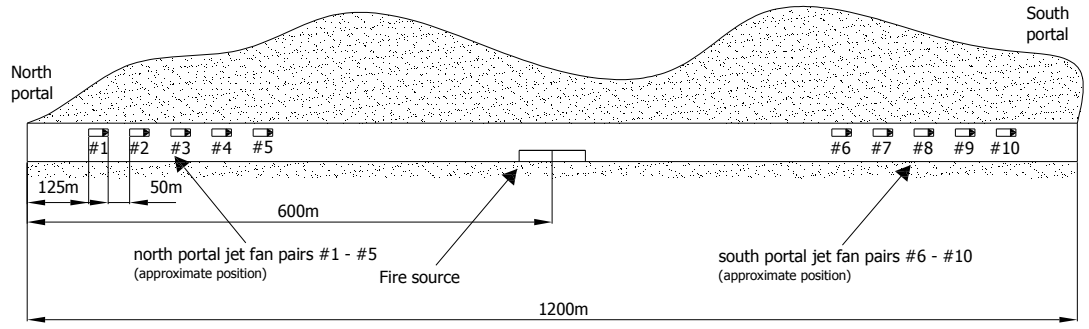

Figure 63: Layout of the tunnel used as case study showing the relative positions of the fire, jet fans and portals (Not to scale).

The fires are located in middle of the tunnel and 4 different sizes ranging from 10 MW to 100 MW are considered. The HRR is assumed to be constant and that steady state conditions are reached within the tunnel. The multiscale analysis includes 7 different scenarios involving different fire sizes and active ventilation devices. The main characteristics of each scenario are resumed in Table 13.

	Fire Size	Jet fan pairs #1- 2	Jet fan pair #3	Jet fan pair #4	Jet fan pair #5	Jet fan pairs #6 - 10
Scenario 1	*30 MW*	*ON*	*ON*	*OFF*	*OFF*	*OFF*
Scenario 2	*30 MW*	*ON*	*ON*	*ON*	*ON*	*OFF*
Scenario 3	*30 MW*	*ON*	*ON*	*ON*	*ON*	*ON*
Scenario 4	*30 MW*	*OFF*	*OFF*	*OFF*	*OFF*	*ON*
Scenario 5	*10 MW*	*ON*	*OFF*	*OFF*	*OFF*	*OFF*
Scenario 6	*50 MW*	*ON*	*ON*	*ON*	*OFF*	*OFF*
Scenario 7	*100 MW*	*ON*	*ON*	*ON*	*ON*	*OFF*

Table 13: Summary of ventilation and fire scenarios analysed with the multiscale technique

The emergency ventilation strategy, as for most longitudinally ventilated tunnels, requires the ventilation system to push all the smoke downstream of the incident region in the same direction as the road traffic flow, thus avoiding the smoke spreading against the ventilation flow (back-layering effect). The vehicles downstream of the fire zone are assumed to leave the tunnel safely. All the studies on back layering show that the maximum critical velocity is in the range from 2.5 m/s to 3 m/s. Thus, an adequate ventilation system has to provide air velocities higher than this range in the region of the fire incident.

6.3. Characterization of the fire near field

The characterization of the fire near field has been conducted by using a multiscale model with direct coupling approach. This approach allows for the computation of detailed flow and temperature field data in the 3D-CFD sub-domain which includes the fire while the rest of tunnel layout is represented by adopting a 1D modelling.

A schematic of the coupling between 1D model of the far field and CFD model of the near field has been depicted in Figure 64.

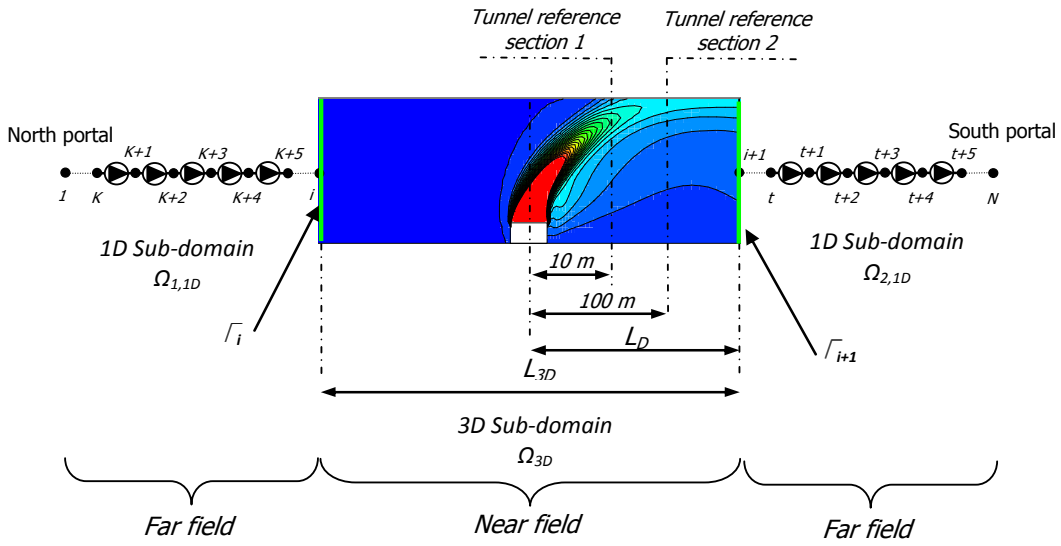

Figure 64: Schematic of the multiscale model of a 1.2 km tunnel including portals, jet fans, and the CFD domain of the fire region. Contours of the temperature field show the fire plume. (Not to scale). The 1D-CFD interfaces have been highlighted in green

As already asserted in the previous sections, a critical point of the multiscale representation is the positioning on the 1D-3D interfaces (Γ_i and Γ_j in Figure 64). Indeed, they must be located in a domain region where the flow is fully developed and is characterized by mild velocity gradients. Thus, it is straightforward that the size of the 3D sub-domain (L_{3D}) plays a crucial role in the accuracy of the global solution. This issue will be addressed in the next sections.

6.3.1. Assessment of the mesh requirements

The computational domain has been discretized using quasi structured meshes with refinements introduced close to each jet fan pairs and close to the fire source. Various full CFD runs of the whole tunnel domain have been conducted to estimate the mesh requirements. Four different meshes were generated and the resulting solutions compared. The mesh characteristics are resumed in Table 14. The symmetry of the solution across the longitudinal plane was also considered. Four examples of the mesh cross sections are presented in Figure 65. The data presented are relative to a 30 MW fire scenario and ventilation conditions slightly above the critical velocity. This condition could be achieved by activating 3 jet fan pairs upstream the fire.

	Mesh density [cells/m]	*predicted air velocity [m/s]*	*deviation from mesh 4*
mesh1	*105*	*3.21*	*-15.25%*
mesh2	*695*	*3.83*	*0.98%*
mesh3	*2525*	*3.80*	*0.32%*
mesh4	*4125*	*3.79*	*-*

Table 14: Grid independence study of the full CFD domain for a 30 MW fire and 3 operating jet fan pairs.

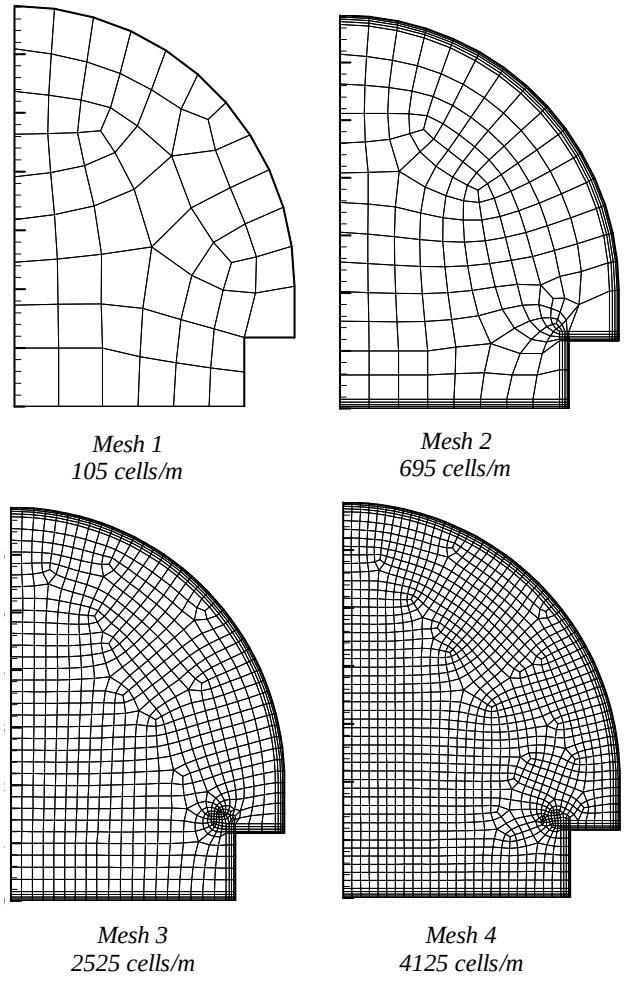

Figure 65: Examples of the different meshes used for half of the tunnel cross section and number of cells per unit length of tunnel.

The solution is shown to converge as the mesh is made finer. A coarse mesh of 100 cells/m leads to a 15% underestimation of the average ventilation velocity. But a finer mesh of 2500 cells/m leads to results within 0.3% of the prediction made with the finest mesh. Besides the comparison of the average quantities, detailed field solutions have

been compared at Reference Sections 1 and 2, located 10 m and 100 m downstream of the fire source location, respectively. The location of these sections is shown in Figure 64. The comparison of the longitudinal velocity and temperature fields is plotted in Figure 66 for the Reference Section 1 and in Figure 67 for the Reference Section 2.

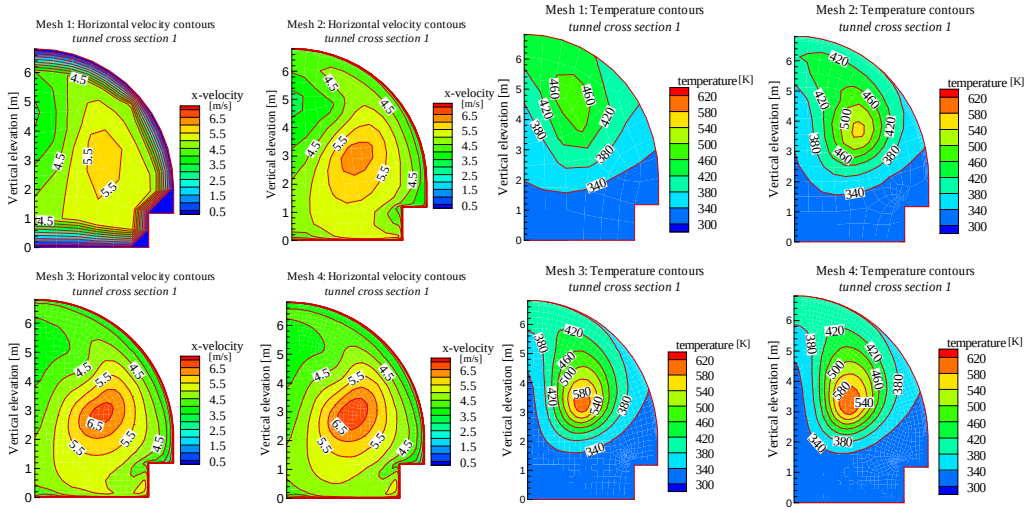

Figure 66: Comparison of the longitudinal velocity (left) and temperature (right) contours for meshes #1 to #4 in the tunnel at Reference Section 1 for a 30 MW fire. The velocity and temperature values are expressed in m/s and K respectively.

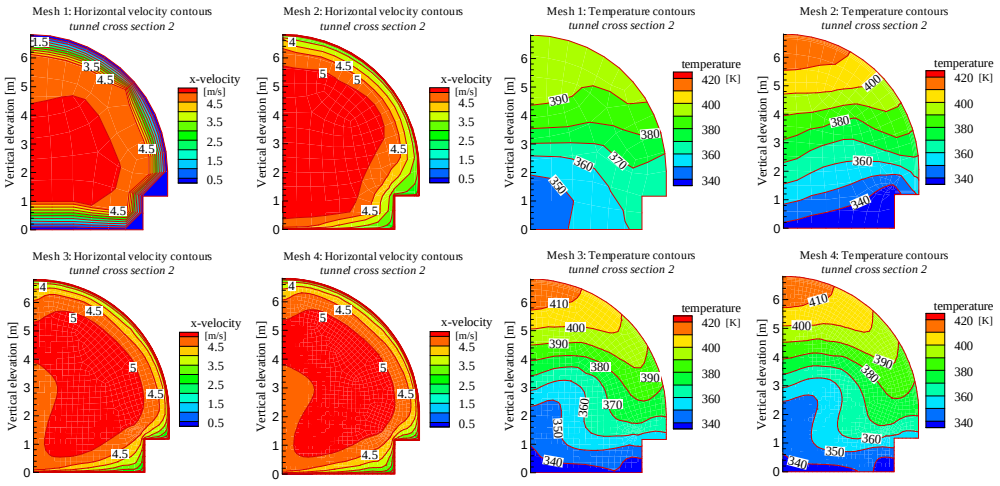

Figure 67: Comparison of the longitudinal velocity (left) and temperature (right) contours for meshes #1 to #4 in the tunnel Reference Section 2 for a 30 MW fire. Velocity and temperature values are expressed in m/s and K respectively

As expected from the previous results, the computed solutions show larger deviations for the courses meshes 1 and 2 while convergence of the temperature and velocity fields

is observed for finer meshes 3 and 4. Based on the results, grid independence is considered reached in mesh 3 and therefore, all the following simulations have been conducted using this mesh.

6.3.2. Effect of the 1D-CFD interface location

The downstream interface boundary between 1D and CFD domain must be located where the flow evolves to fully developed. Otherwise, the coupling would induce an error and the multiscale results would depend on the interface location. The previous chapter on the modelling of tunnel flows provides the sane analysis for cold flow scenarios. The boundary independence study conducted for the specific tunnel and jet fan arrangement showed that notable accuracy in the computed mass flow rate (error smaller than 1%) could be achieved when the ratio between L_D (distance from the fan to the downstream boundary interface) and D_h (tunnel hydraulic diameter) is around 20.

In order to identify the boundary independence limit for cases including fire-induced flows, several runs of the multiscale model were conducted for a range of fire sizes. In each run the interface was placed progressively further downstream of the fire, increasing the longitudinal extension of the CFD domain L_{3D} (see Figure 64) and consequently reducing the extension of the 1D domain by the same amount. The position of the upstream interface between 1D and CFD domain is not as critical as the downstream one where the focus is put here, but fore sake of generality the CFD domain is centered on the fire source. However, if the modeller is sure that during the simulated scenarios the ventilation velocity does not change direction and the air velocity is super-critical (therefore no back-layering occurs), the upstream boundary can be moved significantly closer to the fire. This would produce a further reduction of computing time.

In order to isolate the effect of the interface location on fire-induced flows, the jet fans at this stage are assumed to be located far away from the fire and thus simply modelled as a pressure difference between portals. This pressure difference is given by combining the characteristics curves of the operating fans.

A first analysis has been performed in order to clarify the dependence of the average bulk flow quantities (temperature and velocity) at the outlet boundary of the CFD domain. These values have an additional importance as they represent the input of the 1D model for the far field region located downstream of the fire. Figure 68 represents the average velocities and temperatures for longitudinal dimensions of the CFD domain increasing from 20 m to 600 m. The points plotted for L_{CFD} equal to 1200 m are computed by using the full CFD model and represent the reference values in each scenario. It can be easily seen that, for CFD domain lengths between 20 m and 200 m, the deviations in the average velocity from the reference values range between 6.5% and 40%; the variations in the temperature range between 14% and 21%. No appreciable variations can be observed when the CFD domain length is larger that 200 m.

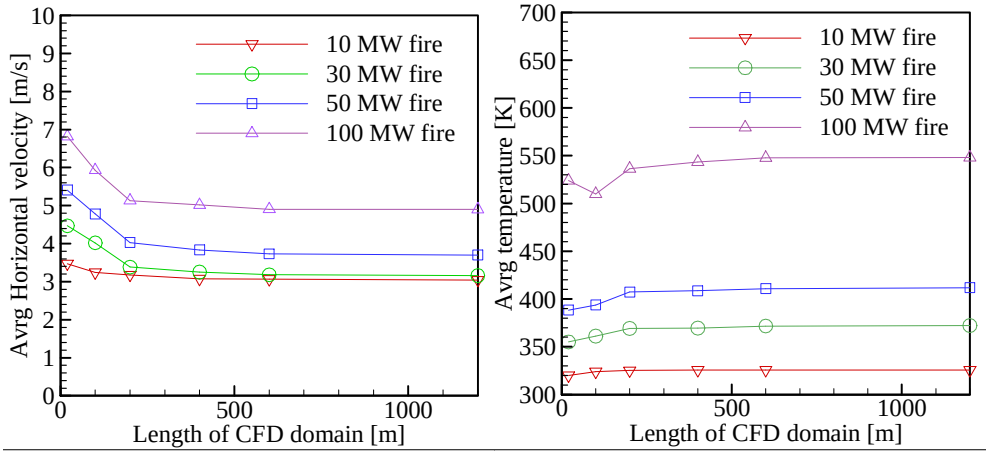

Figure 68: Effect of the CFD domain length, L_{CFD}, on the average longitudinal velocity and temperature at the outlet boundary of the CFD module. Units are in m/s and K respectively. Note that the shortest module length is 20 m.

A second study has been performed in order to identify the dependence of the local flow field solutions on the dimension of the CFD domain. Also in this case, the full CFD data has been taken as reference solution. For a generic flow quantity θ, the associated average error has been calculated with the following norm

$$\varepsilon_{\vartheta} = \frac{\sum_{j=1}^{N} \left| \vartheta_{j,CFD} - \vartheta_{j,ms} \right|}{N \overline{\vartheta_{CFD}}} \tag{76}$$

where $\overline{\vartheta_{CFD}}$ is the average predicted by the full CFD simulation, and $\vartheta_{j,CFD}$ and $\vartheta_{j,ms}$ are the values calculated in each grid point *j* belonging to the Reference Section of interest. The subscript *CFD* and *ms* are referred to the full CFD and multiscale simulation results. Obviously, the summation over *j* is extended to all the grid points belonging to the specific Reference Section.

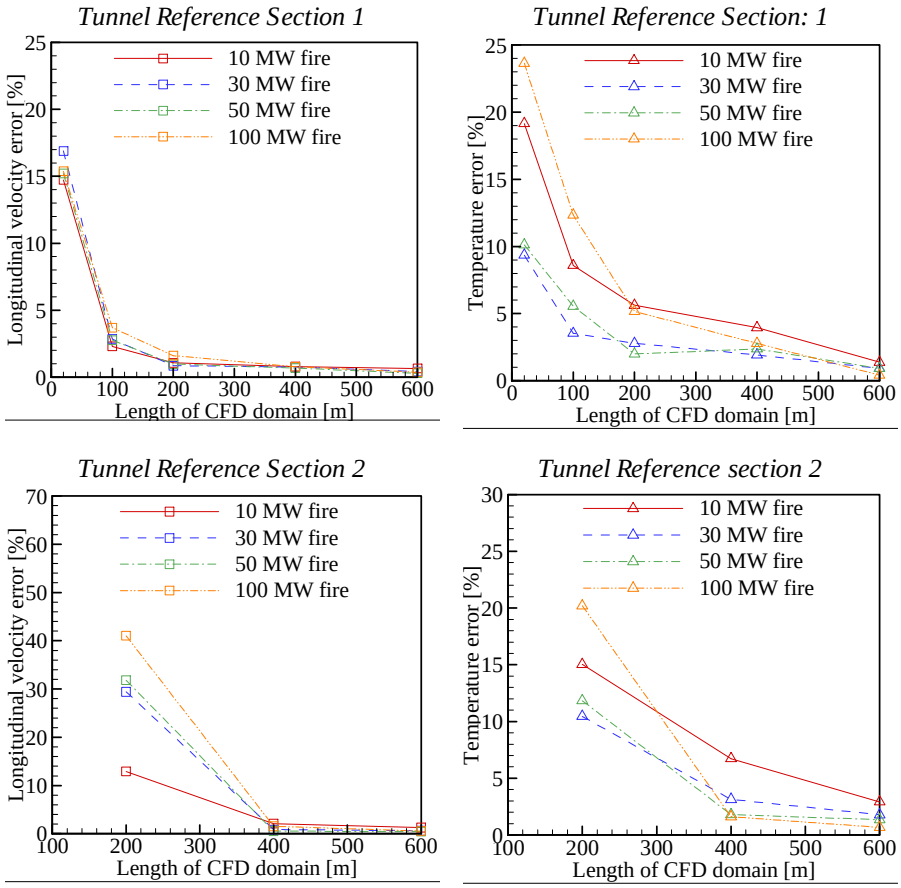

Figure 69: Effect of the CFD domain length L_{CFD} on the error for the average longitudinal velocity and average temperature. Results for top) Reference Section 1; bottom) Reference Section 2. Error calculated using Eq. (76).

The effect of the interface location on average errors has been studied for four different fire sizes (10 MW, 30 MW, 50 MW and 100 MW) and presented in Figure 69. The results show that the error does not depend on the dimension of the fire within that range. Figure 70 and Figure 71 present the field results at Reference Section 1 and Reference Section 2, respectively. The solution obtained with a 20 m long domain provides low accuracy (15% error). The results become boundary independent and provide less than 1% error for domain lengths larger than 200 m (for Reference Section

1 at 10 m downstream of the fire source) and than 400 m (for Reference Section 2 at 100 m downstream of the fire source). Thus, highly accurate results can be achieved with domains whose downstream boundary is at a minimum distance of 100 m from the furthest location where a CFD accurate solution is required.

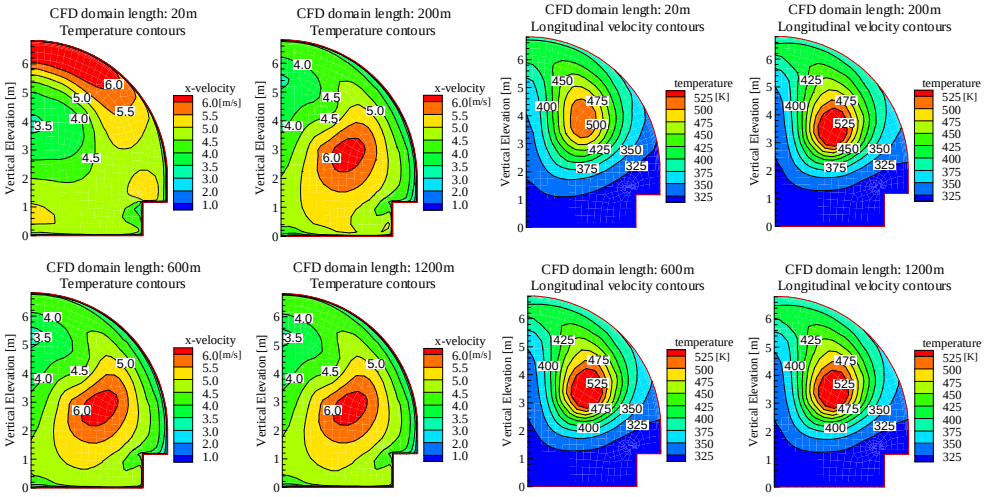

Figure 70: Effect of the CFD domain length L_{CFD} on the horizontal velocity and temperature fields at Reference Section 1 for a 30MW fire. The velocity and temperature values are expressed in m/s and K respectively

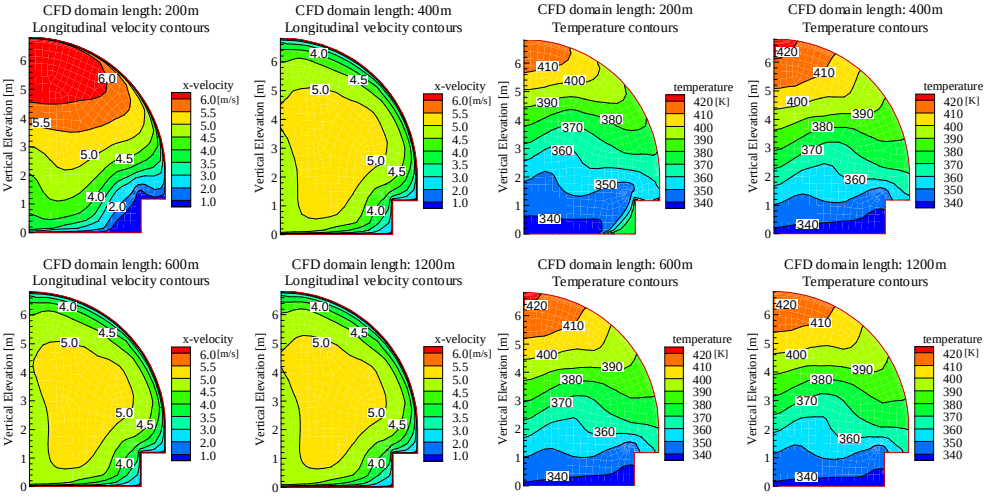

Figure 71: Effect of the CFD domain length L_{CFD} on the horizontal velocity and temperature fields at Reference Section 2 for a 30MW fire. Velocity and temperature values are expressed in m/s and K respectively

In terms of the distance from the fire to the downstream boundary interface L_D (see Figure 64), the minimum ratio between L_D and the tunnel hydraulic diameter D_H is

around 13. In a previous work Van Maele and Merci [97] simulated two different fire scenarios (3 kW and 30 kW) in a small scale tunnel (0.25×0.25 m^2) under ventilation conditions close to the critical velocity. The CFD solution in the vicinity of the fire plume became independent from the boundary location if the distance L_D is at least 12 times the hydraulic diameter. The agreement between the present and previous result is excellent.

Combining Figure 68 to Figure 71 allows identifying a range of CFD sub-domain lengths between 20 and 200 m where the average quantities at the outlet boundary as well as temperature and velocity fields show high deviation from the reference full CFD solution. In particular, average and flow field temperature show a deviation from the CFD solution up to 25%; average and flow field velocities show a deviation up to 40%. However, if the CFD module is larger than 200 m, average and flow field deviations can be significantly reduced with error of few percents.

6.3.3. Comparison to full CFD solutions

The solutions obtained with the multiscale technique and direct coupling have been compared to full CFD solutions of the same scenarios. The full CFD calculation included the full tunnel domain as well as the ventilation devices (i.e. jet fans). Based on the boundary independence study, the near field of the fire region was set to a length of 400 m. A description of the ventilation strategies for each investigated scenario is given in Table 13.

	Fire Size	Full Scale CFD mass flow rate [kg/s]	Multiscale direct mass flow rate [kg/s]	deviation
Scenario 1	*30 MW*	*216.10*	*220.62*	*2.09%*
Scenario 2	*30 MW*	*301.42*	*301.44*	*0.01%*
Scenario 3	*30 MW*	*435.19*	*434.54*	*0.15%*
Scenario 4	*30 MW*	*299.29*	*296.05*	*1.08%*
Scenario 5	*10 MW*	*204.52*	*204.48*	*3.12%*
Scenario 6	*50 MW*	*227.19*	*234.28*	*0.02%*
Scenario 7	*100 MW*	*194.28*	*208.62*	*7.38%*

Table 15: Comparison between Full CFD and Multiscale predictions for the 7 scenarios investigated. The multiscale results are obtained with direct coupling. The table presents only bulk flow data.

The comparison has been performed both in terms of bulk flow and field data from the CFD sub-domain. The bulk flow solutions obtained with the multiscale model and the comparison to the full CFD data are given in Table 15.

The first scenario involves 3 jet fan pairs operating close to the north portal. This is the minimum number of fans required to guarantee velocities above the critical value for a 30 MW fire. The deviation between full CFD and multiscale predictions is very small, around 2%. Figure 72 shows the temperature and velocity fields computed with direct coupling for scenario 1. The multiscale model predictions compare very well to the full CFD predictions. In particular no appreciable differences are observed in the temperature field. Very small differences are observed in the longitudinal velocity field. These small differences are due to the presence of the discharge cone generated by the operating jet fans upstream of the fire source which are included in the full CFD representation.

The same conclusions are reached when analyzing the results for scenarios 2 to 4. The differences in the predicted flow rate range between 0.01% and 1.4%. Field results for scenarios 2 to 4, presented in Figure 73 to Figure 75, confirm that high accuracy can be achieved.

For sake of simplicity, the comparison of the flow field data is not provided for scenario 5 to 7. However the deviations in the bulk flow predictions, resumed in Table 15, range between 0.02% and around 7% for the 100MW fire scenario. However, it must be stressed that the simulations of tunnel ventilation flows and fires suffers of high uncertainty on the real boundary conditions at the portals, effective wall roughness, fire load and its geometry, and throttling effects of vehicles. For these reasons, the largest error induced by using the multiscale model is by far within the uncertainty range of the enforced boundary conditions and it is acceptable.

The computational time required to run the full CFD model ranged between 48 and 72 hr. The multiscale model with direct coupling runs in 2 to 4 hours depending on particular scenario and initialization of the variables.

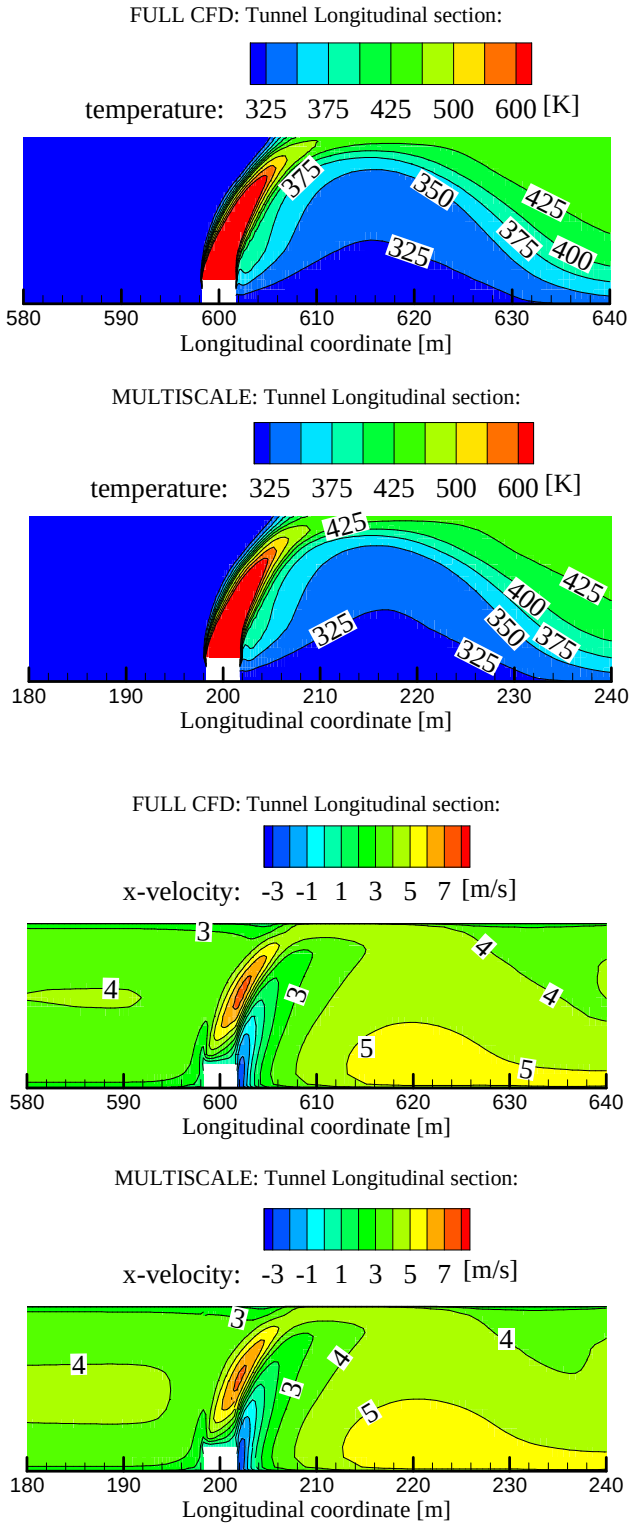

Figure 72: Comparison of results near the fire for the multiscale and the full CFD simulations for a fire of 30 MW and ventilation scenario 1. Velocity and temperature values are expressed in m/s and K respectively. The longitudinal coordinates start at the upstream boundary of the corresponding CFD domain.

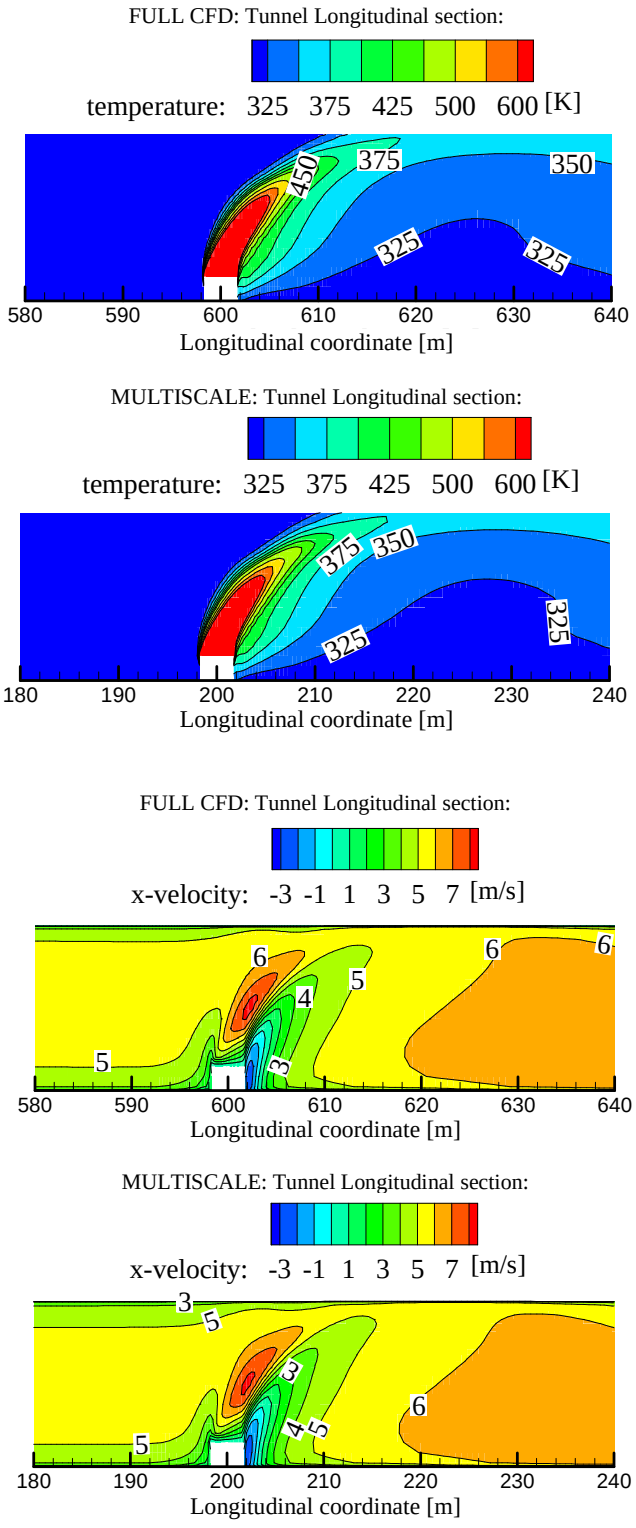

Figure 73: Comparison of results near the fire for the multiscale and the full CFD simulations for a fire of 30 MW and ventilation scenario 2. Velocity and temperature values are expressed in m/s and K respectively. The longitudinal coordinates start at the upstream boundary of the corresponding CFD domain.

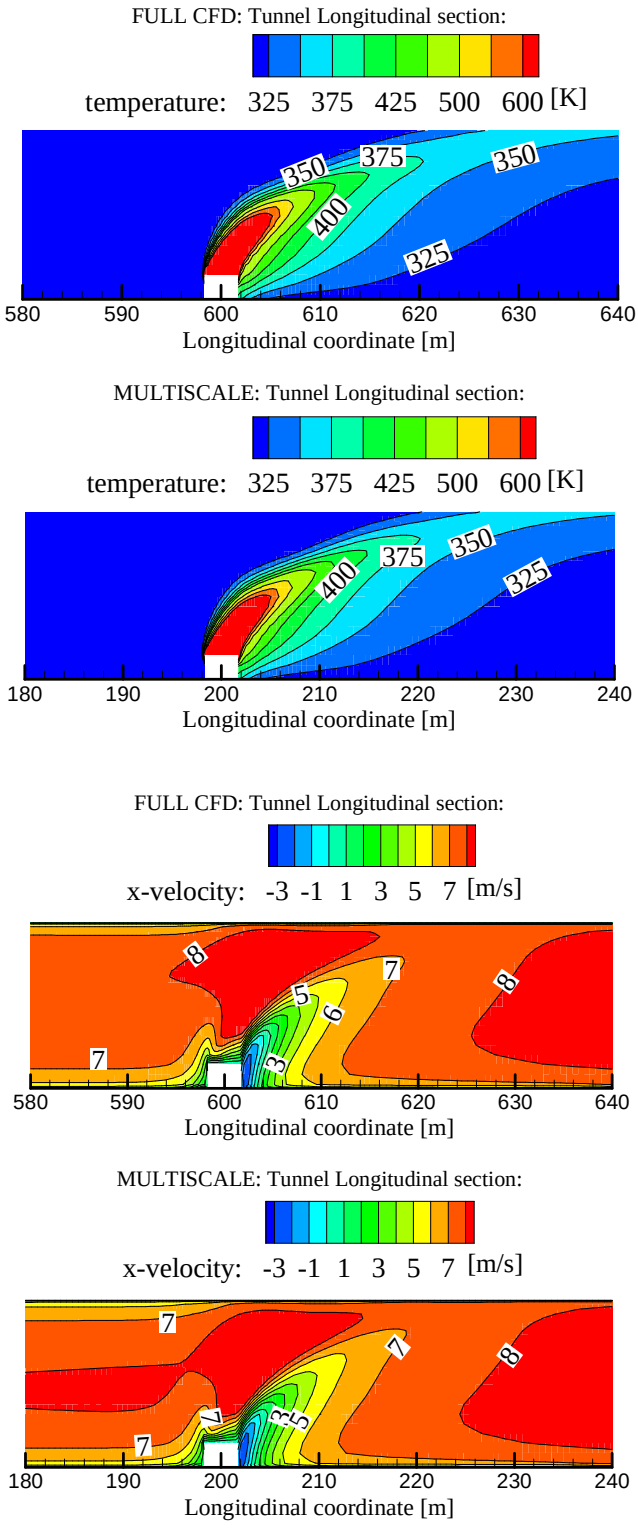

Figure 74: Comparison of results near the fire for the multiscale and the full CFD simulations for a fire of 30 MW and ventilation scenario 3. Velocity and temperature values are expressed in m/s and K respectively. The longitudinal coordinates start at the upstream boundary of the corresponding CFD domain.

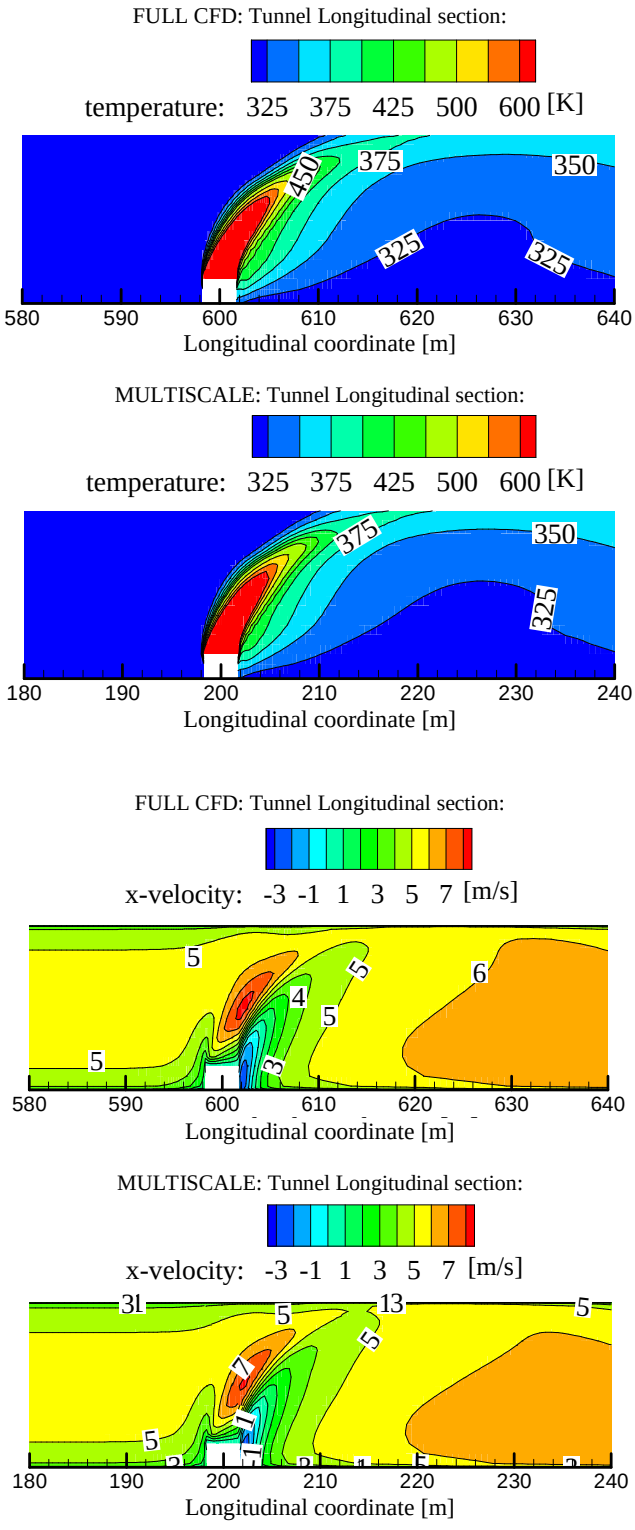

Figure 75: Comparison of results near the fire for the multiscale and the full CFD simulations for a fire of 30 MW and ventilation scenario 4. Velocity and temperature values are expressed in m/s and K respectively. The longitudinal coordinates start at the upstream boundary of the corresponding CFD domain.

6.4. Characterization of the ventilation system performance

The assessment of the ventilation system performance under different fire hazards requires, in most of the cases, only bulk flow data. Such issues can be addressed by using simple 1D models, but the final results can suffer of high uncertainty due to the simplistic representation of the fire source and the corresponding fire induced flows.

A significant improvement in the representation can be introduced by the adoption of a multiscale model with indirect coupling.

6.4.1. Calculation of the fan and fire characteristic curves

The adoption of indirect coupling strategies requires the calculation of the characteristic curves of the near field regions. Several runs of the near field CFD model are conducted, varying the pressure difference across the domain boundaries. The results are presented in terms of bulk flow velocity vs. total pressure difference. Figure 76 shows the characteristic curve of a single and a pair of operating jet fans. The curves describe the capability of jet fans to produce thrust and they are calculated adopting the methodology presented in the previous chapter.

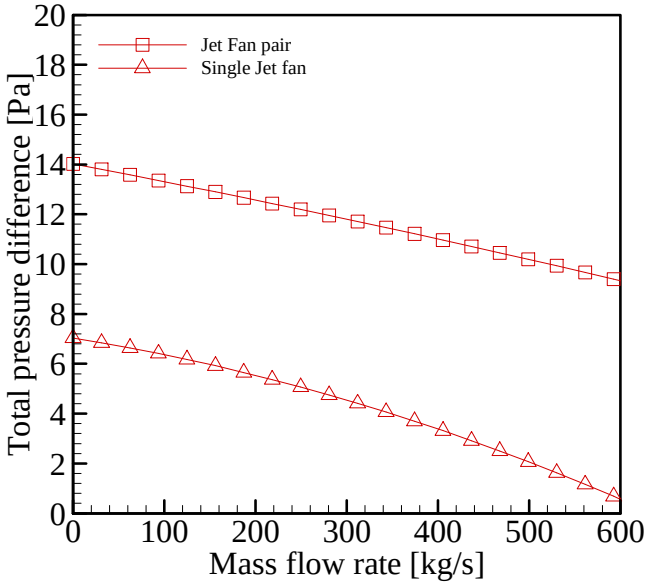

Figure 76: Characteristic curves of a tunnel region 50 m long where an activated jet fan pair (and a single jet fan) is located: Pressure drop between inlet and outlet vs. Mass flow rate across the inlet. (CFD calculated).

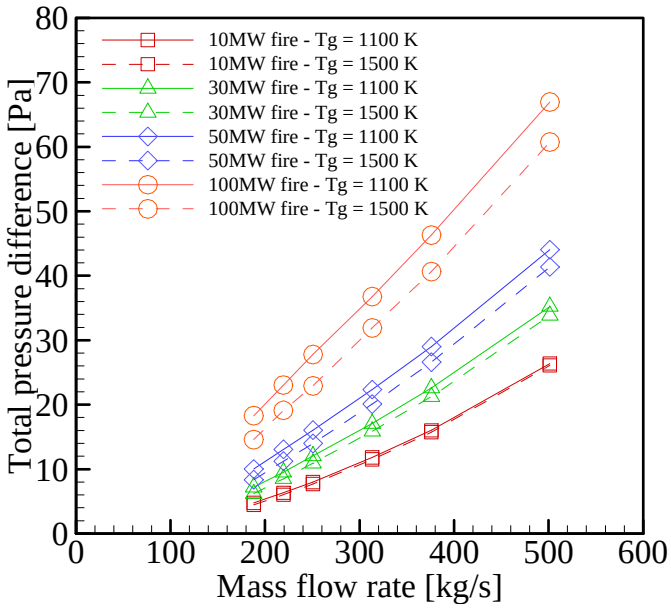

Figure 77: Characteristic curves of the tunnel region 400 m long where the fire is located: Pressure drop between inlet and outlet vs. Mass flow rate across the inlet (CFD calculated)

The same approach has been followed to calculate the characteristic curves of the fire region. Different simulations have been conducted varying the total pressure difference across the domain and calculating the resulting bulk flow velocity. Figure 77 shows the resulting curves for different fire sizes in the range from 10 to 100 MW. The sensitivity of the results to the assumed temperature of the hot gases released by the fire source has been investigated in the experimentally measured range from 1100 to 1500 K. Despite the temperature difference of 400 K (almost 50% increment), the effect on the curve for the 10 MW scenario is negligible (~1%). For the 30 MW and 50 MW scenarios the effect is smaller than 5%, and for the 100 MW it is smaller than 7%. This relatively small sensitivity is a point in favour of the simplified representation of the fire.

6.4.2. Comparison to full CFD solutions

The multiscale results obtained with indirect coupling have been compared to the full CFD solutions for cold flow and fire scenarios.

6.4.2.1. Cold flow scenarios

A previous analysis of cold flow scenarios has been performed to assess the capability of the ventilation system and whether or not the assumption of periodic behaviour for the jet fan train was acceptable. Also in this test case the analysis of the flow pattern

established for 10 operating jet fans pairs confirms the flow periodic behaviour (see Figure 78).

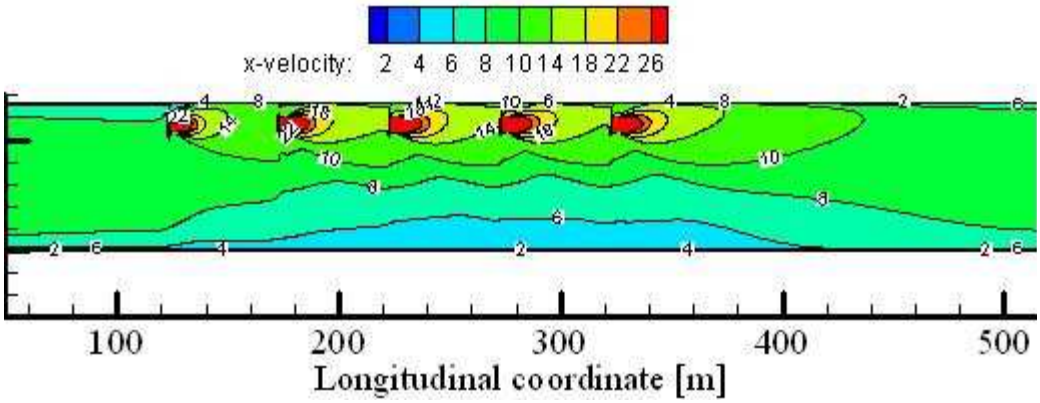

Figure 78: Longitudinal velocity iso-contours, calculated using full CFD for 10 operating jet fans pairs. (Not to scale)

The multiscale calculations have been conducted with the jet fan characteristics curves implemented in the 1D model. The multiscale and full CFD predictions of the bulk flow in the tunnel as function of the number of operating jet fans are shown in Figure 79. It is seen that the adoption of the multiscale model, including the periodic flow hypothesis, induces a numerical error lower than 1.5% in all scenarios. In Figure 79, two different ventilation scenarios with 5 operating jet fans pairs have been considered. The first configurations uses all the north portal jet fans while the second uses all the south portal jet fans (see the configuration of the ventilation system as depicted in Figure 63).

The computational time required to run the full CFD model ranged between 48 and 72 hr. The multiscale model with indirect coupling runs almost instantaneously (few seconds).

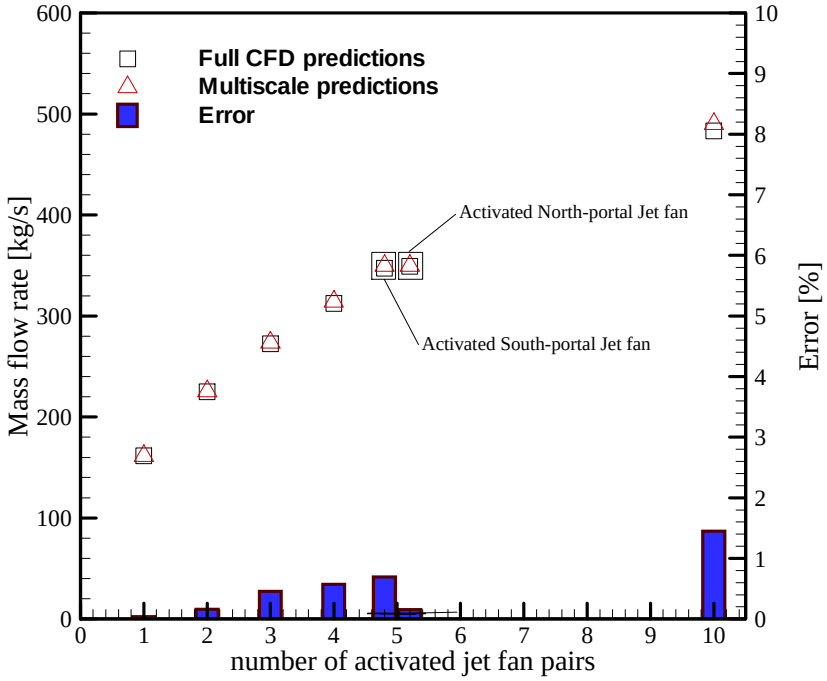

Figure 79: Predictions of average velocity for cold flow scenarios. Comparison and error between multiscale and full CFD results.

6.4.2.2. Fire scenarios

The comparison between bulk flows computed with full CFD model and multiscale model is resumed in Table 16.

	Fire Size	Full Scale CFD mass flow rate [kg/s]	Multiscale indirect mass flow rate [kg/s]	deviation	1D model mass flow rate [kg/s]	deviation
Scenario 1	*30 MW*	*216.10*	*223.53*	*3.44%*	*277.00*	*28.18%*
Scenario 2	*30 MW*	*301.42*	*305.58*	*1.38%*	*356.00*	*18.11%*
Scenario 3	*30 MW*	*435.19*	*445.52*	*2.37%*	*490.00*	*12.59%*
Scenario 4	*30 MW*	*299.29*	*300.25*	*0.32%*	*351.00*	*17.28%*
Scenario 5	*10 MW*	*204.52*	*197.70*	*3.33%*	*236.00*	*15.39%*
Scenario 6	*50 MW*	*227.19*	*242.74*	*6.85%*	*310.00*	*36.45%*
Scenario 7	*100 MW*	*194.28*	*203.01*	*4.50%*	*325.00*	*67.28%*

Table 16: Comparison between Full CFD, Multiscale, and 1D model predictions for the 7 scenarios investigated. The multiscale results are obtained with indirect coupling. The table presents only bulk flow data.

Also in this case, the comparison of the computed bulk flow data is very favourable with deviations ranging between 0.32% and 6.85%. It is worth to note that, the simple representation conducted with a fully 1D model systematically overpredicts the capability of the ventilation system (up to 67% for a 100MW fire). This is due to the

simplistic representation of the fire near field region and the inability in describing the high velocity gradients established in the vicinity of the fire.

The computational time required by full CFD simulations ranged between 48 h and 72 h while multiscale simulations with indirect coupling required few seconds once the characteristics curves are available. This is of great advantage because several ventilation scenarios can be explored and extensive sensitive analysis and parametric studies can be conducted.

6.4.3. A note of the fire throttling effect

The results contained in Table 15 and Table 16 show that the number of operating jet fans required to achieve critical ventilation velocity in the fire region varies with the fire size. In particular 2, 4 and 5 jet fan pairs must be activated to provide super-critical ventilation velocity for a 10 MW, 50 MW and 100 MW fire respectively. These results show that throttling effect of the fire is large.

Comparing the effect of the number of operating jet fans in cold flow scenarios (Figure 78) to the fire scenarios (Table 16), the fire throttling effect can be quantified at least for this specific tunnel layout. For a 100 MW fire, the mass flow when 5 jet fan pairs are activated is ~200 kg/s. When 5 jet fan pairs are activated in cold flow scenarios, the flow is ~290 kg/s. Thus, the effect of the 100 MW is to decrease the ventilation flow by more 30%. This is due to the additional fire induced pressure losses due to sudden air expansion, higher velocities in the tunnel generating higher frictional effects, buoyant effects and localized losses in the plume region. Obviously, such effects will be amplified for larger fires. Besides, it is worth to note that frictional and buoyant effects increase with the tunnel length, so the fire throttling effect can be severely magnified for longer tunnels.

The same conclusions were obtained experimentally on small scale tunnel fires by Lee and Chaiken [36] and very recently by Harvey and Fuster (2009) [131]. The latter provided a rough estimation of the fire induced pressure losses for a 70 MW and a 200 MW fire in a 2 km long tunnel. They concluded that a 200MW fire can induce 2 to 2.5 times higher pressure losses in comparison to the 70 MW one. However they could not

give any conclusion on the actual number of ventilation devices needed to cope with specific fire hazards. In the present work such evaluation can be accurately performed in a relatively short time scale since the main features of fire near field are correctly reproduced by the CFD sub-domain while the behaviour of the remaining tunnel (including frictional losses, ventilation device behaviour, portal boundary conditions etc.) is exactly represented by the 1D model maintaining the coupling between ventilation system and fire.

6.5. Concluding remarks

In this section the multiscale modelling approach has been applied to simulate tunnel ventilation flows also in case of fire. Both direct and indirect coupling strategies are used and compared to full CFD predictions for steady state conditions. The methodology has been applied to a modern tunnel with 53 m^2 cross section and 1.2 km in length. Different fire scenarios ranging from 10 MW to 100 MW are investigated varying the number of operating jet fans.

It is shown that the accuracy of the multiscale model is high when compared to the full CFD solution. In particular, the error for all the studied scenarios is below few percents. The small numerical error is more than acceptable when compared to the large uncertainty of the real meteorological conditions at the portals, actual fire load, effective lining roughness, presence of vehicles and obstructions, etc.

To the best knowledge of the author, this is the first time that a ventilation system has been coupled to a fire. This has allowed, among other things, to quantify the fire throttling effect, which is seen to be large and to reduce the flow up to 30% for a 100 MW fire.

The multiscale model has been demonstrated to be a valid technique for the simulation of complex tunnel ventilation systems under different fire hazards. It can be successfully adopted to conduct parametric and sensitivity studies, to design ventilation systems, to assess system redundancy and to assess the performance under different hazards conditions. Furthermore, the author believes that the multiscale methodology

represents the only feasible tool to conduct accurate simulations in tunnels longer than few kilometres, when the limitation of the computational cost becomes too restrictive.

In this section, the ventilation scenarios are set for super-critical velocities preventing the smoke back-layering. Thus, the assumption of 1D flow at the upstream boundary is guaranteed. In order to use the multiscale model to investigate sub-critical ventilation scenarios, the upstream boundary must be moved to ensure that all the back-layering is captured within the CFD domain. If otherwise, there will be a tunnel region close to the upstream boundary where the computed flow field will present deviation from the full-CFD solution as presented for the downstream boundary apply.

Parts of this work have been published in *Fire Technology [105]*.

7

Multiscale modelling of time-dependent tunnel ventilation flows and fires

7.1. Introduction

In chapter 5 and 6 the multiscale modelling approach has been used to simulate the behaviour of tunnel ventilation flows and fires in steady state conditions. The information provided by this type of simulations is fundamental for analysing the effectiveness of the ventilation system under different fire hazards. Typically such analysis provides data related to the occurrence of back-layering, velocity and temperature distributions within the tunnel domain, velocity profile and temperature fields in the vicinity of operating ventilation devices or close to the fire source.

However, a complete analysis of the ventilation system response and its interaction with the fire is a much more complex task. Indeed, when defining the optimum ventilation strategy for a given fire scenario, other significant issues arise. For instance, information

related to the time required to reach the critical velocity in the fire region, to clear a certain tunnel portion from smoke, or the temporal evolution of the smoke stratification, is fundamental to analyse the development of an emergency scenario. Furthermore, such data are fundamental to determine the evolution of hazardous zones in the tunnel domain, to design evacuation procedures or to determine the correct timing for the activation of fixed fire fighting systems (e.g. water mist, deluge or sprinkler systems).

Obviously, the amount variables that come into play when conducting time dependent analysis increases making sensitivity studies or parametric analysis more complex. Indeed, if steady state analyses require mainly peak HRR and operating ventilation devices, time dependent analyses require inputs data related to the detection times, response time of the ventilation system and fire growth curve. Furthermore, the characteristic transient time ranges from 5 min for the detection and protection activation to 30 min for smoke moment. This last one increases with the tunnel length.

The application the multiscale model for time dependent analysis of tunnel ventilation flows and fires is the subject of this chapter. The great engineering value of multiscale techniques is boosted in this application since the number of input variables, the size of the computational domain and the temporal duration of the event to be simulated are so large that full-scale CFD would demand very large computational resources, most likely out of reach for applications to real systems.

Typically, only few full CDF runs are conducted and sensitivity studies to the main variables (e.g. detection time, fire growth curve and operating ventilation devices) cannot be provided.

7.2. A case study: a modern tunnel 1.2 km in length

The multiscale technique has been used to simulate a 1200 m long tunnel longitudinally ventilated whose layout is the same as the one presented in the chapter 6. A schematic of the tunnel layout is presented in Figure 80. The tunnel is 6.5 m high with standard horseshoe cross section of around 53 m^2 and hydraulic diameter around 7.3 m. The same geometry of the East Dartford tunnel cross section has been used for the scope (see Figure 49).

The tunnel is equipped with two groups of 5 jet fans pairs 50 m spaced, each group installed near a tunnel portal. The jet fans are rated by the manufacturer at the volumetric flow rate of 8.9 m^3/s with a discharge flow velocity of 34 m/s.

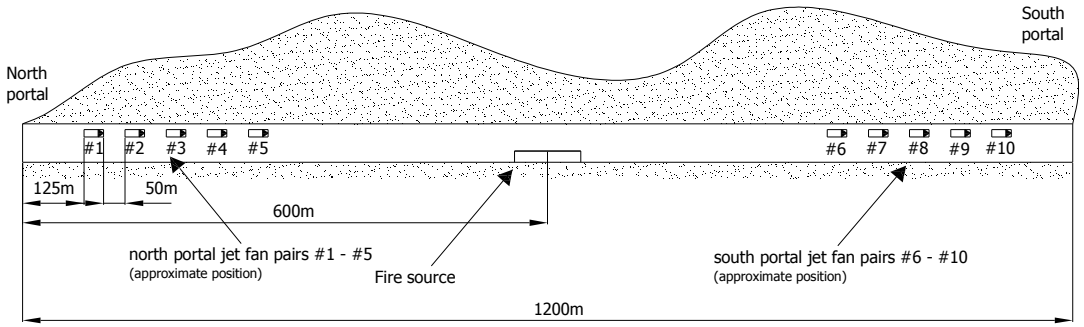

Figure 80: Layout of the tunnel used as case study showing the relative positions of the fire, jet fans and portals (Not to scale).

The fire is located in middle of the tunnel and only a 30 MW fire is considered for this specific application.

The fire growth curve has been built on the basis of the prescriptions proposed by Carvel [17] that apply to tunnel fires involving typical material mixtures for European HGVs cargos [8]. The author observed that the typical t^2 fire representation [6] was not fitting any of the experimental data and proposed a two-step linear approximation. During the first step the fire would grow slowly up to 1÷2 MW, while during the second step, the growth rate would be significantly higher (up to 15 MW/min). The changing of the fire regimes usually takes place after a *delay phase* usually as long as few minutes (from 2 to 6). The author observed also that the delay phase length and the fire growth rate are somehow correlated to the ventilation flows experienced by the fire during its development. For the time dependent analysis conducted in this section an average temporal duration of the delay phase equal to 4 min has been chosen; during this phase the fire growth rate is assumed to be equal to 0.5 MW/min. The following phase is characterized by a higher growth rate equal to 15 MW/min. The peak HRR (30 MW) is reached after around 350 s.

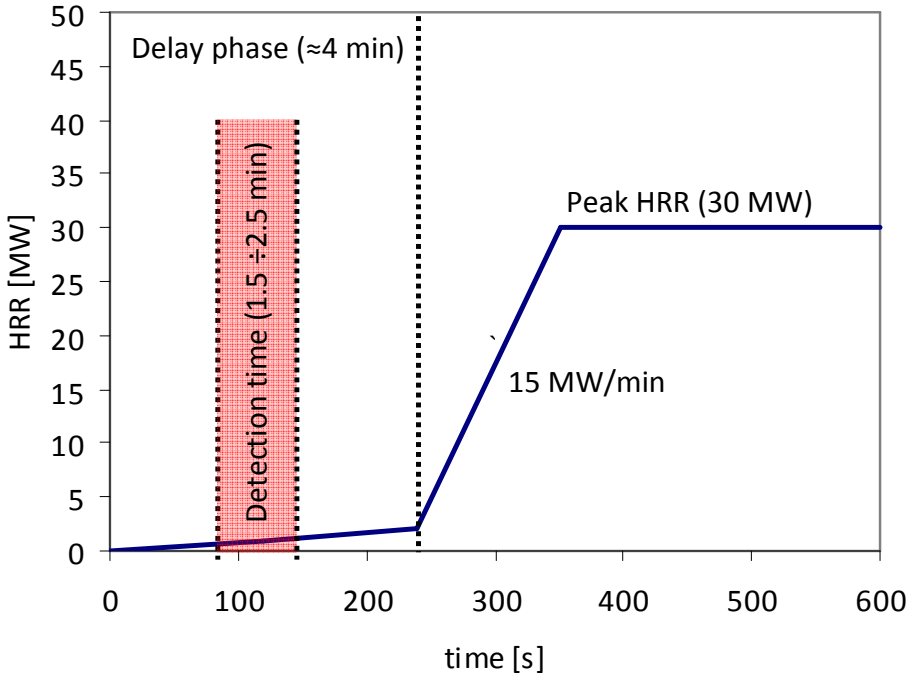

Figure 81: Fire growth curve, delay phase and detection times considered in the time dependent multiscale simulations. The fire growth curve is based on the work of Carvel (2008) [17].

Three different ventilation strategies have been considered for the analysis: 1st strategy involving operating jet fans pairs from #1 to #3; 2nd strategy involving operating jet fans pairs from #1 to #5; 3rd strategy involving operating jet fans pairs from #1 to #10. The fan characteristic curves are the ones computed in the previous chapter and depicted in Figure 76. The jet fans are supposed to reach full thrust after 10 s. However, it has been found that the impact of this variable on the results is negligible being the characteristic time scale of tunnel ventilation flows almost 2 orders of magnitude larger.

Three initial simulations have been run adopting a constant value of detection time (indicated as TD hereafter) equal to 2 min representing an average value for slow growing fire detected by means of fibre optic linear detection cables [132]. Eventually, shorter detection times could be expected for faster growing fires (i.e. pool fires) or more efficient detection techniques based on video analysis systems [133]. On the other hand, longer detection times can be expected if the fire is shielded by obstacles or located underneath the vehicle [134]. For these reasons, after running three base cases characterized by a 2 min detection time, it has been varied to 1.5 min and 2.5 min and the effects on the development of the emergency scenario have been assessed.

The temporal duration of the simulated fire emergency is equal to 10 min being this the time required to reach steady state conditions in the tunnel domain. An overview of the time-dependent ventilation scenarios analysed in this chapter is given in Table 17.

	Fire Size	Jet fan pairs #1- 3	Jet fan pair #4-5	Jet fan pairs #6 - 10	Detection time [min]
Scenario 1	*30 MW*	*ON*	*OFF*	*OFF*	*2*
Scenario 2	*30 MW*	*ON*	*ON*	*OFF*	*2*
Scenario 3	*30 MW*	*ON*	*ON*	*ON*	*2*
Scenario 4	*30 MW*	*ON*	*OFF*	*OFF*	*2.5*
Scenario 5	*30 MW*	*ON*	*ON*	*OFF*	*2.5*
Scenario 6	*30 MW*	*ON*	*ON*	*ON*	*2.5*
Scenario 7	*30 MW*	*ON*	*OFF*	*OFF*	*1.5*
Scenario 8	*30 MW*	*ON*	*ON*	*OFF*	*1.5*
Scenario 9	*30 MW*	*ON*	*ON*	*ON*	*1.5*

Table 17: Summary of the ventilation scenarios considered in the time dependent analysis

The multiscale simulations have been conducted by using a multiscale model with direct coupling approach. As already pointed out in the previous sections this approach allows the computation of detailed flow and temperature field data in the 3D-CFD sub-domain which includes the fire while the rest of tunnel layout is represented by adopting a 1D modelling approach. More details on the coupling technique can be found in chapter 4

A schematic of the coupling between 1D model of the far field and CFD model of the near field has been depicted in Figure 82.

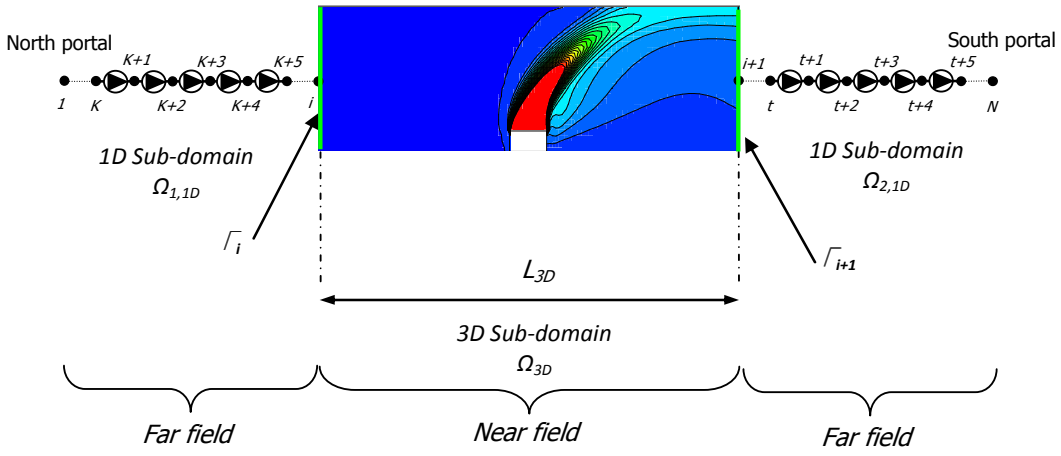

Figure 82: Schematic of the multiscale model of a 1.2 km tunnel including portals, jet fans, and the CFD domain of the fire region. Contours of the temperature field show the fire plume. (Not to scale). The 1D-CFD interfaces have been highlighted in green

As already asserted in the previous chapters, a critical point of the multiscale representation is the positioning of the 1D-3D interfaces (Γ_i and Γ_j in Figure 82). Indeed, they must be located in a domain region where the flow is fully developed and is characterized by mild velocity gradients. This issue was already addressed for the same tunnel layout ad fire sizes in the previous chapter. The analysis confirmed that, if boundary is located at a distance larger that 13 times the tunnel hydraulic diameters, average and flow field deviations can be significantly reduced with error of few percents in comparison to full CFD solutions. On the basis of this estimation, the outlet boundary has been located at distance equal to 20 times the tunnel diameter (~ 150 m) and therefore, the length of the CFD sub-domain is equal to 300 m being the fire located in the middle.

The assumption of 1D flow at the upstream boundary must be maintained during the whole calculation and also during the initial stages of the fire emergency when the ventilation system is not yet operating or the ventilation flow is still sub-critical. In these cases it must be ensured that all the initial back-layering is captured within the CFD domain. If otherwise, there will be a tunnel region close to the upstream boundary where the computed flow field will present deviation from the full-CFD solution as presented for the downstream boundary. For time dependent calculations a rough estimation of the smoke front velocity and the consequent travelled distance can be based on the correlation presented in [135]

$$v_{smoke} = c\left(\frac{gQ(1-\lambda)T}{c_p \rho_o T_o^{\,2} W}\right)^{1/3} \tag{77}$$

where c is an empirical constant equal to 0.8, g is the gravity, T the smoke temperature, Q the fire HRR, λ the fire radiative losses, c_p the air specific heat at constant pressure, W the tunnel width, ρ_o the ambient density and T_o the ambient temperature. The smoke temperature in the fire zone can be assumed to vary between 1100 K and 1500 K (lower values can be expected if the flame does not touch the ceiling). A rough approximation of the temperature evolution beneath the ceiling can be performed by using the energy equation for 1D tunnel bulk flows [5].

However, a posteriori post-processing of the CFD results must always be conducted to clarify this matter.

7.3. Multiscale model results

Figure 83 shows the temporal evolution of the mass flow rate through the tunnel as computed by the multiscale model for the first 3 base scenarios characterized by a TD of 2 min. Supercritical ventilation conditions, corresponding to bulk flow velocity larger than 3m/s, are reached after 244 s, 190 s and 156 s after the fire outbreak (124 s, 70 s and 36 s from the moment of the ventilation system activation) for scenario 1 2 and 3, respectively. At this moment in time the fire is still in its incipient phase and its HRR is lower than 2MW.

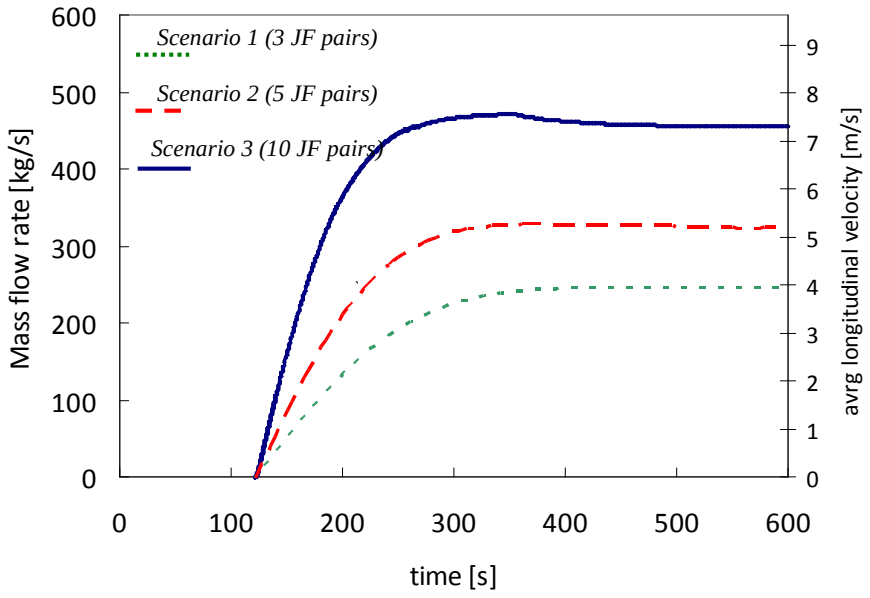

Figure 83: Time dependent evolution of the mass flow rate through the tunnel for scenario 1, 2 and 3 (see Table 17). The time to detection is 2 min. Supercritical conditions (v_{air}> 3m/s) are reached after 244 s, 190 s and 160 s for scenario 2 and 3 respectively

Figure 84 shows the conditions within the tunnel 120 s after the fire outbreak. As it can be seen velocity and temperature profiles are still symmetric since the ventilation system has not been yet activated. The smoke fronts are located around 110 m far away from the fire source (~40 m from the 1D-CFD interfaces). This first result shows that when the ventilation system is activated the back-layering nose is by far within the upstream boundary of the computational domain.

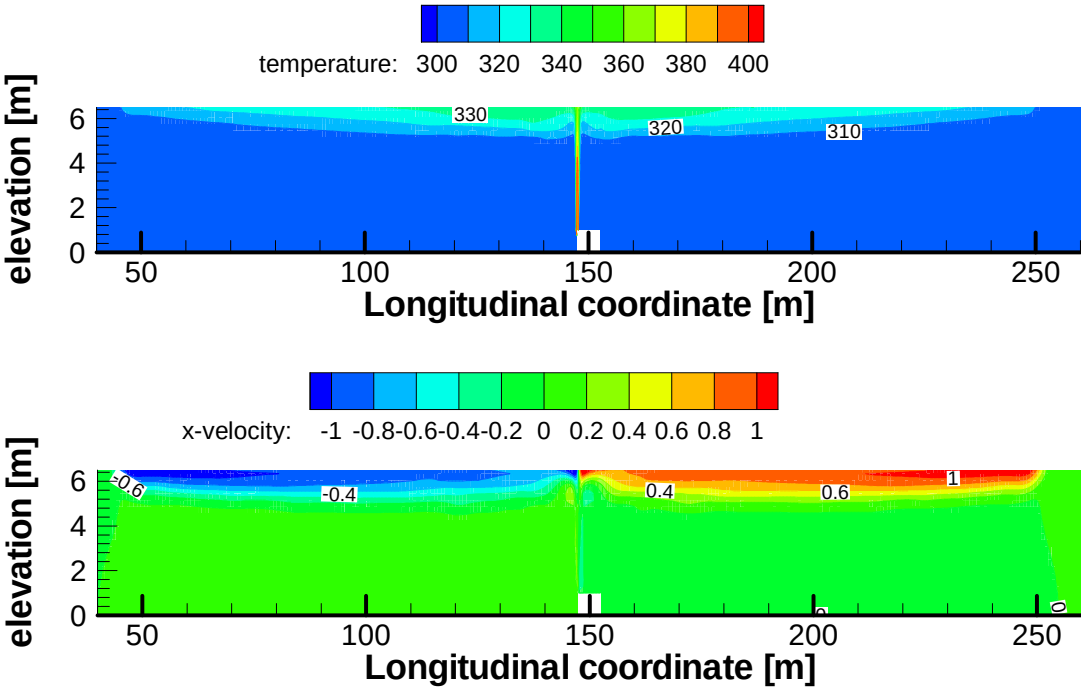

Figure 84: Multiscale results in the vicinity of the fire computed 2 min after the fire outbreak for scenario 1, 2 and 3 (see Table 17). The ventilation system is about to be started. Velocity and temperature values are expressed in m/s and K respectively. The longitudinal coordinates start at the upstream boundary of the corresponding CFD domain. (not to scale)

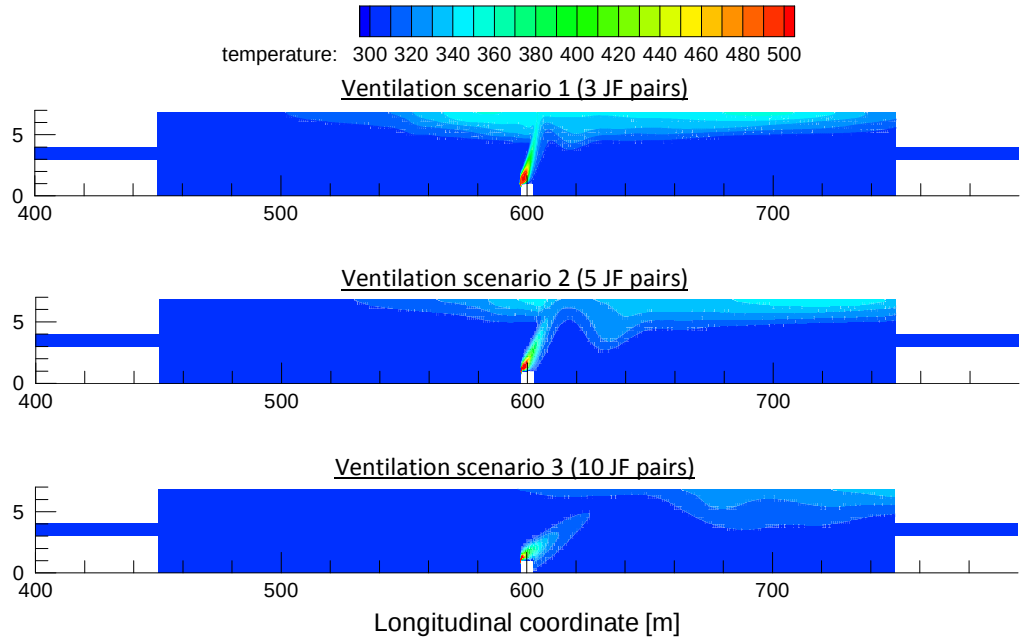

Figure 85: Temperature profiles computed by the multiscale model 3 min after the fire outbreak for scenario 1, 2 and 3 (see Table 17). The ventilation system is operative since 1 min. Temperature values are expressed in K. (not to scale)

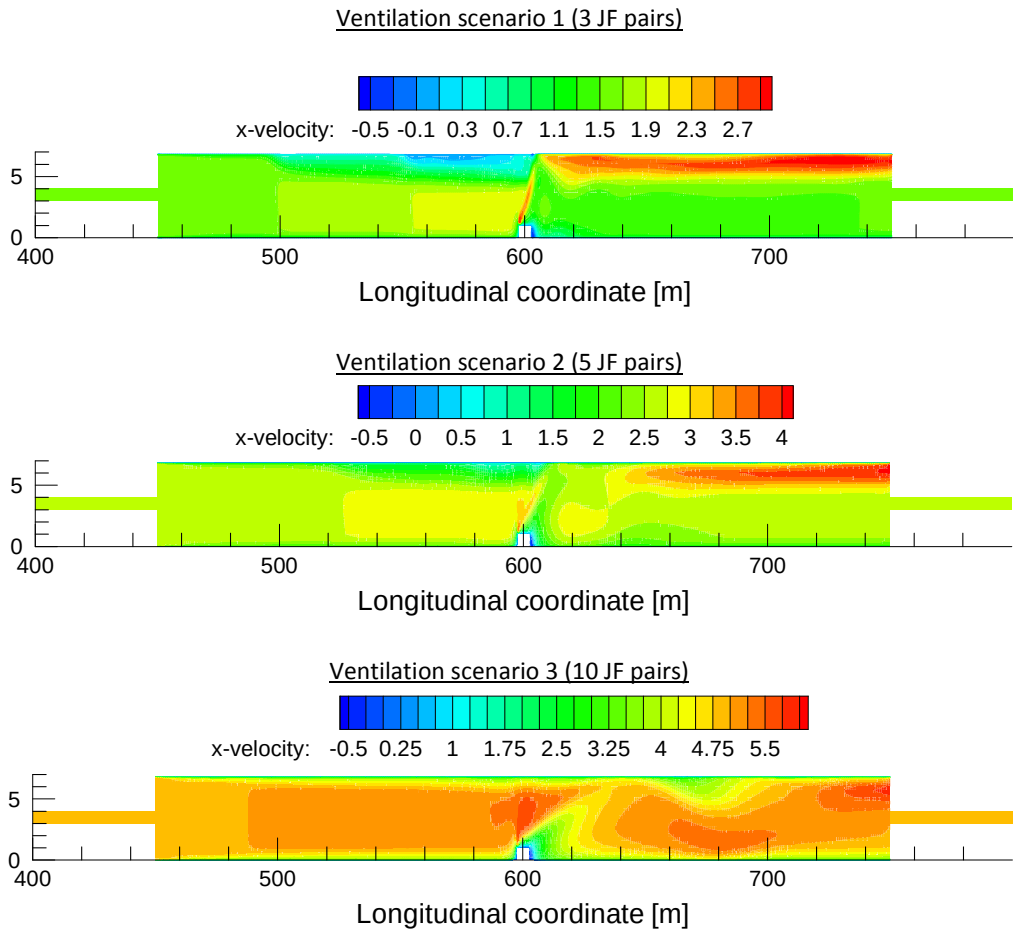

Figure 86: Longitudinal velocity profiles computed by the multiscale model 3 min after the fire outbreak for scenario 1, 2 and 3 (see Table 17). The ventilation system is operative since 1 min. Velocity values are expressed in m/s. (not to scale)

Figure 85 and Figure 86 show the temperature and velocity profiles in the tunnel domain 3 min after the fire outbreak for ventilation scenarios from 1 to 3. The higher performance of ventilation strategy #3 involving 10 operating jet fan pairs is clear since the back-layering nose is completely removed from the tunnel region upstream of the fire. Differently, back-layering regions (100 m and 70 in length) can be still observed for ventilation scenarios #1 and #2 involving 3 and 5 operating jet fan pairs, respectively. The average ventilation velocity in the fire region is around 1.8 m/s, 2.8 m/s and 5 m/s for ventilation scenarios 1, 2 and 3, respectively. Furthermore it can be seen that, given the relatively low ventilation velocity and fire size (smaller that 2 MW), smoke stratification is maintained both in the upstream and downstream regions for all the scenarios. Therefore, both the regions upstream and downstream of the fire can be used for evacuation purposes within the first 3 min from the fire outbreak.

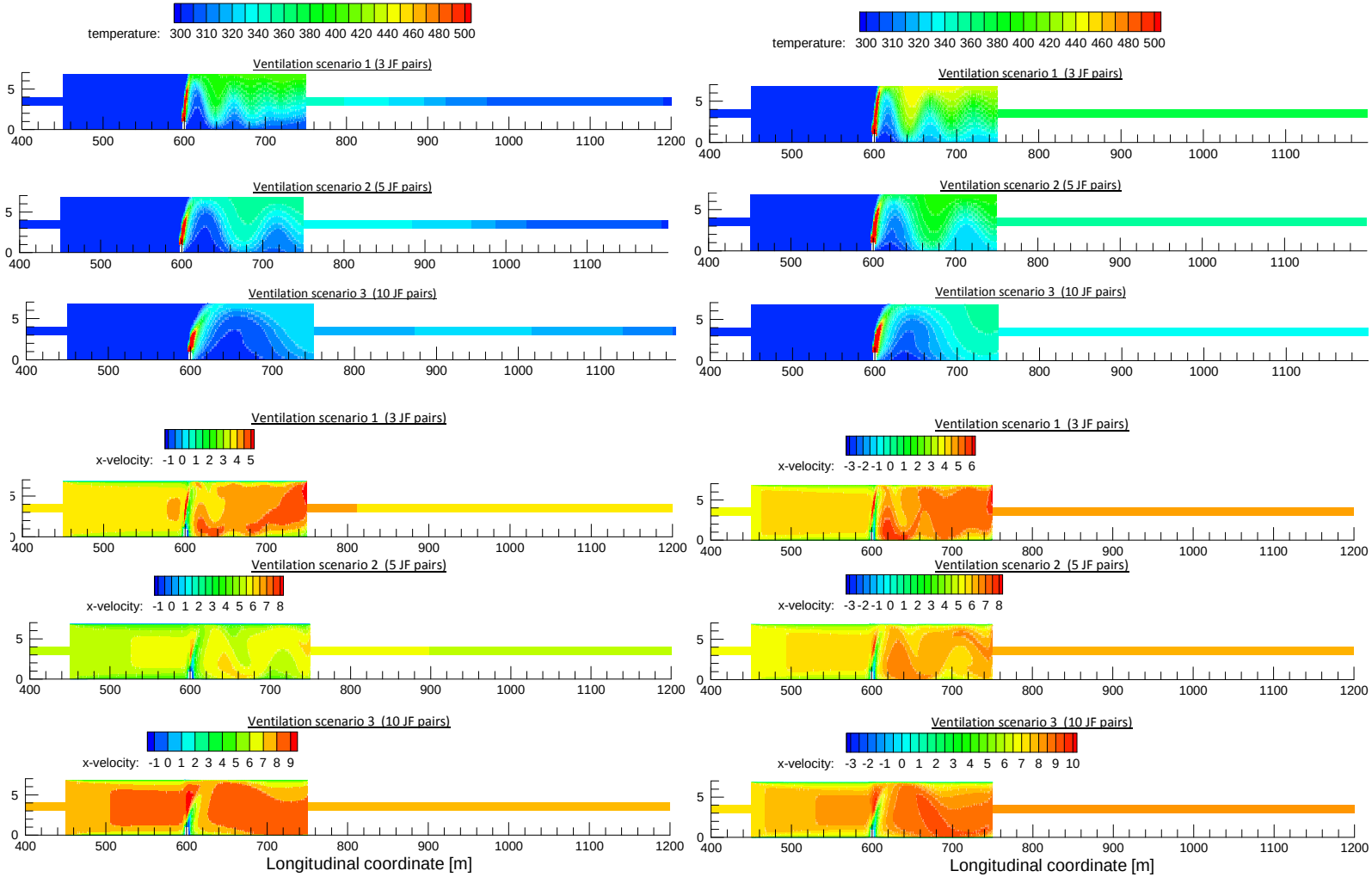

Figure 87: Temperature and velocity profiles 5 min (left column) and 10 min (right column) after the fire outbreak for scenario 1, 2 and 3 (see Table 17). Temperature and velocity values are expressed in K. and m/s, respectively (not to scale)

Figure 87 presents the computed temperature and flow fields 5 min and 10 min after the fire outbreak for ventilation scenarios from #1 to #3. The temperature contours computed 5 min (left column in Figure 87) after the fire outbreak show that the back-layering has been removed in the three ventilation scenarios while the smoke front is located at a distance downstream of the fire source of 350 m and 450 m for scenarios 1 and 2, respectively. Since the ventilation velocities achieved during the emergency scenario 3 are considerably higher (see Figure 83), the smoke front has already reached the tunnel portal 5 min after the fire outbreak. The results show that smoke stratification downstream of the fire is lost at distances of 30, 60 and 100 m for scenarios 1,2 and 3, respectively. Therefore, only the tunnel regions upstream of the fire and these short distances downstream can be used for evacuation purposes. The average ventilation velocity in the fire region is around 3.5 m/s, 5 m/s and 7 m/s for ventilation scenarios 1, 2 and 3, respectively. Given the larger ventilation flows attained in the ventilation scenario 3, considerably lower temperatures (around 100 K lower than for ventilation scenario 1) are achieved within the tunnel domain.

Temperature and velocity profiles within the tunnel domain 10 min after the fire outbreak are resumed in Figure 87 right column. Both the fire and the ventilation flows have reached steady state conditions while the smoke front has reached the downstream portal for scenarios 1, 2 and 3. The average ventilation velocity in the fire region is around 4 m/s, 5.5 m/s and 7.5 m/s for ventilation scenarios 1, 2 and 3, respectively.

Beside the time required to reach supercritical ventilation velocities (indicated as TC hereafter) in the fire region, another important variable is the time required to remove the back-layering (indicated as TB hereafter) from the fire upstream region. In particular it has been computed that the fire upstream region can be cleared after 255 s, 220 s and 187 s after the fire outbreak (135 s, 100 s and 67 s from the moment of the ventilation system activation) for ventilation scenarios 1, 2 and 3, respectively.

The multiscale analysis conducted allows for an assessment of the impact of the number of activated jet fan pairs on TC and TB. In particular it can be calculated that the simultaneous activation of 10 jet fan pairs (ventilation scenario 3) instead of 3 jet fan pairs (ventilation scenario 1) induces a reduction on TC and TB by 36 % and 30 %,

respectively. However, it must be asserted that the TD (120 s) still represents a large portion of TC and TB and therefore its reduction is desirable as it impacts considerably their values. Table 18 gives an overall view on the numerical findings.

	Fire Size	Jet fan pairs #1- 3	Jet fan pair #4-5	Jet fan pairs #6 - 10	Detection time (TD) [min]	Time to critical velocity (TC) [s]	Time to remove back
Scenario 1	*30 MW*	*ON*	*OFF*	*OFF*	*2*	*244*	*255*
Scenario 2	*30 MW*	*ON*	*ON*	*OFF*	*2*	*190*	*220*
Scenario 3	*30 MW*	*ON*	*ON*	*ON*	*2*	*156*	*187*
Scenario 4	*30 MW*	*ON*	*OFF*	*OFF*	*2.5*	*290*	*300*
Scenario 5	*30 MW*	*ON*	*ON*	*OFF*	*2.5*	*220*	*260*
Scenario 6	*30 MW*	*ON*	*ON*	*ON*	*2.5*	*188*	*222*
Scenario 7	*30 MW*	*ON*	*OFF*	*OFF*	*1.5*	*214*	*212*
Scenario 8	*30 MW*	*ON*	*ON*	*OFF*	*1.5*	*160*	*181*
Scenario 9	*30 MW*	*ON*	*ON*	*ON*	*1.5*	*126*	*152*

Table 18: Summary of the ventilation scenarios considered and numerical findings

Among the remaining cases, scenarios 4 to 6 are characterized by a 2.5 min detection time and 3, 5 and 10 operating jet fan pairs, respectively. Scenarios from 7 to 9 are characterized by a 1.5 min detection time and 3, 5 and 10 operating jet fans respectively.

A careful analysis of the TC values shows that a variation in the time to detection produces a simple shift in the time required to attain critical velocity in the fire region. Indeed, for scenarios 1, 4 and 7 characterized by 3 operating jet fan pairs, the system required around 130 s (from the moment of activation) to generate critical ventilation velocities in the fire zone. Similarly, for scenarios 2, 5 and 8 characterized by 5 jet fan pairs, and for scenarios 3, 6, and 9 characterized by 10 jet fan pairs, it requires around 70 s and 40 s, respectively. The previous data show that TC can be reduced by 70% by increasing the number of operating jet fan pairs from 3 to 10.

These results confirm that the values of TC are mainly dependent on detection time and ventilation strategies (e.g. number of operating jet fans) while they are almost insensitive to the specific fire stage. Due to the presence of the initial low HRR stage, the ventilation system is able in most of the ventilation scenarios to generate supercritical ventilation velocity before the fire has reached a considerable size and therefore its impact on the ventilation system response in negligible. Indeed for the fastest response case (scenario 9) the fire size is 1.25 MW while for the slowest response case (scenario 4) the fire size is around 15 MW (half of the full size). It must

be asserted that the fire growth could have a larger impact on the value of TC for faster developing fires (e.g. pool fires).

The analysis conducted provides also information related to the time required to remove the back-layering (TB) defined as the moment when ambient conditions are re-established just upstream of the fire source. The whole set of computed vales is contained in Table 18 and plotted in Figure 88 which highlights the dependence between number of operating jet fans, time to detection and time required to remove back-layering (computed from the moment of the ventilation system activation).

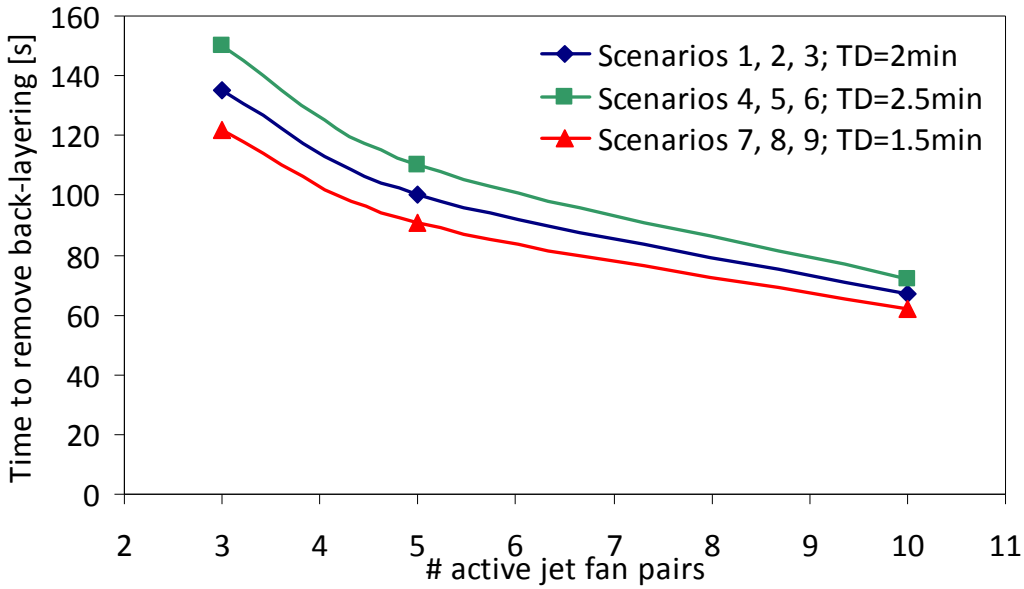

Figure 88: Dependence between number of operating jet fan pairs, TD, and time required to remove back-layering computed from the moment of the ventilation system activation.

It is clearly shown how, due to the further location of the smoke front when the ventilation system is activated, the larger is the time to detection the larger is the time required by a constant number of jet fans (once activated) to remove the back-layering. Figure 88 also clarify that impact of TD on TB becomes smaller when the number of jet fans simultaneously activated is larger; indeed, the curves tend to get closer when the number of operating fans is larger.

Although ventilation scenarios involving 3, 5 or 7 operating jet fan pairs are equivalent from a steady-state point of view since able of removing back-layering, they do not have the same dynamic response. Figure 89 shows the correlations between the number

of active jet fan pairs, detection time and the time required for remove back-layering (computed, in this case, from the fire outbreak). TB values will be the sum of detection time and response time of the ventilation system. While the former depends mainly on the technology used for detection (linear detectors, video analysis or flame detectors), the latter will depends on the ventilation strategy adopted (i.e. number of available jet fan pairs) and on the tunnel geometry.

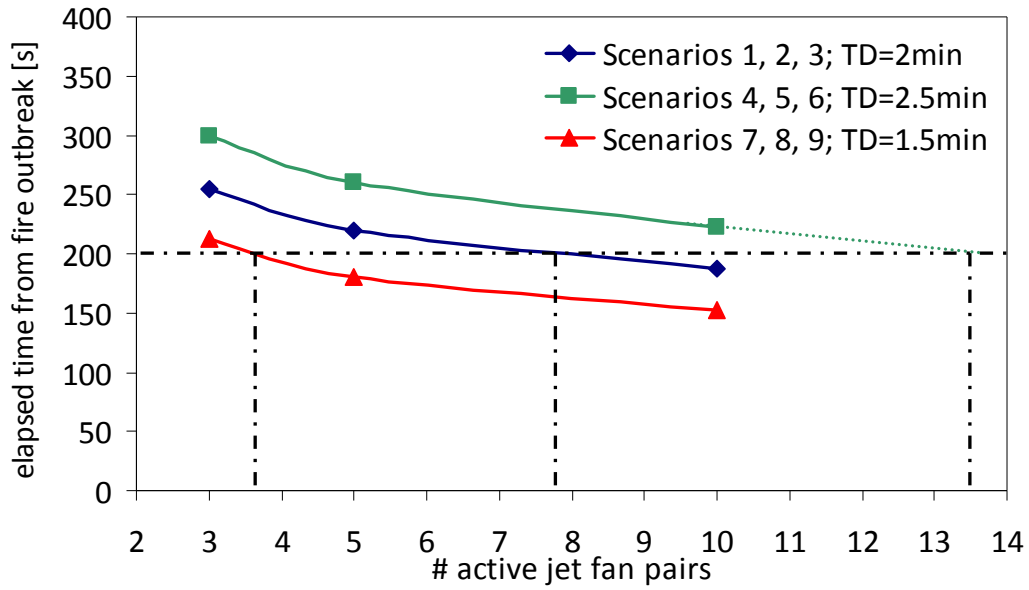

Figure 89: Dependence between number of operating jet fan pairs, TD, and time required to remove back-layering computed from the fire outbreak

Figure 89 clarifies also the great impact of the detection time on the time to remove back-layering. Indeed, a relative small variation on the detection time (30 s) has a huge impact on the minimum number of ventilation devices needed to fulfil a given requirement on TB.

7.4. Concluding remarks

In this section the multiscale modelling approach has been applied to simulate real tunnel fire emergency. The multiscale model, run in direct coupling fashion, has been used to solve time dependent problems.

The methodology has been applied to a 1.2 km long tunnel (53 m^2 cross section) under a 30 MW fire hazard. The fire growth curve has been approximated following a two

linear step approximation. 3 different ventilation scenarios involving 3, 5 and 10 jet fan pairs have been simulated. The time to detection has been ranged between 1.5 and 2.5 min. The simulated time interval was equal to 10 min starting from the fire outbreak.

Being the model run in time dependent fashion, it allows for a complete analysis of the ventilation system response and its interaction with the fire. For instance, information on the time required to reach critical velocity conditions in the fire region, to remove back-layering or related to the evolution of the smoke stratification in the fire region could be obtained. Such data are fundamental to determine the evolution of hazardous zones in the tunnel domain, to design evacuation procedures or to determine the correct timing for the activation of fixed fire fighting systems (e.g. water mist, deluge or sprinkler systems). The computed data confirm the great impact of detection time and number of jet fans on the ventilation system response. A smaller impact is induced by the fire growth curve but this is likely due to the design fire used for the simulations characterized by an initial low growth rate phase. Larger impact could be expected for faster growing design fires. Similar considerations can be done for longer tunnel, where the response of the ventilation system is intrinsically slower and therefore the fire has longer available time to evolve towards significantly larger size.

The effectiveness of the model when dealing with for sub-critical fire scenarios has been also confirmed. The crucial point is represented by the correct sizing of the CFD sub-domain in order to capture the back-layering occurrence. Some empirical correlations related to this issue are provided.

A reduction of the required computing time of almost 2 orders of magnitude is expected also for time dependent calculations. However, a direct assessment of such reduction could not be performed as done for steady state simulations since, based on estimations, each transient full CFD simulation could take up to 3 months. These results confirm that the multiscale methodology represents the only feasible tool to conduct accurate simulations in tunnels longer than few kilometres, when the limitation of the computational cost becomes too restrictive.

Given the low computational complexity of the multiscale model in comparison to traditional computing techniques, the model enables for simultaneous economic

optimizations of the overall ventilation/detection system. For instance, we can think of a coupled ventilation/detection system which is designed to cope with a 30 MW fire and that, for evacuation purposes, requires to be able to fully control the smoke spread (i.e. remove back-layering) within 200 seconds from the fire outbreak. Having this goal fixed, the following combined ventilation/detection systems would be equivalent (see Figure 89):

1. 4 jet fan pairs + detection technique able to detect the fire within 1.5 min
2. 8 jet fan pairs + detection technique able to detect the fire within 2 min
3. 14 jet fan pairs (extrapolated value) + detection technique able to detect the fire within 2.5 min

Being the three different options equally performing, the final design must be chosen on the basis of an economic analysis of the initial investment (including ventilation and detection systems) and maintenance costs.

8

Conclusions and future works

The work presented is related to the numerical simulations of tunnel ventilation flows and fires. Different numerical techniques have been developed and validated against experimental data from real tunnels including 1D models, CFD models and multiscale models.

The developed 1D model has been validated against experimental data from the Frejus tunnel (IT) where it has been shown to be able to predict with reasonable accuracy the evolution of the ventilation conditions within the tunnel during a fire emergency. Typically 1D models are unsuitable to simulate the fluid behaviour in regions characterized by high temperature or velocity gradients typically encountered in the vicinity of the fire plume, ventilation devices or complex interconnections of galleries. In order to deal with such complex flow conditions, they mainly rely on empirical correlations or calibration constants to be defined on the basis of experimental measurements or detailed CFD calculations.

The CFD models have been developed in FLUENT environment and used to simulate tunnel ventilation flows both in cold (i.e. ambient conditions) and fire scenarios. The numerical sub-models have been chosen on the basis of an extensive literature review involving all the related papers published in the last 25 years on archival journals of the field. Great care has also been given to the correct choice of the grid size which has been systematically refined until no substantial variations both in the local field data and integral values were observed.

A first validation work has been undertaken by using cold flow data measured in 9 different ventilation scenarios in the Norfolk Tunnels, Sydney (AU). A significant level of accuracy (average relative deviation around 17%) has been achieved. A comparison to the experimental findings from two small scale tunnel fire scenarios studied by Wu and Bakar [33] confirmed also the ability of the CFD model to predict the critical velocity with a reasonable level of accuracy (~ 25%).

The CFD analyses have also shown that significant computational resources were required to simulate a single steady state ventilation or fire scenario in relatively short tunnels. The computational time become a severe limitation when the full CFD approach is adopted to deal with fire or ventilation in long tunnels or when analysing a broad range of ventilation strategies. Furthermore, the high computational cost leads to the practical problem that arises when the CFD model has to consider boundary conditions in locations far away from the region of interest (i.e. tunnel portals or ventilation stations located long distances away from the fire). In these cases, even if only a limited region of the tunnel has to be investigated, an accurate solution of the flow movement requires that the numerical model includes all the active ventilation devices and the whole tunnel layout. For typical tunnels, this could mean that the computational domain is several kilometres long

Multiscale methods, based on hybrid 1D-CFD computational techniques, represent a way to avoid such high computational complexity. They have never been applied to simulate tunnel ventilation flows and fires and this work represents only the starting point for a more comprehensive use of these techniques addressing tunnel related problems.

Multiscale models are based on the evidence that in the vicinity of operating jet fans or close to the fire source the flow field has a complex 3D behaviour with large transversal and longitudinal temperature and velocity gradients. The flow in these regions needs to be calculated using CFD tools since any other simpler approach would only lead to inaccurate results. However, it has been demonstrated for cold flow scenarios and for fire scenarios that some distance downstream of these regions, the temperature and velocity gradients become milder and the flow behaviour can be accurately represented by 1D models. The work presents also a wide description on the 1D-CFD coupling techniques as well as gives emphasis to the control of the numerical error.

Multiscale modelling techniques have been first applied to simulate steady cold ventilation flows in the Dartford Tunnels (UK) where an extensive experimental campaign has been also undertaken. The comparison to experimental data shows that highly accurate results could be achieved both when modelling the local flow field in the vicinity of operating jet fans as well as bulk flows within the tunnel. The developed multiscale model has also been applied to include the effect of the fire. The comparison to full CFD solutions shows that the maximum flow field error can be reduced to less than few percents, but providing a significant reduction in computational time.

Time dependent analyses of tunnel ventilation flows and fires have also been conducted providing, for instance, information related to the time required to reach the critical velocity in the fire region, to clear a certain tunnel portion from smoke, or the temporal evolution of the smoke stratification in the fire region. These details are indeed fundamental to analyse the development of an emergency scenario to determine the evolution of hazardous zones in the tunnel domain, to design evacuation procedures or to determine the correct timing for the activation of fixed fire fighting systems (e.g. water mist, deluge or sprinkler systems).

The advantages of multiscale modelling techniques when dealing with tunnel ventilation flows and fires are mainly related to the considerable computational time reduction in comparison to traditional full CFD approaches. Indeed, it has been shown that multiscale simulations of steady tunnel ventilation flows and fires in a 1.2 km long tunnel are almost 2 orders of magnitudes faster than full CFD simulations. A direct

assessment of such reduction for time dependent simulations could not be performed since each transient full CFD simulation could take up to 3 months. The reduction in the computing time is likely to be larger for longer tunnels where the multiscale methodology represents the only feasible tool to conduct accurate simulations.

Given the low computation complexities, multiscale techniques can be successfully adopted to conduct parametric and sensitivity studies, to design ventilation systems, to assess their redundancy and performance under different fire hazards. The great engineering value is boosted when conducting time dependent simulations since the number of input variables is larger and includes detection time and fire growth curve. Such broad spectrum of simulations cannot be performed adopting traditional CFD models due to the required computing time.

Another significant advantage is related to the simulation of the whole tunnel domain including the ventilation devices. This allows for an accurate assessment of the fire throttling effect and for a prediction of the minimum number of jet fans needed to cope with a certain fire size. For instance, it has been shown that a 100 MW fire in a 1.2 km long tunnel is likely to decrease the ventilation flow by more 30% due to the additional fire induced pressure losses. Obviously, such effects will be severely amplified for larger fires and longer tunnels. It is worth to note that 1D model could be used to address this issue but it has been shown that they are likely to underestimate the fire induced losses.

One of the most important issues on the use of multiscale model for tunnel ventilation and fires is related to the location of the interfaces between 1D and CFD models. These boundaries must be located in regions of the domain where the temperature or velocity gradients are negligible and the flow behaves largely as 1D. These dictate the length of the CFD domain. This required length is case specific and in general depends on tunnel geometry, installation details of ventilation devices, presence of obstacle, etc. Based on the test cases chosen in this work, which represent real modern tunnel layouts, a minimum length of the CFD domain for an accurate simulation of ventilation and fire induced flows could be provided.

Being this only a pioneering work on the subject, there are several other issues that deserve to be addressed in the next years or so. Some of them are directly related to the sub-models adopted for the simulations while others related to new possible applications and integration with different simulation tools.

A first improvement could be represented by the adoption of more sophisticated combustion models (e.g. Eddy break up or mixture fraction models). The results could be compared to the simplified fire representation based on volumetric heat source as the one used in this work. On the basis of the literature review conducted, it is believed that only marginal improvements on the prediction capabilities can be obtained but this still represents a due step. Eventually, comparisons to detailed flow field and temperature measurements can be introduced to address this issue.

Other possible applications are represented by longer tunnels equipped with different ventilation system types (e.g. transverse and semi-transverse systems). The first application will be the Frejus tunnel where several sets of experimental data are available.

An initial screening of other possible CFD solvers to be coupled to the developed 1D model has been undertaken. Other CFD packages are OpenFoam (general purpose open-source CFD code based on final volumes), FDS (open source CFD code based on finite-differences) and CD-Adapco (general purpose commercial CFD code based on finite volume). The main requirement for the CFD code to be useful for multiscale computing is the accessibility. Indeed, the boundary conditions of the CFD model must be dynamically updated during the solution procedure in order to achieve a global multiscale convergence.

Other interesting applications are represented by the coupling to risk analysis tools in order to perform enhanced studies of ventilation system performance and comprehensive risk analyses involving a large number multiscale runs. The current state-of-the-art, due to the huge time required by full CFD simulations, uses only a limited number of CFD runs and then extrapolates their results to similar scenarios. The lower cost could be of great value also for performing cost optimization during the design process of the tunnel ventilation and detection systems.

REFERENCE LIST

[1] Haack A., (2002), "Current safety issues in traffic tunnels", Tunnelling and Underground space technology, 17: 117-127

[2] Perard, M. (1996), "Statistics on breakdowns, accidents and fires in French road tunnels", Proceedings of the 1st international Conference on Tunnel Incident Management, Korsor, Denmark, 13 - 15 May, 347-365

[3] Carvel R.. Malair G. (2004), "A history of fire incidents in tunnels", In The Handbook of Tunnel Fire Safety (R. O. Carvel and A. N. Beard, Eds.), Thomas Telford Publishing, 231-266, London, 2005.

[4] Carvel R. (2007), "Tunnel fire safety systems", EuroTransport, 5(6): 39-43

[5] Ingason H., Fire Dynamics in tunnel (2005), chapter in, The handbook of tunnel fire safety, Ed A. Beard and R. Carvel, Thomas Telford, London, UK

[6] Drysdale, D. (1998). An Introduction to Fire Dynamics. Wiley, England, 2nd edition.

[7] Carvel, R., (2010), "Fire Dynamics During the Channel Tunnel Fires", Proceedings of the Fourth International Symposium on Tunnel Safety and Security, Frankfurt am Main, Germany, March 17-19, 463-470

[8] H. Ingason and A. Lönnermark, Heat release rates from heavy goods vehicle trailer fires in tunnels, Fire Safety Journal, Volume 40, Issue 7, October 2005, Pages 646-668.

[9] World Road Association, PIARC technical committee on Road Tunnel Operation (C5), (2004), "Fire and smoke control in Road Tunnels"

[10] Babrauskas, V. and Grayson (1992.b) Heat Release in Fires. S.J. Editors, Elsevier Applied Science.

[11] Massachusetts Highway Department (1995) Memorial tunnel fire ventilation test program comprehensive test report

[12] EUREKA 499 Report (1996), Fire in transport tunnels, report on full scale tests. Duesseldorf: Studiengesellschaft Stahlanwendung e.V.

[13] Lemaire T., Kenyon Y., Large Scale Fire Tests in the Second Benelux Tunnel,Fire Technology, 42, 329–350, 2006

[14] Lautenberger, C., Torero, J.L., Fernandez-Pello, C., (2006). Understanding materials flammability. Chapter in Flammability testing of materials used in construction, transport and mining, Woodhead Publishin limited, Cambirdge UK

[15] Bundy M., Ohlemiller, T., (2003). Bench-Scale Flammability Measures for Electronic Equipment, NIST Report 7031

[16] Lonnemark A, Ingason H., The Effect of Air Velocity on Heat Release Rate and Fire Development during Fires in Tunnels, Fire Safety Science-proceedings of the ninth international symposium, 701-712

[17] Carvel, R., "Design fires for tunnel water mist suppression systems", Proceedings of 3rd International Symposium on Tunnel Safety and Security", Stockholm, 12-14 March, 2008

[18] Lemaire A, van de Leur PHE, Kenyon YM, Safety Proef: TNO Metingen Beneluxtunnel—Meetrapport, TNO, TNO-Rapport 2002-CVB-R05572, 2002.

[19] Loennermark A., Ingason, H. (2005), Gas temperatures in heavy goods vehicle fires in tunnels, Fire Safety Journal 40: 506–527

[20] Bendelius A., "Tunnel ventilation – state of the art", In The Handbook of Tunnel Fire Safety (R. O. Carvel and A. N. Beard, Eds.), Thomas Telford Publishing, 231-266, London, 2005.

[21] Chen T.Y., Lee T.T., Hsu C.C. (1998), "Investigation of piston-effect and jet fan-effect in model vehicle tunnels", Journal of Wind Engineering and Industrial Aerodynamics, 73: 99-110

[22] Jang H.M., Chen F. (2000), "A novel approach to the transient ventilation of road tunnels", Journal of Wind Engineering and Industrial Aerodynamics", 28: 15-36.

[23] Torbergsen, L.E., Paaske, P., Schieve, C. (2002), "Numerical simulation of the fire and smoke propagation in long railway tunnels", Proceeding of the 4th International conference on Tunnel Fires, Basel Switzerland, 2-4 December, ITC conferences Ltd, 330-346.

[24] Jagger S., Grant G., "Use of tunnel ventilation for fire safety", In The Handbook of Tunnel Fire Safety (R. O. Carvel and A. N. Beard, Eds.), Thomas Telford Publishing, 231-266, London, 2005

[25] PIARC (2008), "Road tunnels, Operational strategies for emergency ventilation", Technical committee C3.3 Tunnel operations, Working Group No. 6 Ventilation and fire Controll, World Road Association

[26] Jojo S.M. Li, W.K. Chow (2003), Numerical studies on performance evaluation of tunnel ventilation safety systems Tunnelling and Underground Space Technology 18 435–452

[27] Thomas PH (1958) The movement of buoyant fluid against a stream and venting of underground fires. Fire Research note:351.

[28] Oka Y, Atkinson GT (1995) Control of smoke flow in tunnel fires. Fire Safety Journal 25(4): 305–22.

[29] Kunsch JP (2002) Simple model for control of fire gases in a ventilated tunnel. Fire Safety Journal 37(1): 67–81.

[30] Vauquelin O, Wu Y (2006) Influence of tunnel width on longitudinal smoke control. Fire Safety Journal 41: 420–426

[31] Oucherfi, M., Gay, B., Mos, A., Carlotti, P., (2009), "Definition and optimisation of the efficiency of smoke extraction in a road tunnel", 13th international Symposium on Aerodynamics and ventilation of vehicle tunnels

[32] Chasse P., Apvrille J-M. (1999). A new 1D computer model for fires in complex underground networks. Fire in Tunnels Conference, Lion. 201-222.

[33] Wu Y, Bakar MZA (2000) Control of smoke flow in tunnel fires using longitudinal ventilation systems - a study of the critical velocity. Fire Safety Journal 35: 363-390

[34] Hinkley PL. (1970), The flow of hot gases along an enclosed shopping mall. A tentative theory. Fire Research Note No. 807

[35] William D. Kennedy (1997) Critical Velocity - Past, Present and Future (Revised 6 June 1997). American Public Transportation Association's Rail Trail Conference in Washington, DC.

[36] Lee CK, Chaiken RF, J.M. Singer JM (1979) Interaction between duct fires and ventilation flow: an experimental study. Combustion Science & Technology 20: 59-72

[37] Hwang C.C, Edwards J.C. (2005), The critical ventilation velocity in tunnel fires—a computer simulation, Fire Safety Journal 40 (2005) 213–244

[38] Atkinson, G.T. and Wu, Y. (1996). Smoke Control in Sloping Tunnels, Fire Safety Journal, 27(4): 335–34

[39] Ko G.H., Kim, G.R., Ryou H.S. (2010), "An Experimental Study on the Effect of Slope on the Critical Velocity in Tunnel Fires", Journal of fire sciences, 28:27-47

[40] Hu L.H., Huo R., Chow W.K. (2008), Studies on buoyancy-driven back-layering flow in tunnel fires, Experimental Thermal and Fluid Science 32: 1468–1483

[41] Carvel R.O., Beard A.N., Jowitt P.W., Drysdale D., "Variation of heat release rate with forced longitudinal ventilation for vehicle fires in tunnels", Fire Safety Journal 36 (2001) 569–596.

[42] Carvel R., Marlair G. (2005), "A history of experimental tunnel fires", chapter in, The handbook of tunnel fire safety, Ed A. Beard and R. Carvel, Thomas Telford, London, UK

[43] Forney G.P., Moss W.F., "Analyzing and exploiting numerical characteristics of zone fire models", NISTIT 4763, March 1992

[44] Charters D.A., Gray, W.A., McIntosh, A. C., (1994) A computer model to assess fire hazards in tunnels (FASIT), Fire Technology 30,1.

[45] Suzuki, K., Tanaka T., Harada K., Tunnel Fire Simulation Model with Multi-Layer Zone Concept, Fire Safety Science-proceedings of the ninth international symposium, 713-724

[46] Riess I., Bettelini M., Brandt R. (2000). "Sprint – a design tool for fire ventilation", 10th Int. Symp. on Aerodynamics and Ventilation of Vehicle Tunnels, Boston.

[47] Greuer R. E.(1977), Study of mine fires and mine vemtilation, Part I, Computer simulations of mine ventilation systems under the influence of mine fires, Department of the interior bureau of mines, Washington D.C.

[48] Tullis, J. P. (1989), Hydraulics of pipelines, John Wiley & Sons, New York

[49] U. S. Bureau of Mines, (1995), "MFIRE users manual Version 2.20".

[50] Dai G., Vardy A.E. (1994). "Tunnel temperature control by ventilation". Proc 8th int symp on the Aerodynamics and Ventilation of Vehicle Tunnels, Liverpool, UK, 6/8 July, 175-198

[51] West A., Vardy A.E., Middleton B., Lowndes J.F.L. (1994) 'Improving the efficacy and control of the Tyne Tunnel ventilation system', Proceedings of the 1st International Conference on Tunnel Control and Communication, Basel, Switzerland, 28-30 Nov, 473-489

[52] Riess I., Bettelini M. (1999). "The Prediction of Smoke Propagation Due to Tunnel Fires". 1st International Conference Tunnel Fires and Escape from Tunnels, Lyon, May 1999

[53] Riess I., Bettelini M., Brandt R. (2000). "Sprint – a design tool for fire ventilation". 10th Int. Symp. on Aerodynamics and Ventilation of Vehicle Tunnels, Boston, November 2000

[54] NTIS. (1980) "User's guide for the TUNVEN and DUCT programs". Publication PB80141575. National Technical Information Service, Springfield, V A. 27.

[55] Schabacker J., Bettelini M., Rudin Ch. (2002). "CFD study of temperature and smoke distribution in a railway tunnel". Tunnel Management International, Volume 5, Number 3

[56] L.H. Cheng, T.H. Ueng, C.W. Liu. Simulation of ventilation and fire in the underground facilities. Fire Safety Journal 36 (2001) 597–619.

[57] Ferro V., Borchiellini R., Giaretto V. (1991). "Description and Application of a Tunnel Simulation Model" "Aerodynamics and Ventilation of Vehicle Tunnels" Elsevier Applied Science, London, pp. 487÷512.

[58] Borchiellini R., Ferro V., Giaretto V. "Transient Thermal Analvsis of Main Road Tunnel" In "Aerodynamics and Ventilation of Vehicle Tunnels" Mechanical Engineering Publications Limited London 1994, pp. 17÷31 (8th International Symposium on Aerodynamics and Ventilation of Vehicle Tunnels, Liverpool UK, 6-8 July 1994).

[59] Jacques E, (1991) Numerical simulation of complex road tunnels. Proceedings of Aerodynamics and Ventilation of vehicle tunnels conference: 467-486

[60] Parsons Brinckerhoff Quade & Douglas, Inc., "Subway Environmental Design Handbook Volume II Subway Environment Simulation (SES) Computer Program Version 3 Part 1: User's Manual" , prepared in draft for the U.S. Department of Transportation, October 1980.

[61] William D. Kennedy (1997) Critical Velocity - Past, Present and Future (Revised 6 June 1997). American Public Transportation Association's Rail Trail Conference in Washington, DC.

[62] Jang H, Chen F (2002) On the determination of the aerodynamic coefficients of highway tunnels. Journal of wind engineering and industrial aerodynamics 89 (8): 869 – 896.

[63] Fox RW, McDonald AT (1995) Introduction to fluid mechanics 4th edition. John Wiley and Sons, Singapore.

[64] Chandrashekar, M. & Wong, F. C. (1982). Thermodynamic System Analysis – A graph-theoretic Approach. Energy, Vol.7 No.6, pp.539-566.

[65] Quarteroni, A. (2008), "Modellistica numerica di problemi differenziali", Springer, Italy, Milano

[66] Versteeg HK, Malalasekera W (2007) An introduction to computational fluid dynamics, the finite volume method. 2nd ed. Pearson Prentice Hall, Glasgow.

[67] PIARC (1995), Tunnel routiers: emission, ventilation, environnement, Paris.

[68] Incropera, F.P., DeWitt, D.P.(1996), "Introduction to heat transfer, 3rd edition", John Wiley & Sons, New York

[69] Fluent Inc. FLUENT 6.2 User's Guide. 2005.

[70] Ferziger J.H., Peric M. (2002), "Computational methods for fluid-dynamics, 3rd edition", Springer Verlag, Berlin

[71] Patankar, S.V., Spalding, D.B. (1972), "A calculation procedure for Heat, Mass and momentum Tranfer in Three dimensional parabolic Flows", Int. J. Heat Mass Transfer, 15: 1787

[72] Bettelini, M. (2009), "Managing the longitudinal air velocity in long road tunnels", 13th international Symposium on Aerodynamics and ventilation of vehicle tunnels

[73] Bettelini, M., Glarey L., Koeofler A., Croci S., Di Noia L. (2001), "The new Mont Blanc Tunnel – A milestone in Tunnel safety", International conference International tunnel forum", Basel, 4-6 December

[74] Ingason, H., Bergqvist, A., Loennemark, A., Frantzich, H., Hasselrot, K. (2005), "Räddningsinsatser i vägtunnlar", Räddningsverket, Karlstad, ISBN 91-7253-256-4 (in Swedish only).

[75] Idelchik I. E., "Handbook of Hydraulic Resistance 2nd Edition", Hemisphere Publishing Corporation

[76] McGrattan K., Miles S., (2008), "Modeling Enclosure fires using computational Fluid Dynamics" in "The SFPE handbook of Fire Protection Engineering 4th edition", National fire protection association, Quincy, Massachusetts, US

[77] Olenick, S., Carpenter, D. (2003), "An updated international survey of computer models for fire and smokes", journal of fire protection Engineering, 13:87-110.

[78] Cox, G. (1995), "Compartment fire modelling", Combustion fundamental of fire, Academic press, London

[79] Cox, G. (1998), "Turbulent closure and the modelling of fire using CFD", Philosophical transaction of the royal society, A. 356, 2835

[80] Novozhilov, V. (2001), "Computational fluid dynamic modelling of compartment fires", Progress in energy and combustion science, 27: 611-666

[81] Fletcher, D. F., Kent, J. H. (1994),"Numerical Simulations of Smoke Movement from a Pool Fire in a Ventilated Tunnel", Fire Safety Journal 23, 305-325

[82] Woodburn PJ, Britter RE (1996) CFD simulation of tunnel fire – part I. Fire Safety Journal 26: 35-62

[83] Woodburn PJ, Britter RE (1996) CFD simulation of tunnel fire – part II. Fire Safety Journal 26: 63-90

[84] Chow, W.K. (1998)," On Smoke Control for Tunnels by Longitudinal Ventilation", Tunnelling and Underground Space Technology, Vol. 13, No. 3, pp. 271-275, 1998

[85] Karki KC, Patankar SV (2000) CFD model for jet fan ventilation systems. Proceedings of Aerodynamics and Ventilation of vehicle tunnels conference

[86] Gao P.Z.,Liu S.L., Chow W.K., Fong N.K. (2004), "Large eddy simulations for studying tunnel smoke ventilation", Tunnelling and Underground Space Technology 19: 577–586

[87] Bari S., Naser, J., (2005), "Simulation of smoke from a burning vehicle and pollution levels caused by traffic jam in a road tunnel", Tunnelling and Underground Space Technology 20: 281–290

[88] Lee, S.R., Ryou, H.S. (2006), "A numerical study on smoke movement in longitudinal ventilation tunnel fires for different aspect ratio", Building and Environment 41:719–725

[89] McGrattan, K., Hamins, A. (2006), "Numerical Simulation of the Howard Street Tunnel Fire", Fire Technology, 42, 273–281

[90] Ballesteros-Tajadura, R., Santolaria-Morros, C., Blanco-Marigorta E. (2006), "Influence of the slope in the ventilation semi-transversal system of an urban tunnel", Tunnelling and Underground Space Technology 21: 21–28

[91] Lin, C.j., Chuah, Y.K. (2007), "A study on long tunnel smoke extraction strategies by numerical simulation", Tunnel. Underg. Space Technol., doi:10.1016/j.tust.2007.09.003

[92] Jae Seong Roh, J.S., Ryou, H.S., Kim, D.H., Jung, W.S., Jang, Y.J. (2007), "Critical velocity and burning rate in pool fire during longitudinal ventilation", Tunnelling and Underground Space Technology 22: 262–271

[93] Abanto, J., Reggio, M., Barrero, D., Petro, E., (2006), "Prediction of fire and smoke propagation in an underwater tunnel", Tunnelling and Underground Space Technology 22: 90–95

[94] Kim, E. Woycheese, J.P., Dembsey, N.A (2007), "Fire Dynamics Simulator (Version 4.0) Simulation for Tunnel Fire Scenarios with Forced, Transient, Longitudinal Ventilation Flows",Fire Technology DOI: 10.1007/s10694-007-0028-2

[95] Galdo Vega, M., Marıa Arguelles Dıaz, K, Fernandez Oro, J.M., Ballesteros Tajadura, R., Santolaria Morros, C. (2007), "Numerical 3D simulation of a longitudinal ventilation system: Memorial Tunnel case", Tunnelling and Underground Space Technology, doi:10.1016/j.tust.2007.10.001

[96] Rusch, D., Blum, L.,Moser, A., Roesgen, T. (2008), "Turbulence model validation for fire simulation by CFD and experimental investigation of a hot jet in crossflow", Fire Safety Journal, doi:10.1016/j.firesaf.2007.11.005

[97] Van Maele K., Merci B. (2008), Application of RANS and LES field simulations to predict the critical ventilation velocity in longitudinally ventilated horizontal tunnels", Fire Safety Journal 43: 598–609

[98] Kashef, A., Benichou N. (2008), "Investigation of the Performance of Emergency Ventilation Strategies in the Event of Fires in a Road Tunnel – A Case Study", Journal of FIRE PROTECTION ENGINEERING, Vol. 18: 165-198

[99] Jain, S., Kumar, S., Kumar, S., Sharma, T.P. (2008), "Numerical simulation of fire in a tunnel: Comparative study of CFAST and CFX predictions", Tunnelling and Underground Space Technology 23: 160–170

[100] Cheong, M.K., Spearpoint, M.J., Fleischmann, C.M. (2009), "Calibrating an FDS Simulation of Goods-vehicle Fire Growth in a Tunnel Using the Runehamar Experiment", Journal of FIRE PROTECTION ENGINEERING, Vol. 19

[101] Nmira, F., Consalvi, J.L., Kaiss, A., Fernandez-Pello, A.C., Porterie, B., (2009), "A numerical study of water mist mitigation of tunnel fires", Fire Safety Journal, 44: 198-211

[102] Colella F, Rein G, Borchiellini R, Carvel R, Torero JL, V. Verda V, "Calculation and Design of Tunnel Ventilation Systems using a Two-scale Modelling Approach", Building and Environment, 44, 2357-2367, 2009.

[103] Colella, F., Rein, G., Carvel, R., Reszka, P. Torero, J.L. (2010), "Analysis of the ventilation systems in the Dartford tunnels using a multi-scale modelling approach", Tunnel. Underg. Space Technol., doi:10.1016/j.tust.2010.02.007

[104] The Handbook of Tunnel Fire Safety (R. O. Carvel and A. N. Beard, Eds.), Thomas Telford Publishing, 231-266, London, 2005

[105] Colella F., Rein G., Borchiellini R., Torero J.L., "A Novel Multiscale Methodology for Simulating Tunnel Ventilation Flows during Fires", Fire Technology, (in press).

[106] Fluent Inc. FLUENT 6.2 User's Guide. 2005.

[107] B.E. Launder, D.B. Spalding (1974) "The numerical computation of turbulent flows", Comput. Methods Appl. Mech. Engrg; 3 (2): 269-289.

[108] Van Maele, K., Merci, B., (2006), "Application of two buoyancy-modified k-ε turbulence models to different types of buoyant plumes", Fire Safety Journal, 41:122-134

[109] Nam S., Bill Jr. RG. (1993), "Numerical simulation of thermal plumes", Fire Safety journal, 21: 231-256

[110] Hara, T., Kato, S., (2004), "Numerical simulations of thermal plumes in free space using the standard k- ε model", Fire Safety Journal 39. 105-129

[111] Hue, X., Ho, J.C., Cheng, Y.M. (2001), "Comparison of different combustion models in enclosure fire simulation", Fire Safety Journal, 36:37-54

[112] Yan, Z., Holmstedt G. (1999), "A two-equation turbulence mode and its application to a buoyant diffusion flame", Int J. Heat and Mass Transfer, 42:1305-1315

[113] Cox G, Kumar S (2002) Modelling enclosure fires using CFD. In: The SFPE handbook for fire safety engineering, 3rd edn. NFPA, Massachusetts International, Quincy

[114] Lonnemark A, H. Ingason H (2005) Gas temperature in heavy goods vehicles fires in tunnels. Fire safety journal 40: 506-527

[115] Heskestad G (2002) Fire plumes, Flame height and air entrainment. In: The SFPE handbook for fire safety engineering, 3rd edn. NFPA, Massachusetts International, Quincy

[116] Loennermark A. & Ingason H. (2008), The influence of tunnel cross-section on temperature and fire development, 3rd International symposium on Tunnel Safety and Security, Stockholm, Sweden ,March 12-14

[117] Ingason H. (2008), Model scale tunnel tests with water spray, Fire Safety Journal 43: 512–528

[118] Drysdale D. (2000) An introduction to Fire Dynamics II edition, John Wiley & Sons Inc. Hoboken, USA

[119] Schlichting H (1979) Boundary layer theory 7th ed. McGraw-hill, New York

[120] Lacasse, D., Turgeon, E., Pelletier, D. (2004), "On the judicious use of the k-ε model, wall functions and adaptivity", International Journal of Thermal Sciences, 43:925-938

[121] Reszka P, Steinhaus T, Biteau H, Carvel RO, Rein G, Torero JL (2007) A Study of Fire Durability for a Road Tunnel Comparing CFD and Simple Analytical Models. EUROTUN07 Computational Methods in Tunnelling, Wien. http://hdl.handle.net/1842/1892

[122] Merci, B., (2008), "One-dimensional analysis of the global chimney effect in the case of fire in an inclined tunnel", Fire Safety Journal 43: 376–389

[123] Formaggia, L., Gerbeau, J.F., Nobile, F., Quarteroni, A., (2001), "On the coupling of 1D and 3D Navier-Stokes equations for flow problems in compliant vessels" Comput. Methods Appl. Mech. Engrg 191: 561-582

[124] Motenegro, G., (2002), "Simulazione 1D-Multi D di flussi instazionari e reagenti in sistemi di scarico ed aspirazione in motori a combustione interna", PhD thesis, Dipartimento di Energetica, Politecnico di Milano

[125] Mossi. M. (1999), "Simulation of benchmark and industrial unsteady compressible turbulent fluid flows", PhD thesis, Mechanical Engineering Department, EPFL

[126] Rey, B., Mossi, M., Molteni, P., Vos, J., Deville, M. (2009), "Coupling of CFD software for the computation of unsteady flows in tunnel networks", 13th international Symposium on Aerodynamics and ventilation of vehicle tunnels

[127] Geiger, S., Huangfu, Q., Reid, F., Mattha, S., Coumou, D., Belayneh, M., Fricke, C., Schimd, K. (2009), "Massively Parallel Sector Scale Discrete Fracture and Matrix Simulations", SPE Reservoir Simulation Symposium held in The Woodlands, Texas, USA, 2-4 February 2009

[128] Quarteroni, A., Valli, A. (1999), "Domain Decomposition Methods for Partial Differential Equations", Oxford Science Publications, Oxford.

[129] Houzeaux, G., Codina, R. (2004), "A Dirichlet/Neumann domain decomposition method for incompressible turbulent flows on overlapping subdomains", Computers & Fluids: 33: 771–782

[130] Fluent Inc. (2006), "FLUENT 6.3 UDF manual".

[131] Harvey, N., Fuster T. (2009), "Design fire heat release rate selection – impacts for road tunnels", 13th international Symposium on Aerodynamics and ventilation of vehicle tunnels

[132] Koffmane, G., Hoff, H., (2010), "More than Just Fire Detection: Fibre Optic Linear Heat Detection (DTS) enables Fire Monitoring in Road- and Rail-Tunnels", Fourth International Symposium on Tunnel Safety and Security, Frankfurt am Main, Germany, March 17-19

[133] Rogner, A., (2010), "Safety and Reliability of Fire Detection Systems in Road Tunnels", Fourth International Symposium on Tunnel Safety and Security, Frankfurt am Main, Germany, March 17-19

[134] Liu, Z.G., Kashef A., Lougheed, G.D., Crampton, G., Ko, Y., Hadjisophocleous, (2009), "Parameters affecting the performance of detection systems in road tunnels", 13th international Symposium on Aerodynamics and ventilation of vehicle tunnels

[135] Heselden, A.J.M., "Studies of Fire and Smoke Behavior Relevant to Tunnels", Current Paper CP66/78, Building Research Establishment, 1978.